

Chemically Stable Nitrogenous Porous Crystalline Covalent Organic Frameworks for Heterogeneous Catalysis

Thesis Submitted to AcSIR For the Award of
the Degree of
DOCTOR OF PHILOSOPHY
In Chemical Science



By
Mohitosh Bhadra
10CC14A26002

Under the guidance of
Dr. Rahul Banerjee

CSIR-National Chemical Laboratory

Chemically Stable Nitrogenous Crystalline Covalent Organic Frameworks for Heterogeneous Catalysis

Thesis Submitted to AcSIR

For the Award of the Degree of

DOCTOR OF PHILOSOPHY

In

CHEMICAL SCIENCES



By

Mohitosh Bhadra

(Registration Number: 10CC14A26002)

Under the guidance of

Dr. Rahul Banerjee

Physical & Materials Chemistry Division

CSIR-National Chemical Laboratory

Pune - 411008, Maharashtra,

India.

August 2018

*Dedicated to
My Teachers and
My Family for their
Love and Support*



सीएसआईआर - राष्ट्रीय रासायनिक प्रयोगशाला

(वैज्ञानिक तथा औद्योगिक अनुसंधान परिषद)

डॉ. होमी भाभा मार्ग, पुणे - 411 008, भारत

CSIR - NATIONAL CHEMICAL LABORATORY

(Council of Scientific & Industrial Research)

Dr. Homi Bhabha Road, Pune - 411 008, India



Certificate

This is to certify that the work incorporated in this Ph.D. thesis entitled “Chemically Stable Nitrogenous Porous Crystalline Covalent Organic Frameworks for Heterogeneous Catalysis” submitted by Mr. Mohitosh Bhadra to Academy of Scientific and Innovative Research (AcSIR) in fulfillment of the requirements for the award of the Degree of Doctor of Philosophy, embodies original research work under my supervision. I further certify that this work has not been submitted to any other University or Institution in part or full for the award of any degree or diploma. Research material obtained from other sources has been duly acknowledged in the thesis. Any text, illustration, table etc., used in the thesis from other sources, have been duly cited and acknowledged.

Mohitosh Bhadra

Mr. Mohitosh Bhadra

(Student)

Rahul Banerjee


Dr. Rahul Banerjee

(Supervisor)

9th August, 2018

Pune.

Communication Channels

 NCL Level DID : 2590
NCL Board No. : +91-20-25902000
EPABX : +91-20-25893300
: +91-20-25893400

FAX

Director's Office : +91-20-25902601
COA's Office : +91-20-25902660
SPO's Office : +91-20-25902664

WEBSITE

www.ncl-india.org

STATEMENT

I hereby declare that the matter embodied in this thesis entitled “Chemically Stable Nitrogenous Porous Crystalline Covalent Organic Frameworks for Heterogeneous Catalysis” is the result of investigations carried out by me in the Physical & Materials Chemistry Division, CSIR-National Chemical Laboratory, Pune, India under the supervision of Dr. Rahul Banerjee.

In keeping with the general practice of reporting scientific observations due acknowledgements have been made wherever the work described is based on the findings of other investigators.

*Pune,
August, 2018*

Mohitosh Bhadra
Mohitosh Bhadra

ACKNOWLEDGEMENT

*I would take this opportunity to express my sincere gratitude to my supervisor **Dr. Rahul Banerjee**. My heartfelt thanks go to him for introducing me to the wonders of scientific research, for his persistent guidance, encouragement, inspiration and support during every stage of my doctoral research work. Again I warmly thank him for his precious advice, analysis, criticism and discussions on my research work. I am very much thankful to him for his pursuance for improving me as a person as well as my scientific skills. I would also like to sincerely thank my research co-supervisor **Dr. Shatabdi Porel Mukherjee** and my DAC committee members **Dr. Ulhas K. Kharul**, **Dr. Kumar Vanka** and **Dr. Narendra Y. Kadoo** for their constructive, innovative suggestion and comments throughout my Ph.D. work period at CSIR-NCL, Pune.*

*I extend my sincere thanks to the Director of CSIR-NCL **Prof. Ashwani Kumar Nangia**, former Directors **Dr. Vijayamohanan K. Pillai** and **Dr. Sourav Pal**, Head of Physical and Materials Chemistry Division **Dr. P. A. Joy** and **Dr. Anil Kumar (Ex-HoD)** for their kind help and encouragement during the course of this work. I must earnestly acknowledge the collaborative assistance, valuable scientific discussions and suggestions that I received from **Dr. Ekambaram Balaraman**, **Dr. Sreekumar Kurungot**, **Dr. Manjusha V. Shelke**, **Dr. Chinnakonda S. Gopinath**, **Dr. Sayam Sen Gupta**, **Dr. Sakya S. Sen**, **Dr. S.K. Asha**, and **Dr. Rajesh G. Gonnade** from CSIR NCL and **Prof. Avinash S. Kumbhar** from Savitribai Phule Pune University, Pune. My sincere thanks and kind acknowledgment to **Dr. Matthew Addicoat** from School of Science and Technology, Nottingham Trent University, Clifton Lane, NG11 8NS Nottingham, United Kingdom, **Dr. Thomas Hein**, from School of Engineering and Science, Jacobs University, Germany, **Dr. Arne Thomas** and **Amitava Acharjya** from Technische Universität Berlin, Hardenbergstr. 4010623 Berlin, Germany for their theoretical calculations and experimental help in my projects.*

*I am very much grateful to CSIR, New Delhi for fellowship support to carry out my research work and **AcSIR** for allowing me to submit my work in the form of a thesis. I thank all the non-teaching staff of CSIR-NCL for their assistance on various occasions. I wish to thank all my friendly and cooperative labmates **Arijit Da**, **Tamas Da**, **Pradip da**, **Chandan Da**, **Subhadeep Da**, **Tanay Da**, **Sharath da**, **Bishnu da**, **Suman da**, **Bikash Da**, **Shouvik Da**, **Govinda da**, **Sujit Da**, **Digamber Ji**, **Jayashri Mam**, **Manas da**, **Amit da**, **Tapan da**, **Arghya***

Da, Sushil Bhaya, Srinu Anna, Gargi Di, Abdul, Arjun, Saibal, Suwendu, Kaushik, Himadri, Shebeeb and Kanhu da for creating a cheerful and enjoyable working atmosphere in the lab. They were extremely supportive as well as helpful during my tenure. I also thank project student Neethu T. V., Tusar and Junior Joy Pramani who helped me in various projects.

*My stay on this campus has been pleasing with the association of all the research scholars at CSIR-NCL. I am thankful to **Krishanu da, Anup da, Pravat da, Jayasis da, Kanak da, Achintya da, Susanta da, Basab da, Arpan da, Shyam da, Chandan da, Munmun di, Soumen da, Santanu da, Saibal da, Hridesh da, Arunava da, Firoj da, Moumita di, Atanu da, Manik da, Santanu Da, Sudip Da, Monalisa di, Poulami di, Debasree di, Atryee di, Manoj Da, Soumyajyoti Da, Praveen, Bhawana di, Sushma ji, Vinita di, Shrikanth, Suresh ji, Farsa Ram, Samir, Propat ji, Harshal ji, Bharat ji, Vipin, Varre Swamy, Prabhakar, Sagar, Kshirodra ji, Rangarajan, Shibin, Indrapal, Pravin ji, Priyanka ji, Leena ji, Venkannababu, Sarabjot ji, Preeti, Shrikant ji, Sandeep, Prajitha ji, Ganesh ji, Harsha, Venkatesh, Goudappa ji, Brijesh ji, Shekhar ji, Nagesh ji, Manoj ji, Garima, Vinod, Sulfur, Shivakumar, Amarnath, Subramanian, Vinita, Santosh ji, Kashyap, Veer, Vidyand and Rajith** for their support and advice.*

*I would like to especially thank **Sandipan** for supporting me in my hard time. Also I would like to thank **Siba, Santigopal, Bipul, Tapas, Tamal, Subhrasis, Pranab, Manzoor, Indradweep, Abhijit, Basudeb, Pranoy, Rahul, Asish, Arghya, Sandipan, Sutanu, Somsuvra, Anirban, Anagh, Meena, Moumita, Gargi, Milan, Sanjukta, Bittu, Debu, Prasenjit, Sourik, Jagannath, Akash, Pankaj and Narugopal** as my Pune stay would have been boring without you people. I am thankful to for their support and advice.*

*I would also like to thanks my previous mentors **Prof. Debabrata Maiti (IITB)** and **Prof. Suvarn S. Kulkarni (IITB)** for giving me the opportunity to work under their supervision during my postgraduate studying in IIT Bombay. Also I would like to express my sincere gratitude to my teachers **Sk. Year Ali, Chandrasekhar Sasmal, Anadiranjan Dutta, Srikanta Hasda, Animesh Patra, Kanak Kar, Manik Babu, Balai Dhara, Madhusudan Samanta, Uttam Maity, Anupam Tripathi, Mrinalkanti, Sankar Mishra, Late Prof. Arunava Sen, Prof. Chandrakanta Bandyopadhyay, Prof. Subhabrata Banerjee, Prof. Kalipada Giri, Prof. Atanu Bhattacharya, Prof. Shouvik Chattopadhyay, Prof. Dhruba***

*Prosad Chatterjee, Prof. Anindya Dutta (IITB), and Prof. Sambasivarao Kotha (IITB) for their help, suggestions and encouragement in different part of my life. Also I want to thank to all my seniors and friends from IIT, Bombay specially **Someswara Rao, Vikram ji, Madhu anna, Sanjoy da, Mrityunjoy da, Atanu da, Arghya da, Tuhin da, Sohom da, Sujoy da, Tamal da, Srimanta da, Manas da, Sayan, Saptarshi, Uttam, Sukdev, Sourav, Jyoti prasad, Narashima, Ananda Rao, Archana di, Santanu, Ravikumar, Chinnam anna and Rajesh anna.***

*I thank the entire members of my family for their constant care and wishes. I would like to thank my uncles **Rajib kaku, Bhabani kaku, Utpal kaku, Alok kaku, Tarapada kaku, Prasanta kaku and Subhendu kaku** for their support. Last but not least, I would like to pay high regards to my father **Mrityunjoy Bhadra**, mother **Shantilata Bhadra**, my brother (**Paritosh**) and sisters (**Nandita, Sambita, Sanchita, Rakhi**) for their constant encouragement and inspiration throughout my research work and lifting me uphill this phase of life. Dedicating this thesis to them is a minor recognition for their valuable support and encouragement.*

Mohitosh Bhadra

PREFACE

Design and synthesis of heterogeneous catalyst for organic transformation reactions are very challenging. The key research objective of the chemical and pharmaceutical industries is to convert homogeneous catalytic reaction centers into heterogeneous versions through the attachment of catalytic sites on stable porous supports. Heterogeneous catalysts offer many advantages, over the homogeneous ones which include high recyclability, easy recovery from the reaction mixture and their use in continuous flow processes. Over the past decades, different porous materials have been developed like Porous Carbon, Zeolite, Porous Silica and MOFs and have been utilized for different applications. But applications of these porous materials as heterogeneous catalyst are limited although Zeolite is being used extensively in petroleum industries for hydrocarbon cracking process. In mesoporous silica, the surface silanol groups hamper the catalytic process. Although MOFs possess high surface area, tunable pore size, adjustable skeletons but the potential drawback of the utilizing of MOFs as solid catalysts is that MOFs are constructed by dative (coordinate) covalent bonds, which are usually only of moderate strength and result in a certain degree of instability that can be detrimental for catalytic applications. Therefore chemically robust porous crystalline materials constructed from covalent bonds have shown significant interest for catalytic applications. Porous Organic Polymers (POPs) could be a promising candidate owing to its high chemical stability which arises from the strong covalent bonds. But POPs consist of non-uniform pores with disordered random structure. Thus, their behaviors in catalysis in terms of selectivity and reaction yield are often difficult to predict. Thus there is an urgent need for developing new crystalline heterogeneous catalyst having well defined ordered pore channels.

In this regards, crystalline Covalent Organic Frameworks (COFs), constructed by light elements through a covalent bond, exhibit large surface areas and uniform porous structures with tunable pore size will be a promising candidate for this heterogeneous catalytic application. As the nitrogen-rich polymers are used as a suitable support to stabilize metal nanoparticles or in photocatalysis, therefore the presence of more heteroatom, like nitrogen in Covalent Organic Frameworks (COFs), can improve the catalytic activity by chelating the metal catalyst or stabilizing the catalytic active metal nanoparticles in the frameworks.

Although there is a significant research has been done to synthesize Covalent Organic Frameworks (COFs) but applied as a heterogeneous catalyst is not explored so far due to its poor stability especially in the field of catalysis. But the problem is overcome by simply introducing an irreversible keto-enol tautomerization within the COF skeleton. Therefore synthesis of Chemically Stable Nitrogenous Porous Crystalline Covalent Organic Frameworks is still demanding and challenging. The synthesis of this material can open up a new area in heterogeneous catalysis.

Chapter 2 we have discussed that bipyridine moiety is a very important chelating tool for different metal ions and those are used in homogeneous catalysis for different organic transformation. Therefore we have synthesized bipyridine based covalent organic frameworks by choosing bipyridine diamine (Bpy) and triformylphloroglucinol (Tp) as precursor using solvothermal and mechanochemical way. The solvothermally synthesized COF (TpBpy-ST) is found highly crystalline compared to mechanochemical one (TpBpy-MC) but both the COFs are stable in acid (9N HCl, 3M H₃PO₄), water and base (3N NaOH) due to the irreversible enol to keto tautomerized structure. The surface area of the activated COFs calculated using the Brunauer-Emmett-Teller model is found to be 1746 and 293 m²g⁻¹ respectively. TpBpy-ST shows good CO₂ uptake 165 cc/g compared to TpBpy-MC, 95 cc/g at 0 °C 1 atm pressure whereas H₂ uptake for TpBpy-ST is also higher 150 cc/g with respect to TpBpy-MC 115 cc/g at 77 K 1 atm pressure. Also, we have found that TpBpy-ST adsorbs more water 450 cc/g compared to TpBpy-MC 260 cc/g.

Chapter 3 we have developed a novel synthetic strategy by choosing predesigned metal anchored building block for *in situ* generation of metal (Pd) nanoparticles in the stable, porous and crystalline covalent organic framework (COF), without using conventional reducing agents. *In situ* generation of Pd nanoparticles in COF skeleton is explicitly confirmed from PXRD, XPS, TEM images, and ¹⁵N NMR spectral analysis. This hybrid material is found to be an excellent reusable heterogeneous catalyst for the synthesis of biologically and pharmaceutically important 2-substituted benzofurans from 2-bromophenols and terminal alkynes *via* tandem process with TON up to 1101. The heterogeneity of the catalytic process is unambiguously verified by mercury poisoning experiment and leaching test. This hybrid material shows superior catalytic performance compared to commercially available homogeneous as well as heterogeneous Pd catalysts.

Chapter 4 we have discussed the difficulty of synthesizing crystalline covalent organic frameworks from presynthesized catalytically active ligand keeping the catalytically active site intact during COF formation. Herein we have synthesized palladium chloride (PdCl₂) coordinated bipyridine based covalent organic framework *via* pre-synthesis method by reacting with bipyridine Diamine - palladium chloride (Bpy-PdCl₂) and triformylphloroglucinol (Tp) through Schiff base reaction. The +2 oxidation state of palladium was confirmed from XPS analysis. The surface area of the activated COF is found to be 300 m²g⁻¹ calculated using the Brunauer-Emmett-Teller model. This material was successfully utilized for chelation assisted direct C(sp²)-H bond hydroxylation reaction of 2-phenyl pyridine with good yield. The heterogeneity of the catalytic process is verified by mercury poisoning experiment and leaching test.

In chapter 5, we have discussed that visible light mediated photocatalytic organic transformation has drawn significant attention compared to thermally promoted reactions due to clean, safe, infinitely available easy to handle energy source. However, most photocatalytic bond forming reaction requires the involvement of precious metals or organic dyes which face the drawbacks of high cost, a problem associated with recyclability or both. Therefore metal free heterogeneous catalysis can address the above-mentioned issues. Therefore we have synthesized metal free photocatalytic covalent organic frameworks by reacting with melamine, triformylphloroglucinol (Tp) and trimethoxybenzenetricarbaldehyde (TpOMe) respectively. The synthesized COFs acts as a metal-free semiconductor with an optical band gap in the range 2.6 to 2.7 eV and successfully utilized for photocatalytic hydrogen evolution from the water. Whereas the COF synthesized from melamine and triformylphloroglucinol (Tp) shows better catalytic *trans* to *cis* isomerization of stilbene derivatives in presence of blue LED compared to other one.

Finally, Chapter 6 will describe the conclusion of the overall work presented in this thesis. The future direction based on the understanding of this thesis work also presented in the last section of this chapter.

Mohitosh Bhadra

CONTENTS	PAGE
Certificate	iii
Statement	iv
Acknowledgement	v
Preface	viii

CHAPTER 1

Introduction to Different Porous Heterogeneous Catalysts and Covalent Organic Frameworks

	1-33
1.1	General Background of the Different Porous Heterogeneous Materials 2
1.2	Covalent Organic Frameworks 5
1.3	Types of Reversible Reaction Used the Synthesis of COFs 9
	1.3.1 Boronic Acid Trimerisation Reaction 9
	1.3.2 Boronate Ester Formation Reaction 10
	1.3.3 Schiff Base Reaction 11
	1.3.4 Hydrazone formation 11
	1.3.5 Trimerization of Nitriles 11
1.4	Different Methods COF Synthesis 12
	1.4.1 Solvothermal Synthesis 12
	1.4.2 Ionothermal synthesis 13
	1.4.3 Microwave synthesis 13
	1.4.4 Mechanochemical Synthesis 14
	1.4.5 Synthesis of Mono Layers on Surface 14
1.5	Applications of COFs 15
	1.5.1 Gas storage application 16
	1.5.2 Photoelectric and Semi Conduction Applications 18
	1.5.3 Energy storage 18
	1.5.4 Separation 19

1.5.5	Proton conduction	19
1.5.6	Drug storage and Delivery	20
1.6	Chemical Stability of COFs	20
1.7	Different Methods for Covalent Organic Frameworks Functionalization	22
1.7.1	Post Synthetic Strategy	22
1.7.2	Pre Synthetic Strategy	23
1.8	Importance of Nitrogen-Rich Porous Material	23
1.9	Heterogeneous Catalysis by Covalent Organic Frameworks	24
1.9.1	Metal Loaded Catalysis	25
1.9.1.a	Metal Coordinated COF:	22
1.9.1.b	Metal Nanoparticles Loaded COF	26
1.9.2	Organocatalysis	27
1.9.3	Photocatalysis	30
1.9.4	Electrocatalysis	32

CHAPTER 2

Synthesis and Gas Adsorption Properties of a Stable Crystalline and Ultraporous Covalent Organic Framework with Bipyridyl Backbone **34-53**

2.1	Introduction	35
2.1.1	Importance of Nitrogen-Rich Porous Material	35
2.1.2	Importance of 2,2'-Bipyridine Ligand	37
2.1.3.	The Drawbacks of Solvothermal Method for Synthesizing Covalent Organic Frameworks	38
2.1.4	Statement of the Problem	39
2.2	Synthesis and Characterization	39
2.2.1	TpBpy COF Synthesis via Solvothermal Process	39
2.2.2	TpBpy COF Synthesis via Solvent-Assisted Mechanochemical Process	40
2.2.3	Synthesis of 2,2'-bipyridine-5,5'-diamine (Bpy)	41

2.2.4	Synthesis of 5-amino-2,2'-bipyridine	42
2.2.5	Monomer (2E,4E,6E)-2,4,6-tris((2,2'-bipyridin]-5-yl-amino)methylene)cyclohex-ane-1,3,5-trione Synthesis	42
2.2.6	Structural Simulation and Characterization	43
2.2.7	Chemical Characterization	44
2.2.8	Chemical Stability Investigation	49
2.3	Conclusions	52
2.4	General Methods for Characterization	53

CHAPTER 3

Pre-designed Metal Anchored Building Block for *In Situ* Generation of Pd Nanoparticles in Porous Covalent Organic Framework for Heterogeneous Tandem Catalysis 54-89

3.1	Introduction	55
3.1.1	Different Approaches for Conversion of Homogeneous Catalyst into Heterogeneous Version	55
3.1.2	Tandem Catalysis	57
3.1.3	Importance of 2-Substituted Benzofurans Synthesis	57
3.1.4	Synthesis of Pd Nanoparticles in Covalent Organic Framework via ex situ Process and the Disadvantages	58
3.2	Statement of the Problem	59
3.3	Synthesis and Characterization	59
3.3.1	Pd@TpBpy COF Synthesis	59
3.3.2	Structural simulation and characterization	60
3.3.3	Chemical characterization	62
3.3.4	Tandem Catalysis by Pd@TpBpy Catalyst for Co-catalyst Free Benzofuran Synthesis	66
3.3.5	Heterogeneity Test	69
3.3.5.1	Mercury Poisoning Experiment	69
3.3.5.2	Pd Leaching Test	70

3.3.5.3	Catalyst Recyclability Experiment	70
3.4	Conclusions	71
3.5	Experimental procedures	71
3.5.1	Synthesis of 2,2'-bipyridine-5,5'-diamine palladium chloride (Bpy-PdCl ₂)	71
3.5.2	X-Ray Investigation of Single Crystals of Bpy-PdCl ₂	74
3.5.3	Synthesis of Pd@TpBpy	75
3.5.4	Structure Modelling and Powder X-Ray Diffraction Analysis	76
3.5.5	FT-IR Spectra and Energy Dispersive X-ray Analysis (EDX)	77
3.5.6	General Procedure for the Tandem Catalysis	77
3.5.7	Optimization Details for Tandem Catalysis	78
3.5.8	Characteristic Data of Synthesized Compounds	80
3.5.9	X-Ray Investigation of 2-Phenylbenzofuran-5-Carbaldehyde (3b)	86
3.5.10	Catalyst Recyclability Experiment	87
3.5.11	Large-scale Synthesis (TON and TOF)	87
3.5.12	Characterization of Pd@TpBpy after Catalysis	88
3.5.13	General methods for characterization	88

CHAPTER 4

Presynthesized Metal Coordinated Stable Covalent Organic Framework as Heterogeneous Catalyst for Chelation Assisted Direct C(sp²)-H Bond Hydroxylation Reaction.

90-111

4.1	Introduction	91
4.1.1	Mechanism of Pd(II) complex During Catalytical Process	92
4.1.2	Importance of Chelation Assisted Direct C(sp ²)-H Bond Hydroxylation Reaction	93
4.1.3	Different Methods and their Problems for Covalent Organic Frameworks Functionalization	94
4.1.3.1	Post Synthetic Strategy	94

4.1.3.2	Pre Synthetic Strategy	95
4.2	Statement of the Problem	95
4.3	Synthesis and Characterization	96
4.3.1	TpBpy-PdCl ₂ COF Synthesis	96
4.3.2	Structural simulation and characterization	97
4.3.3	Chemical characterization	99
4.3.4	Optimization Details for Chelation Assisted Direct C(sp ²)-H Bond Hydroxylation Reaction	102
4.3.5	Heterogeneity Test	107
4.3.5.1	Mercury Poisoning Experiment	107
4.4	Conclusions	107
4.5	Experimental procedures	108
4.5.1	Synthesis of TpBpy-PdCl ₂	108
4.5.2	Synthesis of 2,2'-bipyridine-5,5'-diamine palladium chloride (Bpy-PdCl ₂)	109
4.5.3	General Procedure for selective hydroxylation of 2-phenylpyridine via direct C(sp ²)-H bond activation	109
4.5.4	Characteristic Data of Synthesized Compounds	110
4.5.5	Characterization of TpBpy-PdCl ₂ after Catalysis	110
4.5.6	General methods for characterization	110

CHAPTER 5

Photocatalytic Covalent Organic Frameworks: Metal Free Photocatalyst for Trans to Cis Isomerization of Stilbenes and Hydrogen Evolution **112-142**

5.1	Introduction	113
5.1.1	Water Splitting	115
5.1.2	Importance of Trans (E) to Cis (Z) Isomerization Reaction and the Problems	117
5.2	Synthesis and Characterization	118
5.2.1	TpTt COF Synthesis	118

5.2.2	Tp-OMeTt COF Synthesis	119
5.2.3	Structural Simulation and Characterization	120
5.2.4	Chemical Characterization	124
5.2.5	Photocatalytic trans to cis Isomerization Reaction	129
5.2.6	Catalyst Recyclability Experiment	133
5.2.7	Photocatalytic Hydrogen Evolution Reaction	134
5.3	Conclusions	134
5.4	Experimental procedures	135
5.4.1	Synthesis of 2,4,6-trimethoxybenzene-1,3,5-tricarbaldehyde (Tp-OMe)	135
5.4.2	General Procedure for Photocatalytic trans to cis Isomerization	137
5.4.3	General Procedure for Photocatalytic Hydrogen Evolution Reaction	137
5.4.4	Optimization Details for trans to cis Isomerization Reaction	138
5.4.5	Characteristic Data of Synthesized Compounds	139
5.4.6	General Methods for Characterization	141
CHAPTER 6		
Conclusions of All Chapters and Future Directive		143-146
6.1	Conclusions	143
6.2	Future directives	146
REFERENCES		147-169
About the Author		170
List of Publications, Conferences and Presentations		171

LIST OF FIGURES

Figure		Page
1.1	<i>(a) Classifications of porous materials based on pore diameter. (b) Different porous heterogeneous catalysts. Images are taken from Google.</i>	2
1.2	<i>Classifications of porous organic frameworks. Images are taken from Google.</i>	4
1.3	<i>Different linker used for COF synthesis. (a) Boronic acid-based building blocks for boron-containing COFs. (b) Different catechol-based linkers for another type of boron-based COFs. (c,d) Aldehyde and amine building units used for imine based COF synthesis.</i>	6
1.4	<i>Schematic representation of different organic symmetric combination used in COF framework construction.</i>	7
1.5	<i>Schematic representation of a) and c) COF formation by the reversible reaction, b) PAF formation by the irreversible reaction.</i>	8
1.6	<i>Type of reversible organic reactions used for COFs formation.</i>	10
1.7	<i>Different synthetic methods used for the synthesis of COFs. Images are taken from Google.</i>	12
1.8	<i>(a) Synthesis of COF-5 on the surface of few-layer graphene. (b) & (c) STM images of COF-1 and (d) STM images of COF 10 on HOPG surface. Figures are reproduced with permission from Science.</i>	15
1.9	<i>Various applications of COFs such as drug/bio molecules storage, proton conduction, gas storage, photo-conducting materials, energy storage and gas separation.</i>	16
1.10	<i>Comparison of excess hydrogen uptake of different COFs (a) at 1 bar and (b) high pressure (open symbols represent experimental results, filled symbols simulated results). (c) Methane adsorption isotherms of COFs at high pressure. (d) Carbon dioxide adsorption isotherms of COFs at high pressure. Figures are reproduced with permission from ACS publications.</i>	17
1.11	<i>Schematic representation of (a) as-synthesized COF (b) partial hydrolysis and release of monomers into solution upon submersion in water (c)</i>	20

completely hydrolyzed COF. Figures are reproduced with permission from ACS publications.

- 1.12** *Synthesis scheme for chemically stable COFs via Schiff base condensation reaction with the combination of reversible and irreversible reaction.* 21
- 1.13** *Schematic diagram of COF functionalization.* 22
- 1.14** *Schematic diagram of COF catalysis.* 24
- 1.15** *Chemical and extended structures of COF-LZU1, Pd/COF-LZU1 and Suzuki–Miyaura coupling reaction. Figures are reproduced with permission from ACS publications.* 25
- 1.16** *Synthesis of Pd nanoparticles on TpTa-1 COF via ex-situ process and applied for Sonogashira and Heck coupling reactions. Figures are reproduced with permission from RSC publications.* 26
- 1.17** *(a), (b), (c), (d) Schematic representation of the strategy for preparing 3D microporous base-functionalized COFs and applied in size selective Knoevenagel condensation reaction. Figures are reproduced with permission from Willey VCH publications.* 27
- 1.18** *Schematic representation of chiral COFs synthesis and their asymmetric catalysis. Figures are reproduced with permission from ACS publications.* 28
- 1.19** *Schematic representation of preparing chiral COFs from chiral building unit for asymmetric aldol reaction. Figures are reproduced with permission from ACS publications.* 29
- 1.20** *Schematic representation of a tunable triphenylarene based COFs for photocatalytic hydrogen evolution. Figures are reproduced with permission from Nature publications.* 30
- 1.21** *Schematic representation of a CdS loaded COF for photocatalytic hydrogen evolution. Figures are reproduced with permission from Willey VCH publications.* 31
- 1.22** *Design and synthesis of metalloporphyrin-derived 2D covalent organic frameworks for electrocatalytically CO₂ reduction. Figures are reproduced with permission from Science.* 32

Sch. 2.1	<i>Different applications of the nitrogen-rich framework. Figures are taken from Google.</i>	36
Sch. 2.2	<i>Different 2,2'-bipyridine metal complexes are used for different catalytic applications.</i>	37
Sch. 2.3	<i>Schematic representation of solvothermal synthesis steps.</i>	38
2.1	<i>((a) Schematic representation of solvothermal (ST) and mechanochemical (MC) synthesis of TpBpy COF. (b) Comparison of the experimental PXRD patterns of TpBpy-MC (blue), TpBpy-ST (black) with the simulated eclipsed (red) and staggered (green). (c), (d) Space-filling AA eclipsed stacking models of TpBpy along a and c direction. (e) Space-filling staggered stacking models of TpBpy along c direction.</i>	40
2.2	<i>General synthetic scheme for the preparation of 2,2'-bipyridine-5,5'-diamine (Bpy).</i>	41
2.4	<i>General synthetic scheme for the preparation of monomer</i>	43
2.5	<i>(a) Comparison of the PXRD pattern of experimental TpBpy-ST (blue) and simulated (red) TpBpy-ST in eclipsed stacking mode. Difference plot is depicted in black line. Pawley refinement demonstrates good agreement between experimental and simulated eclipsed PXRD pattern (Rwp: 1.94%, Rp: 5.29%). (b) Comparison of PXRD pattern of experimental TpBpy-MC (blue) and simulated (red) TpBpy-MC in eclipsed stacking mode. Difference plot is depicted in black line. Pawley refinement demonstrates good agreement between experimental and simulated eclipsed PXRD pattern (Rwp: 5.05%, Rp: 8.81%)</i>	44
2.6	<i>(a) FTIR spectra of Bpy (brown), Tp (blue) and TpBpy-ST (black). (b) FTIR spectra of Monomer (blue), TpBpy-ST (black) and TpBpy-MC (red).</i>	45
2.7	<i>(a) Comparison of solid state ¹³C NMR spectra of Monomer (green) TpBpy-ST (red) and TpBpy-MC (black). (b) Comparison of N₂ adsorption isotherm of TpBpy-ST (red) and TpBpy-MC (blue).</i>	45
2.8	<i>Gas uptake properties of TpBpy-ST and TpBpy-MC. (a) CO₂ adsorption</i>	46

	<i>isotherm of TpBpy-ST (red) and TpBpy-MC (blue) at zero degree. (b) Water adsorption isotherm of TpBpy-ST. (c), (d) H_2 adsorption isotherm of TpBpy-ST (red) and TpBpy-MC (blue).</i>	
2.9	<i>(a), (b) Experimental pore size distributions of TpBpy-ST and TpBpy-MC respectively calculated using NLDFT model.</i>	47
2.10	<i>(a) TGA spectra of TpBpy-ST (red). (b) TGA spectra of TpBpy-MC (blue).</i>	47
2.11	<i>(a), (b), (c) SEM images and (d), (e), (f) TEM images of TpBpy-ST showing interwoven thread like morphology.</i>	48
2.12	<i>(a), (b), (c) SEM images and (d), (e), (f) TEM images of TpBpy-ST showing interwoven thread like morphology.</i>	48
2.13	<i>(a) FTIR spectra of TpBpy-ST as synthesized (black), after water treatment (red), acid treatment (blue) and base treatment (green). (b) FTIR spectra of TpBpy-MC as synthesized (black), after water treatment (red), acid treatment (blue) and base treatment (green).</i>	49
2.14	<i>(a) Comparison of PXRD pattern for TpBpy-ST as synthesized (black), after water treatment (blue), acid treatment (red) and base treatment (green). (b) Comparison of PXRD pattern for TpBpy-MC as synthesized (black), after water treatment (blue), acid treatment (red) and base treatment (green).</i>	50
2.15	<i>(a) Comparison of N_2 adsorption isotherm of TpBpy-ST as synthesized (red), after water treatment (orange), acid treatment (green) and base treatment (brown). (b) Comparison of N_2 adsorption isotherm of TpBpy-MC as synthesized (red), after water treatment (orange), acid treatment (green) and base treatment (brown).</i>	50
2.16	<i>(a) Stability of different tautomeric forms in (a) mono substituted <i>N</i>-Salicylidene-anilines and (b) tri substituted <i>N</i>-Salicylideneanilines</i>	51
Sch. 3.1	<i>a),b),c) are reported approaches are used to convert a homogeneous catalyst into the reusable heterogeneous version.</i>	56
Sch. 3.2	<i>Schematic representation of tandem catalysis.</i>	57
Sch. 3.3	<i>Selected biologically active benzofuran natural products.</i>	57

Sch. 3.4	<i>Synthesis of Pd nanoparticles on TpTa-1 COF via ex-situ process.</i>	58
Sch. 3.5	<i>Synthesis of Pd nanoparticles on TpBpy COF via in situ process.</i>	59
3.1	<i>(a) Synthesis details of the in situ generation of highly dispersed Pd nanoparticles in the TpBpy skeleton. The size of Pd nanoparticles and the COF pore organization is not exactly based on a scale to scale. (b) Comparison of PXRD patterns of simulated TpBpy (black) with experimental TpBpy (blue), Pd nanoparticles (cyan) and experimental Pd@TpBpy (red).</i>	60
3.2	<i>Characterization details of Pd@TpBpy and TpBpy. (a) FTIR spectra of TpBpy (blue) and Pd@TpBpy (red). (b) Comparison of solid state ¹³C NMR spectra of Bpy-PdCl₂ (black), TpBpy (blue) and Pd@TpBpy (red). (c) Comparison of solid-state ¹⁵N NMR spectra of Bpy-PdCl₂ (black), TpBpy (blue) and Pd@TpBpy (red). (d) TGA spectra of Pd@TpBpy (red) and TpBpy (blue).</i>	62
3.3	<i>(a) N₂ adsorption isotherms of Pd@TpBpy (red) and TpBpy (blue). (b) XPS spectra of Pd in Pd@TpBpy (black) and Bpy-PdCl₂ (red). Experimental pore size distributions for (c) Pd@TpBpy, (d) TpBpy calculated using the non-local density functional theory (NLDFE) model.</i>	63
3.4	<i>Characterization details of Pd@TpBpy. (a, b) SEM images of Pd@TpBpy showing flake-like morphology. (c, d) TEM images of Pd@TpBpy showing a uniform distribution of Pd nanoparticles. (e, f) TEM images of Pd@TpBpy showing the lattice fringes of Pd nanoparticles in Pd@TpBpy. (g) HAADF-STEM image of Pd@TpBpy. (h) SAED pattern of Pd@TpBpy before catalysis. (i) Size distribution histogram of Pd nanoparticles in Pd@TpBpy.</i>	64
3.5	<i>Evaluation of the substrate scope.^{a,b}. ^aAll the reaction were conducted with 0.5 mmol of 2-bromophenols (1 equiv), 0.6 mmol of alkynes (1.2 equiv), 0.6 mol% of Pd@TpBpy catalyst, K₂CO₃ (0.5 equiv) in DMF. ^bIsolated yields. ^cUsing 5 mmol of 3-bromo-4-hydroxybenzotrile. ^dBased on GC analysis.</i>	67
3.6	<i>Probable catalytic mechanism of the tandem process</i>	68
3.7	<i>Recyclability test of Pd@TpBpy catalyst used for tandem catalysis. Yields</i>	70

are calculated by GC peak integration using *m*-Xylene as an internal standard.

3.8	General synthetic scheme for the preparation of 2,2'-bipyridine-5,5'-diamine palladium chloride (Bpy-PdCl₂).	72
3.9	¹ H NMR spectrum (in DMSO- <i>d</i> ₆) of 2,2'-bipyridine-5,5'-diamine palladium chloride (Bpy-PdCl₂).	73
3.10	¹³ C NMR spectrum (in DMSO- <i>d</i> ₆) of 2,2'-bipyridine-5,5'-diamine palladium chloride (Bpy-PdCl₂).	73
3.11	(a) Single Crystal X-ray diffraction structure of the reference compound Bpy-PdCl₂ . In the ORTEP (with 50% probability level); Carbon (light gray), Nitrogen (blue), Palladium (orange), Chloride (green) and Hydrogen (white) have been shown. (b) Crystal packing along <i>c</i> axis.	75
3.12	PXRD comparison between as-synthesized (red) and simulated (black) pattern of 2,2'-bipyridine-5,5'-diamine-palladium chloride (Bpy-PdCl₂).	75
3.13	(a) Unit cell and (b) Eclipsed crystal lattice packing of cis TpBpy .	76
3.14	(a) FT-IR spectra of 2,2'-bipyridine-5,5'-diamine palladium chloride (Bpy-PdCl₂) (blue), 1,3,5-triformylphloroglucinol (Tp) (red) and Pd@TpBpy (pink). (b) Energy dispersive x-ray analysis of Pd@TpBpy showing the presence of C, N, O, Cl and Pd elements.	77
3.15	Single Crystal X-ray diffraction structure of 2-phenylbenzofuran-5-carbaldehyde (3b). In the ORTEP (with 50% probability level); Carbon (light gray), Oxygen (red), and Hydrogen (white) have been shown.	87
3.16	(a), (b) are the SEM images; (c), (d) are the TEM images of Pd@TpBpy after catalysis.	88
Sch. 4.1	Schematic representation of the catalytic mechanism of Pd (II) complex. a) Cycle-I: Pd (II) / Pd (0) reductive cycle, b) Cycle-II: Pd (II) / Pd (IV) oxidative cycle.	92
Sch. 4.2	Schematic representation of the synthesis of 2-(2-pyridyl)phenol from 2-phenylpyridine.	93
Sch. 4.3	Schematic diagram of COF functionalization.	94

Sch. 4.4	<i>Chemical and extended structures of COF-LZU1, Pd/COF-LZU1 and Suzuki–Miyaura coupling reaction. Figures are reproduced with permission from ACS publications.</i>	95
4.1	<i>(a) Synthesis of the TpBpy-PdCl₂ using the pre-synthetic method. (b, c) Space-filling models of the AA eclipsed stacking model along c and a axis direction. (d) Comparison of the experimental PXRD patterns of TpBpy-PdCl₂ (black) with the simulated (blue) simulated after Pawley refinement (red), and difference plot (cyan).</i>	97
4.2	<i>(a) Comparison of the PXRD pattern of experimental (crossed) and simulated (blue) TpBpy-PdCl₂ in eclipsed stacking mode. Difference plot is depicted in black line. Pawley refinement demonstrates good agreement between experimental and simulated eclipsed PXRD pattern (Rwp: 7.66%, Rp: 5.37%). (b) Unit cell and (c) eclipsed crystal lattice packing of TpBpy-PdCl₂.</i>	98
4.3	<i>(a) FTIR spectra of Bpy-PdCl₂ (blue), Tp (red) and TpBpy-PdCl₂ (pink). (b) Comparison of solid state ¹³C NMR spectra of Bpy-PdCl₂ (red) and TpBpy-PdCl₂ (pink).</i>	99
4.4	<i>(a) N₂ adsorption isotherm of TpBpy-PdCl₂. (b) Experimental pore size distributions of TpBpy-PdCl₂ calculated using the N₂ at 77 K on carbon (cylindr./sphere pores, QSDFT adsorption branch) model. (c) CO₂ adsorption isotherm, (d) Hydrogen adsorption isotherm of TpBpy-PdCl₂.</i>	100
4.5	<i>(a) XPS spectra of Pd (II) in Bpy-PdCl₂ (red) and TpBpy-PdCl₂ (pink). (b) TGA spectra of TpBpy-PdCl₂.</i>	101
4.6	<i>Characterization details of TpBpy-PdCl₂. (a, b, c) SEM images and (d, e, f) TEM images of TpBpy-PdCl₂ showing fibrillar morphology.</i>	102
4.7	<i>General synthetic scheme for the preparation of 2,2'-bipyridine-5,5'-diamine palladium chloride (Bpy-PdCl₂).</i>	109
4.8	<i>(a), (b) are the SEM images; (c), (d) are the TEM images of TpBpy-PdCl₂ after catalysis.</i>	110
Sch. 5.1	<i>Chemical structure of some common photoredox catalysts.</i>	113

Sch. 5.2	<i>Schematic representation of photocatalysis and the description of possible mechanisms.</i>	114
Sch. 5.3	<i>(a) Mechanism of triplet-triplet energy transfer (TTET) from photocatalyst to the acceptor. (b) Photoredox catalysis with visible light: reductive and oxidative quenching cycle. PC = photocatalyst, RQ = reductive quencher, OQ = oxidative quencher, A = electron acceptor, D = electron donor.</i>	115
Sch. 5.4	<i>Band gap energies and band position of different semiconductors in relation with the redox potential of water splitting. Figures are reproduced with permission from ACS publications.</i>	116
Sch. 5.5	<i>Synthetic scheme for (a) graphitic carbon nitride (g-C₃N₄) and (b) covalent triazine framework (CTF).</i>	117
5.1	<i>5.1: (a) Synthesis details of Tp-OMeTt (imine based COF) and TpTt (Ketoamine based COF).(b) Comparison of the experimental PXRD patterns of Tp-OMeTt (black) with the simulated (blue) simulated after Pawley refinement (red), and difference plot (green). (c) Comparison of the experimental PXRD patterns of TpTt (black) with the simulated (blue) simulated after Pawley refinement (red), and difference plot (green). (d),(e) Space-filling AA eclipsed stacking models of Tp-OMeTt and TpTt respectively along c direction.</i>	119
5.2	<i>(a) Comparison of PXRD pattern of experimental (crossed) and simulated (blue) Tp-OMeTt in eclipsed stacking mode. Difference plot is depicted in black line. Pawley refinement demonstrates good agreement between experimental and simulated eclipsed PXRD pattern (Rwp: 8.43%, Rp: 12.71%). (b) Unit cell and (c) eclipsed crystal lattice packing of Tp-OMeTt.</i>	121
5.3	<i>(a) Comparison of the PXRD pattern of experimental (crossed) and simulated (blue) TpTt in eclipsed stacking mode. Difference plot is depicted in black line. Pawley refinement demonstrates good agreement between experimental and simulated eclipsed PXRD pattern (Rwp: 8.19%, Rp: 4.74%). (b) Unit cell and (c) eclipsed crystal lattice packing of TpTt.</i>	121
5.4	<i>(a) FTIR spectra of Melamine (Tt) (blue), Tp-OMe (red) and Tp-OMeTt</i>	124

	<i>(pink). (b) FTIR spectra of Melamine (Tt) (blue), Tp (red) and TPTt (pink).</i>	
5.5	<i>(a) Comparison of solid state ¹³C NMR spectra of Melamine (blue) and Tp-OMeTt (pink). (b) Comparison of solid state ¹³C NMR spectra of Melamine (blue) and TpTt (pink).</i>	125
5.6	<i>(a), (c) N₂ adsorption isotherm of Tp-OMeTt and TpTt. (b), (d) Experimental pore size distributions of Tp-OMeTt and TpTt calculated using the N₂ at 77 K on carbon (slit/cylindr. Pores, NLDFT equilibrium) model.</i>	125
5.7	<i>(a), (b) H₂ adsorption isotherm of Tp-OMeTt and TpTt. (c), (d) CO₂ adsorption isotherm of Tp-OMeTt and TpTt.</i>	126
5.8	<i>(a) TGA spectra of Melamine (Tt) (blue), Tp-OMe (red) and Tp-OMeTt (pink). (b) TGA spectra of Melamine (Tt) (blue), Tp (red) and TPTt (pink).</i>	127
5.9	<i>(a), (b), (c) SEM images and (d), (e), (f) TEM images of Tp-OMeTt showing spherical morphology.</i>	127
5.10	<i>(a), (b), (c) SEM images and (d), (e), (f) TEM images of TpTt showing fibrillar morphology.</i>	128
5.11	<i>(a) Solid state UV-Vis diffuse reflectance spectra of Melamine (Tt) (blue), Tp-OMe (red) and TP-OMeTt (pink). (b) Solid state UV-Vis diffuse reflectance spectra of Melamine (Tt) (blue), Tp (red) and TPTt (pink).</i>	128
5.12	<i>Tauc plots. (a) The optical band gap of Tp-OMeTt. (b) The optical band gap of TpTt.</i>	129
5.13	<i>Evaluation of the substrate scope.^{a,b} ^aAll the reactions are conducted with 0.5 mmol of trans-stilbene (1 equiv), 4 mg TpTt catalyst, in 5 mL N,N-dimethylformamide at rt under blue LED for 18h. ^bIsolated yields. ^cBased on GC analysis (2h).</i>	131
5.14	<i>(a) Photocatalytic mechanism of TpTt COF during trans to cis isomerization process. (b) Light on off experiment study over time.</i>	132
5.15	<i>(a) Recyclability test of TpTt catalyst used in trans to cis isomerization reaction. Yields are calculated by GC peak integration using n-decane as an internal standard. (b) Photocatalytic hydrogen evolution experiments of</i>	133

TpTt under visible light irradiation ($\lambda \geq 395$ nm).

5.16	<i>5.16: General synthetic scheme for the preparation of 2,4,6-trimethoxybenzene-1,3,5-tricarbaldehyde (Tp-OMe).</i>	135
5.17	<i>¹H NMR spectrum of TpOMe.</i>	136
5.18	<i>¹³C NMR spectrum of TpOMe.</i>	136
6.1	<i>A synthetic scheme of TpPQ COF and utilization for photocatalytic C-F bond formation (Approach-1), Alcohol oxidation (Approach-2) and Phenazine formation (Approach-3).</i>	146

LIST OF TABLES

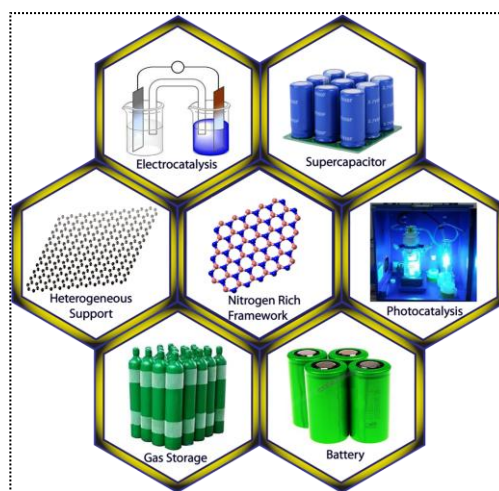
Table		Page
2.1	<i>Optimization table for the synthesis of TpBpy-MC at different milling frequency and time.</i>	41
2.2	<i>Fractional atomic coordinates for the unit cell of TpBpy-(ST/MC) (Eclipsed)</i>	44
3.1	<i>Fractional atomic coordinates for the unit cell of cis TpBpy (Eclipsed)</i>	61
3.2	<i>Optimization table for tandem catalysis</i>	66
3.3	<i>Structural information of Bpy-PdCl₂ single crystal</i>	74
3.4	<i>Optimization of Solvents</i>	78
3.5	<i>Optimization of Bases</i>	78
3.6	<i>Temperature Optimization</i>	79
3.7	<i>Optimization of Amount of Catalyst</i>	79
3.8	<i>Time Optimization</i>	79
3.9	<i>Structural information of 2-phenylbenzofuran-5-carbaldehyde (3b) single crystal</i>	86
4.1	<i>Fractional atomic coordinates for the unit cell of TpBpy-PdCl₂ (Eclipsed)</i>	98
4.2	<i>Optimization of Solvents</i>	103

4.3	<i>Optimization in presence of Acid and Water</i>	104
4.4	<i>Temperature Optimization</i>	104
4.5	<i>Optimization of Oxidant</i>	105
4.6	<i>Optimization of Amount of Oxidant</i>	105
4.7	<i>Optimization of Amount of Catalyst</i>	106
4.8	<i>Time Optimization</i>	106
5.1	<i>Fractional atomic coordinates for the unit cell of Tp-OMeTt (Eclipsed)</i>	121
5.2	<i>Fractional atomic coordinates for the unit cell of TpTt (Eclipsed)</i>	123
5.3	<i>Optimization table for trans to cis isomerization process</i>	130
5.4	<i>Optimization of Solvents</i>	138
5.5	<i>Optimization of Catalyst Amount</i>	138
5.6	<i>Optimization of Solvent Amount</i>	139
5.7	<i>Time Optimization</i>	139

CHAPTER 1

Introduction to Different Porous Heterogeneous Catalysts and Covalent Organic Frameworks

Abstract: *Converting homogeneous catalyst into heterogeneous is more important in the chemical and pharmaceutical industries. Heterogeneous catalysts are easily recoverable from the reaction mixture, have recyclability and reproducibility property, cost-effective and produce less waste compared to the homogeneous catalyst. Therefore significant research has been done on developing porous stable heterogeneous catalyst compare to an amorphous one. The uniform pores and the high surface area will allow the reactants to access the catalytically active sites and helps mass transfer process which will increase the TON of the catalyst. Many porous catalysts like Porous Carbon, Zeolite, Mesoporous silica and MOF have been developed and applied as heterogeneous catalysts. Recently another porous crystalline thermally stable lightweight material has been developed called Covalent Organic Frameworks (COFs). The uniform pore size with tenability and high surface area with long-range order make them suitable for gas uptake, separation, drug delivery, sensing, and energy storage purpose. But it can be used as a heterogeneous catalyst or as a stable support. The chemical stability of the material was the main drawback which limits its application as a heterogeneous catalyst. After the discovery of ketoenamine based thermally and chemically stable COFs, researchers have utilized COFs for heterogeneous catalysis. Nitrogen-rich materials are well known for photocatalysis, electrocatalysis and stabilizing metal nanoparticles. Therefore design and synthesis of nitrogen-rich porous covalent organic frameworks may open up a new domain of exciting research area in the field of heterogeneous catalysis.*



1.1 General Background of the Different Porous Heterogeneous Materials

Developing green, clean, atom-economy and cost-effective methods for synthesizing porous heterogeneous materials is the key research objective of the chemical and pharmaceutical industries. The homogeneous catalyst can be converted into heterogeneous by attaching the catalytically active sites on a stable support [1.1]. The advantages of using heterogeneous catalyst over homogeneous are easily recoverable from the reaction mixture, minimizes waste production, shows recyclability property and are used in continuous flow processes [1.2]. Porous materials have utilized for different applications because of their unique pore size and high surface area. Therefore both academia and industries have shown more attention for synthesizing new porous materials. Activated charcoal is a porous material has been used for water purification and removal of toxic gases from the air since ancient time. The smaller and uniform pores present in the charcoal are appropriate for separating small impurities through adsorption based interaction [1.3]. According to the International Union of Pure and Applied Chemistry (IUPAC), the porous materials are classified into three categories [1.4] 1) Microporous, 2) Mesoporous and 3) Macroporous materials depending on their pore size (Figure 1.1a). The porous materials having a pore size less than 2 nm are called Microporous material while the pore aperture lies in the range of 2-50 nm are called Mesoporous materials. The materials having a pore size in the range of 50-1000 nm are called Macroporous material. After porous carbon, many porous materials have been

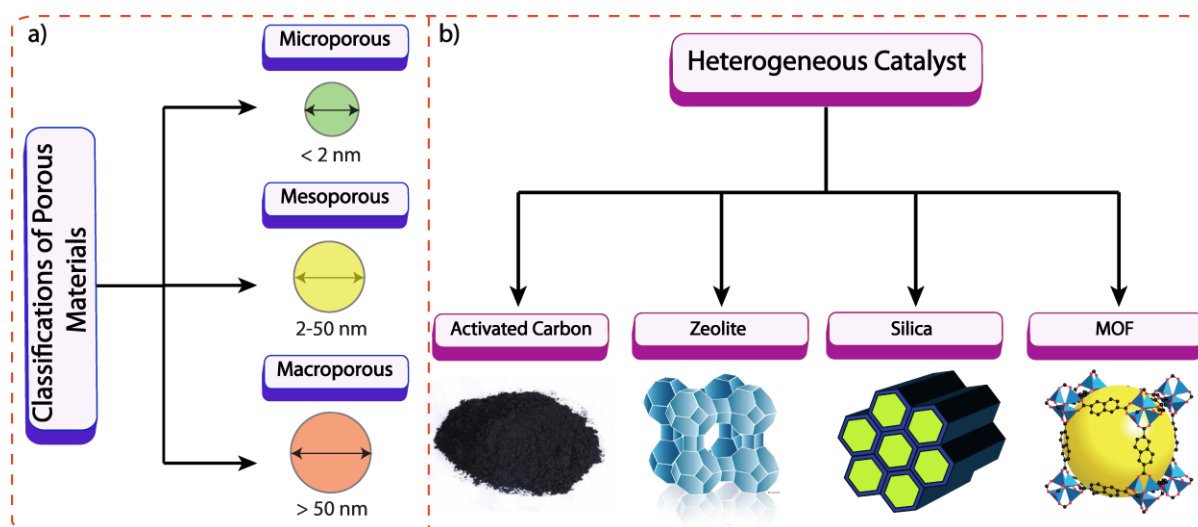


Figure 1.1: (a) Classifications of porous materials based on pore diameter. (b) Different porous heterogeneous catalysts. Images are taken from Google.

developed like Zeolite, mesoporous silica and Metal Organic Frameworks (Figure 1.1b). **Zeolites** are one kind of porous three dimensional materials are constructed by aluminosilicate where the tetrahedral aluminate (AlO_4) and silicates (SiO_4) are linked by terminal oxygen atoms [1.5]. This inorganic material is highly porous, has long-range periodicity, rigid and is chemically and thermally stable. Therefore it has been extensively used as a heterogeneous catalyst in industrial applications [1.6]. The material can be used in extreme catalytic condition even though no change in catalytic activity is observed which indicates the framework stability. Some of the Zeolites have been commercialized for industrial applications like Zeolite Y, ZSM-5 and Mordenite mainly in petroleum industries [1.6]. Although many Zeolites have been synthesized to date are belongs to the microporous region. The pore size of Zeolites is varying from 0.3 nm to 0.8 nm which is the major drawback of utilizing Zeolite as a heterogeneous catalyst. The small pore resists in the mass transfer process for bigger molecule during catalysis. Also, it consists of Al, O, and Si where the ratio of Si/Al is more than one but difficulties in functionalization of the framework due to the fulfillment of the coordination number of all the atoms limits its applications for different organic transformations in heterogeneous catalysis process. After several research scientists discover **porous silica** which is mesoporous in nature. The framework is constituted by strong Si-O bonds which make the framework stable and rigid in nature. The long-range periodicity, large pore volume, and tunable pore size make the material suitable as a heterogeneous catalyst. Therefore different porous silica MCM-48, FSM-16, SBA-15, and MCM-50 has been utilized for sensing, adsorption, and catalysis. Also, the mesoporous nature helps for mass transfer process during catalysis. But the strong interaction of surface silanol groups with catalytically active metal complexes hampers the catalytic process which cannot be resolved by surface modification also. Although the materials are heterogeneous in nature but the above factors limit their applications for the chemoselective process.

After several research Prof. Omar M. Yaghi and co-workers have introduced a new class of heterogeneous porous materials in 1998 is called **Metal Organic Frameworks (MOFs)** [1.7]. MOFs are inorganic-organic hybrid materials which are synthesized from different metal ions and organic linkers through coordination bonds. The long-range periodicity, high surface area, and tunable pore size make the material suitable for different applications like gas adsorption, sensing, separation, and energy storage purpose [1.8]. But

the application of MOFs as a heterogeneous catalyst is limited because the MOFs are unstable in acid, base and water medium. The dative/coordination bonds are not as stronger as covalent bonds [1.9]. Hence scientists have shown more interest for synthesizing heterogeneous catalyst constructed through covalent bonds [1.10].

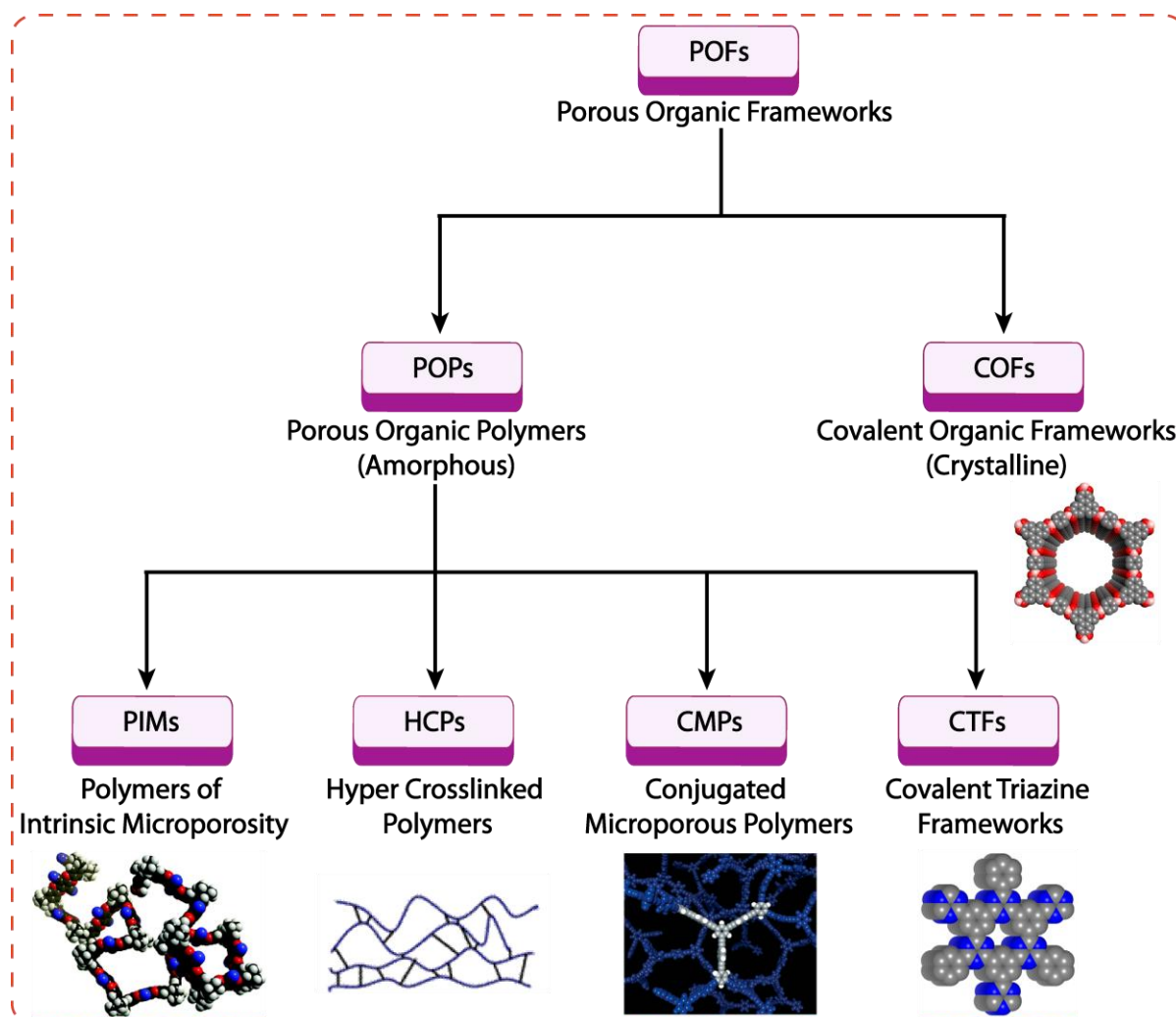


Figure 1.2: Classifications of porous organic frameworks. Images are taken from Google.

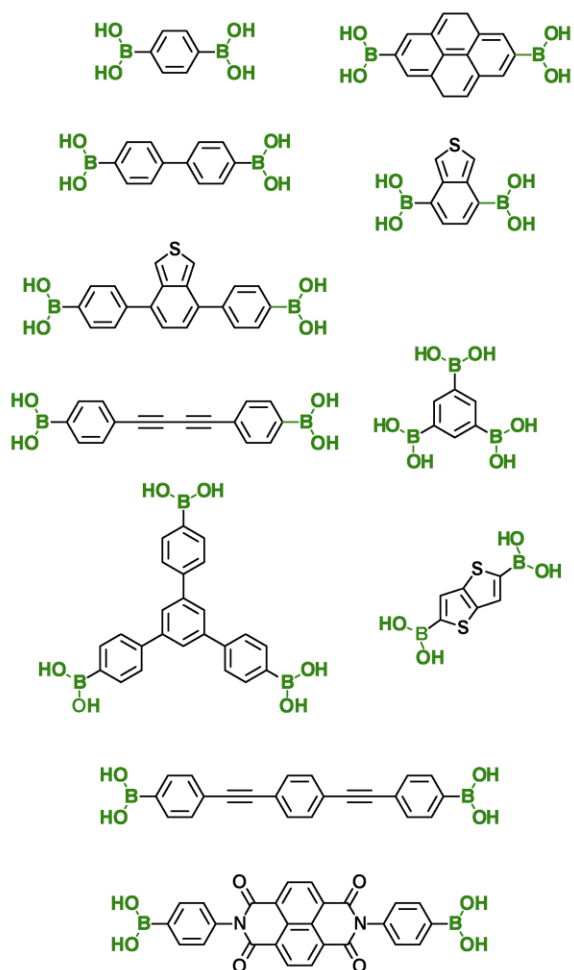
Porous organic frameworks (POFs) are new classes of porous material similar to MOFs offer several advantages in catalysis over MOFs. The covalent bonds are much less polar in nature than coordination bonds between metals and organic linkers. Porous organic frameworks (POFs) can be classified into two groups depending on the crystallinity of materials (Figure 1.2): 1) Porous Organic Polymers (POPs) which are amorphous and 2) Covalent Organic Frameworks (COFs) which are crystalline in nature [1.11]. Also, Porous Organic Polymers (POPs) can be sub classified into four categories; a) Polymers of Intrinsic

Microporosity (PIMs), b) Hyper-Cross-linked Polymers (HCPs), c) Conjugated Microporous Polymers (CMPs), and d) Covalent Triazine Frameworks (CTFs), are synthesized from numerous metal-catalyzed couplings, such as Yamamoto, oxidative couplings, Sonogashira-Hagihara, Friedel-Crafts, Suzuki-Miyaura, olefin metathesis, nitrile cyclotrimerization, terminal alkyne trimerization, and CuAAC click which are well established methods [1.12]. Although Porous Organic Polymers possess non-uniform pores but they are highly thermally and chemically stable due to the strong covalent bond formation. Therefore POPs are used for many real-life applications like catalysis, gas storage, and separation. Even though POPs are the easiest to make but they have non-uniform pores and are not crystalline in nature. Therefore it is very difficult to control their design and difficult to understand their behaviors in catalysis. Also, the uses of the stoichiometric hazardous metal catalyst during the synthesis of amorphous polymer make the process costly and inefficient because the removal of metal catalyst from the polymer is not an easy process even after using strong acidic condition also. But crystalline covalent organic frameworks (COFs) are one kind of porous organic frameworks (POFs) are made by organic linker having light elements, such as boron, oxygen, carbon, and silicon in periodic manner using metal free different reversible condensation reactions which show large surface area and uniform porous structures. The size and shapes of the pore can be tuned and can be functionalized into various functional groups by varying different building blocks. As the synthesized materials are not soluble in any solvent and thermally stable, therefore it can be used as a heterogeneous catalyst or as a support in heterogeneous catalysis. Furthermore, we will discuss the development of the synthetic strategy involved to improve the stability and specific functional groups incorporation into the covalent organic frameworks to make an ideal catalyst in any area and in any medium for heterogeneous catalysis.

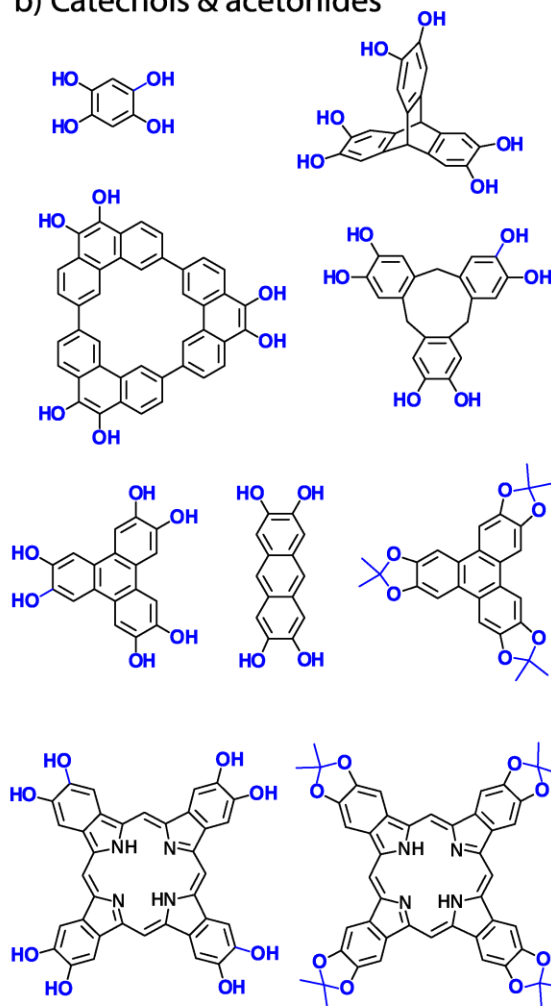
1.2 Covalent Organic Frameworks

Another new class of porous organic material is developed by Prof. Yaghi and co-workers termed as Covalent Organic Frameworks (COFs) [1.13]. The COFs are totally organic in nature and are constructed from different organic building blocks, unlike Zeolite and MOF. The major difference between COFs and Porous Organic Polymers (POPs) is that COFs are crystalline and having uniform pore size compared to POPs although both are formed *via* covalent bonds. Therefore COFs are thermodynamically and chemically more

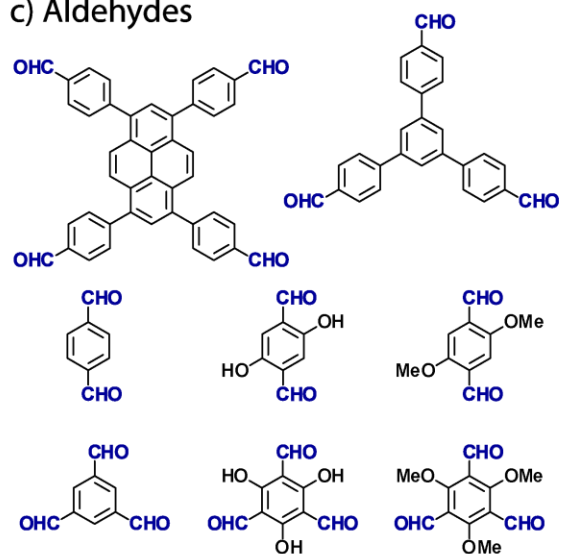
a) Boronic acids



b) Catechols & acetonides



c) Aldehydes



d) Amines

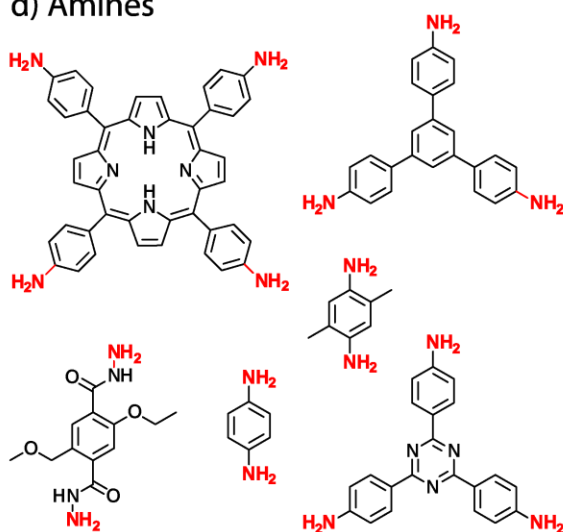


Figure 1.3: Different linker used for COF synthesis. (a) Boronic acid-based building blocks for boron-containing COFs. (b) Different catechol-based linkers for another type of boron-based COFs. (c,d) Aldehyde and amine building units used for imine based COF synthesis.

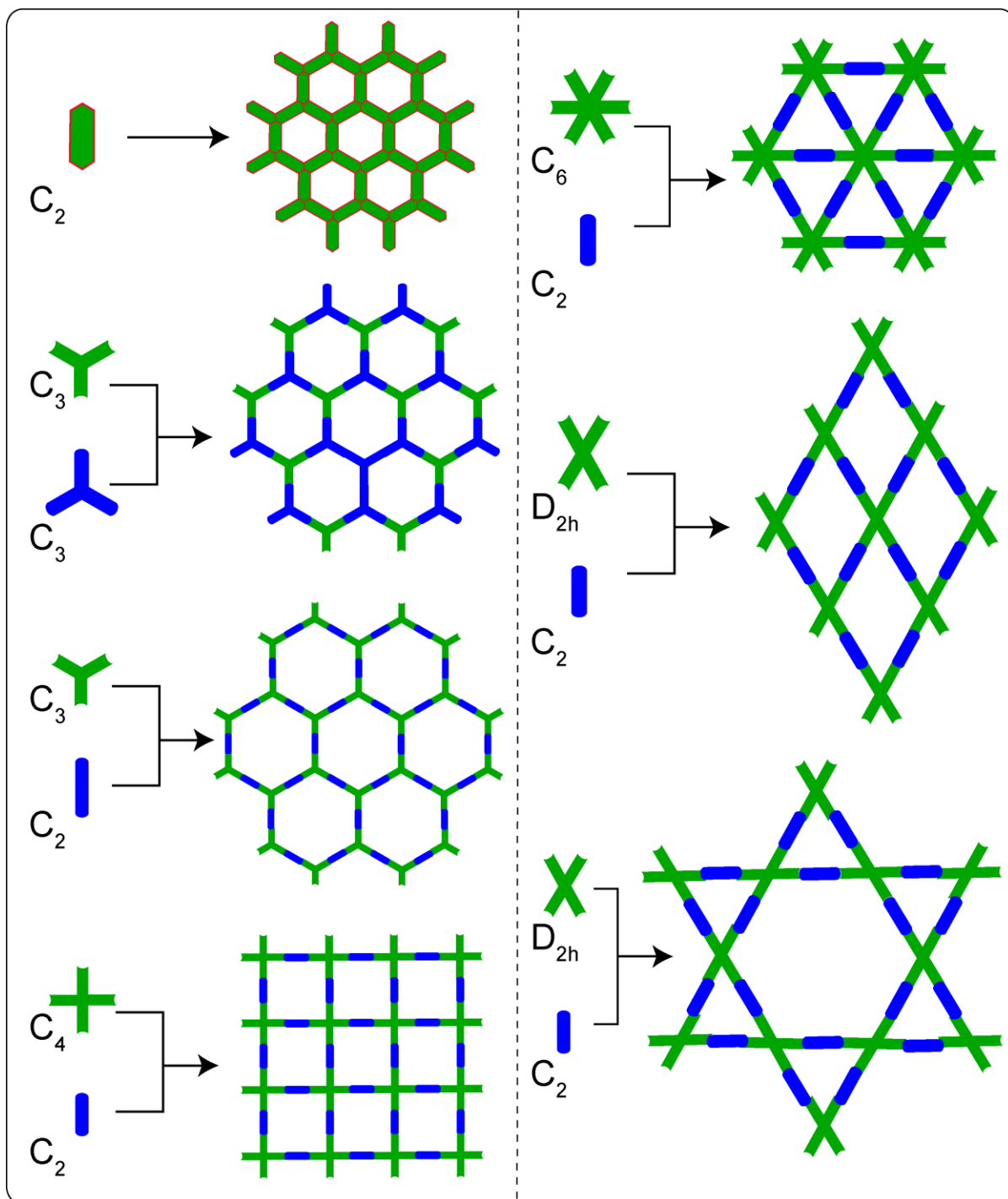


Figure 1.4: Schematic representation of different organic symmetric combination used in COF framework construction.

stable than MOFs. Generally, lightweight elements B, C, N, O, Si are used for COF formation. Hence the synthesized COFs become lightweight and show high surface area which makes the material suitable for gas storage purpose [1.14]. The different pore size and pore volume can be obtained by choosing different size building blocks with proper symmetry combination which will produce more crystalline material instead of amorphous polymer formation. Symmetry combinations of the organic building blocks play an important role for 2D and 3D crystalline COF formation (Figure 1.3). For synthesizing 2D COFs generally C_3+C_2 , C_3+C_3 , C_4+C_2 , C_4+C_4 , C_6+C_2 symmetry combinations are used [1.15]. Among them C_3+C_2 , C_3+C_3 combination will produce 2D COFs with hexagonal pores. The unit cell of these COFs fall in $P6/m$ (eclipsed structure) and $P6_3/m$ (staggered structure) space group [1.16]. The 2D COFs with tetragonal pores are obtained by C_4+C_2 and C_4+C_4 symmetry combination. Generally, porphyrin-based COFs are the examples of this category and $P4/m$ space group is used for modeling the structure. C_6+C_2 combination is rarely used for COF formation [1.17]. There are a limited number of 3D COFs are reported so far due to

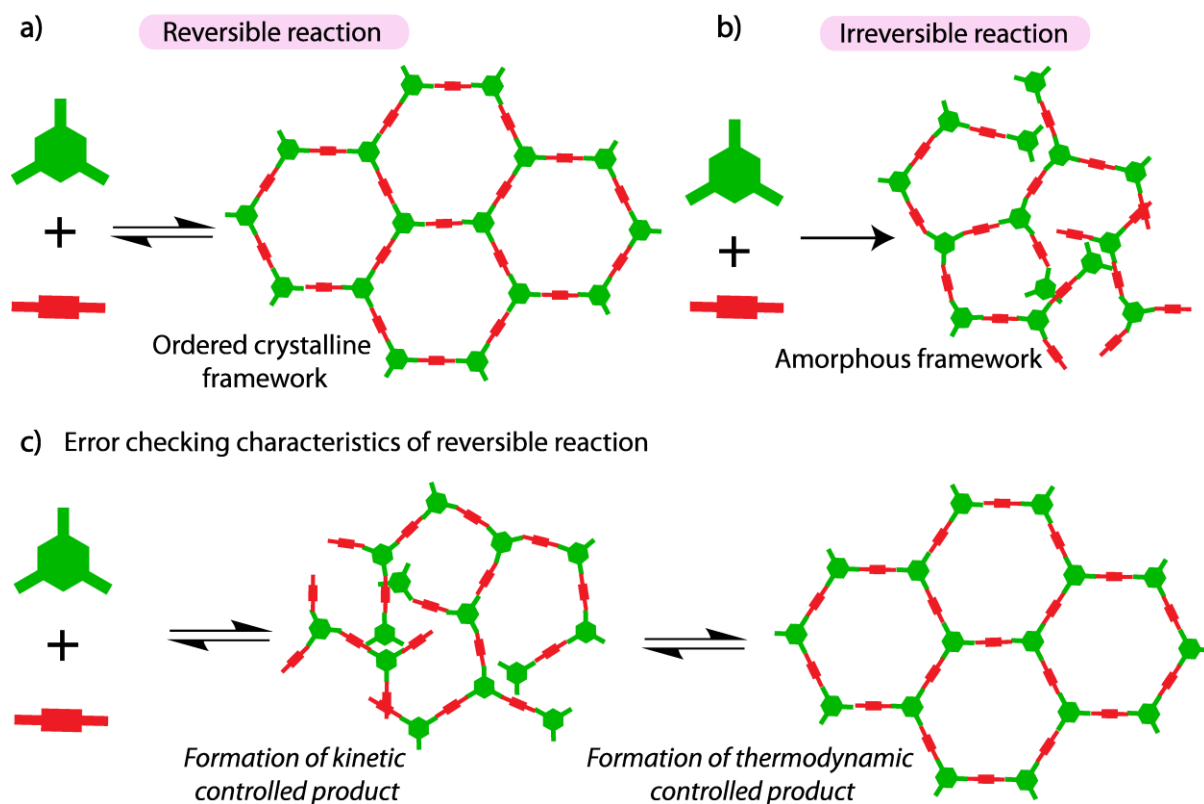


Figure 1.5: Schematic representation of a) and c) COF formation by the reversible reaction, b) PAF formation by the irreversible reaction.

the limited availability of the higher symmetry organic building unit (T_d) [1.18]. The combinations of symmetry elements $T_d + T_d$, $T_d + C_2$, $T_d + C_3$ and $T_d + C_4$ are used for 3D COFs synthesis. In general, the pore diameter of the 2D COFs are obtained in the microporous region but applying the above symmetry combination and changing the organic linker length 4.7 nm highest mesoporous 2D COF is made so far [1.19]. The choosing of a reversible reaction is another important factor responsible for synthesizing highly crystalline COFs rather than an irreversible one. Reversible reaction allows the system to form disorder structure (kinetically control) to order structure (thermodynamically control) by multiple reversible bond formation through self-repairing or self-correcting the defects, present in the system where irreversible reaction produces amorphous polymer due to the lack of self-correction during the reaction process. Many reversible reactions like 1) boronic acid trimerization, [1.20] 2) boronate ester formation, [1.21] 3) nitrile group trimerization [1.22] and 4) Schiff base reaction [1.23] are used for synthesizing highly porous stable crystalline COFs with long-range periodicity which is obtained for π - π interaction between COF layers. The above cumulative properties of COFs make as an ideal candidate for gas storage and separation, sensing, energy storing material, heterogeneous catalyst, and drug delivering agent. But the pore stability and lack of large-scale production limit their applications in heterogeneous catalysis.

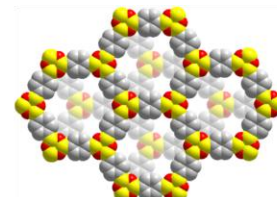
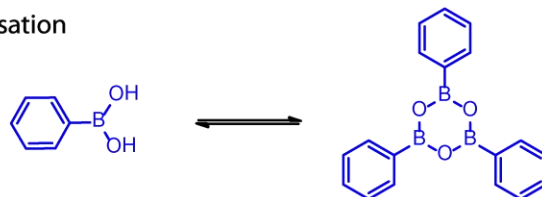
1.3 Types of Reversible Reaction Used the Synthesis of COFs

Chemical bonds are stronger than a coordinative bond. Therefore chemical bond forming reactions are used for synthesizing porous materials which makes material highly thermally and chemically stable. Among them, reversible reactions are preferred for highly crystalline framework formation with uniform pore size and high surface area because reversible reaction allows the material for self-corrections of defects to form a more stable thermodynamically stable product. Although there are very few reversible reactions are reported so far are used for COFs formation purpose. Those are 1) boronic acid trimerization, 2) boronate ester formation, 3) imine formation, 4) hydrazone formation and 5) trimerization of nitrile.

1.3.1 Boronic Acid Trimerisation Reaction: Here boronic acid trimerizes and forms 2D COFs. Three 1,4-benzene diboronic acids are reversibly condensed and form a planar six-membered boroxines ring (B_3O_3 ring) and water (Figure 1.6-1). COF-1, COF-102, COF-103,

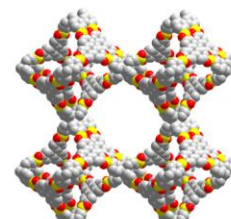
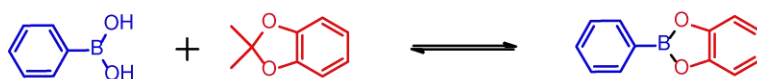
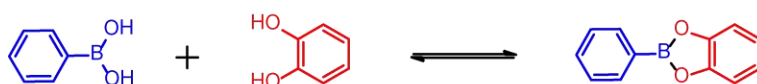
and PPy-COF are synthesized using this method. Moreover, the first COF was made by Prof. Yaghi and co-workers by using this protocol. The synthesized COFs are highly crystalline and porous but unstable in presence of moisture.

1) Boronic acid trimerisation



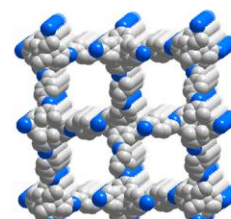
COF-1

2) Boronate ester formation



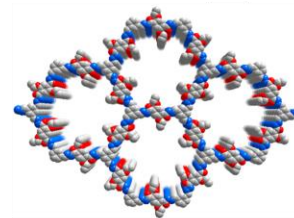
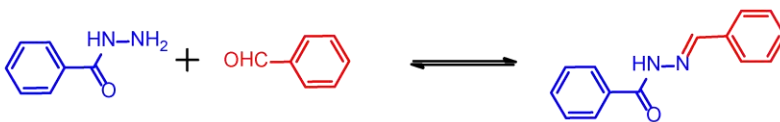
COF-108

3) Imine formation



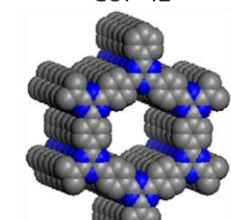
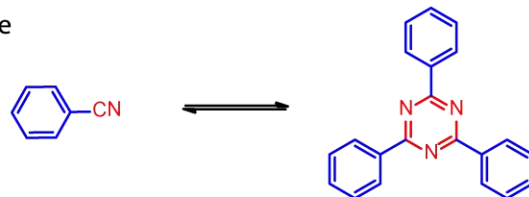
COF-300

4) Hydrazone formation



COF-42

5) Trimerisation of nitrile



CTF-1

Figure 1.6: Type of reversible organic reactions used for COFs formation.

1.3.2 Boronate Ester Formation Reaction: The another class of boron-containing COFs are synthesized by reversible condensation reaction of the boronic acid with aromatic diols or protected diols to form five membered boronate ester rings (C_2O_2B rings) (Figure 1.6-2).

Two or more building blocks are condensed for COF formation. One the building unit will be aromatic boronic acid (usually di or tri) and the second one will be poly-hydroxy aromatic compounds like 2,3,6,7,10,11-hexahydroxytriphenylene (HHTP). The common examples of COFs synthesized by this reaction are COF-5, COF-8, COF-10, HHTP-DPB COF, ZnPc-Py COF etc. Three dimensional COF-8 is prepared by reacting between HHTP and TBPM to produce three dimensional pore with extremely low dense material 0.17 g cm^{-1} using this method [1.24].

1.3.3 Schiff Base Reaction: Another class of COFs made via C-N bond formation by using a reversible Schiff base reaction between aldehyde and amine precursors (Figure 1.6-3). Prof. Yaghi and co-workers have first introduced Schiff based COF-300 by reacting between tetra-(4-anilyl) methane (T_d) and terephthalaldehyde (C_2) to produce three-dimensional imine based COFs. After this report, several 2D imine based COFs COF-42, COF-43, COF-366, COF-LZU-1 are also reported by using a symmetric combination such as $C_3 + C_3$ or $C_3 + C_2$. As Schiff base reactions are completely reversible under acid condition (pH=4-5), therefore the catalytic amount of mild acids are used for the successful crystallization of imine COFs. Imine based COFs are much more hydrolytically stable in comparison to boronic acid COFs. However, at lower pH imine COFs also get completely decomposed. The stability of the imine based COFs is remarkably enhanced by Prof. Banerjee and co-workers by introducing reversible Schiff base reaction followed by irreversible tautomerization to produced more stable keto-enamine based COFs which are stable in acidic, basic and in water medium. After that several keto-enamine based COFs TpPa-1, TpPa-2, TpBD, TpBpy are synthesized and applied to different real-life applications [1.23].

1.3.4 Hydrazone formation: After imine bond formation another C-N bonded COFs are synthesized via hydrazone bond formation (Figure 1.6-4). Here condensation reaction happens between aldehydes and hydrazide building blocks. COF-42 and COF-43 are the examples of hydrazone based COFs. COF-42 is prepared by reacting with DETH and TFB. This method is developed to stabilize the imine bonded COFs.

1.3.5 Trimerization of Nitriles: Another class of porous material is developed termed as Covalent Triazine Frameworks (CTFs) by trimerization of nitriles at a higher temperature in presence of Lewis acid catalyst (Figure 1.6-5). Prof. Arne Thomas and co-workers have first synthesized CTF-1 in 2008 by reversible trimerization of the nitrile in ionothermal method at

high temperature (400 °C) and in presence of Lewis acid (ZnCl_2). However, this process happens at a higher temperature and in presence of a toxic metal catalyst which limits the application of this procedure [1.22].

1.4 Different Methods COF Synthesis

Reversible covalent bond forming reactions are mainly used for crystalline COF formation. The reversible reaction allows the materials for self-corrections to produce the thermodynamically more stable ordered structure. Therefore the amount of solvents, different solvent combination, pressure, temperature, and catalysts plays an important role in making the reaction reversible. Here we will discuss the different methods are used so far for the synthesis of crystalline COFs.

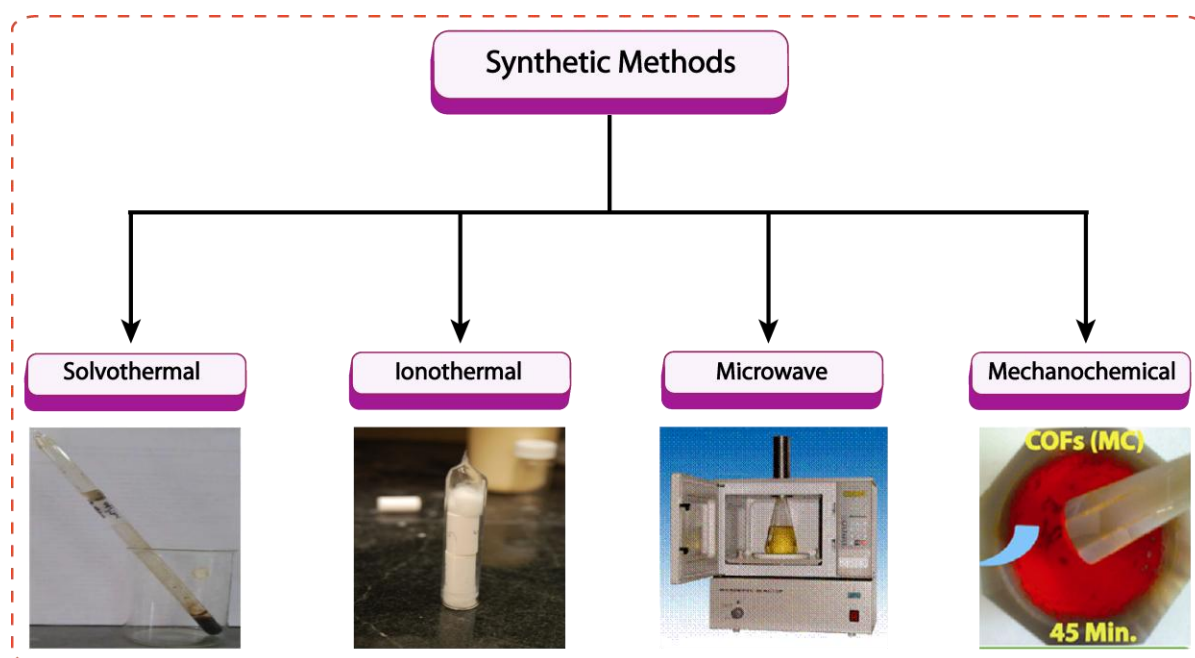


Figure 1.7. Different synthetic methods used for the synthesis of COFs. Images are taken from Google.

1.4.1 Solvothermal Synthesis.

Among different methods solvothermal is utilized for different COFs formation purpose and it produces more crystalline and porous COFs compared to other methods (Figure 1.7) [1.15]. During this process, different solvent combinations are used to solubilize the starting materials partially and sealed glass/pyrex tubes are used to get more crystalline materials. Several steps are involved in this process:

- 1) First starting materials are kept inside the glass tube and proper solvent combinations are used in presence of very catalytic amount acetic acid.
- 2) The reaction mixture is sonicated and degassed for 30 min and then the tube is properly closed and is flash frozen in liquid nitrogen.
- 3) Then the reaction mixture is kept in vacuum and freeze-pump-thaw cycles are continued for three times. After that, the tube is sealed in flame in presence of a vacuum.
- 4) Now the reaction mixture is allowed to reach room temperature and then it is kept in a hot air oven (90-120 °C) for 3-7 days in an undisturbed condition.
- 5) After 3-7 days the seal tube is broken and the phase pure material is washed with DMAc, water and acetone solvents to get pure COF material.

Although this process is widely used for synthesizing more crystalline and high surface area COFs but a special reaction set up and longer reaction time limits their applications for bulk scale production.

1.4.2 Ionothermal synthesis

Prof. Arne Thomas and co-workers have exploited ionothermal reactions for the synthesis of covalent triazine frameworks (CTFs) (Figure 1.7). Here aromatic nitriles are trimerized to produce hexagonal frameworks. This reaction is performed in a high temperature and in presence of Lewis Acid $ZnCl_2$. Here $ZnCl_2$ not only acts as a solvent but the molten $ZnCl_2$ helps to form a more crystalline product. The high temperature, uses of toxic metal and limited organic ligands make the methods not suitable for commercialization process although the materials produced in this method are highly thermally and chemically stable [1.22].

1.4.3 Microwave synthesis

Prof. Andrew I. Cooper and co-workers introduced a microwave-based method for COF synthesis. The reaction is performed inside the microwave oven having the reactants in the closed heating tube (Figure 1.7). Microwave reaction methods are faster compared to the sealed tube method. COF-5 and COF-102 are synthesized by Prof. Andrew I. Cooper and co-workers in 20 minutes under microwave conditions. This method is a greener, cleaner, faster process and produces minimum impurities during COF synthesis with comparable crystallinity surface area to the solvothermally synthesized COFs [1.25].

1.4.4 Mechanochemical Synthesis

As we have discussed that solvothermal is not suitable for large-scale production of COFs. Therefore developing a method which is cost effective, time efficient, easy to handle at room temperature in an open atmosphere without using special equipment is required for bulk scale production of COFs. The discovery of the mechanochemical process has drawn significant attention in chemical and pharmaceutical industries due to the greener, cleaner, safe, time efficient and eco-friendly process. This process avoids of using plenty of solvents, heater, and stirrer for chemical transformation by simply replacing by using ball mills and mortar and pestle. This process is already applied for synthesizing industrially important zeolites and metal organic frameworks. Therefore finding a suitable method for synthesizing COFs *via* mechanochemical process is industrially important for bulk scale production. It has been observed that using a small amount of solvent during the grinding process accelerates the reaction in a faster rate compared to net grinding. This process is often called as Liquid-Assisted Grinding (LAG) process in Mechanochemistry. Prof. Banerjee and co-workers are developed first-time COFs synthesis *via* the mechanochemical process. The process involves the grinding of reactants in a mortar and pestle (15 minutes) followed by heating them at high temperature (120 °C for 45 minutes). The COFs synthesized in this methods show low crystallinity porosity, which was due to the delimitation of the COF layer during the grinding process. Later Prof. Banerjee and co-workers have developed a mechanochemical method for COFs synthesis in presence of *p*-toluene sulfonic acid. The COFs are produced in this method are highly crystalline and porous comparable with solvothermal method within a short reaction period. Therefore this method is suitable for bulk scale production of COFs [1.26].

1.4.5 Synthesis of Mono Layers on Surface

Solvothermally synthesized powder COFs are not suitable for electrochemical applications like energy storage, optoelectronics etc. Therefore researchers have developed a method for synthesis of single COF layer on support like HOPG and metal surfaces [Ag(111)] by the condensation of the building blocks in UHV condition at high temperature. Louis Porte and coworkers are able to synthesize surface covalent organic frameworks (SCOFs) COF-1 and COF-5 on the clean Ag (111) surface at a higher temperature by vacuum sublimation of reactants in presence of a water reservoir ($\text{CuSO}_4 \cdot 5\text{H}_2\text{O}$). The growth

of the COF layer is monitored by STM images. Prof. Ditchel and co-workers developed a new method by which COFs thin films can be directly fabricated on to single-layer graphene attached to a SiO₂ surface (Figure 1.8a) [1.27].

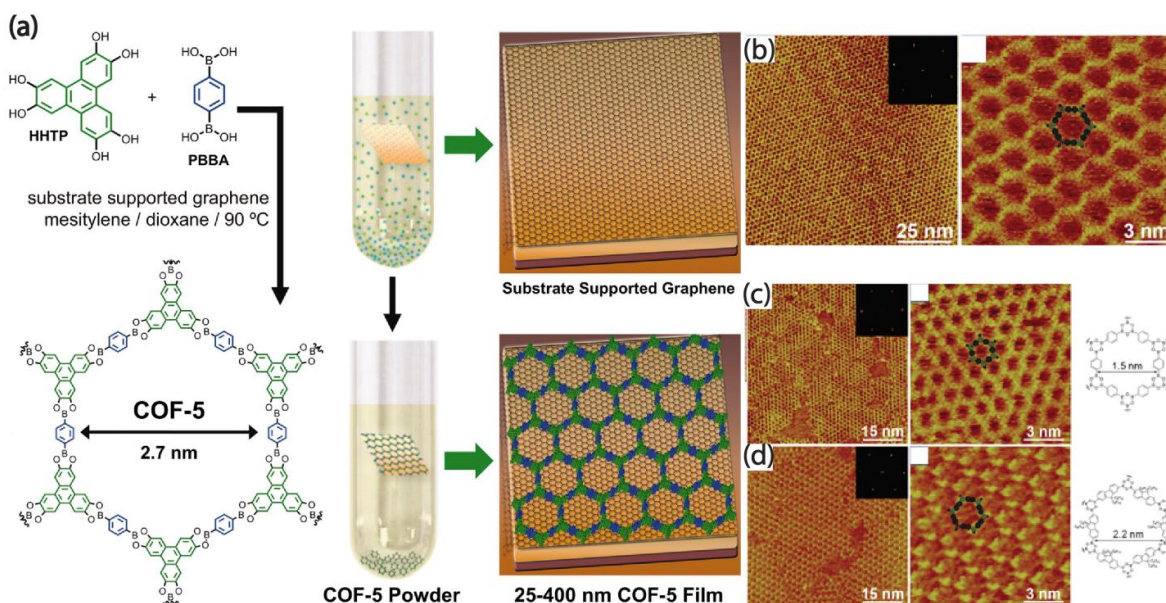


Figure 1.8.: (a) Synthesis of COF-5 on the surface of few-layer graphene. (b) & (c) STM images of COF-1 and (d) STM images of COF 10 on HOPG surface. Figures are reproduced with permission from Science.

1.5 Applications of COFs

Covalent Organic Frameworks are crystalline, porous organic material composed of light elements boron, carbon, nitrogen, oxygen, and silicon atoms. Therefore COFs are lightweight and low dense material useful for high gas uptake and storage purpose. Already different COFs have been utilized for hydrogen, carbon dioxide, methane and ammonia gas uptake, and storage purpose. Choosing reversible reactions is very important criteria for synthesizing highly crystalline covalent organic frameworks because reversible reactions allow the system for self-correction of defects during the reaction and produce the more thermodynamically stable ordered structure. The long-range periodicity comes from the π - π interactions between two COF layers which help to improve the charge carrier mobility in COF frameworks suitable for photoelectric and semiconducting materials. Another important factor for constructing more crystalline COF is the choosing of proper symmetry combinations. The different pore size and the volume can be tuned by changing the symmetry combination of the respective precursor. Also, different pores can be generated

inside the materials suitable for selective gas separation. COFs can be functionalized by using reticular chemistry and different functionalized COFs have been used for different applications like drug delivery, proton conduction and as energy storage material (Fig 1.9).

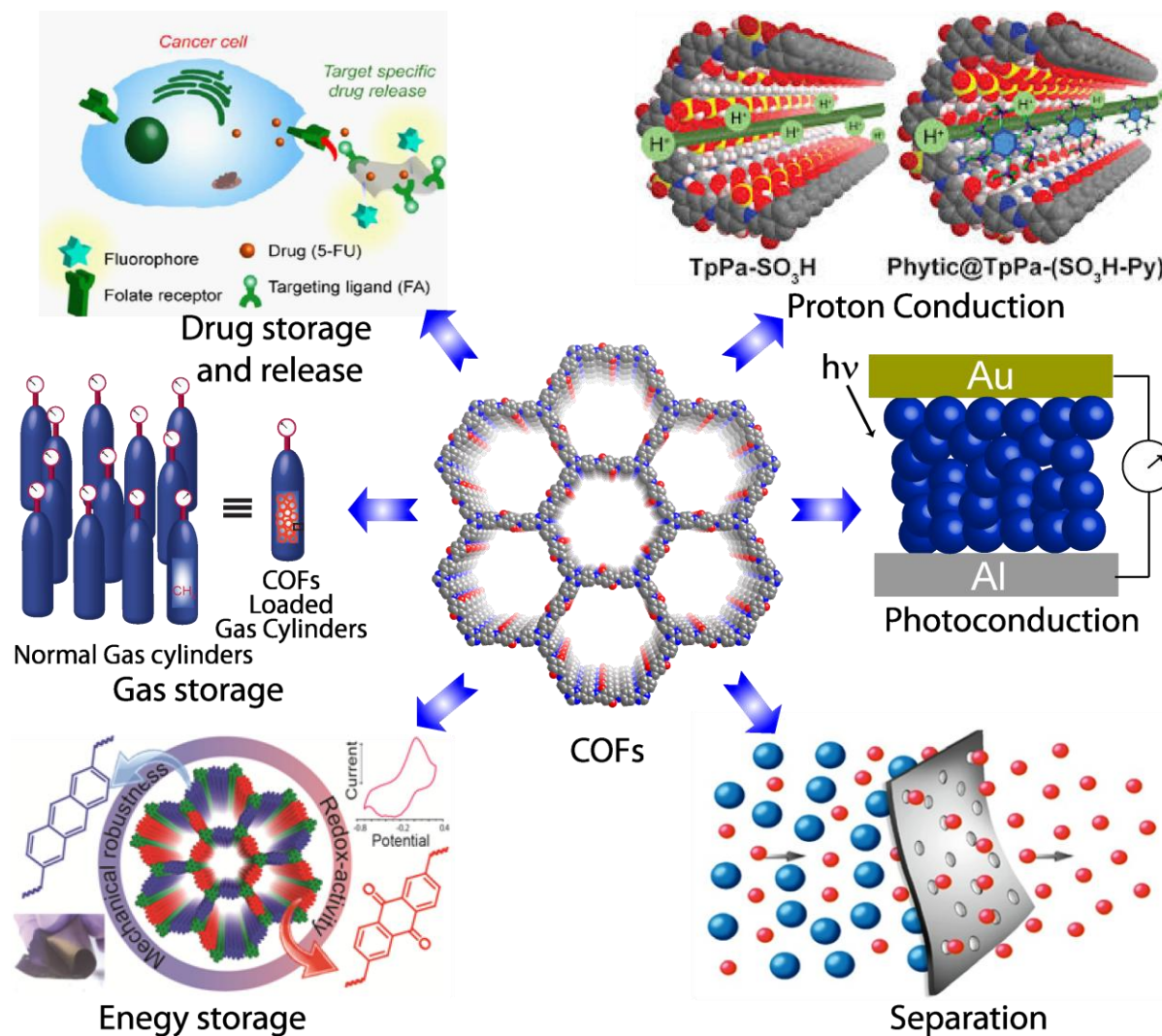


Figure 1.9: Various applications of COFs such as drug/bio molecules storage, proton conduction, gas storage, photo-conducting materials, energy storage and gas separation.

1.5.1 Gas storage application

Highly porous low density and uniform pore size make COF materials suitable for different gas uptake and storage application such as hydrogen (H_2), carbon dioxide (CO_2), methane (CH_4) and ammonia (NH_3). Hydrogen is the alternative renewable energy source can replace the uses of fossil fuels. Therefore storage of hydrogen is very important. The US Department of Energy (DOE) has set the target of H_2 storage for 2017 to be 5.5 wt% at a

temperature of -40 to 60 °C and a maximum pressure of 100 atm. Till now, many porous materials have been tested for H_2 storage. In COFs the hydrogen uptake can be increased in two ways: 1) increasing the surface area and pore volume of the COFs without changing the optimum pore size and 2) by metallation like Li^+ , Ca^{2+} , Sc^{3+} , Pd^{2+} etc in COF. Among 3D COFs COF-102 and COF-103 have shown the highest H_2 uptake of 7.24 and 7.05 wt% at 77K and 85 bar. Among 2D COFs COF-10 has shown H_2 uptake of 3.9 wt% at 77K and 85 bar. Lithium-ion intercalated COF-105 and COF-108 exhibit H_2 uptake of 6.84 and 6.73 wt% respectively at 100 bar and 298 K. Among natural gases methane is abundant, cheap and an alternative to the fossil fuel for clean energy. The current US DOE target for methane storage is 180 (v/v) at 298K and 35 bar. Among COFs, 3D COF-102 and COF-103 have shown the highest gravimetric methane uptake of 187 $mg\ g^{-1}$ and 175 $mg\ g^{-1}$ respectively at 35 bar and

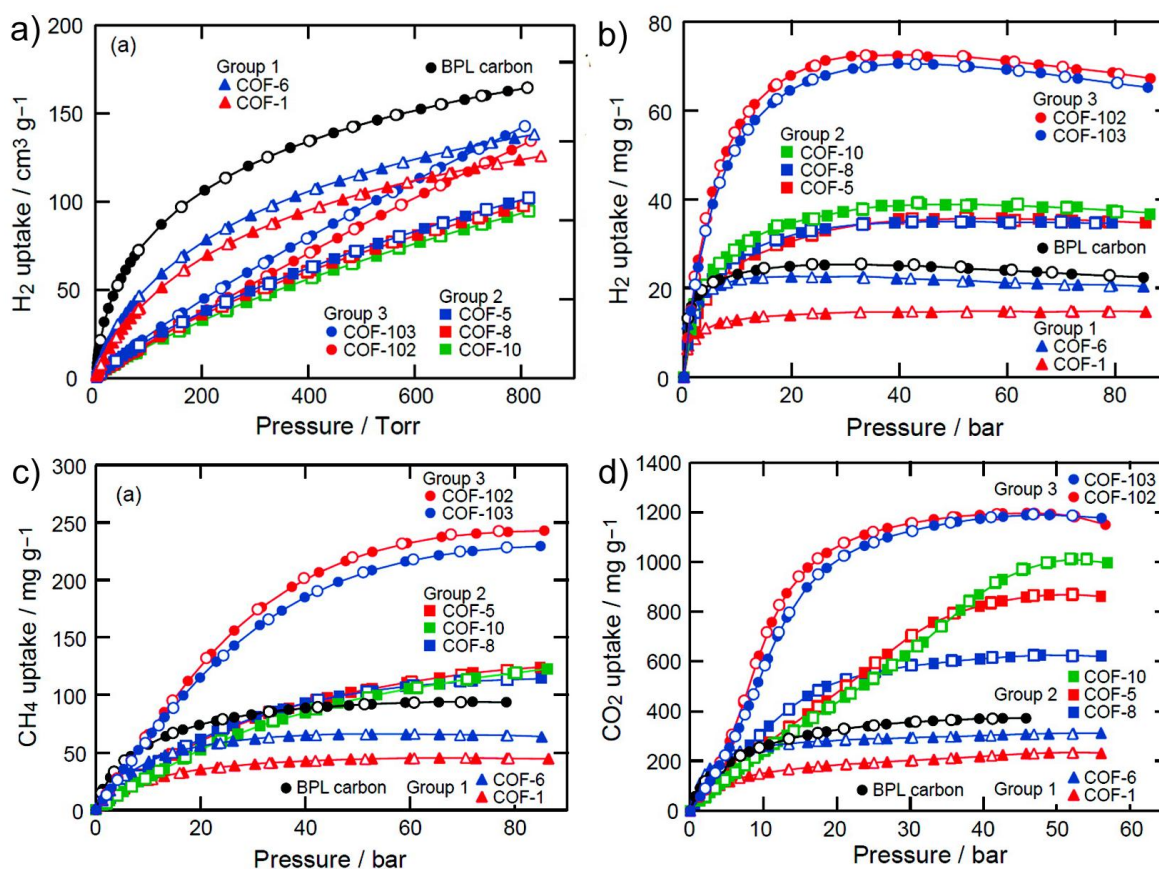


Figure 1.10. Comparison of excess hydrogen uptake of different COFs (a) at 1 bar and (b) high pressure (open symbols represent experimental results, filled symbols simulated results). (c) Methane adsorption isotherms of COFs at high pressure. (d) Carbon dioxide adsorption isotherms of COFs at high pressure. Figures are reproduced with permission from ACS publications.

298K. The increase in CO₂ amount day by day in nature is responsible for global warming and environment pollution. Therefore adsorption of CO₂ gas and storage are becoming more significant research area. Although many porous materials like porous carbon, silicas, zeolites, MOFs and CTFs have been tested for CO₂ gas adsorption and storage. Among COFs COF-102 exhibits the highest uptake of 27 mmol g⁻¹ at 298 K and 35 bar, which is higher than the uptake of both zeolites (5-8 mmol g⁻¹) and MOF-5 (22 mmol g⁻¹). Also, it has been observed that the incorporation of basic nitrogen atoms inside the frameworks increases the acidic CO₂ gas uptake. Prof. Banerjee and co-workers have synthesized bipyridine based COF which shows high CO₂ uptake 170 cc/g at 0 °C 1 atm pressure. Ammonia is widely used for the production of fertilizer and therefore suitable storage medium is necessary for safe storage and transportation purpose of both liquid and gaseous ammonia as the handling of liquid NH₃ is very risky due to its toxicity and corrosive nature. Among COFs the boronate ester COF-10, synthesized by the condensation of 2,3,6,7,10,11-hexahydroxytriphenylene (HHTP) and 4,4'-biphenyldiboronic acid (BPDA), exhibits the highest ammonia uptake of 15 mol kg⁻¹ at 1 bar and 298K [1.28].

1.5.2 Photoelectric and Semi Conduction Applications

Apart from the high porosity 2D-COFs also possess conjugated 2D sheet-like structure analogous to graphene. The efficient long-range π - π stacking interaction of the COF layers makes them suitable for semi conduction applications. PPy-COF is the first COF tested for a photoelectric application which is synthesized by boronic trimerization reaction between pyrene-2,7-diyldiboronic acid. Upon irradiation with visible light, Ppy-COF generates photocurrent of 5 nA. Another TP-COFs is synthesized by boronate ester formation reaction exhibits p-type semiconducting character, and displays a linear I-V curve. Prof. Donglin Jiang and co-workers have also synthesized three porphyrin-based COFs, with different metal ions (Cu²⁺ and Zn²⁺) at the porphyrin centers and have shown different charge transport behavior in three COF [1.29].

1.5.3 Energy storage

The long-range ordered structure with the high surface area and tunable pore functionality makes COFs for ideal electrode materials for energy storage purpose. Therefore COFs has been used as active electrode materials for battery and electrochemical capacitor

(Supercapacitor) by introducing redox active moieties into the frameworks. Prof. William Dichtel and co-workers have synthesized an anthraquinone-based β -ketoenamine COF (DAAQ-TFP COF) by the Schiff base reaction between 1,3,5-triformylphloroglucinol and 2,6-diaminoanthraquinone which shows specific capacitance of $40 \pm 9 \text{ Fg}^{-1}$ after 5000 cycles. Prof. Tang, Li, and coworkers have synthesized pyridine functionalized TaPa-Py COF which shows redox activity of pyridine groups with a specific capacitance value of 209 Fg^{-1} along with high capacitance retention (92%) after 6000 cycles. Prof. Banerjee and co-workers have synthesized ketoenamine based COF TpTa-(OH)₂ which shows specific capacitance 416 F/g at 0.5 A/g current density in three electrode system [1.30].

1.5.4 Separation

The ordered channels and pore functionalization of COFs are utilized for the gas separation applications. Prof. Yanan Gao and coworkers have used COF-320 for H₂/CH₄ and N₂/H₂ separation application. The membrane fabrication is fabricated on the surface of porous alumina ceramic support by the Schiff base reaction between reactants. Recently Prof. Banerjee and coworkers are able to fabricate hybrid membranes of COF with PBI polymers. These hybrid membranes display moderate selectivity in CO₂/CH₄ and CO₂/N₂ separation [1.31].

1.5.5 Proton conduction

The channel structure of COFs has been used for loading and transporting of proton carrier molecules inside COFs. Prof Banerjee and coworkers have demonstrated first-time proton conductivity in COFs. They have loaded phosphoric acid into synthesized azo (N=N) functionalized chemically stable Tp-Azo COF. Chemical stable and basic nature of azo groups in Tp-Azo COF helps to bind phosphoric acid and proton hopping process inside the nanochannel. The H₃PO₄@Tp-Azo COF exhibit proton conductivity of $9.9 \times 10^{-4} \text{ Scm}^{-1}$ in hydrous condition. Sulfonic acid based COF (TpPa-SO₃H) is also synthesized by the same group for intrinsic proton conduction. The periodic alignment of sulfonic acid groups in two-dimensional (2D) layers promotes the proton hopping inside the hexagonal one-dimensional channel. The intrinsic proton conductivity of TpPa-SO₃H is measured and shows $1.7 \times 10^{-5} \text{ Scm}^{-1}$ at $120 \text{ }^\circ\text{C}$ under anhydrous conditions. In another work, Prof. Banerjee and coworkers have synthesized bipyridine based TpBpy-COF *via* the mechanochemical method and used as a proton exchange membrane. It showed proton conductivity of $1.4 \times 10^{-2} \text{ Scm}^{-1}$ at $120 \text{ }^\circ\text{C}$

and an open circuit voltage of 0.93 V. This clearly indicates the potential of COFs as solid electrolytes in hydrogen fuel cell [1.32].

1.5.6 Drug storage and Delivery

Since COF porosity can be extended to the mesoporous region, scientists have attempted to load bigger sized drug/ bio-molecules into the COF pores. Prof. Yushan Yan and coworkers have designed a 3D polyimide-based COF (PI-COF-4) for drug delivery application. PI-COF-4 displayed a high surface area of $2403\text{m}^2\text{g}^{-1}$ which makes them capable of storing ibuprofen (IBU) drug molecule. The authors are calculated drug loading capacity of PI-COF-4 as 20 wt% from the UV-Vis studies. The slow diffusion of drug molecules from the framework pores are observed from drug release profile. The complete removal of ibuprofen (IBU) happens from the COF pores after 6 days [1.33].

1.6 Chemical Stability of COFs

Although different COFs have been synthesized using various methods but the applications of COFs in real life is limited. The major reason behind this is the chemical stability of COFs. COFs are not stable in acid base and water medium. For highly crystalline COFs formation reversible reactions (Boronic acid, Schiff base etc) are used so far. But the major drawback of using reversible reaction is that there is a possibility of backward reaction where the final compound may get decomposed and forms the respective starting materials. Therefore, in general COFs get completely decomposed to the starting materials coming in contact to water or humid conditions (Figure 1.11). Few attempts have already done to improve the chemical stability of COFs but little improvement is achieved by pyridine doping and alkylation of COF pore walls. But it decreases the gas uptake properties of the

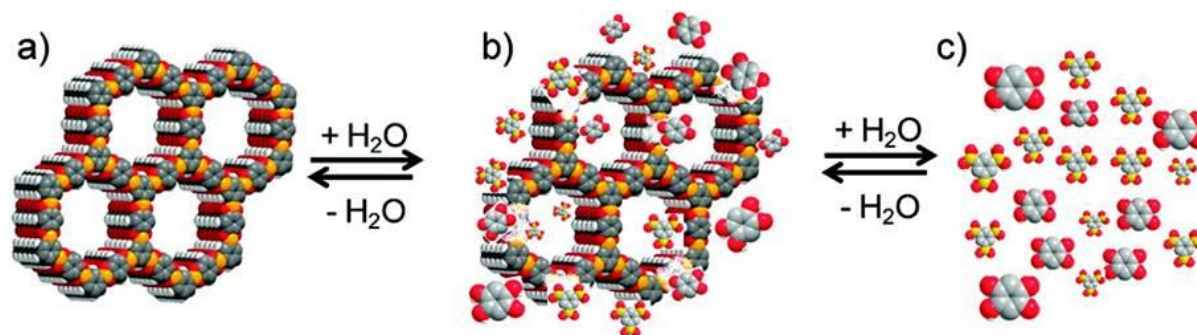


Figure 1.11: Schematic representation of (a) as-synthesized COF (b) partial hydrolysis and release of monomers into solution upon submersion in water (c) completely hydrolyzed COF. Figures are reproduced with permission from ACS publications.

respective COFs. Therefore the real-life application of the porous materials, chemical stability of the framework is one of the important aspects which should take into consideration. The problem is overcome by Prof. Banerjee and co-workers by simply introducing an irreversible enol-keto tautomerization within the COF skeleton to produce stable COFs which are stable in boiling water and highly acidic (9N HCl) condition.

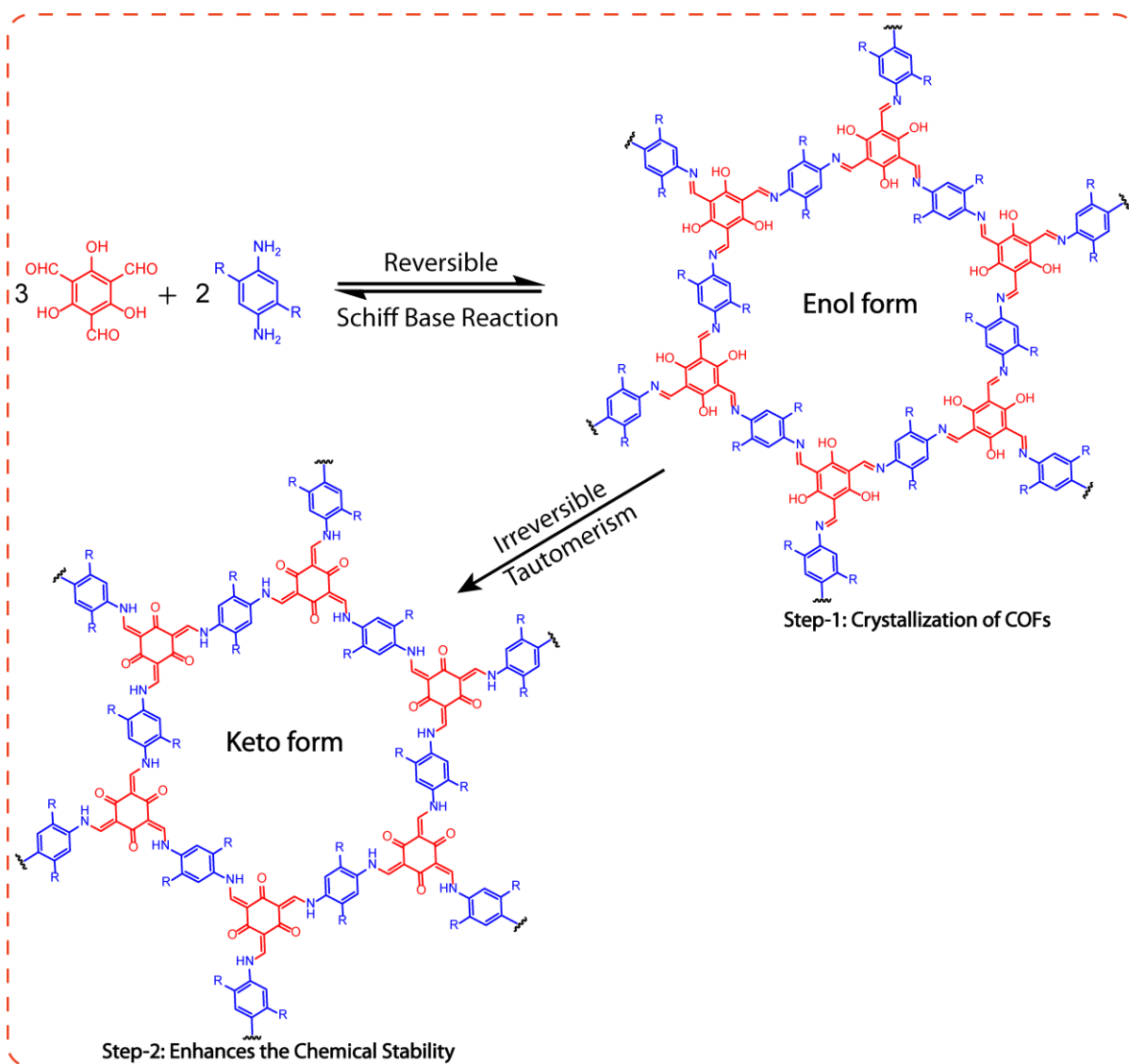


Figure 1.12: Synthesis scheme for chemically stable COFs via Schiff base condensation reaction with the combination of reversible and irreversible reaction.

The reason behind these materials to show high stability is that the COFs are synthesized by a combination of reversible and irreversible organic reaction. The total reactions are divided into two steps. Reversible Schiff base reaction leads to the formation of the crystalline

framework in the first step, followed by irreversible enol to keto tautomerization in the second step (Figure 1.12) which enhances the chemical stability. The irreversible nature of the tautomerization does not affect the crystallinity of the COF since the transformation involves only shifting of bonds keeping atomic positions almost same in both the cases [1.34].

1.7 Different Methods for Covalent Organic Frameworks Functionalization:

Covalent organic frameworks have been utilized for different applications. It has been observed that different functional groups in the covalent organic framework (COF) are responsible for different applications. Therefore the development of methods for introducing different functional group in the covalent organic framework is a very important and challenging research topic. So far there are two methods for COF functionalization: a) Post Synthetic Method and b) Pre Synthetic Method (Figure 1.13).

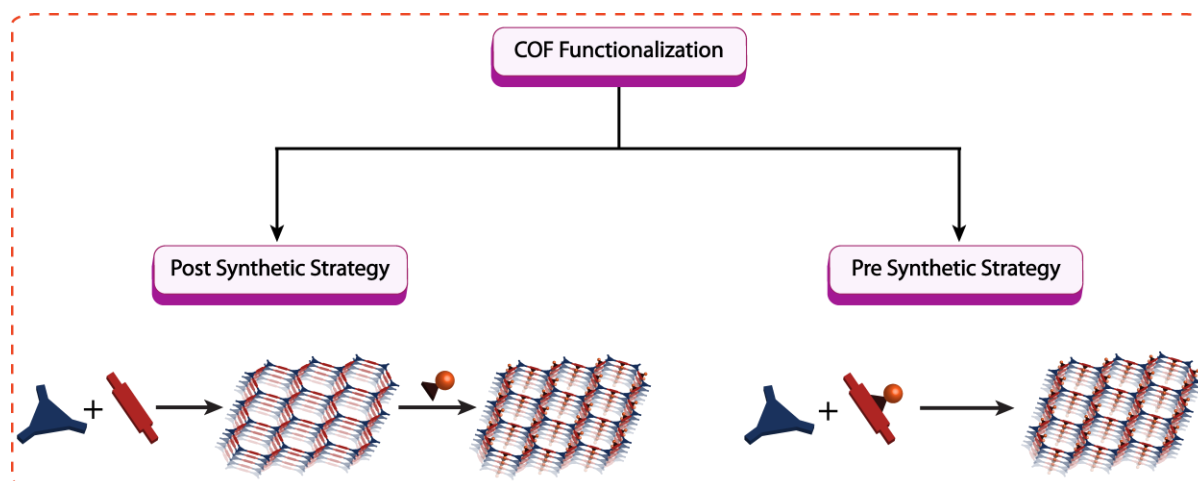


Figure 1.13: Schematic diagram of COF functionalization.

1.7.1 Post Synthetic Strategy:

This is the most used method for introducing new functional moiety into the covalent organic framework backbone through chemical transformation or coordinative incorporation. In this strategy, the catalytically active species or functional group is attached after formation of the COF. Therefore, there are several disadvantages of using this method. Uneven distribution of catalytically active species: catalytically active species are not homogeneously distributed in the framework. Hence, lower loading of catalytically active species into the framework may give lower yield during catalytic process. During this process, the

crystallinity of the original material will hamper and the framework may lose long-range structural periodicity. Prof. Wang and coworkers have synthesized Pd/COF-LZU1, Pd(OAc)₂ coordinated imine based covalent organic framework using this strategy and the metal loaded COF has been utilized for Suzuki–Miyaura coupling reaction (Scheme 4.4) [1.35].

1.7.2 Pre Synthetic Strategy:

This strategy is more straightforward but difficult for covalent organic framework functionalization. Here the functional group should directly attach to the predesigned building block before covalent organic framework synthesis. The advantage of this method is the homogeneous distribution of the functional group in the covalent organic framework will occur and which may improve the thermal and chemical stability compared to the previous framework. During this process, crystallinity and porosity should also get equal priority. Therefore it is always becoming more challenging for synthesizing highly crystalline and porous functionalized covalent organic framework. COFs synthesized *via* pre-synthetic method have shown good performance in ammonia gas uptake, catalysis, and photoelectric application [1.36].

1.8 Importance of Nitrogen-Rich Porous Material:

The problem is overcome by introducing the heteroatom into the material. Among different heteroatom (B, N, S, F, P) nitrogen incorporating material shows better activity due to the change in electronic distribution in the material. Also, the atomic radius of the nitrogen is similar to carbon which significantly reduces the lattice mismatch. Moreover, nitrogen has the good chelating ability for different metal ion which is useful for stabilizing different metal nanoparticles to form uniform particles distribution all over the material. The incorporation of nitrogen into the material also increases the overall thermal stability. The basic nature of the nitrogen shows higher acidic gas (CO₂) uptake and selective CO₂/N₂ gas separation through the membrane. Moreover, this material is useful for abstracting acidic protons which will help in proton conduction or as a useful membrane in a fuel cell. Nitrogen doping to the material makes the neighboring carbon atoms more electron deficient as electronegativity of nitrogen is higher compared to carbon. Therefore it promotes more oxygen adsorption into catalyst and applicable for oxygen reduction reaction (ORR) in fuel cell and as an energy storage material (EDLC supercapacitor). But the main drawback of this method is that finding the accurate position of the nitrogen after doping is more difficult due

to the limited instrumental technique and huge defects in the material. Therefore nitrogen-rich porous crystalline material design and synthesis from nitrogen-containing precursor will be the most alternative approach to short out the problem [1.37].

1.9 Heterogeneous Catalysis by Covalent Organic Frameworks:

The use of porous materials as heterogeneous catalysts is of great interest because heterogeneous catalyst offers many advantages combined with the greater accessibility of active sites over homogeneous. However, despite their high porosity and great tunability, the use of COFs in heterogeneous catalysis remains largely unexplored relative to other classes of porous materials. As imine based and enol-keto tautomerized COFs have shown good crystallinity, easy to synthesize and moreover stable in water, acid and base medium. Therefore, a variety of COFs based on Schiff-base chemistry has been used to catalyze different organic reactions. Here we will discuss the different types of heterogeneous catalysis has been done by using COFs where it acts as a catalyst or as a support to stabilize different metal nanoparticles required for catalysis. The types of catalysis are as follows 1) Metal loaded catalysis (metal coordinated and metal nano (*in-situ/ex-situ*)) 2) Organocatalysis (acid, base, asymmetric) 3) Photocatalysis 4) Electrocatalysis (Figure 1.14).

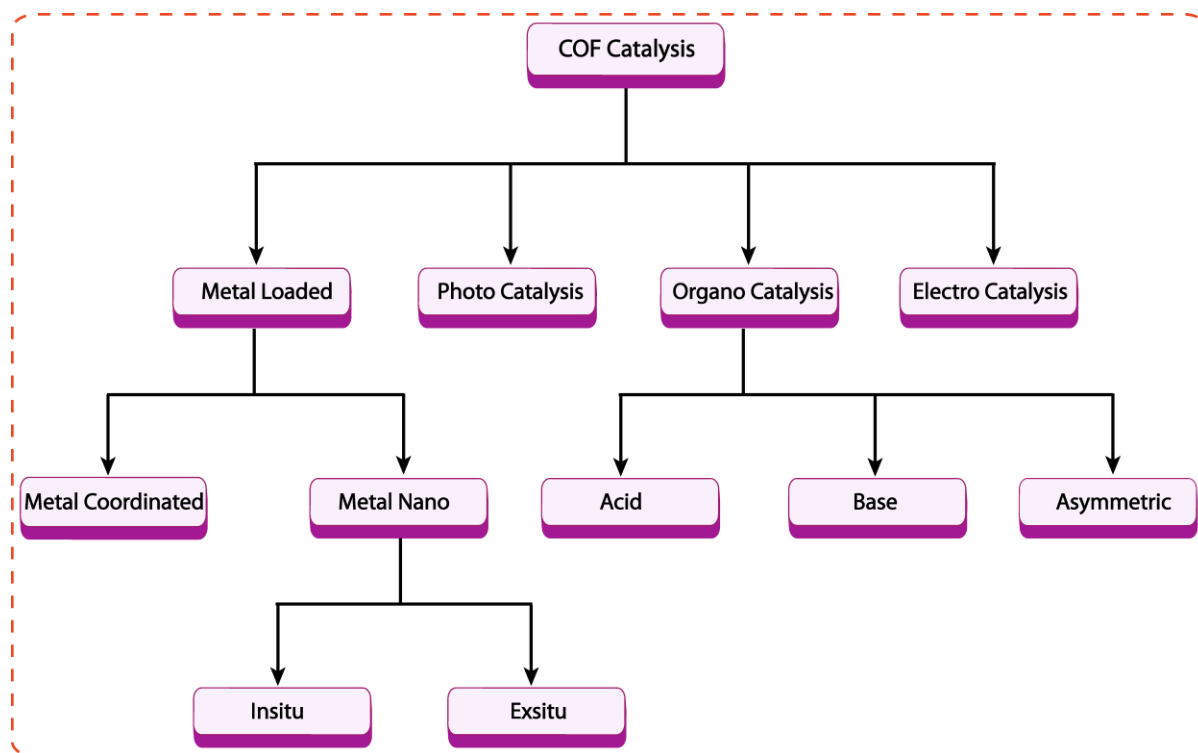


Figure 1.14: Schematic diagram of COF catalysis.

1.9.1 Metal Loaded Catalysis:

Metal loaded COFs which have been used for heterogeneous catalysis are classified into two categories: a) Metal coordinated COFs b) Metal nanoparticles loaded COFs. Metal nanoparticles loaded COFs can be subcategories into two classes based on their synthetic methodologies i) *Exsitu* synthesis and ii) *Insitu* synthesis.

1.9.1.a Metal Coordinated COF:

Pd(II) Coordinated COF (COF-LZU1) for Suzuki Reactions:

Prof. Wang and co-workers have synthesized 2D imine bonded covalent organic frameworks (COF-LZU1) by reacting with 1,3,5-triformylbenzene and 1,4-diaminobenzene (Figure 1.15). The distance between imine nitrogen between two adjacent layers in eclipsed form is 3.7 Å which is suitable for incorporation of different metal ions into the framework. The large pore width 1.8 nm of the synthesized material helps bulky product diffusion in a faster rate and appropriate to access the catalytically active sites. They have synthesized Pd(OAc)₂ coordinated Pd/COF-LZU1 at room temperature by adding palladium metal to the

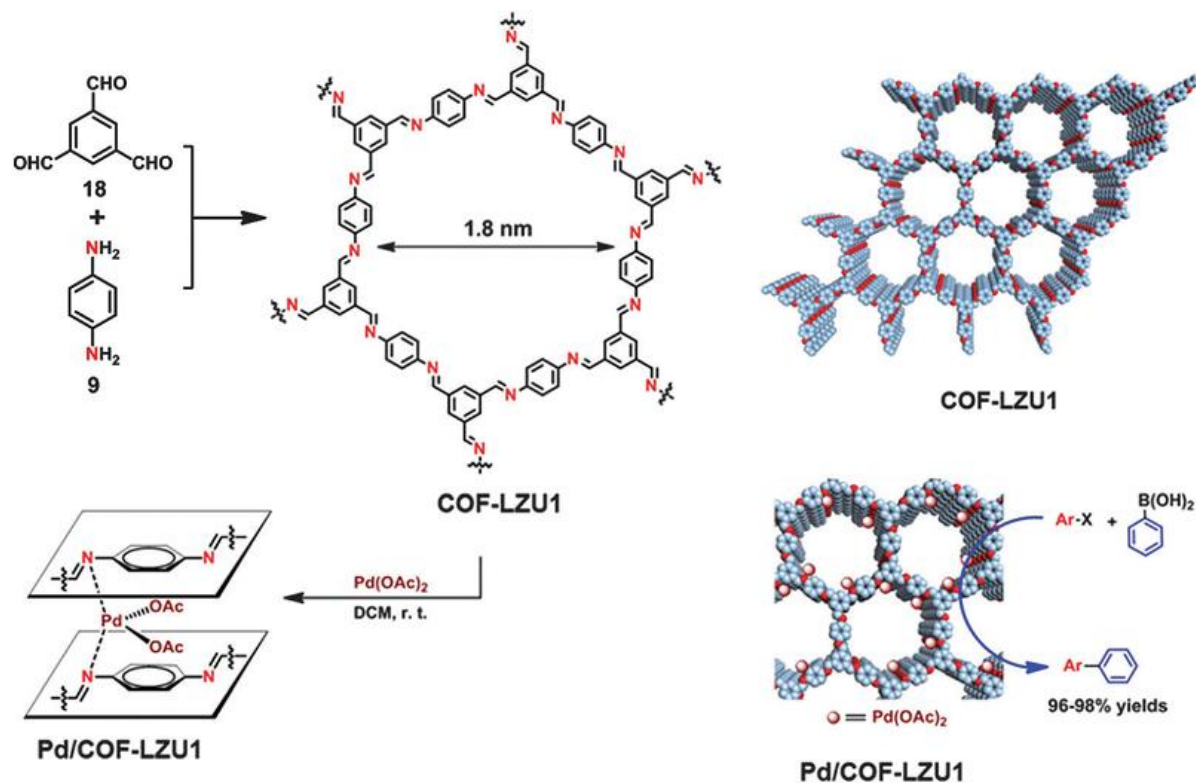


Figure 1.15: Chemical and extended structures of COF-LZU1, Pd/COF-LZU1 and Suzuki-Miyaura coupling reaction. Figures are reproduced with permission from ACS publications.

synthesized COF-LZU1 by post-synthetic modification. The metal loaded COF has been successfully utilized for Suzuki-Miyaura coupling reaction with broad substrates scope, high selectivity and with good recyclability [1.38].

1.9.1.b Metal Nanoparticles Loaded COF:

Pd(0) nanoparticles Loaded COFs for Sonogashira and Heck Coupling Reactions (Ex Situ Method):

Prof. Banerjee and co-workers have realized that COFs can be used as a heterogeneous support to stabilized different metal nanoparticles to make heterogeneous catalyst. Therefore they have first synthesized ketoenamine based chemically and thermodynamically stable TpPa-1 COF. Then the metal nanoparticles are generated by adding Pd(OAc)₂ to the synthesized COF in presence of reducing agent (NaBH₄) at room temperature (Figure 1.16). The presence of more nitrogen and oxygen atoms in the frameworks makes the metal

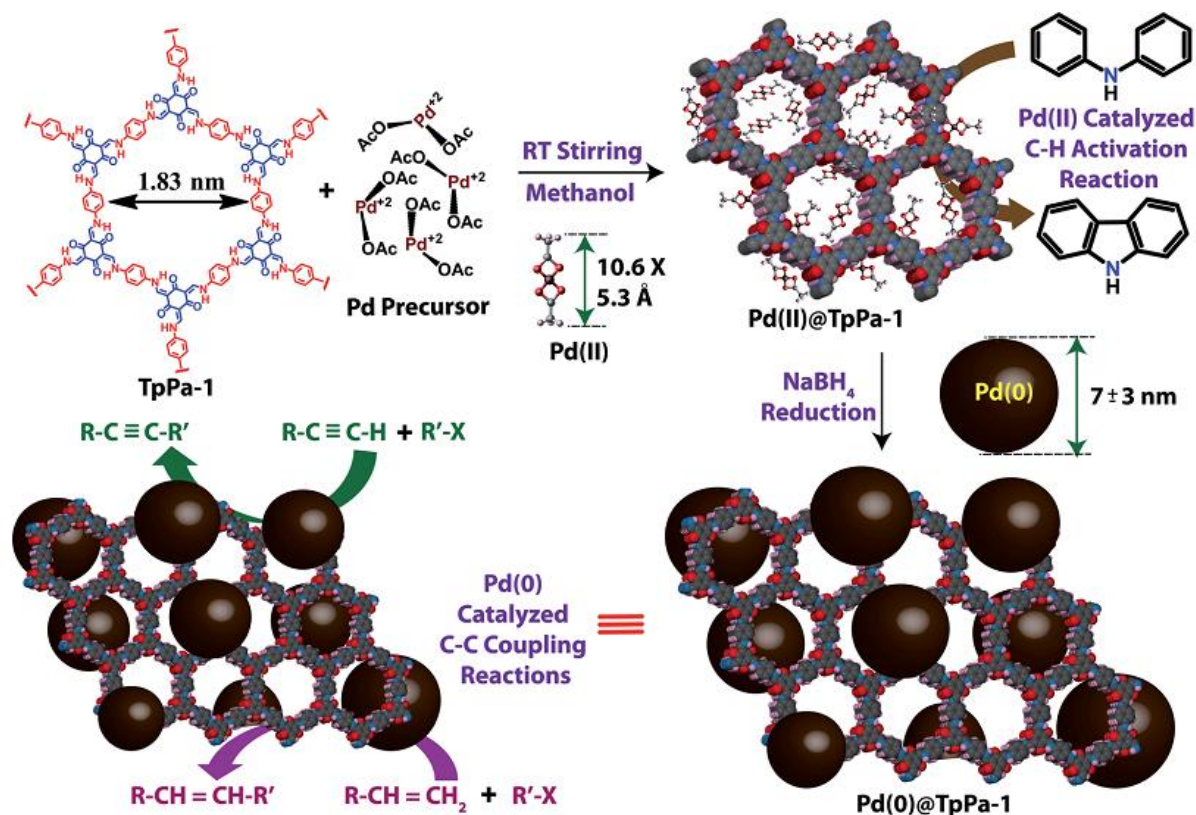


Figure 1.16: Synthesis of Pd nanoparticles on TpPa-1 COF via ex-situ process and applied for Sonogashira and Heck coupling reactions. Figures are reproduced with permission from RSC publications.

nanoparticles immobilized and resist from agglomeration process. The synthesized material Pd(0)@TpPa-1 has shown superior catalytic activity for Sonogashira and Heck coupling reactions compared to commercial Pd/C catalyst with broad substrates scope, and good recyclability [1.39].

1.9.2 Organocatalysis:

Base Functionalized COFs for Knoevenagel Condensation Reaction:

Prof. Yan and co-workers have synthesized BF-COF-1 and BF-COF-2 three dimensional COFs by reacting 1,3,5,7-tetraaminoadamantane (TAA) with 1,3,5-triformylbenzene (TFB) or triformylphloroglucinol (TFP) respective aldehydes (Figure 1.17). The synthesized COFs are basic in nature. Further, they have simulated the structure and have measured the microporous cavities for both the COFs. BF-COF-1 shows the diameter of 7.8 Å with the size of 7.8*11.3 Å² rectangular windows whereas in case of BF-COF-2 diameter is 7.7 Å with the size of 7.7*10.5 Å² rectangular windows. There they have observed that the cavity

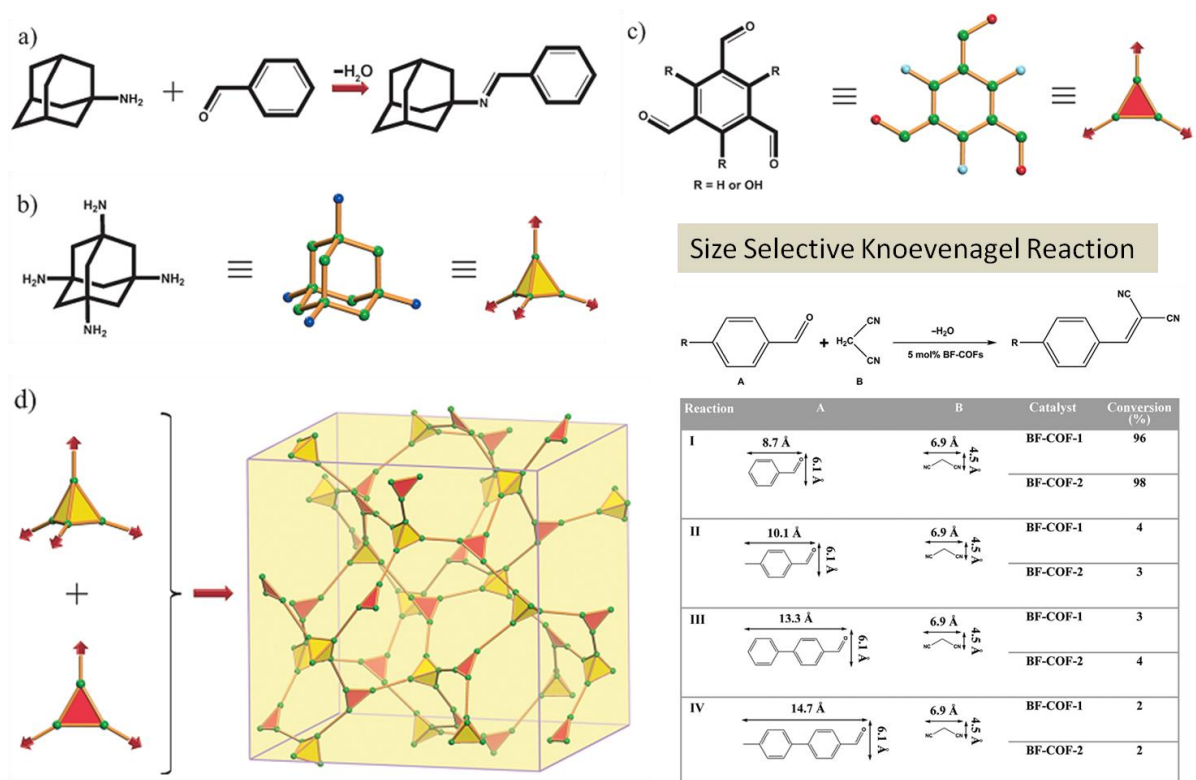


Figure 1.17: (a), (b), (c), (d) Schematic representation of the strategy for preparing 3D microporous base-functionalized COFs and applied in size selective Knoevenagel condensation reaction. Figures are reproduced with permission from Willey VCH publications.

plays an important role for size-selective Knoevenagel condensation reactions. The molecule having a size less than mentioned cavities has shown good reactivity with good selectivity. They have found that BF-COF-1 gave 96% and BF-COF-2 gave 98% conversion of benzaldehyde to a Knoevenagel condensed product whereas other aldehydes having bigger size compared to cavities size are failed to produce corresponding products [1.40].

Asymmetric Addition of Diethylzinc to Aromatic Aldehydes:

Synthesis of chiral COFs remains a great challenge. Prof. Cui and co-workers have reported 2D imine based enantiopure chiral CCOFs CCOF-1 and COF-2 respectively by reacting with tetraaryl-1,3-dioxolane-4,5-dimethanols (TADDOLs) derived enantiopure tetraaldehydes TTA or TTPA with 4,4'-diaminodiphenylmethane (4,4'-DADPM) in solvothermal method (Figure 1.18). Powder X-ray diffraction and computer modeling together with pore size distribution analysis showed that one COF has a twofold-interpenetrated grid-type network and the other has a non-interpenetrated grid network. The dihydroxy groups of TADDOLs react with $\text{Ti}(\text{O}^i\text{Pr})_4$ to produce Lewis acidic (TADDOLate) $\text{Ti}(\text{O}^i\text{Pr})_2$ compounds which are an effective heterogeneous catalyst for asymmetric addition of diethylzinc to aromatic aldehyde for enantioselective secondary alcohol production with 90% ee [1.41].

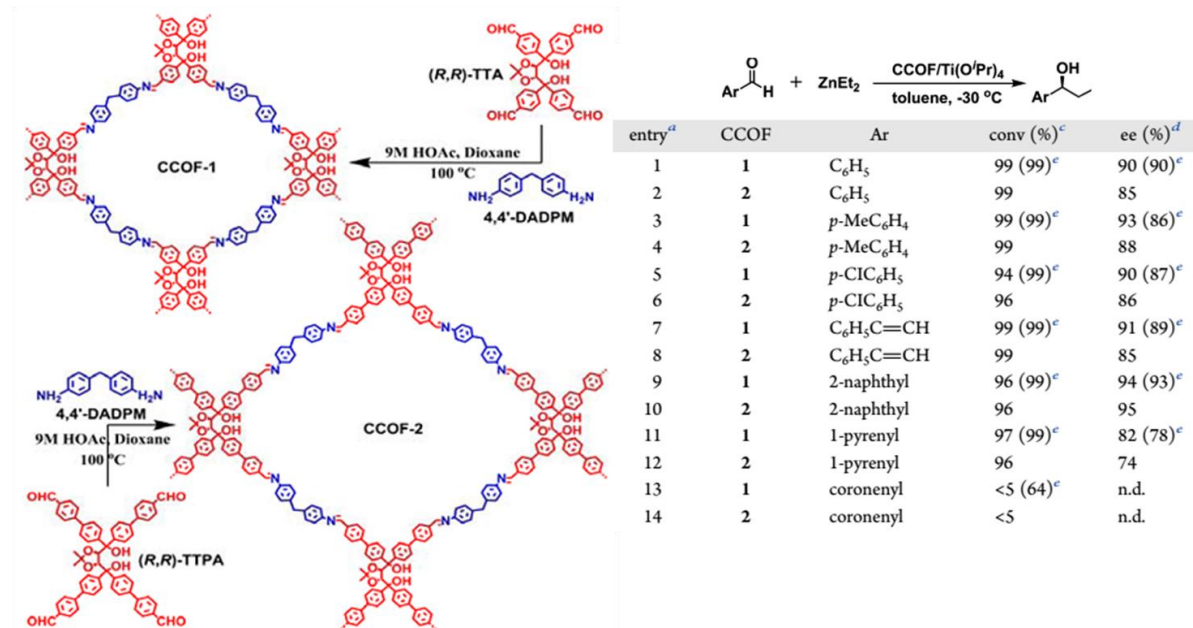


Figure 1.18: Schematic representation of chiral COFs synthesis and their asymmetric catalysis.

Figures are reproduced with permission from ACS publications.

Asymmetric Aldol Reaction:

Asymmetric catalysis is important in chemical and pharmaceutical industries for the production of enantiopure product formation. Therefore synthesizing of the porous chiral heterogeneous catalyst has drawn significant attention towards science community. COFs are interesting porous materials can be used for asymmetric catalysis. The incorporation of chiral moiety into the framework is done by post-synthesis methods. Asymmetric COFs synthesis *via* direct method from chiral building unit is challenging. Prof. Wan and co-workers have developed the synthesis of chiral COFs LZU-72 (imine based), LZU-76 (keto-enamine) from enantiopure building unit **3** (*S*)-4,4'-(2-(pyrrolidin-2-yl)-1*H*-benzo[*d*]imidazole-4,7-diyl)dianiline (Figure 1.19). As keto-enamine COFs are stable in acid water medium. Therefore they have successfully utilized COF LZU-76 for asymmetric aldol reaction with excellent enantioselectivity [1.42].

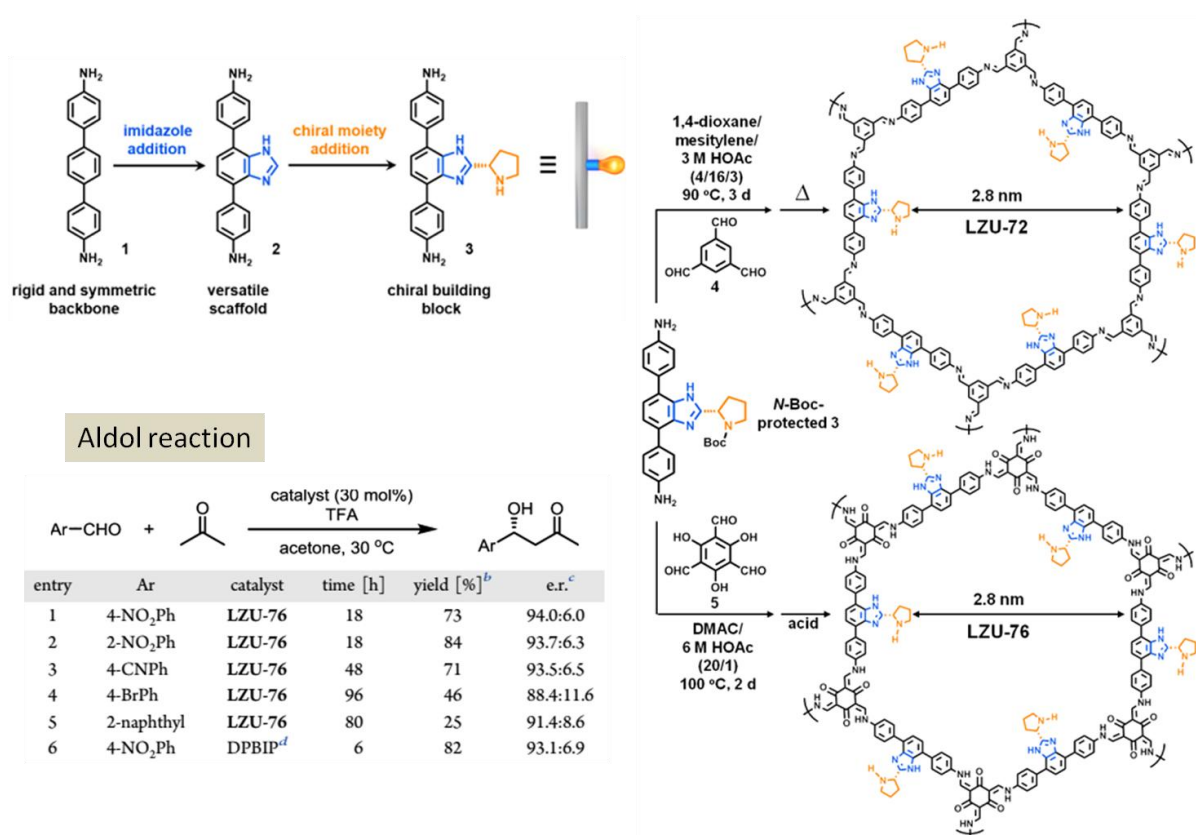


Figure 1.19: Schematic representation of preparing chiral COFs from chiral building unit for asymmetric aldol reaction. Figures are reproduced with permission from ACS publications.

1.9.3 Photocatalysis:

COFs Used for Photocatalytic Hydrogen Evolution Reaction:

The day by day increasing energy demand and the climate change due to the consumption of fossil fuels (limited) producing greenhouse gases are becoming a serious concern to the scientific community. Hence conversion of most abundant solar energy to renewable energy will be the most alternative approach. The lack of visible light absorption capability of the most common organic molecule becomes a major obstacle for utilization of visible light in the photocatalytic process. Therefore the criteria for good photocatalyst should be 1) it should absorb more light in the visible region, 2) should have proper band gap and position for splitting the water molecule, 3) should be stable and dispersive during the reaction. Prof. Lostz and co-workers have synthesized hydrazone based COFs by reacting with triphenylarylaldehydes with hydrazine. In the central aromatic ring, nitrogen is varied by replacing carbon atoms from 0-3. They have found that when central ring contains three

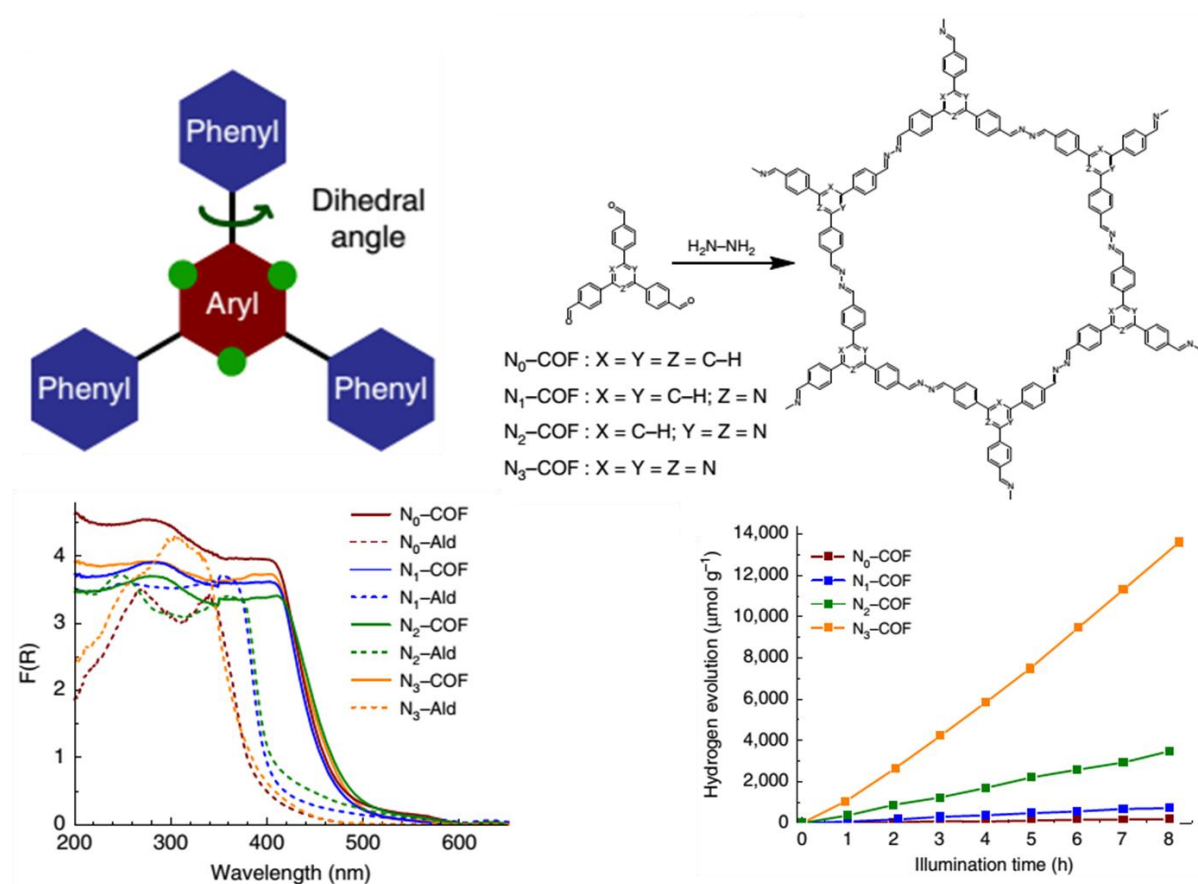


Figure 1.20: Schematic representation of a tunable triphenylarene based COFs for photocatalytic hydrogen evolution. Figures are reproduced with permission from Nature publications.

nitrogen atoms, the COF is in planer form. Therefore the conjugation inside the framework increases. Among other COFs three nitrogen-containing COFs in the central ring produces more hydrogen at 25 °C under visible light irradiation (≥ 420 nm) at pH 7 in PBS. During the process, Pt is used as co-catalyst and triethanolamine (TEOA) as a sacrificial electron donor [1.43].

Covalent organic frameworks can be used as a support to stabilize metal nanoparticles. Metal oxide and sulfide nanoparticles are well-known photocatalyst for photocatalytic hydrogen evolution reaction. The activity of the photocatalyst is increased when the nanoparticles are in a uniformly distributed form compared to bulk agglomerated form. Prof. Banerjee and co-workers have synthesized CdS nanoparticles on stable ketoenamine TpPa-2 COFs. The nanoparticles are well distributed into frameworks have been observed from TEM images and the particles size are in the range of 20-25 nm. The COF-nanoparticles hybrid material shows higher hydrogen production ($1320 \mu\text{molg}^{-1}\text{h}^{-1}$) compared to bulk CdS ($128 \mu\text{molg}^{-1}\text{h}^{-1}$)

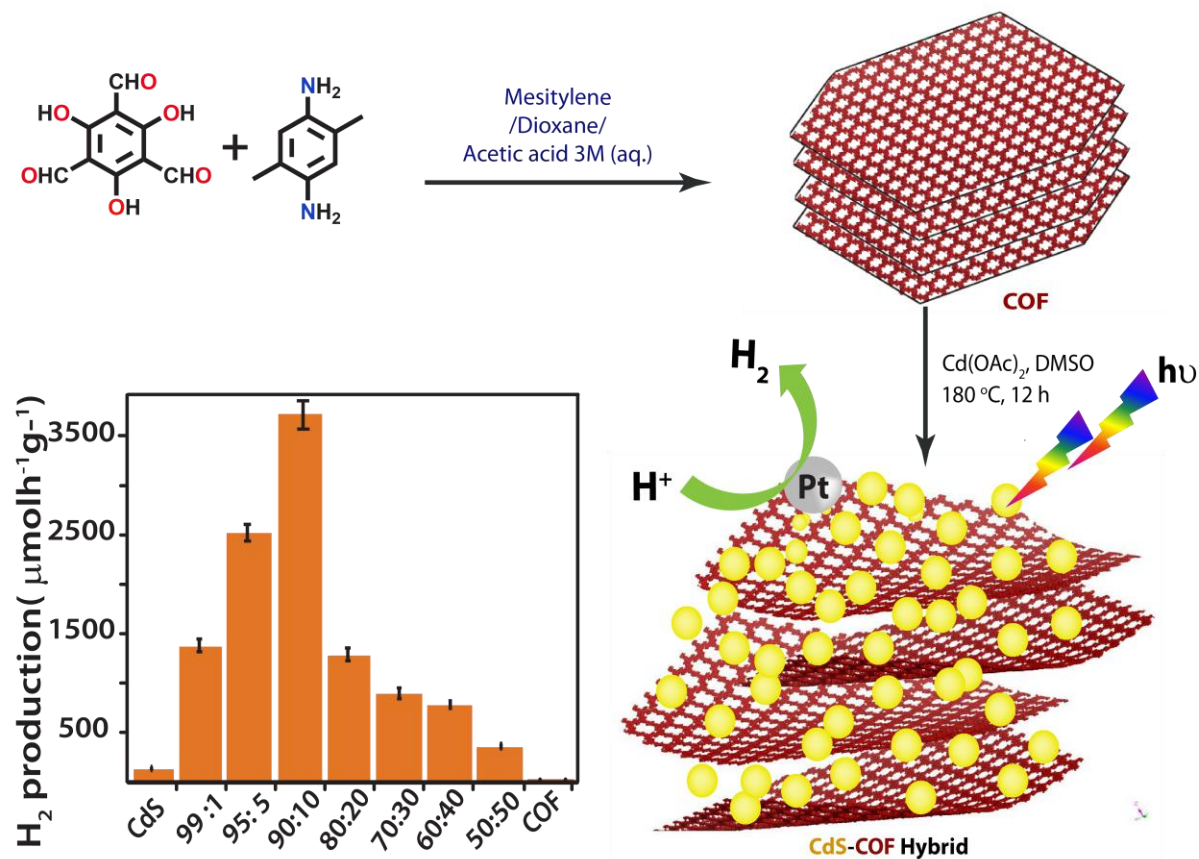


Figure 1.21: Schematic representation of a CdS loaded COF for photocatalytic hydrogen evolution. Figures are reproduced with permission from Willey VCH publications.

and only COF ($28 \mu\text{molg}^{-1}\text{h}^{-1}$) in presence of 0.5 wt% Pt co-catalyst and lactic acid under visible light irradiation ($\geq 420 \text{ nm}$) (Figure 1.21). Later they have prepared different wt% of CdS loaded COFs and found that 90:10 combination of COF and CdS have shown maximum hydrogen production activity ($3678 \mu\text{molg}^{-1}\text{h}^{-1}$) [1.44].

1.9.4 Electrocatalysis:

COFs Used for Electrocatalytic CO_2 Reduction:

Electrocatalytic conversion of CO_2 to value-added carbon product CO is becoming more interesting research area in terms of climate change and global energy demand. Electrocatalytic CO_2 reduction in a water medium is challenging because during the reaction proton reduction can also happen. The reason behind choosing water as solvent is that water is more abundant, cheap and environmentally friendly solvent. Therefore developing a suitable catalyst for CO_2 reduction is a challenging task keeping the proton reduction reaction optimum under the reaction condition. Prof. Yaghi and co-workers have synthesized cobalt porphyrin-based 2D imine COF-366-Co by reacting with 5,10,15,20-tetrakis(4-aminophenyl)porphyrato]cobalt [Co(TAP)] with 1,4-benzenedicarboxaldehyde (BDA). The

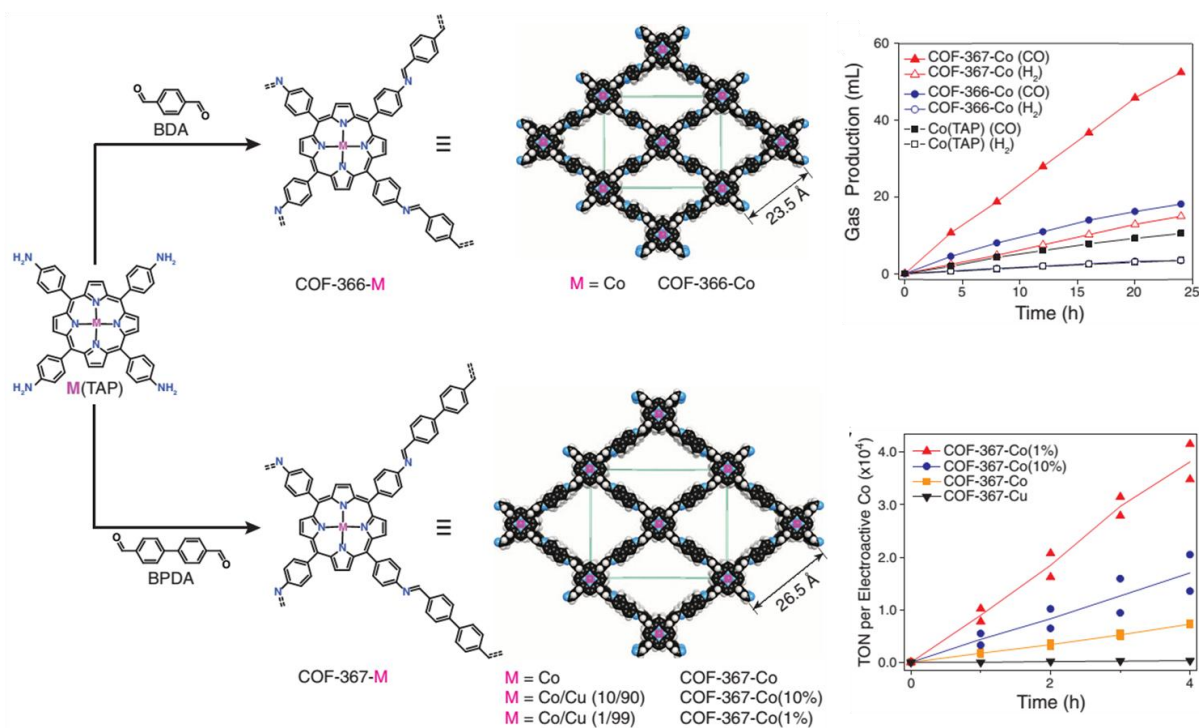


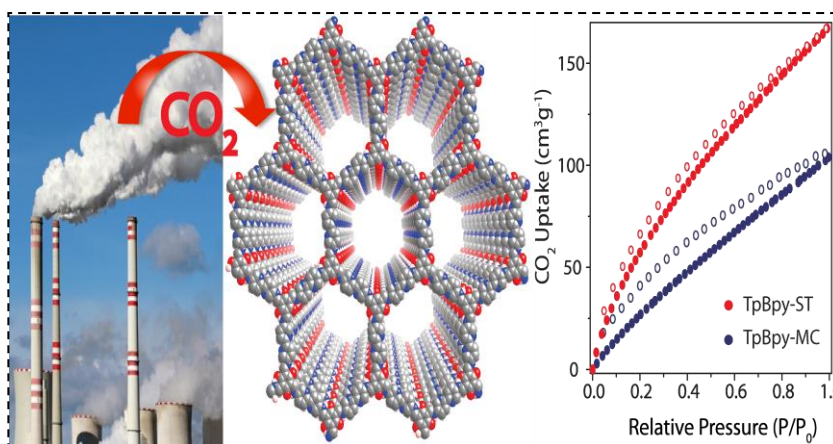
Figure 1.22: Design and synthesis of metalloporphyrin-derived 2D covalent organic frameworks for electrocatalytically CO_2 reduction. Figures are reproduced with permission from Science.

electrocatalysis is performed in carbon dioxide-saturated aqueous bicarbonate buffer (pH = 7.3) under applied potentials between -0.57 and -0.97 V (vs.RHE) and at -0.67 V COF-366-Co produces 36 mL carbon monoxide at STP after 24 h with TON 1352 (Figure 1.22). Simultaneously they have synthesized the extended COF-367-Co by increasing the linker length assuming that the bigger pores and the high surface area may uptake more CO₂ and will give more access to the all catalytically active centers to perform the reaction. They have found that bigger COF-367-Co produces more carbon monoxide 100 mL at STP after 24 h with TON 3901 at -0.67 V [1.45].

CHAPTER 2

Synthesis and Gas Adsorption Properties of a Stable Crystalline and Ultraporous Covalent Organic Framework with Bipyridyl Backbone

Abstract: Synthesizing porous nitrogen-rich heterogeneous materials are industrially important. The basic nature of the nitrogenous materials not only applicable for acidic greenhouse gas (CO_2) adsorption and separation (CO_2/N_2) but also applicable for stabilizing different metal nanoparticles for making heterogeneous catalyst, energy storing material and proton conducting material. Moreover, methods for synthesizing such materials are limited for bulk scale production. 2,2'-Bipyridine is a very good chelating



ligand for anchoring different metal ions and is applied for different catalytic organic transformation in homogeneous catalysis. Mechanochemistry is a greener, time-efficient, cost-effective and eco-friendly process for large-scale production. Therefore we have developed methods for synthesizing bipyridine based crystalline porous heterogeneous materials in solvothermal (**TpBpy-ST**) and mechanochemical process (**TpBpy-MC**). Both the materials are porous crystalline and have shown excellent gas uptake properties towards CO_2 , H_2 , and H_2O . Moreover, the materials are highly thermally as well as chemically (acid, base, and water medium) stable.

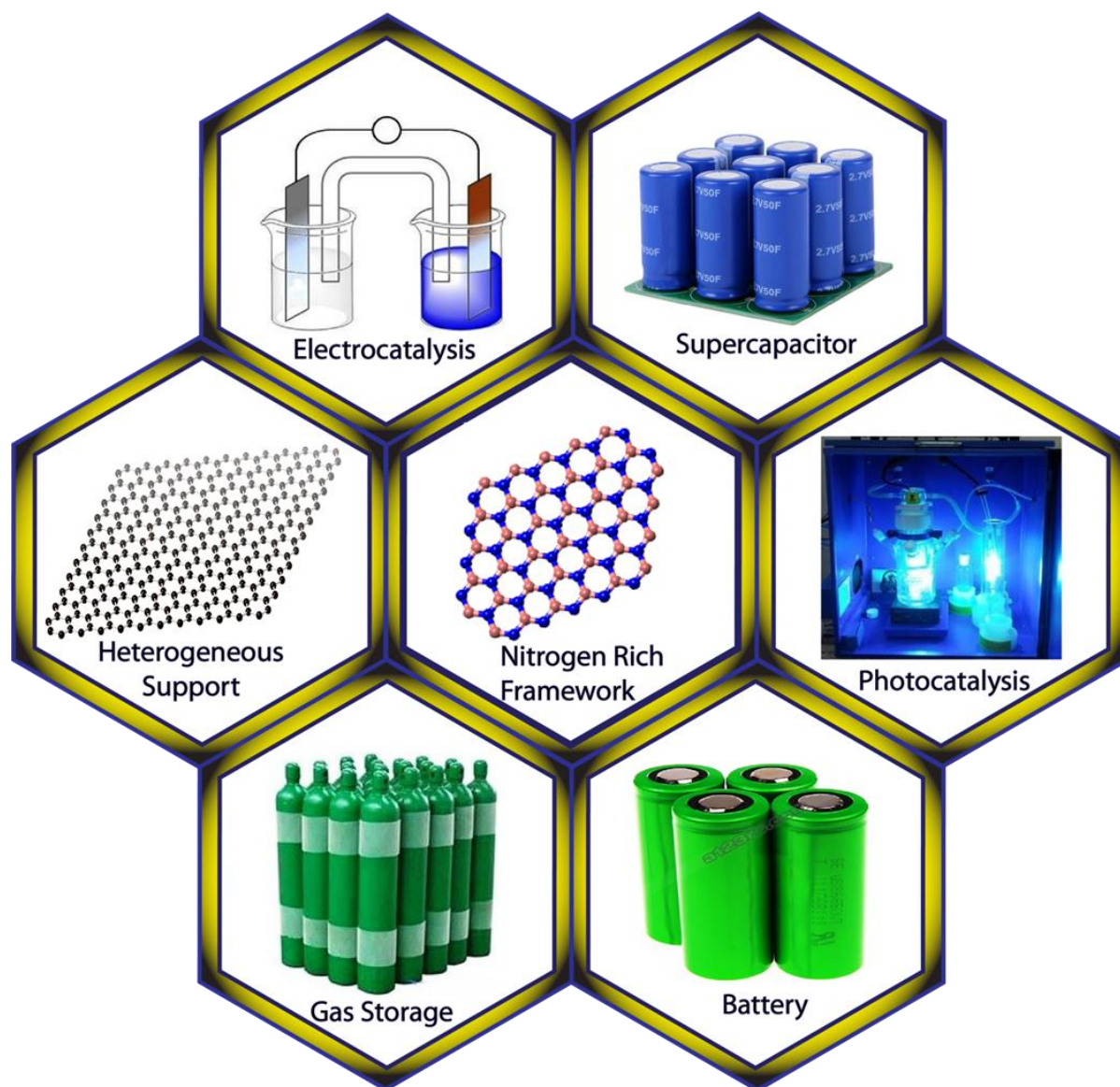
2.1 Introduction:

Catalyst makes our life easier. Today all pharmaceutical, petrochemical, automobile and chemical industries use catalysts for different chemical transformation and large-scale production [2.1]. Therefore the contribution of catalyst to the modern science is remarkable [2.2]. Although significant research has been done in homogeneous catalysis for synthesizing different catalysts and different organic reactions but high cost, miscible and unrecoverable nature of the catalyst makes them inappropriate for large-scale synthesis [2.3]. Therefore suitable method development for synthesizing heterogeneous catalyst is more important now a day. Previously porous carbon is used as a heterogeneous catalyst and heterogeneous support for different metal catalysts [2.4]. The low manufacturing cost, high surface area, good thermal conductivity and high pore volume make porous carbon as a promising heterogeneous candidate [2.5]. Commercially available Pd/C catalyst is one of the best examples in this category which is extensively used for carbon-carbon bond formation reaction, nitro reduction and hydrogenation reaction of olefin [2.6]. But microporous nature which restricts the mass transfer and absence of anchoring site in the material limit its application in stabilizing different metal nanoparticles. Therefore agglomeration, leaching and sintering of nanoparticles are observed in the repeated cycles which simultaneously decreases the formation of products also in the respective cycles [2.7]. Hence developing a method by modifying the material can solve the problem.

2.1.1 Importance of Nitrogen-Rich Porous Material:

The problem is overcome by introducing the heteroatom into the material. Among different heteroatom (B, N, S, F, P) nitrogen incorporating material shows better activity due to the change in electronic distribution in the material [2.8]. Also, the atomic radius of the nitrogen is similar to carbon which significantly reduces the lattice mismatch [2.9]. Moreover nitrogen has good chelating ability for different metal ion which is useful for stabilizing different metal nanoparticles to form uniform particles distribution all over the material [2.10]. The incorporation of nitrogen into the material also increases the overall thermal stability [2.11]. The basic nature of the nitrogen shows higher acidic gas (CO₂) uptake and selective CO₂/N₂ gas separation through the membrane [2.12]. Moreover, this material is useful for abstracting acidic protons which will help in proton conduction or as a useful membrane in a fuel cell. Nitrogen doping to the material makes the neighboring carbon

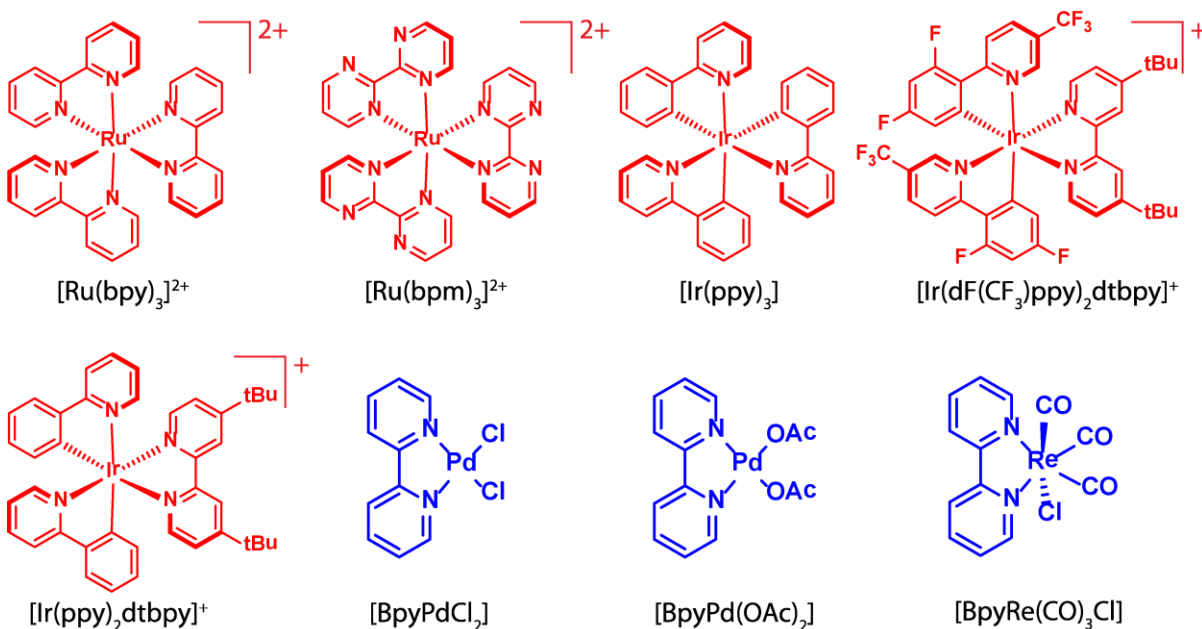
atoms more electron deficient as electronegativity of nitrogen is higher compared to carbon. Therefore it promotes more oxygen adsorption in to catalyst and applicable for oxygen reduction reaction (ORR) [2.13] in fuel cell and as an energy storage material (EDLC supercapacitor) [2.14] (Scheme 2.1). But the main drawback of this method is that finding the accurate position of the nitrogen after doping is more difficult due to the limited instrumental technique and huge defects in the material [2.15]. Therefore nitrogen-rich porous crystalline material design and synthesis from nitrogen-containing precursor will be the most alternative approach to sort out the problem.



Scheme 2.1: Different applications of the nitrogen-rich framework. Figures are taken from Google.

2.1.2 Importance of 2,2'-Bipyridine Ligand:

2,2'-Bipyridine is a good promising nitrogen-rich chelating ligand which can coordinate different metal centers through its nitrogen moieties present in the same side by forming five-member stable chelating complexes. In homogeneous catalysis, different bipyridine based metal complexes have already been synthesized and applied for Carbon-Hydrogen bond activation reaction and Carbon-Carbon bond formation reaction [2.16], carbon dioxide reduction [2.17], photocatalytic hydrogen evolution reaction and different photocatalytic organic transformation reactions [2.18] (Scheme 2.2).



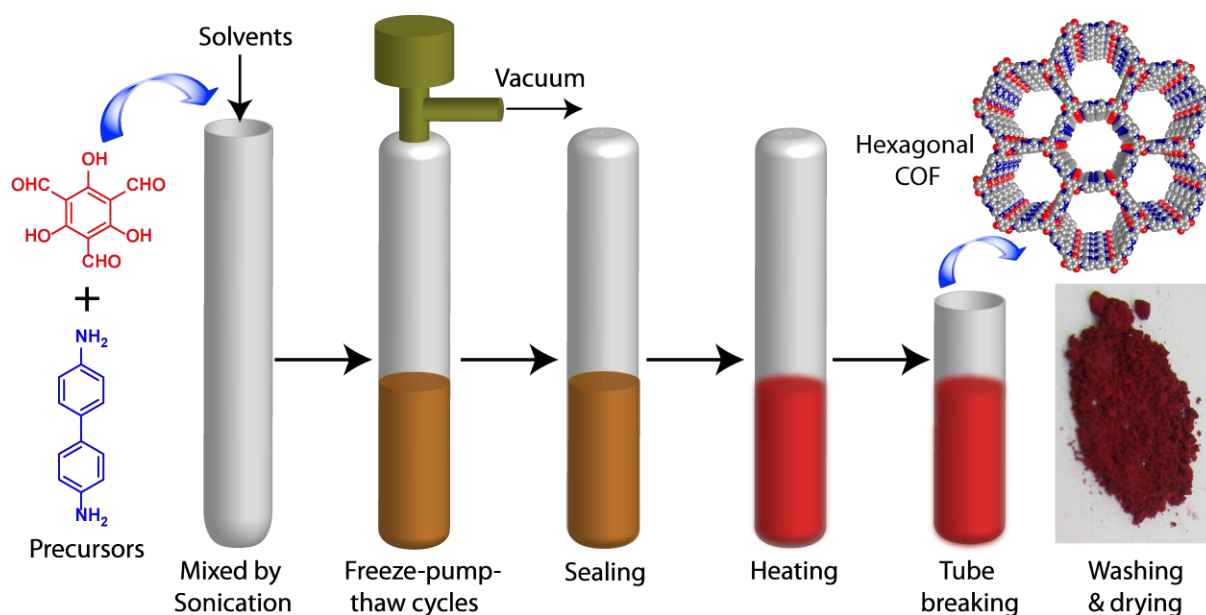
Scheme 2.2: Different 2,2'-bipyridine metal complexes are used for different catalytic applications.

Therefore synthesis of 2,2'-bipyridine based porous crystalline stable framework has drawn remarkable attention. Covalent organic frameworks are one kind of crystalline porous polymer constituted by repeating organic building blocks in a periodic manner. The frameworks are constituted by light elements like boron, carbon, oxygen, nitrogen, silicon and have uniform pore size [2.19]. The pore can be tuned by choosing proper organic linker and can be functionalized by varying different functional group in the linker using reticular chemistry which is quite difficult in case of zeolites and silica compounds. The different functionalized covalent organic frameworks have been applied to different applications like gas adsorption, drug delivery, sensing, supercapacitor and in the field of catalysis [2.20]. Different methods have been used for synthesizing covalent organic frameworks like

solvothermal [2.21], ionothermal [2.22], microwave [2.23] and layering methods [2.24]. Among them solvothermal gives a more crystalline porous covalent organic framework and been successfully used for different COF formation reaction.

2.1.3 The Drawbacks of Solvothermal Method for Synthesizing Covalent Organic Frameworks:

Among different methods solvothermal is utilized for different COFs formation purpose and it produces more crystalline and porous COFs compared to other methods. During this process, different solvent combinations are used to solubilize the starting materials partially and sealed glass/pyrex tubes are used to get more crystalline materials. Several steps are involved in this process:



Scheme 2.3: Schematic representation of solvothermal synthesis steps.

- 1) First starting materials are kept inside the glass tube and proper solvent combinations are used in presence of very catalytic amount acetic acid.
- 2) The reaction mixture is sonicated and degassed for 30 min and then the tube is properly closed and is flash frozen in liquid nitrogen.
- 3) Then the reaction mixture is kept in vacuum and freeze-pump-thaw cycles are continued for three times. After that, the tube is sealed in flame in presence of a vacuum.
- 4) Now the reaction mixture is allowed to reach room temperature and then it is kept in a hot air oven (90-120 °C) for 3-7 days in an undisturbed condition.

5) After 3-7 days the seal tube is broken and the phase pure material is washed with DMAc, water and acetone solvents to get pure COF material.

This whole process is time-consuming and is required special set up which is difficult to handle. Therefore this process is not suitable for bulk scale production of COF.

2.1.4 Statement of the Problem

As we have discussed that solvothermal is not suitable for large-scale production of COFs. Therefore developing a method which is cost effective, time efficient, easy to handle at room temperature in an open atmosphere without using special equipment is required for bulk scale production of COFs. The discovery of the mechanochemical process has drawn significant attention in chemical and pharmaceutical industries due to the greener, cleaner, safe, time efficient and eco-friendly process [2.25]. This process avoids of using plenty of solvents, heater, and stirrer for chemical transformation by simply replacing by using ball mills and mortar and pestle. This process is already applied for synthesizing industrially important zeolites and metal organic frameworks [2.26]. Therefore finding a suitable method for synthesizing COFs *via* mechanochemical process is industrially important for bulk scale production. It has been observed that using a small amount of solvent during the grinding process accelerates the reaction in a faster rate compared to net grinding. This process is often called as Liquid-Assisted Grinding (LAG) process in Mechanochemistry [2.27].

Keeping this idea in mind we have synthesized industrially important 2,2'-bipyridine based covalent organic frameworks in solvothermal and mechanochemical process. Also, we have thoroughly studied the change in physical and chemical properties of the materials synthesized using both the process.

2.2 Synthesis and Characterization

2.2.1 *TpBpy COF Synthesis via Solvothermal Process:*

A pyrex tube (o.d. \times i.d. = 18 \times 10 mm² and length 16 cm) is charged with 1,3,5-triformylphloroglucinol (**Tp**) (63.0 mg, 0.3) and 2,2'-bipyridine-5,5'-diamine (**Bpy**) (83.7 mg, 0.45 mmol) and 4.5 mL of dimethylacetamide (DMAc) and 1.5 mL of o-dichlorobenzene (o-DCB), 0.6 mL of 6.0 M aqueous acetic acid (AcOH). This mixture is sonicated for 10-15 minutes in order to get a homogenous dispersion. The tube is flash frozen at 77 K (liquid N₂ bath) and degassed by three freeze-pump-thaw cycles. Then the tube is sealed off and is

heated at 120 °C for 3 days. A dark red colored precipitate formed is collected and washed with dimethylacetamide (DMAc), water and then acetone. The collected powder is solvent exchanged with acetone three times and dried at 150 °C under vacuum for 24 h to give a dark red colored powder in ~ 79 % isolated yield (**TpBpy-ST**) (Figure 2.1). The elemental micro analysis (C, N, H) of the **TpBpy-ST**, the experimental data are very well matched with the theoretical one, indicating the purity of the material. **IR (powder, cm⁻¹):** 1607, 1579, 1458, 1397, 1270, 1095, 992, 826, 732, 640. **Elemental Analysis;** Anal. Calcd. For C₈H₆N₂O: C, 65.75; H, 4.14; N, 19.17; found: C, 66.84; H, 4.21; N, 18.69.

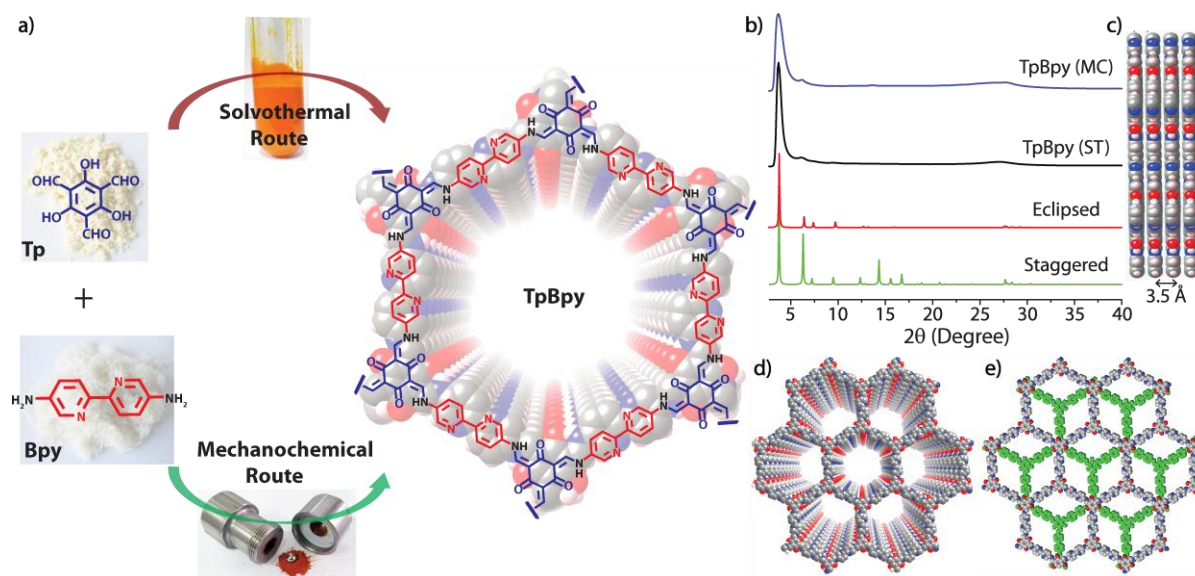


Figure 2.1: (a) Schematic representation of solvothermal (ST) and mechanochemical (MC) synthesis of **TpBpy** COF. (b) Comparison of the experimental PXRD patterns of **TpBpy-MC** (blue), **TpBpy-ST** (black) with the simulated eclipsed (red) and staggered (green). (c),(d) Space-filling AA eclipsed stacking models of **TpBpy** along a and c direction. (e) Space-filling staggered stacking models of **TpBpy** along c direction.

2.2.2 **TpBpy** COF Synthesis via Solvent-Assisted Mechanochemical Process:

1,3,5-triformylphloroglucinol (**Tp**) (63.0 mg, 0.3) and 2,2'-bipyridine-5,5'-diamine (**Bpy**) (83.7 mg, 0.45 mmol) are placed in a 5 mL stainless steel jar, with one 7 mm diameter stainless steel ball the addition of ~60 μL of DMAc, ~30 μL of o-DCB and ~15 μL of 6 M acetic acid. The synthesis of **TpBpy-MC** has been done at different ball milling time and frequency (Table 2.1) and found optimized process grinding for 90 min at 30 Hz gives the highest surface area and yield of the product compared to other mechanochemical processes.

Then the ground material is washed with minimal amount of DMAc followed by water and acetone. Then the powder is dried at 150 °C under vacuum for 24 h to get a red colored powder in 84 % isolated yield (**TpBpy-MC**) (Figure 2.1). **IR (powder, cm⁻¹):** 1607, 1579, 1458, 1397, 1270, 1095, 992, 826, 732, 640. **Elemental Analysis;** Anal. Calcd. For C₈H₆N₂O: C, 65.75; H, 4.14; N, 19.17; found: C, 66.84; H, 4.21; N, 18.69.

Table 2.1 Optimization table for the synthesis of TpBpy-MC at different milling frequency and time.

Condition	Time (min)	Frequency (Hz)	Yield (%)	BET Surface Area (m ² g ⁻¹)
LAG	30	30	52	59
LAG	60	30	76	219
LAG	90	30	84	293
LAG	120	30	84	293
LAG	120	20	68	156
NEAT	120	30	72	72

2.2.3 Synthesis of 2,2'-bipyridine-5,5'-diamine (**Bpy**):

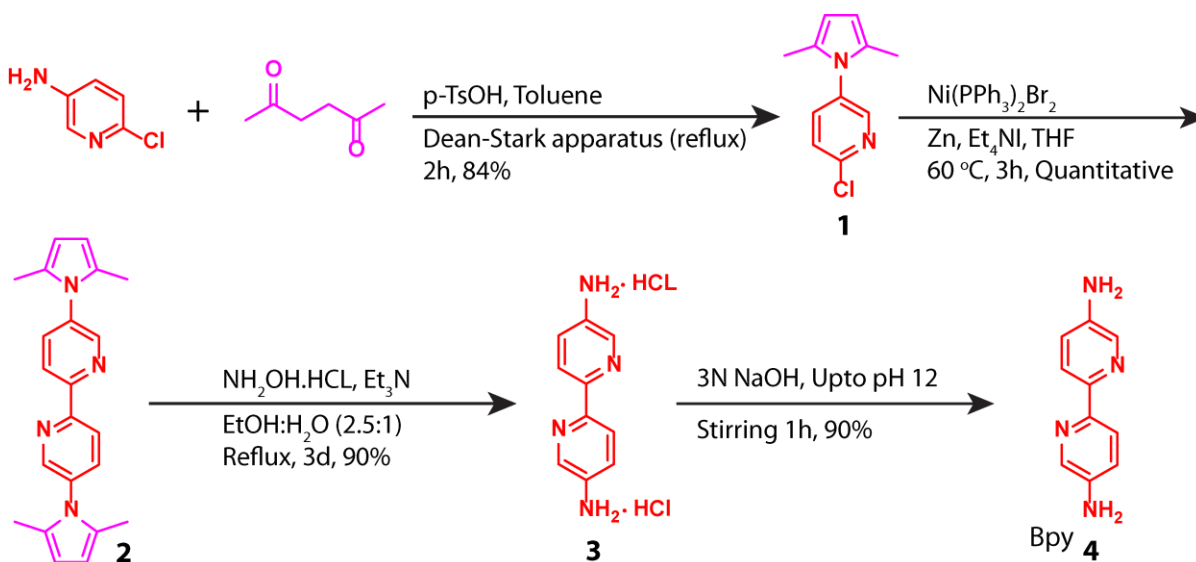


Figure 2.2: General synthetic scheme for the preparation of 2,2'-bipyridine-5,5'-diamine (**Bpy**).

1,3,5-triformylphloroglucinol (**Tp**) was synthesized using a previously reported method and confirmed by IR, ¹HNMR, and ¹³CNMR [2.28].

As shown in Figure 2.2, the compounds, 1-(2-Chloropyridine-5-yl)-2,5-dimethyl-1H-pyrrole (**1**), 5,5'-Bis(2,5-dimethyl-1H-pyrrole)-2,2'-bipyridine (**2**), and 2,2'-bipyridine-5,5'-diamine (**Bpy**) are synthesized using previously reported methods and confirmed by IR, ¹HNMR, and ¹³CNMR [2.29].

2.2.4 Synthesis of 5-amino-2,2'-bipyridine:

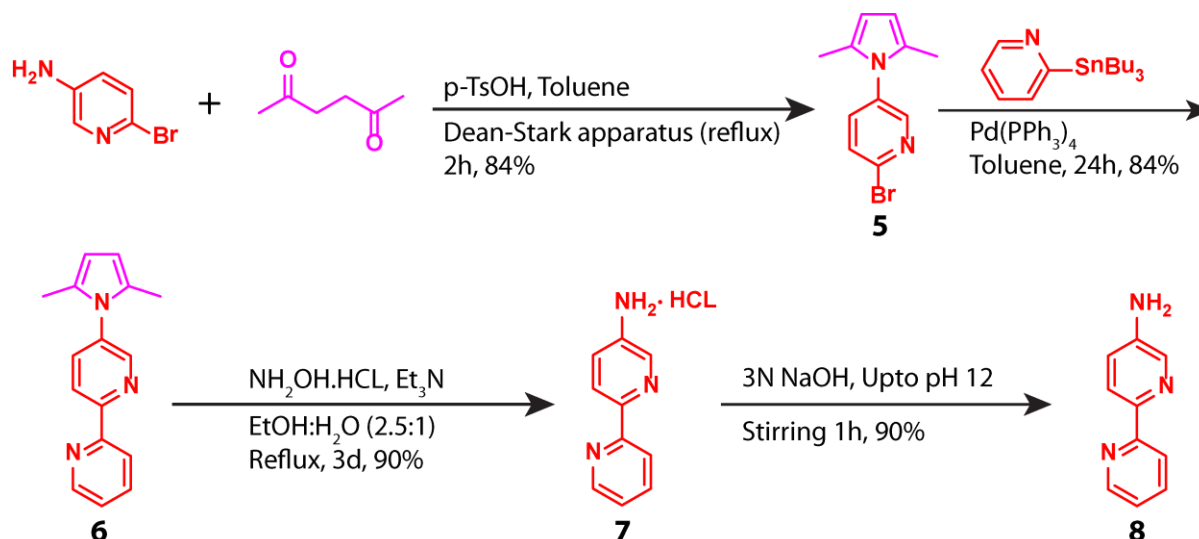


Figure 2.3: General synthetic scheme for the preparation of 5-amino-2,2'-bipyridine.

These compounds in Figure 2.3 1-(2-Bromopyridine-5-yl)-2,5-dimethyl-1H-pyrrole (**5**), 1-(2,2'-Bipyridine-5-yl)-2,5-dimethyl-1H-pyrrole (**6**) and 5-Amino-2,2'-bipyridine (**8**) are synthesized using reported methods and confirmed by IR, ¹HNMR, and ¹³C NMR [2.29].

2.2.5 Monomer (2E,4E,6E)-2,4,6-tris([(2,2'-bipyridin]-5-yl-amino)methylene)cyclohexane-1,3,5-trione Synthesis:

The monomer is synthesized by the reaction between 1,3,5-triformylphloroglucinol (**Tp**) (0.105 g, 0.5 mmol) and 5-Amino-2,2'-bipyridine (0.370 g, 2.0 mmol) in 25 mL of ethanol under refluxing condition for 48 h. The solution is cooled to room temperature and the precipitate is collected by filtration, washed with copious amount of ethanol, and finally dried under vacuum to give 0.274 g (82%) of a yellow solid (Figure 2.4). **IR (powder, cm⁻¹):** 1610, 1565, 1447, 1396, 1207, 1095, 991, 826, 731, 640. **¹H NMR (300 MHz, CDCl₃):** δ = 13.80 (d, *J* = 12.3 Hz, 1H), 13.60 (d, *J* = 12.3 Hz, 2H), 13.19 (d, *J* = 12.3 Hz, 3H), 9.95 (d, *J* = 12.3 Hz, 3H), 8.92 (d, *J* = 12.3 Hz, 1H), 8.78 (d, *J* = 12.3 Hz, 2H), 8.62-8.60 (m, 6H), 8.42-8.40 (m, 6H), 7.90-7.73 (m, 24H), 7.27-7.42 (m, 6H).

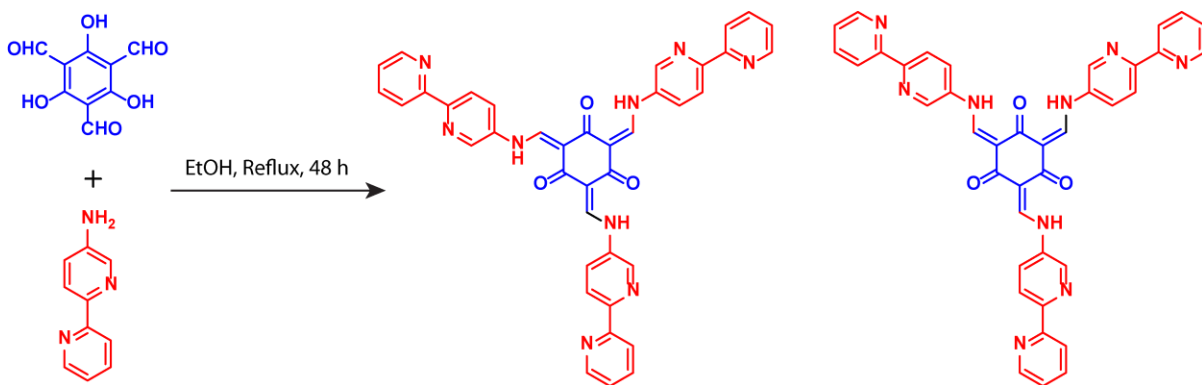


Figure 2.4: General synthetic scheme for the preparation of monomer.

2.2.6 Structural Simulation and Characterization

The crystallinity of the synthesized **TpBpy-ST** and **TpBpy-MC** are investigated by PXRD analysis. The high crystallinity of **TpBpy-ST** is observed from intense peak arise at 3.6° (2θ). This intense peak corresponding to the reflection from 100 planes. The other minor peaks appear at 6.0° , 6.9° , 9.2° , 12.1° , 12.5° , 15.2° and 25.1 - 28.6° (2θ). The peak at $2\theta = 25.1$ - 28.6° corresponding to the reflection of 001 planes indicates the presence of π - π stacking between the 2D COF layers. The d -spacing between the COF layers is 3.5 \AA . The similar pattern is also observed in the case of **TpBpy-MC**. But the intensity of the first peak corresponding to the reflection of 100 planes is lower in this case compared to the solvothermal method. This indicates that the loss of crystallinity is due to random displacement of COF layers for continuous applying mechanical force during the synthesis. Therefore the layers are formed during this process are not fully eclipsed. The peak appears at higher 2θ value 26° is corresponding to the reflection of 001 planes indicates the presence of π - π stacking between the 2D COF layers.

In order to find out a reasonably fitting modeled structure of **TpBpy-ST** and **TpBpy-MC**, several stacking possibilities such as AA eclipsed and AB staggered are constructed using Material Studio-6.1 software. The simulated structure of the eclipse model is well matching with the experimental PXRD pattern of both the COFs. The eclipse models of **TpBpy-ST** and **TpBpy-MC** are simulated in $P6/m$ space group. To determine the exact unit cell parameter we have performed Pawley refinement. After refinement the final unit cell values are $a = b = 29.3 \text{ \AA}$, $c = 3.5 \text{ \AA}$, $\alpha = \beta = 90^\circ$, $\gamma = 120^\circ$ with $R_p = 5.2\%$ and $R_{wp} = 1.9\%$ for

TpBpy-ST (Figure 2.5a) and with $R_p = 8.8\%$ and $R_{wp} = 5.0\%$ for **TpBpy-MC** (Figure 2.5b and Table 2.2).

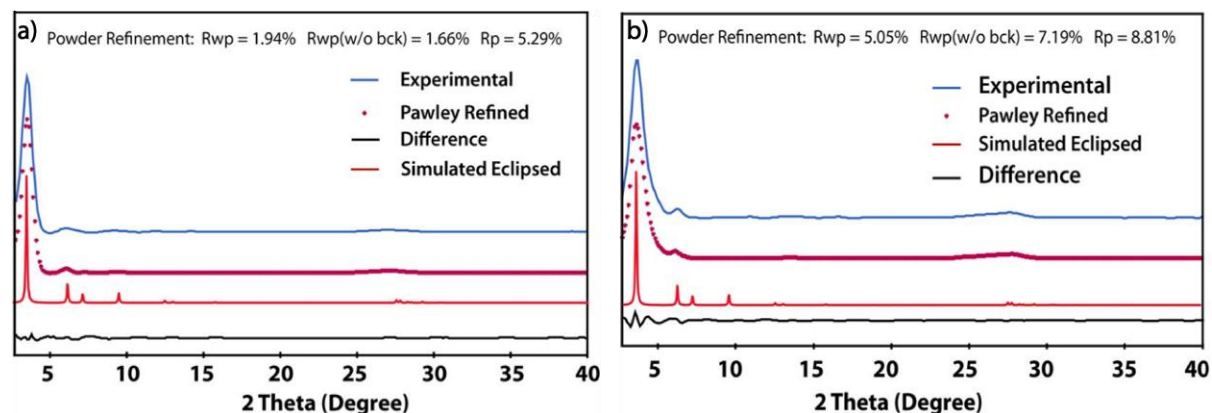


Figure 2.5: (a) Comparison of the PXR D pattern of experimental **TpBpy-ST** (blue) and simulated (red) **TpBpy-ST** in eclipsed stacking mode. Difference plot is depicted in black line. Pawley refinement demonstrates good agreement between experimental and simulated eclipsed PXR D pattern (R_{wp} : 1.94%, R_p : 5.29%). (b) Comparison of PXR D pattern of experimental **TpBpy-MC** (blue) and simulated (red) **TpBpy-MC** in eclipsed stacking mode. Difference plot is depicted in black line. Pawley refinement demonstrates good agreement between experimental and simulated eclipsed PXR D pattern (R_{wp} : 5.05%, R_p : 8.81%).

Table 2.2 Fractional atomic coordinates for the unit cell of **TpBpy-(ST/MC)** (Eclipsed)

TpBpy							
Hexagonal, $P6/m$							
$a = b = 29.3 \text{ \AA}$, $c = 3.5 \text{ \AA}$							
$\alpha = \beta = 90$, $\gamma = 120$							
C1	0.51519	0.49086	0.47194	N2	0.61501	0.42795	0.46881
C2	0.56958	0.52323	0.46886	C6	0.63085	0.35423	0.46981
C3	0.60194	0.50122	0.46782	C7	0.59597	0.37453	0.47085
C4	0.57993	0.44683	0.46986	C8	0.61035	0.29759	0.47184
C5	0.52555	0.41446	0.47293	O1	0.55671	0.26495	0.47492
N1	0.49318	0.43648	0.47397				

2.2.7 Chemical Characterization

The formation of enol to keto tautomerized **TpBpy-(ST/MC)** covalent organic frameworks are investigated by FT-IR and ^{13}C CP-MAS solid-state NMR spectra. The FT-IR

spectra of **TpBpy-(ST/MC)** show the consumption of starting materials. The characteristics stretching band -C=O (1637 cm^{-1}) of 1,3,5-triformylphloroglucinol (**Tp**) and -N-H ($3317\text{-}3112\text{ cm}^{-1}$) stretching band of 2,2'-bipyridine-5,5'-diamine (**Bpy**) are totally disappeared. In addition, the new intense peaks arise at 1608 cm^{-1} (-C=O) and 1579 cm^{-1} (-C=C) indicate the formation of the most stable keto structure (Figure 2.6) which are exactly matching with the synthesized enol-keto tautomerized monomer also. Here the -C=O peak at 1608 cm^{-1} of **TpBpy-ST** is merged with -C=C peak at 1579 cm^{-1} .

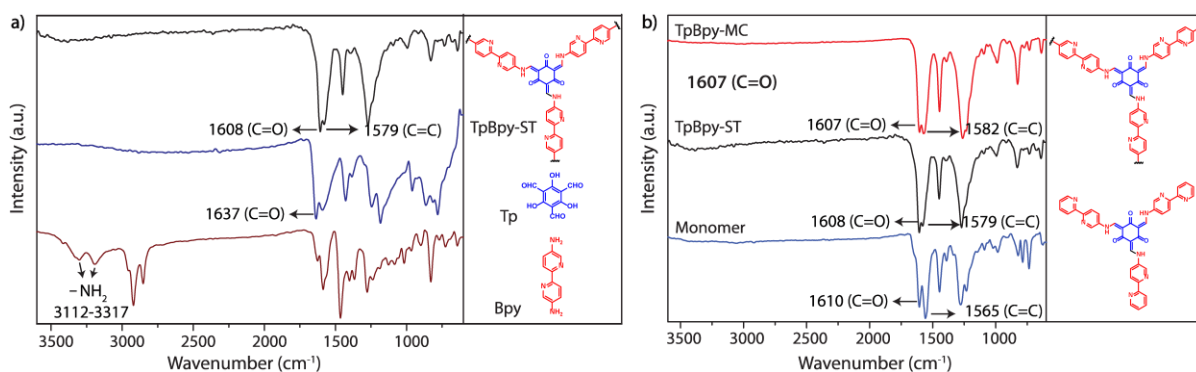


Figure 2.6: (a) FTIR spectra of **Bpy** (brown), **Tp** (blue) and **TpBpy-ST** (black). (b) FTIR spectra of **Monomer** (blue), **TpBpy-ST** (black) and **TpBpy-MC** (red).

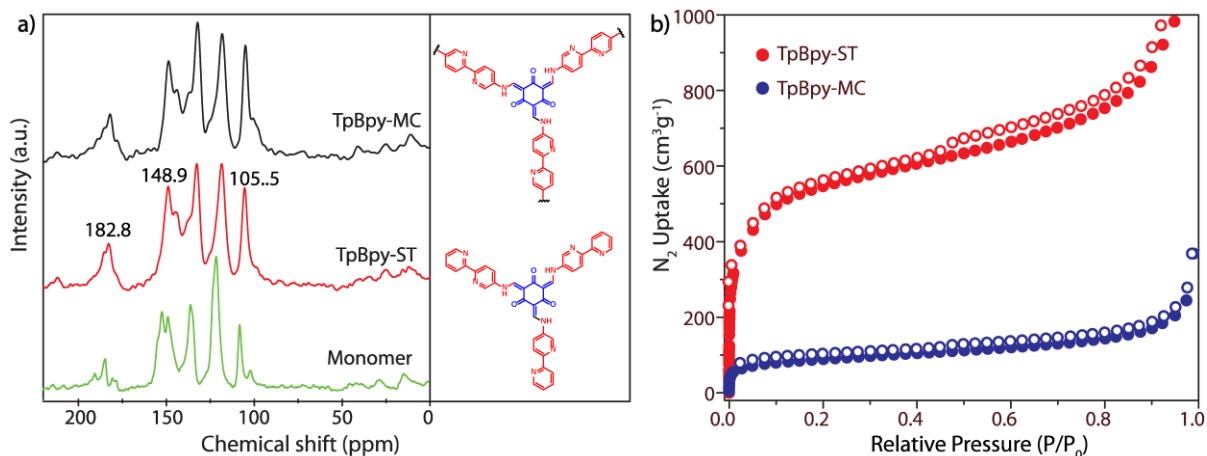


Figure 2.7: (a) Comparison of solid state ^{13}C NMR spectra of **Monomer** (green) **TpBpy-ST** (red) and **TpBpy-MC** (black). (b) Comparison of N_2 adsorption isotherm of **TpBpy-ST** (red) and **TpBpy-MC** (blue).

The ^{13}C CP-MAS solid-state NMR of **TpBpy-MC**, **TpBpy-ST**, and **Monomer** are performed. The signal appears at 182.8 ppm in case of **TpBpy-ST** and 181.5 ppm for **TpBpy-MC** are corresponding to carbonyl (-C=O) carbon which appears at 181.2 ppm in

case of synthesized enol keto tautomerized **Monomer** also. The remaining sp^2 carbons appear in the aromatic region (Figure 2.7a).

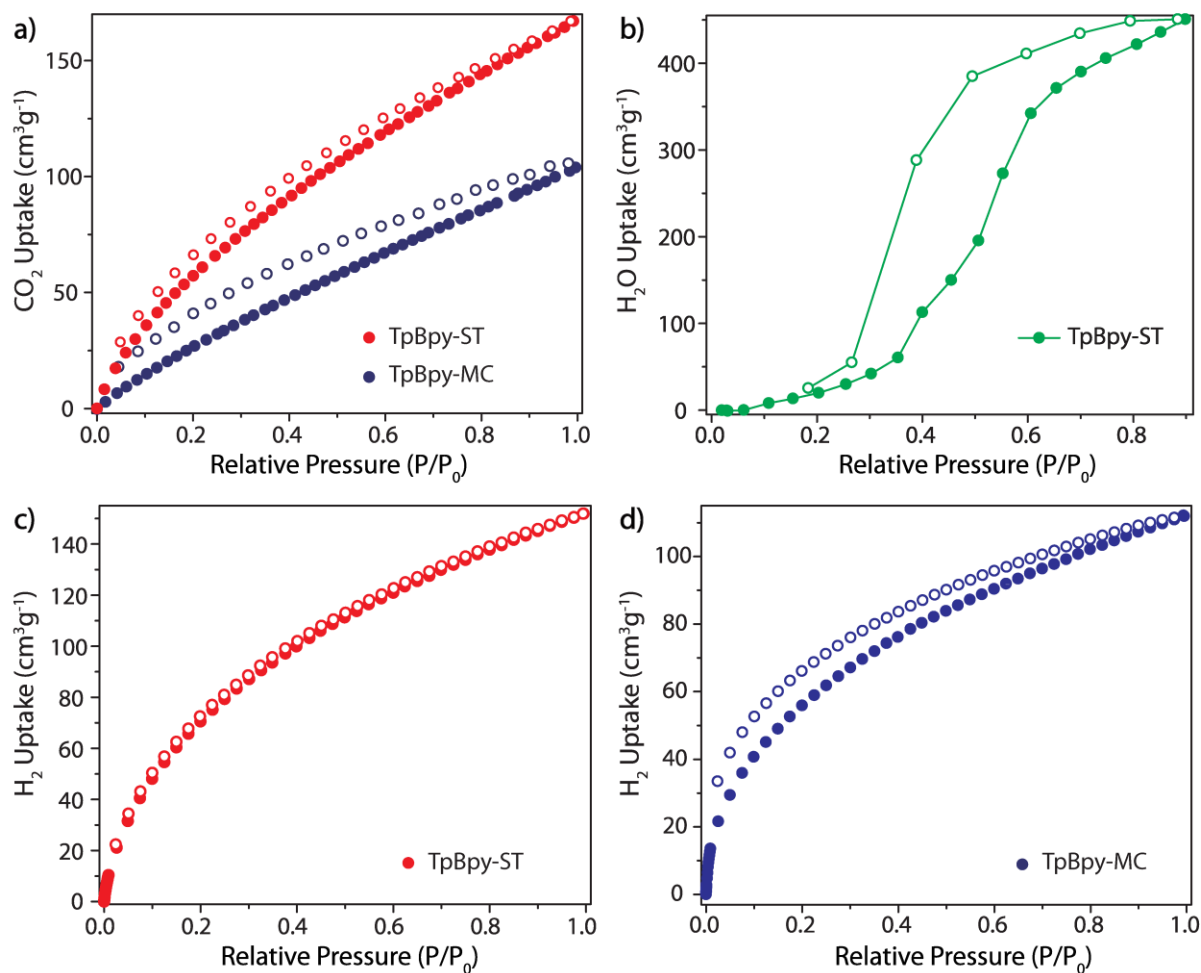


Figure 2.8: Gas uptake properties of **TpBpy-ST** and **TpBpy-MC**. (a) CO₂ adsorption isotherm of **TpBpy-ST** (red) and **TpBpy-MC** (blue) at zero degree. (b) Water adsorption isotherm of **TpBpy-ST**. (c), (d) H₂ adsorption isotherm of **TpBpy-ST** (red) and **TpBpy-MC** (blue).

We have carried out N₂ adsorption isotherm of activated **TpBpy-ST** and **TpBpy-MC** at 77K to evaluate permanent porosity of the respective COFs. Both the COFs show type IV reversible N₂ adsorption isotherm. The Brunauer–Emmett–Teller (BET) surface areas of **TpBpy-ST** and **TpBpy-MC** are found to be 1746 and 293 m²g⁻¹ respectively (Figure 2.7b). The decrease of surface area in case of **TpBpy-MC** is higher compared to **TpBpy-ST** is due to random displacement of COF sheet layers for continuous applying mechanical force during the synthesis. Therefore the layers are formed during this process are not fully eclipsed or perfectly ordered which is supporting the broadness of first 100 peak appeared in

PXRD pattern for **TpBpy-MC**. Also, we have performed the CO₂, H₂O and H₂ uptake study for both the COFs. The materials have shown high CO₂ uptake 165 cc/g for **TpBpy-ST** and 95 cc/g for **TpBpy-MC** respectively at 0 °C 1 atm pressure (Figure 2.8a). The water uptake properties of both the COFs have been measured and have shown 450 cc/g water uptake for

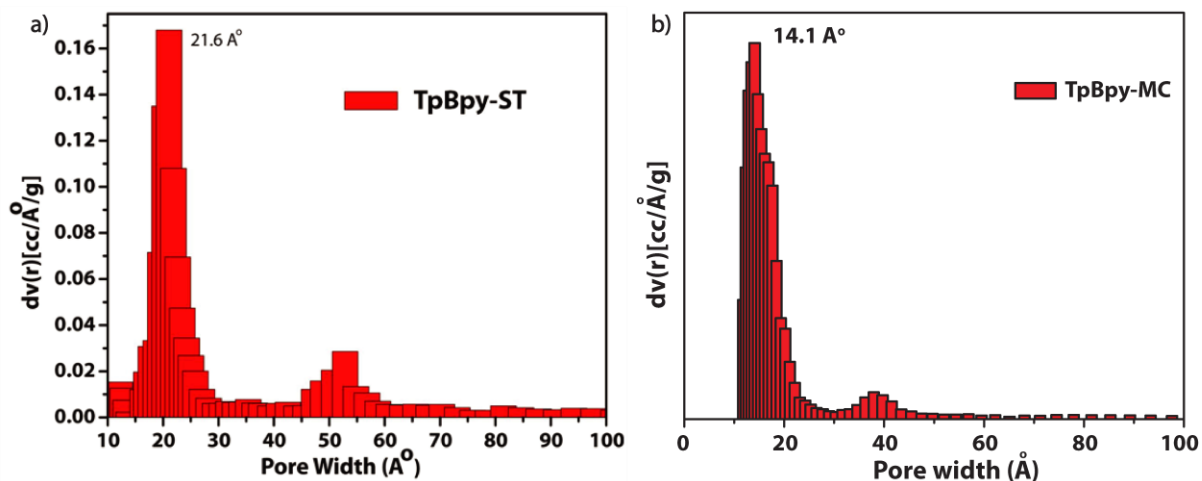


Figure 2.9: (a), (b) Experimental pore size distributions of **TpBpy-ST** and **TpBpy-MC** respectively calculated using NLDFT model.

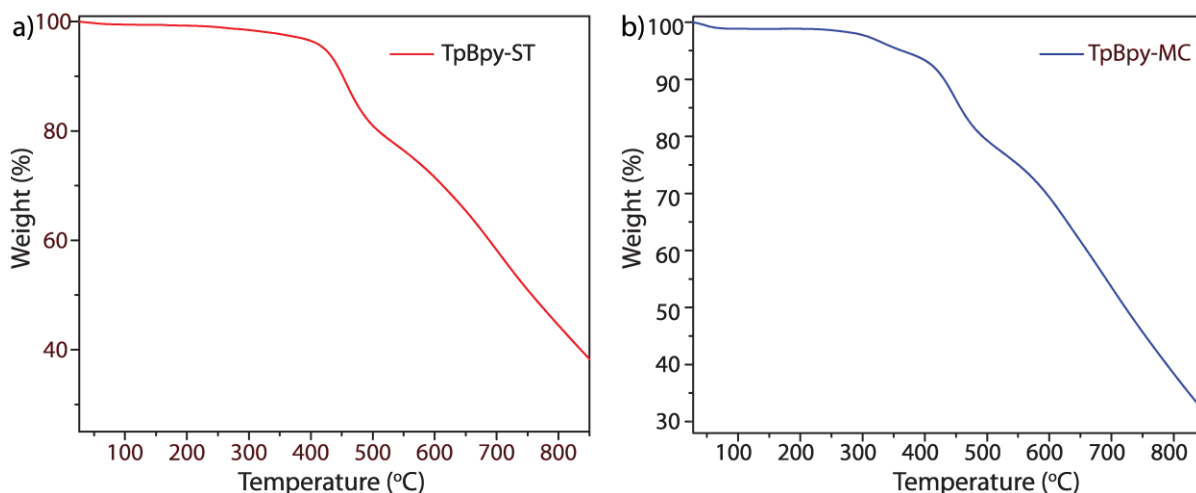


Figure 2.10: (a) TGA spectra of **TpBpy-ST** (red). (b) TGA spectra of **TpBpy-MC** (blue).

TpBpy-ST and 260 cc/g water uptake for **TpBpy-MC** respectively at 1atm pressure (Figure 2.8b). The hydrogen uptake properties for **TpBpy-ST** and **TpBpy-MC** are 150 cc/g and 115 cc/g respectively at 77 K 1atm pressure (Figure 2.8 c,d). The pore size distribution is measured on the basis of nonlocal density functional theory (NLDFT) which shows the narrow pore size distribution in the range of 2.1 nm for **TpBpy-ST** and 1.4 nm for **TpBpy-MC** (Figure 2.9).

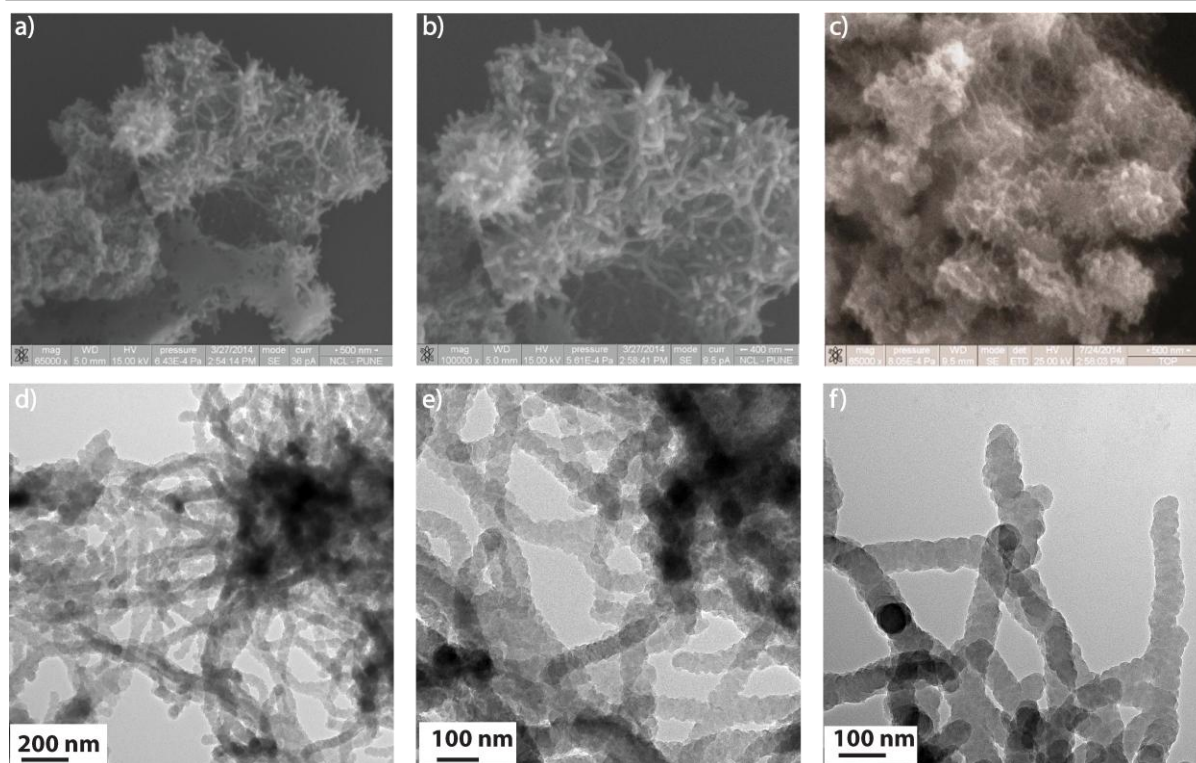


Figure 2.11: (a), (b), (c) SEM images and (d), (e), (f) TEM images of **TpBpy-ST** showing interwoven thread like morphology.

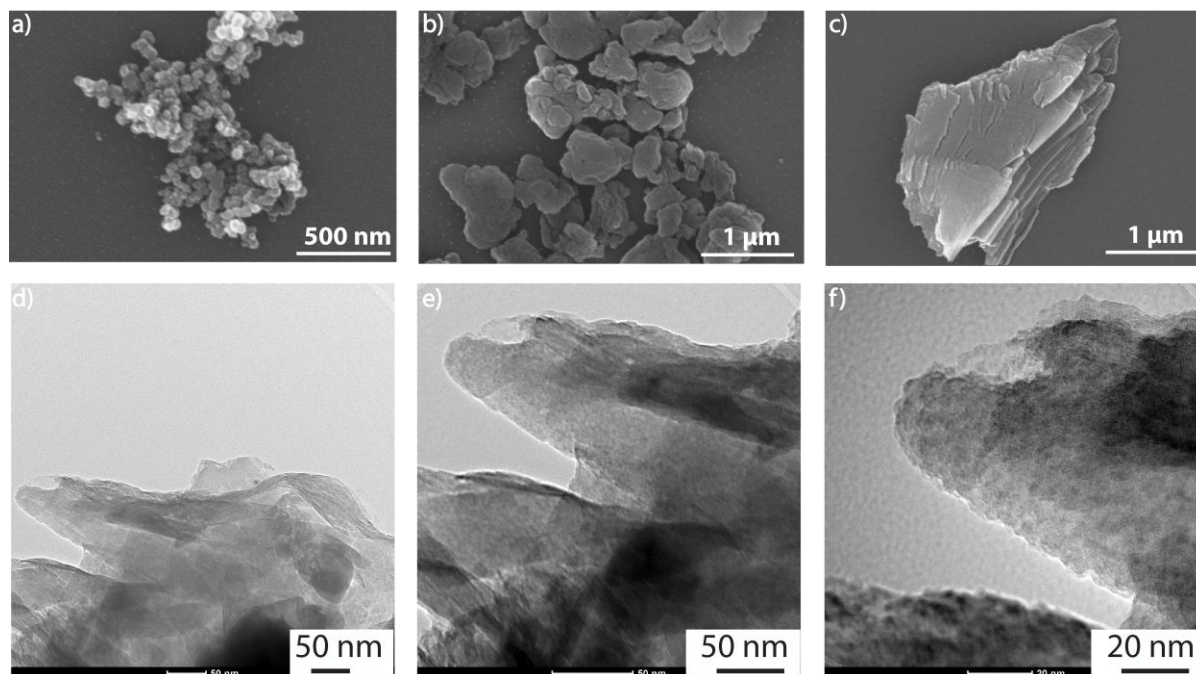


Figure 2.12: (a), (b), (c) SEM images and (d), (e), (f) TEM images of **TpBpy-MC** showing sheet-like morphology.

The thermal stability of the frameworks is analyzed by thermogravimetric analysis (TGA). It shows that the materials **TpBpy-ST** and **TpBpy-MC** are stable up to 350 °C and after 360 °C gradual weight losses are observed due to the decomposition of frameworks (Figure 2.10). In order to investigate the internal morphology of the synthesized materials we have performed Scanning Electron Microscopy (SEM) and Transmission Electron Microscopy (TEM) analysis. The SEM and TEM images of **TpBpy-ST** show interwoven thread-like morphology which generates by the aggregation of small crystallites (Figure 2.11). Whereas the SEM and TEM images of **TpBpy-MC** show sheet-like morphology (Figure 2.12).

2.2.8 Chemical Stability Investigation:

For real-life practical applications like gas storage and separation, the adsorbent material should be stable in acid, base and water medium. The rate of the performance mainly depends on the stability of the material for humid operating conditions in fuels cells and CO₂ capture from humidified bio-fuel stream applications. Therefore we have checked the stability of the synthesized **TpBpy-ST** and **TpBpy-MC** COFs in water, acid and base medium. First 50 mg of both the COFs are kept separately in 10 ml of water for 7 days. After one week the materials are separated, dried and performed IR, PXRD and N₂ gas adsorption analysis. From IR and PXRD analysis no change in peak position and intensity of the spectra is observed from the as-synthesized materials. Also from N₂ adsorption isotherm, it shows

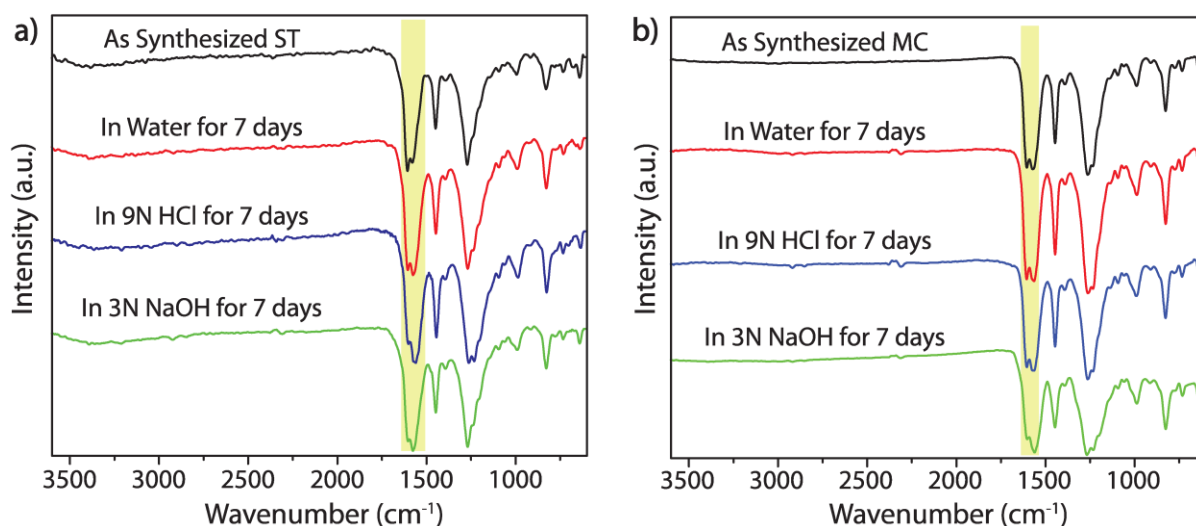


Figure 2.13: (a) FTIR spectra of **TpBpy-ST** as synthesized (black), after water treatment (red), acid treatment (blue) and base treatment (green). (b) FTIR spectra of **TpBpy-MC** as synthesized (black), after water treatment (red), acid treatment (blue) and base treatment (green).

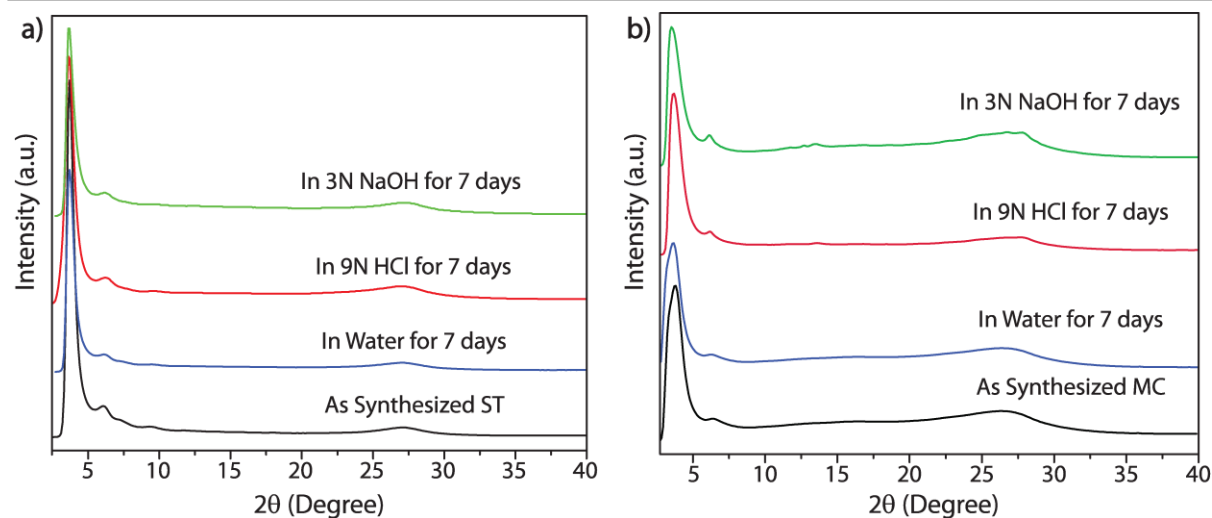


Figure 2.14: (a) Comparison of PXRD pattern for **TpBpy-ST** as synthesized (black), after water treatment (blue), acid treatment (red) and base treatment (green). (b) Comparison of PXRD pattern for **TpBpy-MC** as synthesized (black), after water treatment (blue), acid treatment (red) and base treatment (green).

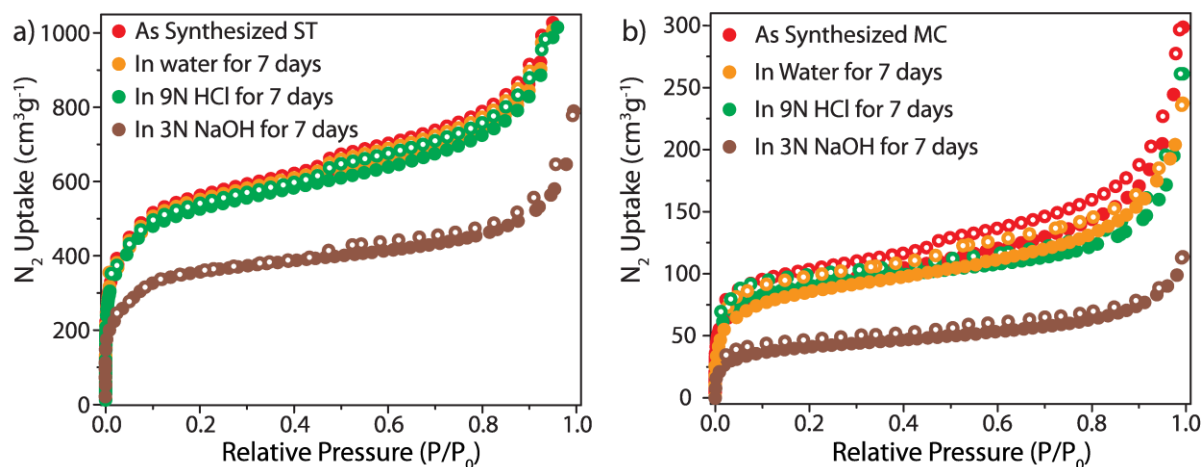


Figure 2.15: (a) Comparison of N_2 adsorption isotherm of **TpBpy-ST** as synthesized (red), after water treatment (orange), acid treatment (green) and base treatment (brown). (b) Comparison of N_2 adsorption isotherm of **TpBpy-MC** as synthesized (red), after water treatment (orange), acid treatment (green) and base treatment (brown).

a similar pattern and surface area as like synthesized materials which prove that the materials are exceptionally stable in water medium. Then we have tested the materials stability in acid medium. The 50 mg of each materials are treated in 10 mL 9(N) HCl for 7 days. After a week the materials are separated, dried and performed IR, PXRD and N_2 gas adsorption analysis. From IR and PXRD analysis no change in peak position and intensity of the spectra

is observed from the as-synthesized materials. Also from N_2 adsorption isotherm, it shows a similar pattern and but a slight decrease in surface area as compared to synthesized materials which prove that the materials are stable in acid medium also. Finally, we have checked the material stability in the basic medium. The 50 mg each materials are dipped in 10 mL 3(N) NaOH for 7 days. After a week the materials are separated, dried and performed IR, PXRD and N_2 gas adsorption analysis. From IR and PXRD analysis no change in peak position but a little decrease in the intensity of the spectra is observed. Also from N_2 adsorption isotherm, it shows a similar pattern and but significant loss in surface area as compared to synthesized materials. The decrease in surface area is due to the loss in intra-molecular hydrogen bonding in the frameworks of the materials in a basic medium which subsequently decreases the framework stability and rigidity. The unusual stability of the materials is observed due to the irreversible nature of the COF formation reaction which prevents the frameworks to go back to the imine/enol form rather than β - ketoenamine form. Similar type of enol-keto tautomerism is possible in monosubstituted N-Salicylideneanilines but here only enol form is observed. Acid-base interaction between imine nitrogen (C=N) phenolic oxygen (O-H) and aromaticity are two main factors which decide the stability of the tautomeric forms. The system loses the aromaticity after the tautomerization in mono substituted Schiff base

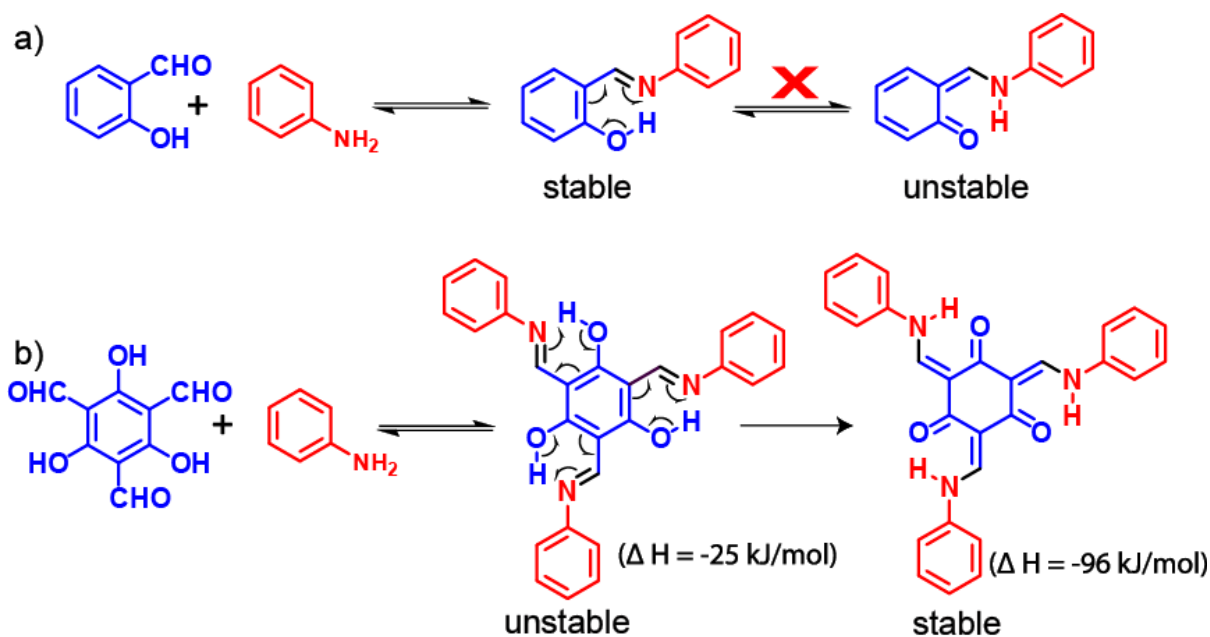


Figure 2.16: (a) Stability of different tautomeric forms in (a) mono substituted N-Salicylideneanilines and (b) tri substituted N-Salicylideneanilines

compounds (N-Salicylideneanilines). Here aromaticity is the most dominating factor which allow the compound to get stabilized in enol form (Figure 2.16a). But in the case of tri substituted Schiff base compounds tris (N-salicylideneaniline) the co-operative effect of basicity of imine functional group surpasses the aromaticity stabilization effect, and as a result the compound gets stabilized in β - ketoenamine form (Figure 2.16b). However, the existence of the enol-form intermediate is difficult to prove experimentally because of the rapid tautomerization step. In order to find the stability of the enol intermediate, energy calculations are performed on the single unit of COF using the Turbo mole 6.0s programs. It is found that keto-form gets stabilized over the enol-form with a huge energy difference of $\Delta E = -74.06$ kcal/mol (Figure 2.16b).

2.3 Conclusion

In this chapter, we have discussed the synthesis of industrially important bipyridine based COFs in solvothermal and mechanochemical methods. Both the COFs are fully characterized by different instrumental analysis. Although solvothermally synthesized COF shows better crystallinity and surface area compared to the mechanochemical one. The different morphology of two COFs is observed from SEM and TEM analysis. But both the COFs have shown exceptional chemical stability in water, acid, and base even after immersion for a week. The reason behind stability is due to the irreversible enol-keto tautomerization process. Both the COFs shows high uptake of greenhouse gas (CO_2), renewable energy source H_2 and H_2O at 1 atm pressure. Although solvothermally synthesized COF has performed better gas uptake compared to mechano one due to the high crystallinity and surface area. Here we have first time synthesized industrially important bipyridine based COF in greener, time efficient and cost effective mechanochemical process for large-scale synthesis. Finally, we believe our developed method for synthesizing bipyridine based Covalent Organic Frameworks will be applicable as heterogeneous support for stabilizing metal nanoparticles in making heterogeneous catalyst, proton conduction, energy storage, gas storage and separation purpose.

2.4 General Methods for Characterization

All reagents were commercially available and used as received.

a) Wide-angle X-Ray Diffraction (WAXD): The Powder X-ray diffraction (PXRD) patterns were recorded on a Phillips PAN analytical diffractometer for Cu K α radiation ($\alpha = 1.5406 \text{ \AA}$), with a scan speed of 1° min^{-1} and a step size of 0.02° in 2θ . The instrument was previously calibrated using a silicon standard.

b) FT-IR spectroscopy: The Fourier Transform Infrared (FTIR) spectra were taken on a Bruker Optics ALPHA-E spectrometer with a universal Zn-Se ATR (attenuated total reflection) accessory in the $600\text{--}4000 \text{ cm}^{-1}$ region.

c) Thermogravimetric analysis: TGA was carried out on a TG50 analyzer (Mettler-Toledo) or a SDT Q600 TG-DTA analyzer under N $_2$ atmosphere at a heating rate of $10^\circ \text{ C min}^{-1}$ within a temperature range of $30\text{--}900^\circ \text{ C}$.

d) Scanning Electron Microscopy: SEM images were obtained with a Zeiss DSM 950 scanning electron microscope and FEI-QUANTA 200 3D Scanning Electron Microscope with tungsten filament as electron source operated at 10 kV. The samples were sputtered with Au (nano-sized film) prior to imaging by a SCD 040 Balzers Union.

e) Transmission Electron Microscopy: TEM images were recorded using FEI Tecnai G2 F20 X-TWIN TEM at an accelerating voltage of 200 kV. The TEM Samples were prepared by drop-casting the sample from isopropanol on copper grids (TED PELLA, INC. 200 mesh). The metal nanoparticles size distribution was determined by measuring the size of 700 particles from TEM images.

f) BET surface area: BET surface area of the synthesized COFs was measured through N $_2$ adsorption studies. N $_2$ adsorption isotherms were collected with a Quantachrome make Autosorb IQ $_2$ automated surface area analyzer.

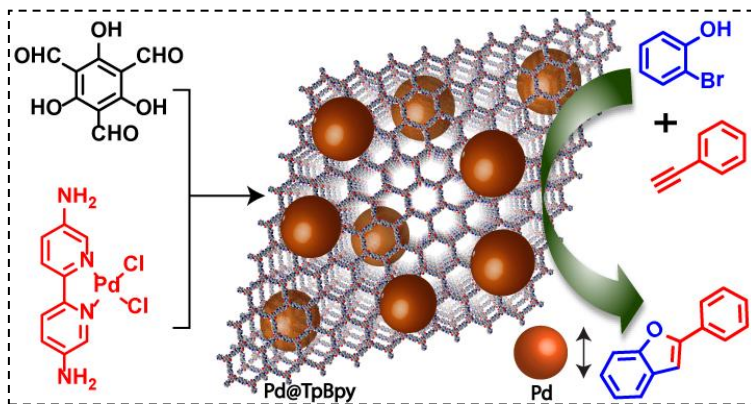
g) Solid-state NMR (SSNMR): Solid-state NMR (SSNMR) was taken in a Bruker 300 MHz NMR spectrometer and ligand NMR data were taken in Bruker 200/400/500 MHz NMR spectrometer.

NOTE: The results of this chapter have already been published in *J. Mater Chem. A*, **2016**, *4*, 2682-2690 with the title: “A mechanochemically synthesized covalent organic framework as a proton-conducting solid electrolyte”. Here I have equally contributed.

CHAPTER 3

Predesigned Metal Anchored Building Block for *In Situ* Generation of Pd Nanoparticles in Porous Covalent Organic Framework for Heterogeneous Tandem Catalysis

Abstract: The nanoparticle-polymer hybrid based heterogeneous catalysts development is highly desired for their applications in the pharmaceutical and chemical industries. Also, the catalyst should show high reactivity and good recyclability. Herein, metal (Pd) nanoparticles are generated *in situ* way using our developed novel synthetic strategy in the porous, stable, and crystalline covalent organic framework (COF) by using predesigned metal anchored building block. Here nanoparticles are generated without using conventional reducing agents. From PXRD, XPS, TEM images, and ^{15}N NMR spectral analysis, it is confirmed the *in situ* generation of Pd nanoparticles in COF skeleton. This hybrid material is used as an excellent heterogeneous reusable catalyst for the synthesis of biologically and pharmaceutically important 2-substituted benzofurans from 2-bromophenols and terminal alkynes via tandem process which shows TON up to 1101. Mercury poisoning experiment and leaching test prove the heterogeneity of the catalytic process. The catalytic performance of the hybrid material is superior compared to commercially available heterogeneous as well as homogeneous Pd catalysts.



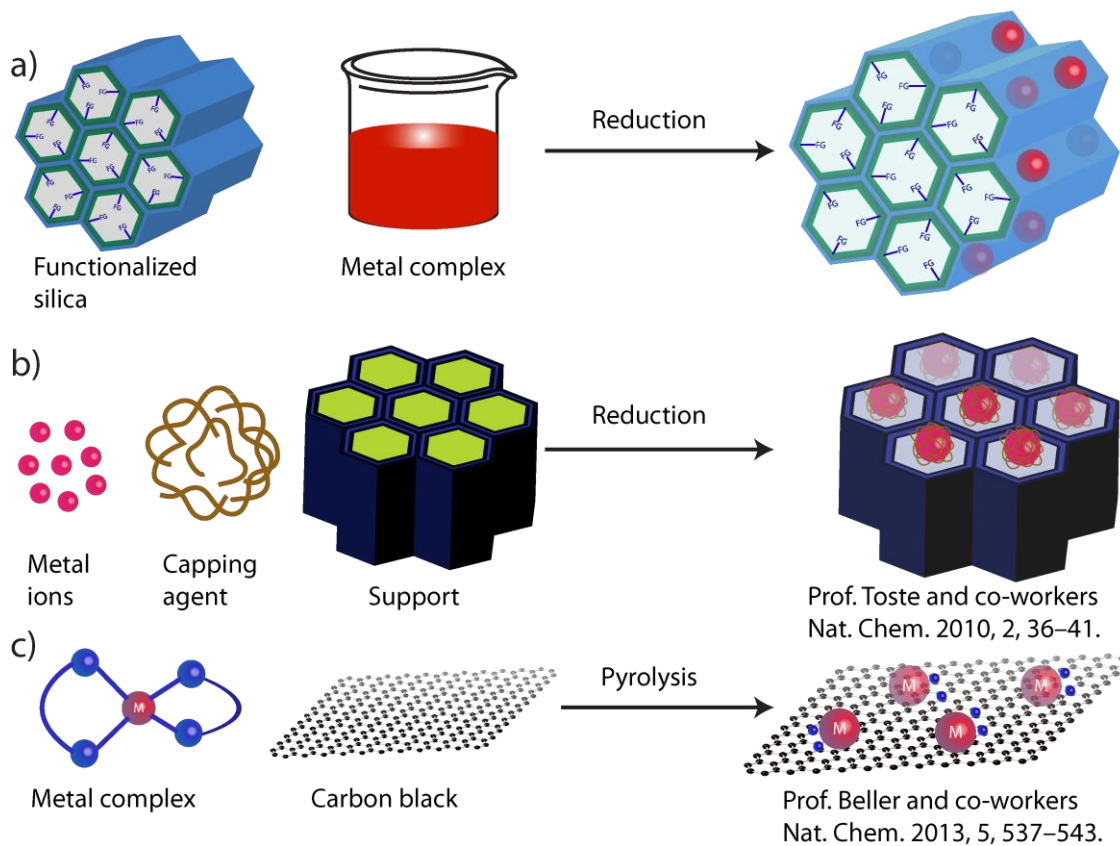
3.1 Introduction:

It has been always a key research objective in the chemical and pharmaceutical industries, to convert homogeneous catalytic reactions into heterogeneous versions through the attachment of catalytic sites on stable supports. There are many advantages of heterogeneous catalysts, over the homogeneous ones which include easy recovery from the reaction mixture, high recyclability and their use in continuous flow processes [3.1]. In the literature, there are different approaches reported for converting homogeneous catalyst into reusable heterogeneous version (Scheme 3.1) [3.2]. Moreover, metal nanoparticles are the excellent candidates for heterogeneous catalysis. Because not only due to their unique properties such as high surface area and narrow size distribution but also due to their vast application in catalytic transformations [3.3]. Metal nanoparticles have already been used to catalyze conventional oxidation and reduction, cross-coupling reactions in solution. But the synthesis of such metal nanoparticles based heterogeneous catalyst is highly challenging and demanding for keeping the nanoparticles mono-dispersed and non-aggregated during the decoration onto the matrix support [3.4].

3.1.1 Different Approaches for Conversion of Homogeneous Catalyst into Heterogeneous Version :

Although there is a significant research has been done on metal-based homogeneous catalysis but converting a homogeneous catalyst to its heterogeneous version is highly challenging. As a heterogeneous catalyst offers many advantages than the homogeneous version, therefore designing and synthesis of different heterogeneous catalyst and their catalytic applications for various organic transformations becoming more prominent research area nowadays. In the literature, there are different approaches reported for converting a homogeneous metal catalyst into its heterogeneous version (Scheme-3.1). In case of a) this is the conventional method for the preparation of silica supported metal nanoparticles loaded catalyst where functionalized silica (SBA-15) has been taken as heterogeneous support. Then the homogeneous metal complex solution is added to the functionalized silica (SBA-15) with vigorous stirring. The resultant material is washed with solvents, dried and reduced in presence of hydrogen at a higher temperature will produce the silica supported metal nanoparticles loaded heterogeneous catalyst. In the case of b) Prof. Toste and co-workers have synthesized Pt nanoparticles on silica support (SBA-15). First metal nanoparticles are

Previous approaches

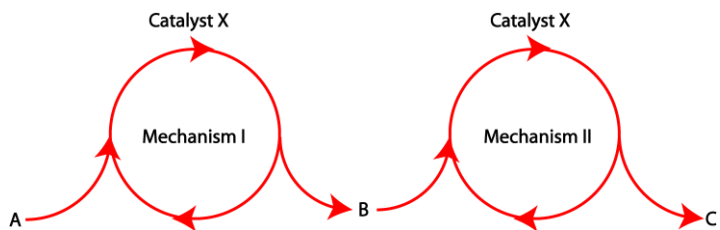


Scheme 3.1: a), b), c) are reported approaches are used to convert a homogeneous catalyst into the reusable heterogeneous version.

generated from corresponding metal complex in solution. The synthesized nanoparticles are stabilized from agglomeration by using PVP (polymer) as a capping agent. After that, the polymer encapsulated nanoparticles are deposited on SBA-15 which will finally produce the metal nanoparticles loaded catalyst. In case of c) Prof. Beller and co-workers have synthesized an active cobalt oxide–nitrogen/carbon catalyst for reduction of nitroarenes by pyrolyzing a cobalt (II) acetate–phenanthroline complex on commercially available carbon (Vulcan XC72R). All the above cases heterogeneous catalyst is synthesized at a higher temperature by taking heterogeneous support as a synthetic precursor.

3.1.2 Tandem Catalysis:

Among the different catalytic processes, tandem catalysis is a greener process with high atom economy, in which sequential transformation of the substrate occurs *via* two (or more) mechanistically distinct processes (Scheme 3.2). This process not only reduces the workup and purification steps but also minimizes the by-products formation [3.5]. Therefore, developing new heterogeneous catalytic systems capable of performing versatile synthetic transformations *via* tandem processes is highly desirable.



Scheme 3.2: Schematic representation of tandem catalysis.

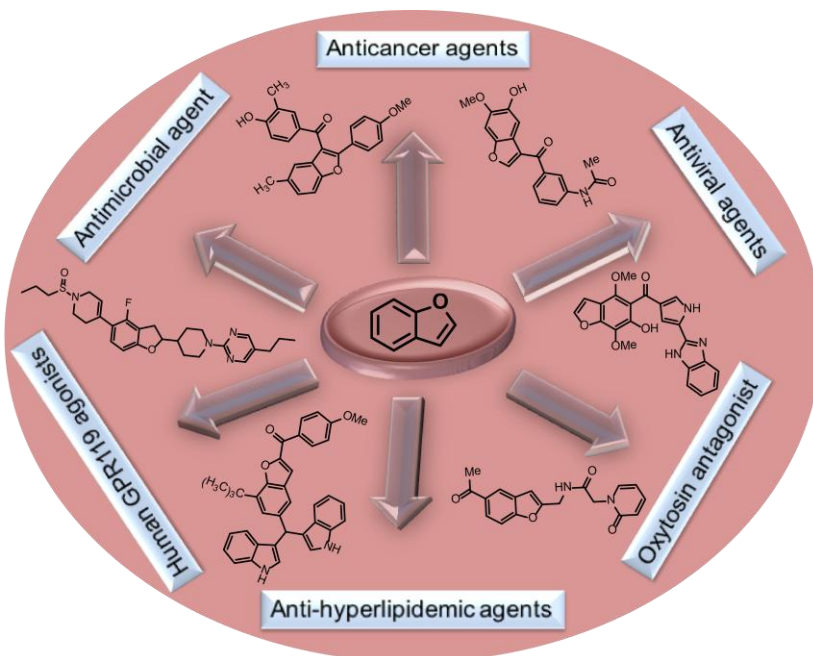
3.1.3 Importance of 2-Substituted Benzofurans Synthesis:

The benzofuran framework is omnipresent in natural products, pharmaceuticals and its derivatives exhibit different biological antimicrobial, antiparasitic, antihyperglycemic, antitumor activities

(Scheme 3.3). Therefore benzofuran derivatives synthesis has drawn significant attention from the past few years.

Although there are various methods developed for 2-substituted benzofurans synthesis but Pd-catalyzed one-pot synthesis of benzofurans from 2-

halophenols and terminal alkynes by a Sonogashira

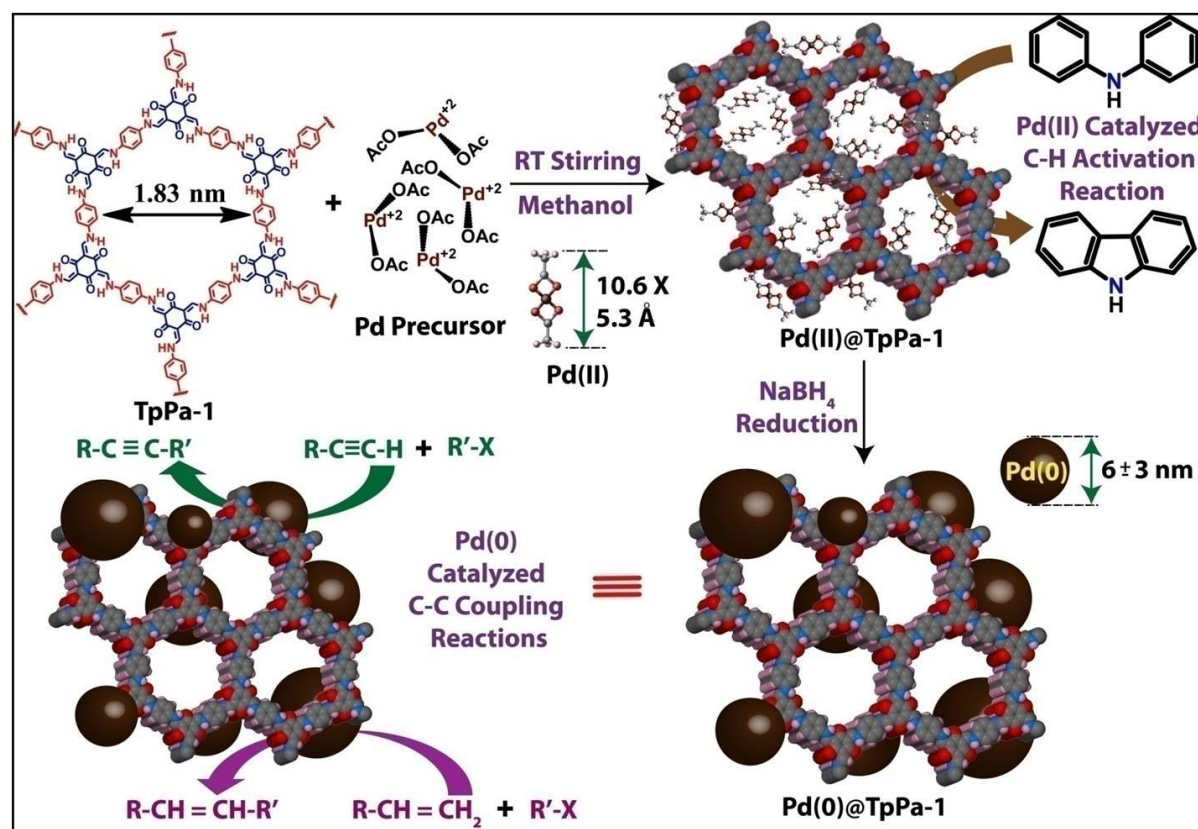


Scheme 3.3: Selected biologically active benzofuran natural products.

coupling followed by cyclization in presence of copper salt as co-catalyst seems to be the most convenient homogeneous method. But the synthesis of 2-substituted benzofuran using heterogeneous catalyst in one-pot way *via* tandem process is rare.

3.1.4 Synthesis of Pd Nanoparticles in Covalent Organic Framework *via ex situ* Process and the Disadvantages:

Covalent organic frameworks (COFs) are crystalline porous polymers made by organic building blocks in a periodic manner [3.6]. COFs have already been used for different applications like gas sensing [3.7], storage [3.8], opto-electronics [3.9] and catalysis [3.10]. COFs can be used as ideal supports for anchoring various catalytically active metal nanoparticles due to the availability of the coordination sites for uniform nucleation of nanoparticles within the internal microenvironment, along with high porosity, chemical tunability and ordered structural integrities [3.11]. However, the poor stability of the COFs become a barrier to their applications in the field of catalysis. The stability issues were overcome by simply introducing an irreversible keto-enol tautomerization within the COF skeleton [3.12]. Although, there are very few reports of COF-metal nanoparticle hybrids. In most of the cases, metal nanoparticles loading have been done *via ex-situ* processes on pre-synthesized COF-materials (Scheme 3.4) [3.13]. These synthetic procedures have several disadvantages such as (a) additional synthetic steps and (b) usage of the strong reducing



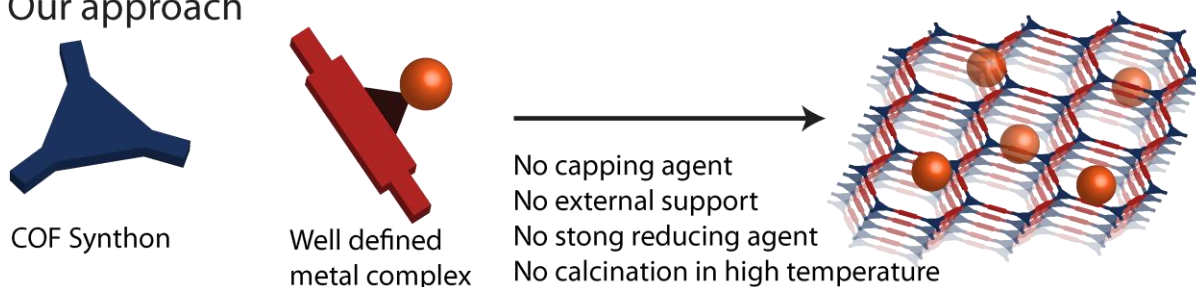
Scheme 3.4: Synthesis of Pd nanoparticles on TpPa-1 COF *via ex-situ* process.

agent. The usage of the external reducing agent changes the internal structure of COFs. Subsequently, it affects the crystallinity and porosity of these materials. The interaction between the support and nanoparticles decreases due to the loss of crystallinity and rigidity of these COF supports which results in the loss of catalytic activity due to leaching and sintering of nanoparticles during the repeated cycles.

3.2 Statement of the Problem

As we have discussed introduction section that most of the heterogeneous catalysts are prepared by taking external support, capping agent, reducing agent and pyrolyzed at a higher temperature. The strong reducing agent hampers the crystallinity and porosity of the framework during nanoparticles synthesis. The simple alternative to conquer this problem is to load metal nanoparticles in the COF skeleton by *in situ* synthetic methods without using any external reducing agents (Scheme 3.5).

Our approach



Scheme 3.5: Synthesis of Pd nanoparticles on TpBpy COF via *in situ* process.

Keeping this idea in our mind, we have strategically developed an *in situ* process to synthesize Pd nanoparticles within a chemically stable COF (**Pd@TpBpy**) via a judicious choice of Pd metal anchored tailored building units. To our knowledge, this is the first report of *in situ* generated COF–Pd nanoparticle hybrids and their utilization as a heterogeneous catalyst for the synthesis of 2-substituted benzofurans via tandem process [3.14]. Such type of solution-phase carbon-carbon and carbon-heteroatom bond forming reactivity by using single heterogeneous catalyst is rare in literature [3.15].

3.3 Synthesis and Characterization

3.3.1 Pd@TpBpy COF Synthesis

The **Pd@TpBpy** is synthesized by the Schiff-base reaction between C₃ linker 1,3,5-triformylphloroglucinol (**Tp**) (21 mg, 0.1 mmol) with C₂ linker 2,2'-bipyridine-5,5'-diamine

palladium chloride (**Bpy-PdCl₂**) (54.5 mg, 0.15 mmol) with 0.3 mL of 6M aqueous acetic acid in presence of *N,N*-dimethylacetamide (DMAc) and 1,4-dioxane solvent combination (2.3 : 0.7 mL) using solvothermal process. Then the reactants are ultrasonicated for 15 min for homogeneous dispersion and degassed through three successive freeze-pump-thaw cycles. In vacuum condition, the tube is sealed and kept for heating at 90 °C in the isothermal oven for 3 days. To remove the residues of the starting materials, the phase pure material is washed with DMAc and DMSO solvents. The collected reddish black material is solvent exchanged with DMSO and washed with excess acetone. Then the synthesized **Pd@TpBpy** COF material was dried at 110 °C for 12 h under vacuum.

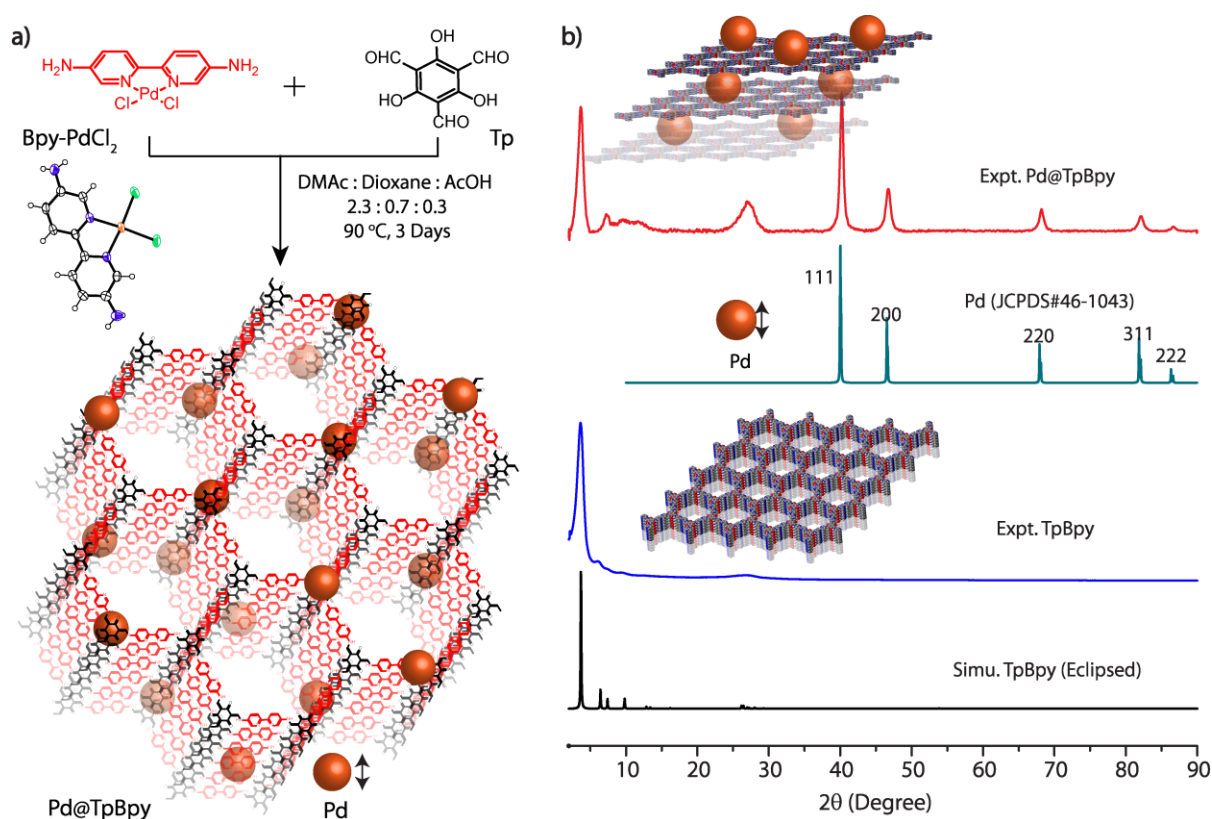


Figure 3.1: (a) Synthesis details of the *in situ* generation of highly dispersed Pd nanoparticles in the **TpBpy** skeleton. The size of Pd nanoparticles and the COF pore organization is not exactly based on a scale to scale. (b) Comparison of PXRD patterns of simulated **TpBpy** (black) with experimental **TpBpy** (blue), Pd nanoparticles (cyan) and experimental **Pd@TpBpy** (red).

3.3.2 Structural simulation and characterization

The Pd nanoparticles are formed *via* breakage of Pd–N bond during the COF formation reaction. It is important to mention that the overall crystallinity and structural

integrity of isolated COF remain intact after the formation of Pd nanoparticles during the COF synthesis. The high crystallinity of **Pd@TpBpy** is observed from the intense peak in the PXRD patterns at 3.6° (2θ) corresponding to the reflection from (100) plane and the minor peaks arise at 7.2° , and 26.9° (2θ) are attributed to (200) and (002) reflections. The peak at $2\theta = 26.9^\circ$ indicates the presence of π - π stacking between the 2D COF layers corresponding to (002) reflection. Since eclipsed model of the simulated COF structure matches well with the experimental PXRD pattern of **Pd@TpBpy** (Figure 3.1(b)). Therefore we have proposed a structure close to the hexagonal $P6_3$ space group ($a = b = 27.5 \text{ \AA}$, $c = 6.8 \text{ \AA}$, $\alpha = \beta = 90^\circ$, $\gamma = 120^\circ$). The d -spacing between the COF layers is 3.4 \AA (Table 3.1). The additional peaks arise at higher (2θ) values of 40.2 , 46.7 , 68.1 , 82.1 and 86.6° correspond to the reflections from (111), (200), (220), (311) and (222) planes of Pd (JCPDS#46-1043).

Table 3.1 Fractional atomic coordinates for the unit cell of *cis* **TpBpy** (Eclipsed)

<i>cis</i> TpBpy							
Hexagonal; $P6_3$							
$a = b = 27.5 \text{ \AA}$, $c = 6.8 \text{ \AA}$							
$\alpha = \beta = 90$, $\gamma = 120$							
C2	0.36415	0.64415	0.23756	N74	0.44360	0.48701	0.77285
C3	0.38904	0.69786	0.23644	C75	0.53787	0.42485	0.76195
O9	0.44360	0.72938	0.23513	C76	0.42183	0.55632	0.76466
C10	0.39804	0.62389	0.23703	C77	0.51218	0.57682	0.76438
N19	0.37778	0.56975	0.23805	C78	0.58676	0.53225	0.76969
N28	0.61501	0.42795	0.23441	C79	0.47561	0.59321	0.75977
C31	0.63410	0.35748	0.23495	C80	0.61719	0.50860	0.76716
C32	0.59740	0.37771	0.23583	C81	0.53180	0.50168	0.76795
C33	0.60839	0.29941	0.23592	C82	0.49599	0.52314	0.76967
O48	0.55424	0.26552	0.23746	C83	0.40733	0.50256	0.77112
H54	0.66124	0.45468	0.26084	H84	0.60303	0.56918	0.77250
H57	0.34596	0.54762	0.26670	H85	0.65412	0.52940	0.76694
H58	0.44533	0.65128	0.26344	H86	0.37140	0.47690	0.77432
H65	0.56453	0.35492	0.26369	H87	0.48689	0.62934	0.75342
N72	0.50836	0.44813	0.76264	H88	0.54831	0.60189	0.76397
C73	0.59312	0.45351	0.76496	H104	0.51790	0.37957	0.25879

3.3.3 Chemical characterization

The FT-IR spectra of **Pd@TpBpy** suggest that the starting materials are totally consumed during the reaction. The characteristics $\text{C}=\text{O}$ (1641 cm^{-1}) stretching band of 1,3,5-triformylphloroglucinol (**Tp**) and $\text{N}-\text{H}$ ($3318, 3204\text{ cm}^{-1}$) stretching band of 2,2'-bipyridine-5,5'-diamine palladium chloride (**Bpy-PdCl₂**) are totally disappeared. In addition, the intense peaks appear at 1606 cm^{-1} ($\text{C}=\text{O}$), 1566 cm^{-1} ($\text{C}=\text{C}$) and 1243 cm^{-1} ($\text{C}-\text{N}$) which indicates the most stable keto bond formation *via* keto-enol tautomerization during Schiff base reaction which is similar to the **TpBpy** (Figure 3.2a). Also, it is observed that the $\text{C}=\text{O}$ peak of **Pd@TpBpy** at 1606 cm^{-1} is merged with $\text{C}=\text{C}$ peak at 1566 cm^{-1} in this case. The ^{13}C CP-MAS solid-state NMR of **Pd@TpBpy** shows the signal at 184.4 ppm

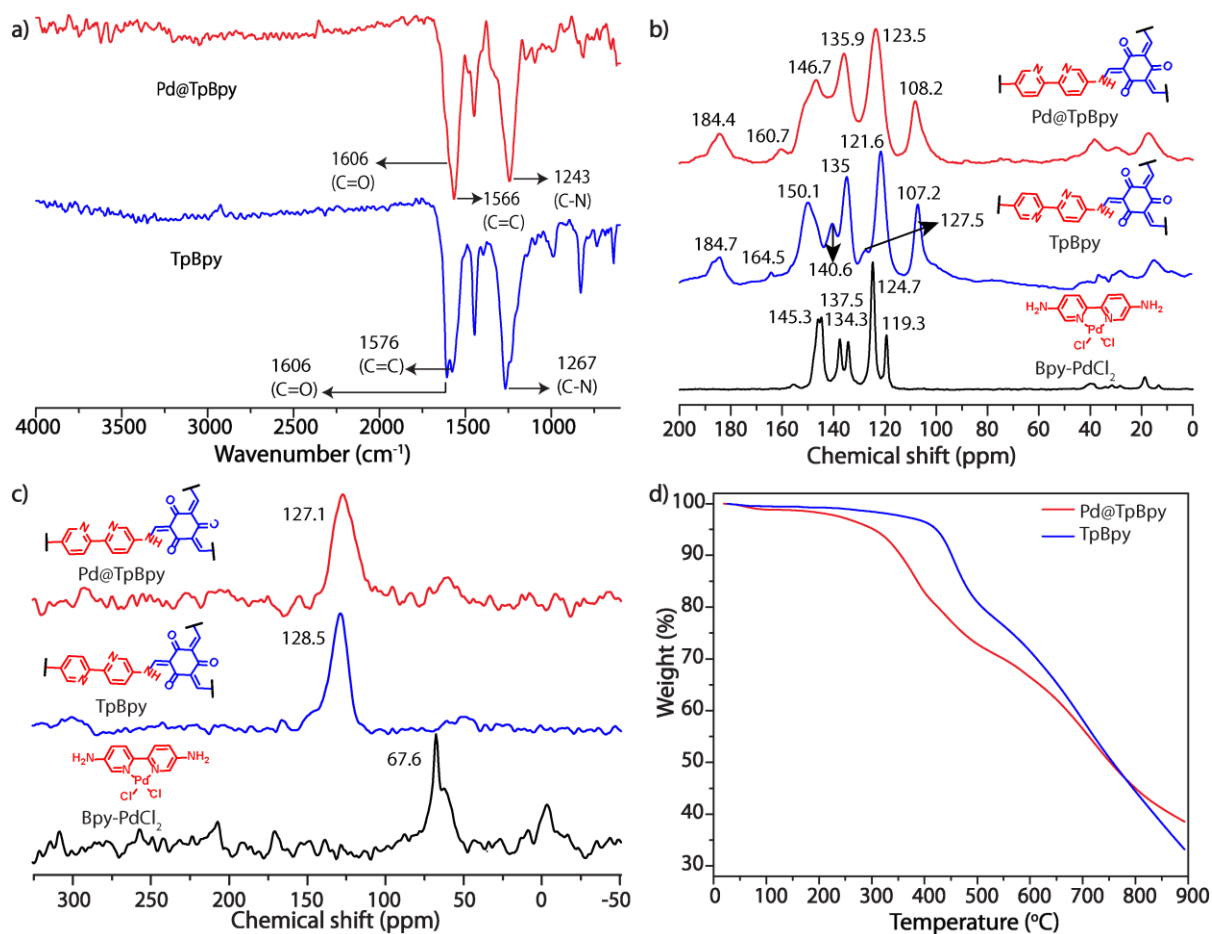


Figure 3.2: Characterization details of **Pd@TpBpy** and **TpBpy**. (a) FTIR spectra of **TpBpy** (blue) and **Pd@TpBpy** (red). (b) Comparison of solid state ^{13}C NMR spectra of **Bpy-PdCl₂** (black), **TpBpy** (blue) and **Pd@TpBpy** (red). (c) Comparison of solid-state ^{15}N NMR spectra of **Bpy-PdCl₂** (black), **TpBpy** (blue) and **Pd@TpBpy** (red). (d) TGA spectra of **Pd@TpBpy** (red) and **TpBpy** (blue).

corresponding to carbonyl ($-\text{C}=\text{O}$) carbon. The remaining sp^2 carbons appear together in the range of 108 to 161 ppm (Figure 3.2b). we have performed the ^{15}N CP-MAS solid-state NMR of **Pd@TpBpy**, **TpBpy** [3.16] and **Bpy-PdCl₂** complex, using NH_4Cl as an internal standard to assess the chemical environments of the nitrogen atoms present in the as-synthesized materials, (Figure 3.2c). In the case of **Bpy-PdCl₂**, the Pd metal coordinated pyridinic nitrogen signal arises at 67.6 ppm. In contrast, the pyridinic nitrogen of **Pd@TpBpy** and pyridinic nitrogens of **TpBpy** signals appear at 127.1 ppm and 128.5 ppm respectively which suggest that the pyridinic nitrogens of **Pd@TpBpy** are not strongly coordinated to the Pd metal centers as like in the **Bpy-PdCl₂** complex [3.17]. However, the Pd nanoparticles in **Pd@TpBpy** are stabilized by the weak nonbonding interactions with the pyridinic nitrogens of the bipyridine unit has been observed by the significant upfield shift

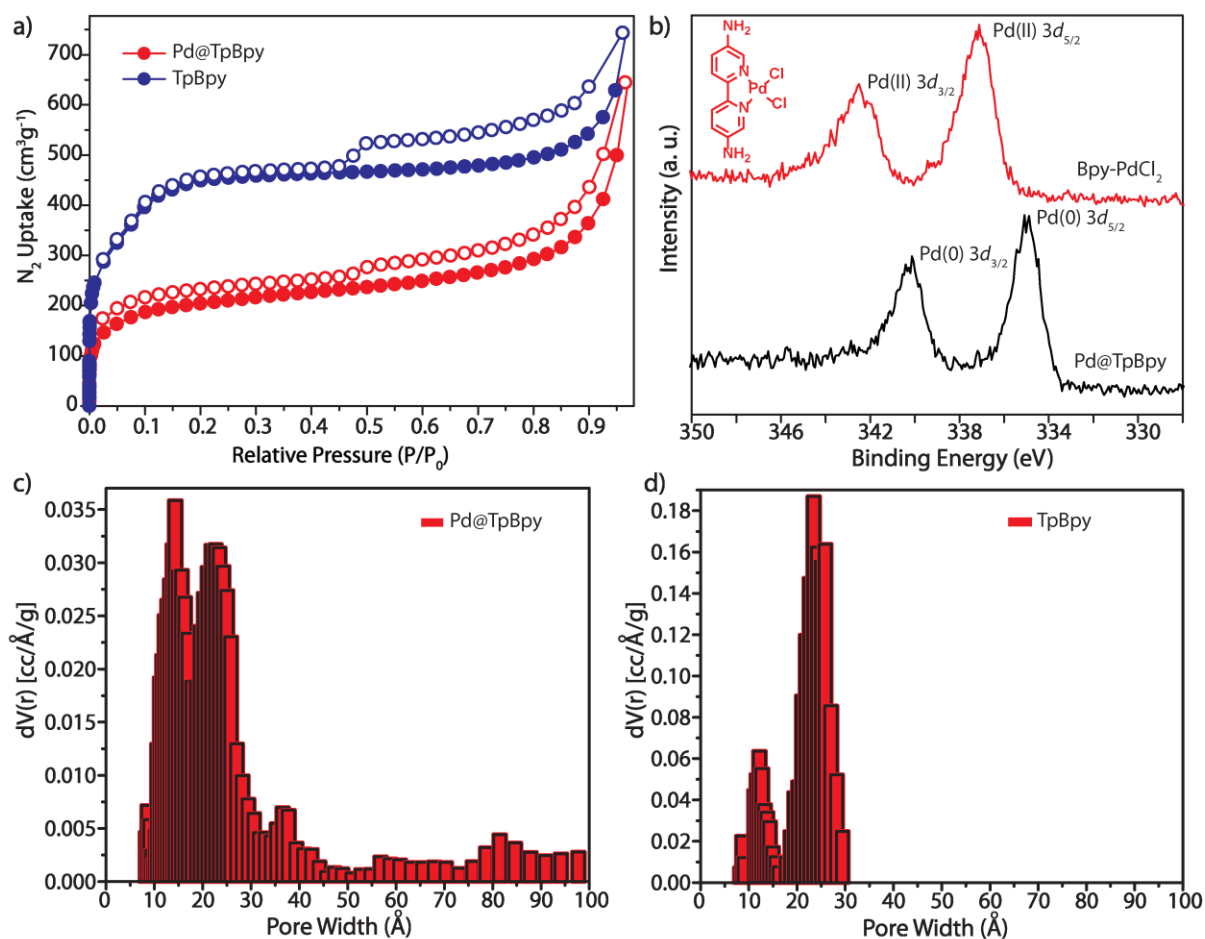


Figure 3.3: (a) N_2 adsorption isotherms of **Pd@TpBpy** (red) and **TpBpy** (blue). (b) XPS spectra of Pd in **Pd@TpBpy** (black) and **Bpy-PdCl₂** (red). Experimental pore size distributions for (c) **Pd@TpBpy**, (d) **TpBpy** calculated using the non-local density functional theory (NLDFT) model.

(1.4 ppm) of the pyridinic nitrogens in case of **Pd@TpBpy** compared to **TpBpy**. This result also proves our initial speculation that the breakage of Pd–N bond of **Bpy-PdCl₂** complex takes place during the course of **Pd@TpBpy** formation, which leads to the *in situ* synthesis of Pd nanoparticles in **Pd@TpBpy** hybrid. To determine the framework thermal stability,

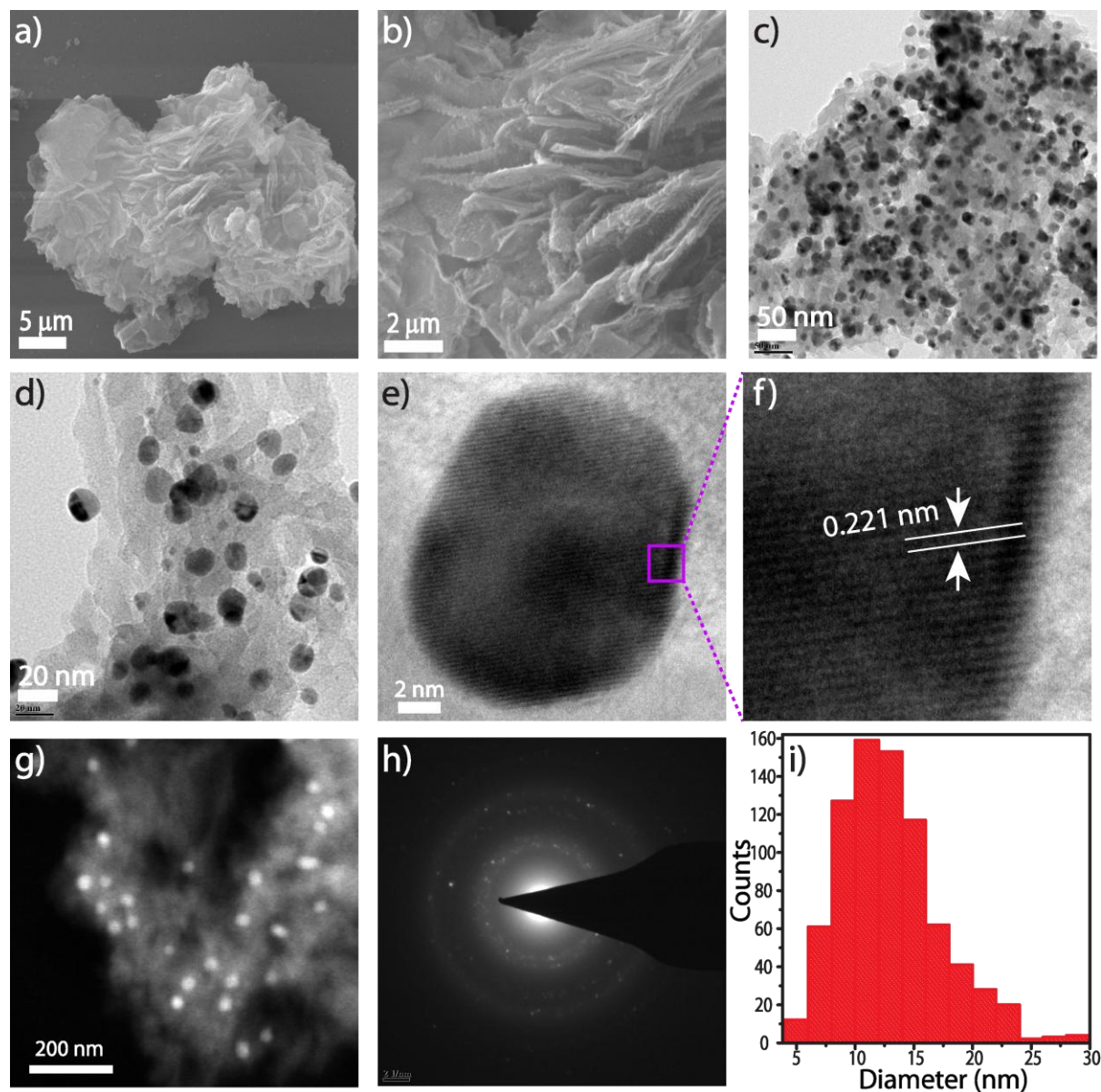


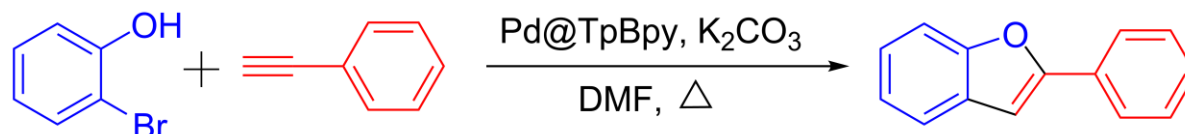
Figure 3.4: Characterization details of **Pd@TpBpy**. (a, b) SEM images of **Pd@TpBpy** showing flake-like morphology. (c, d) TEM images of **Pd@TpBpy** showing a uniform distribution of Pd nanoparticles. (e, f) TEM images of **Pd@TpBpy** showing the lattice fringes of Pd nanoparticles in **Pd@TpBpy**. (g) HAADF-STEM image of **Pd@TpBpy**. (h) SAED pattern of **Pd@TpBpy** before catalysis. (i) Size distribution histogram of Pd nanoparticles in **Pd@TpBpy**.

thermogravimetric analysis (TGA) was performed on activated COF samples. TGA of **Pd@TpBpy** and **TpBpy** show that both the COFs are highly thermally stable up to 300 and 350 °C respectively (Figure 3.2d). We have performed N₂ adsorption isotherm of activated **Pd@TpBpy** and pure **TpBpy** at 77K to evaluate permanent porosity of the respective COFs. Both the COFs show type IV reversible N₂ adsorption isotherm with mesoporous in nature. The Brunauer–Emmett–Teller (BET) surface areas of **Pd@TpBpy** and **TpBpy** are found to be 653 and 1462 m²g⁻¹ respectively (Figure 3.3a). The decrease in surface area of **Pd@TpBpy** with respect to **TpBpy** is due to the distribution of fine Pd nanoparticles around the pore surface and interlayer spacing of the host framework which block the pores of the host framework. The pore size distribution is measured on the basis of nonlocal density functional theory (NLDFIT) which shows the narrow pore size distribution in the range of 1.4 nm and 2.3 nm for **Pd@TpBpy** and 2.3 nm for **TpBpy** (Figure 3.3 c,d). We have carried out detail XPS analysis of both **Bpy-PdCl₂** complex and **Pd@TpBpy** COF in order to confirm the oxidation state of Pd, the presence of characteristic binding energy peaks at 337 and 342.5 eV of Pd 3d_{5/2} and Pd 3d_{3/2} are corresponding to Pd(II) species. Whereas, Pd 3d_{5/2} and Pd 3d_{3/2} peaks arising at 335 and 340.2 eV unambiguously confirm the formation of Pd(0) species in **Pd@TpBpy** (Figure 3.3b). On the other hand, in order to understand the inner structure and properties of the synthesized material we have performed SEM and TEM analysis. Flake-like morphology of **Pd@TpBpy** is observed from Scanning Electron Microscopy images (Figure 3.4 a,b). From Transmission Electron Microscopy (TEM) images it is clear that the Pd nanoparticles are well distributed over COF matrices (Figure 3.4 c,d). The average size of the Pd nanoparticles is found to be 12±4 nm from the nanoparticle size distribution plot (Figure 3.4 i). The good distribution of the Pd nanoparticles in both the surface and interlayer spacing of the COF framework is well understood from both high and low-contrast Pd nanoparticles in TEM images (Figure 3.4 g,d). The lattice fringes of the Pd nanoparticles are found to be 0.221 nm from the TEM image (Figure 3.4 e,f,h). The percentage of elements present in the material is observed from Energy Dispersive X-ray (EDX) analysis (Figure 3.14b). But in order to know the quantity of Pd metal present in **Pd@TpBpy** accurately, we have performed Inductively Coupled Plasma Atomic Emission Spectroscopy (ICP-OES) analysis and found 15.2 wt% Pd metal present in the matrix.

3.3.4 Tandem Catalysis by Pd@TpBpy Catalyst for Co-catalyst Free Benzofuran Synthesis:

The benzofuran framework is omnipresent in natural products, pharmaceuticals and its derivatives exhibit different biological antimicrobial, antiparasitic, antihyperglycemic, antitumor activities [3.18]. Therefore benzofuran derivatives synthesis has drawn significant

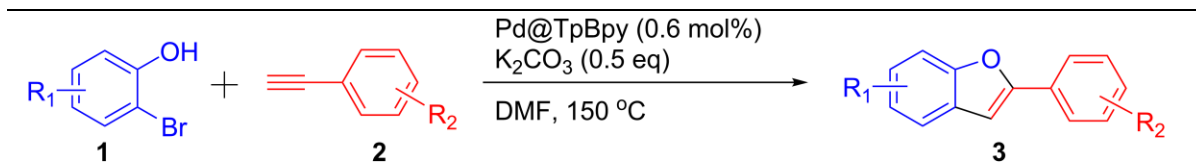
Table 3.2 Optimization table for tandem catalysis.^a



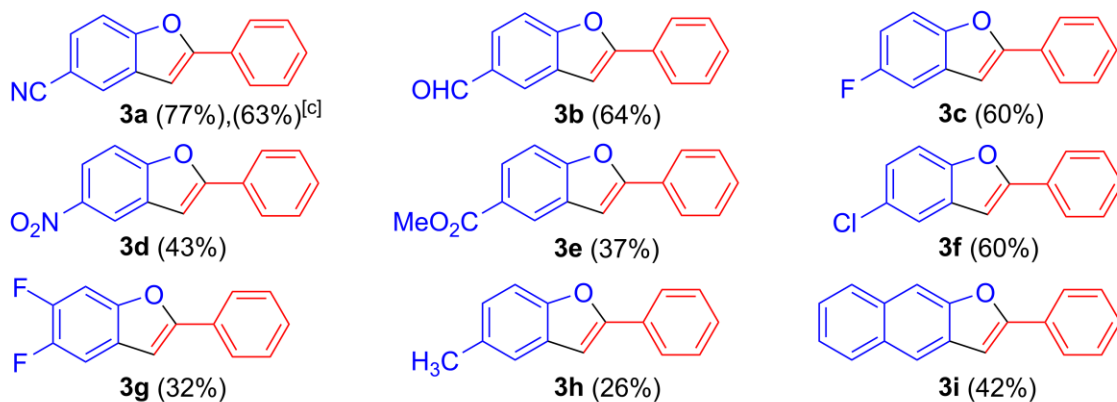
Entry	Pd Catalyst	Base	Solvent	Yield (%) ^b
1	Pd@TpBpy	K ₂ CO ₃	DMF	70
2	Pd@TpBpy	K ₂ CO ₃	Toluene	44
3	Pd@TpBpy	K ₂ CO ₃	<i>m</i> -Xylene	30
4	Pd@TpBpy	K ₂ CO ₃	THF	32
5	Pd@TpBpy	K ₂ CO ₃	DMSO	16
6	Pd@TpBpy	K ₂ CO ₃	Mesitylene	25
7	Pd@TpBpy	Cs ₂ CO ₃	DMF	21
8	Pd@TpBpy	Li ₂ CO ₃	DMF	10
9	Pd@TpBpy	Ag ₂ CO ₃	DMF	-
10	Pd@TpBpy	KO ^t Bu	DMF	10
11	Pd@TpBpy	KOAc	DMF	18
12	Pd@TpBpy	-	DMF	-
13	-	K ₂ CO ₃	DMF	-
14	Pd/C(10 wt%)	K ₂ CO ₃	DMF	23
15	PdCl ₂	K ₂ CO ₃	DMF	3
16	Bpy-PdCl ₂	K ₂ CO ₃	DMF	6
17	TpBpy	K ₂ CO ₃	DMF	4

^aAll the reactions were conducted with 0.5 mmol of 2-bromophenol (1 equiv), 0.6 mmol of phenyl acetylene (1.2 equiv), 0.6 mol% of Pd@TpBpy catalyst, K₂CO₃ (0.5 equiv) in *N,N*-dimethylformamide (heated at 150 °C). ^bBased on GC analysis using *m*-Xylene as an internal standard.

attention from past few years. Although there are various methods developed for 2-substituted benzofurans synthesis but Pd-catalyzed one-pot synthesis of benzofurans from 2-halophenols and terminal alkynes by a Sonogashira coupling followed by cyclization in presence of copper salt as co-catalyst seems to be the most convenient homogeneous method.



a) Scope of 2-bromo phenols



b) Scope of alkynes

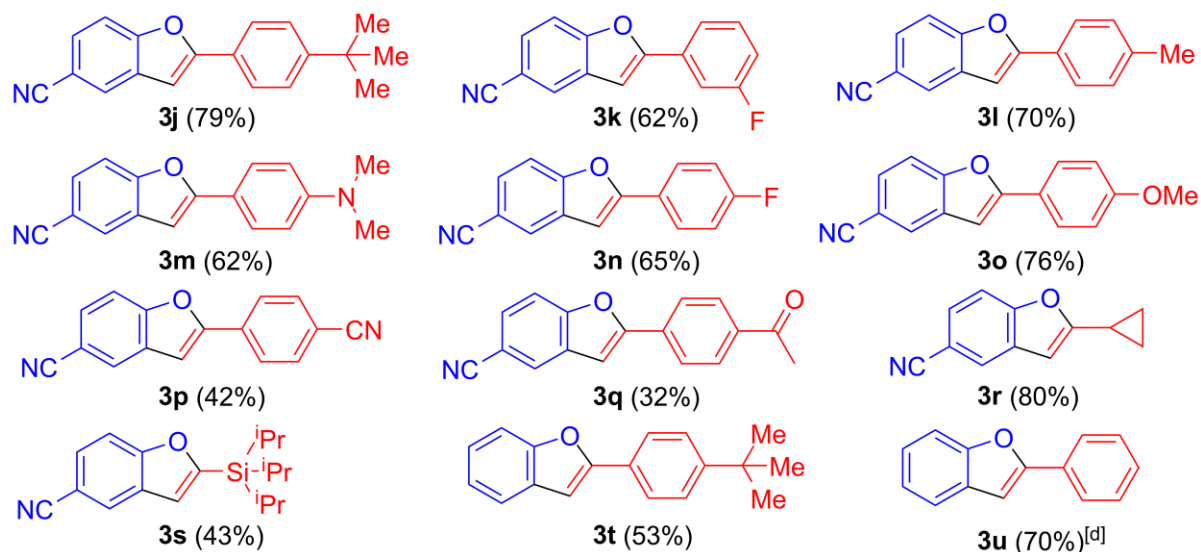


Figure 3.5: Evaluation of the substrate scope.^{a,b} ^aAll the reaction were conducted with 0.5 mmol of 2-bromophenols (1 equiv), 0.6 mmol of alkynes (1.2 equiv), 0.6 mol% of Pd@TpBpy catalyst, K₂CO₃ (0.5 equiv) in DMF. ^bIsolated yields. ^cUsing 5 mmol of 3-bromo-4-hydroxybenzonitril. ^dBased on GC analysis.

But the synthesis of 2-substituted benzofuran using heterogeneous catalyst in one-pot way *via* tandem process is rare (Figure 3.6). Here we set out to evaluate the performance of the stable porous crystalline **Pd@TpBpy** catalyst in the tandem process for the effective synthesis of 2-arylbenzofurans in absence of additive/co-catalyst. We have started the optimization of the reaction by taking 2-bromophenol and phenylacetylene as substrates, and 70% yield of the desired product 2-arylbenzofuran (Table 3.2) is obtained by using the catalytic amount of **Pd@TpBpy** (0.6 mol%) in presence of K_2CO_3 (0.5 eq) in DMF solvent at 150 °C under N_2 atmosphere. Notably, the efficiency of the reaction is decreased by lowering the temperature and the optimum temperature for this reaction is 150 °C. Interestingly, no conversion is observed in absence of a base. Among the various tested bases, K_2CO_3 gives the highest yield. Whereas, in term of solvent, DMF afforded the highest yield. As expected, no product formation is observed in absence of **Pd@TpBpy**. We have performed control reactions using **PdCl₂**, **Bpy-PdCl₂**, and **TpBpy** materials as catalysts to confirm the superiority of our catalyst. It was found that **PdCl₂**, **Bpy-PdCl₂**, and **TpBpy** are ineffective and gave trace amounts of the

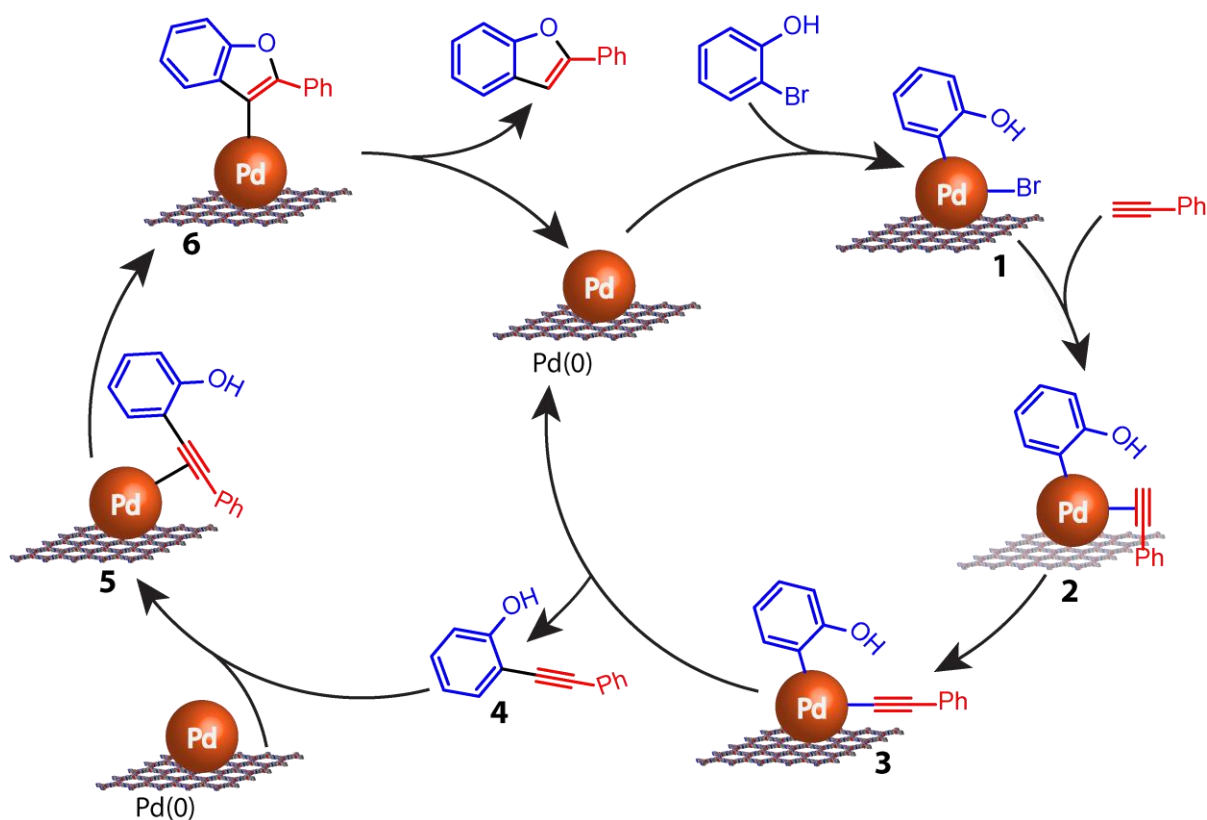


Figure 3.6: Probable catalytic mechanism of the tandem process

desired product 3%, 6%, 4% yield respectively (Table 3.2). Notably, commercially available palladium on carbon, a heterogeneous catalyst, gave the expected product in low yield (23% yield) under optimized condition. In order to prove the versatility of the reaction condition, we have synthesized different benzofuran derivatives by taking various 2-bromophenol and terminal alkynes *via* tandem catalysis process (Figure 3.5). First, we have tested the reaction conversion of different electron donating and withdrawing substituent of 2-bromophenol in the optimized condition keeping the terminal alkyne (phenylacetylene) constant. It has been observed that electron withdrawing groups showed good to excellent yield compared to electron donating groups. Thus, the electron-withdrawing groups such as $-\text{CN}$ (**3a**), $-\text{CHO}$ (**3b**), $-\text{CO}_2\text{Me}$ (**3e**) and $-\text{NO}_2$ (**3d**) gave 37% to 77% yields of the desired products. A decrease in the yield (26%) of the desired product was observed in the case of methyl (**3h**). Also, different halogen substituents such as $-\text{F}$ (**3c**, **3g**), $-\text{Cl}$ (**3f**) and extended conjugated systems like naphthalene (**3i**) gave the desired products in 32% to 60% yields. Moreover, we have also varied different electron donating, electron withdrawing, aliphatic and aromatic substituents on the terminal alkyne side keeping 3-bromo-4-hydroxybenzotrile as coupling partner unchanged. Thus, electron-donating groups i.e. $-\text{CH}_3$ (**3l**), $-\text{OMe}$ (**3o**), $-\text{N}(\text{Me})_2$ (**3m**), $-\text{tBu}$ (**3j**) and electron-withdrawing groups such as, $-\text{F}$ (**3k** and **3n**), $-\text{CN}$ (**3p**) and $-\text{COCH}_3$ (**3q**) gave the corresponding 2-arylbenzofuran with 32% to 79% yields. Also, like cyclopropyl (**3r**) and silicon substituent $-\text{Si}(\text{iPr})_3$ (**3s**) aliphatic substituent yielded 80% and 43% of the corresponding products, respectively. Moreover, the optimized condition has shown broad substrates scope and large functional group tolerance which implies that it will be most suitable, easiest and economical process for the synthesis of biological demanding benzofuran derivatives.

3.3.5 Heterogeneity Test:

The heterogeneity of the **Pd@TpBpy** catalyst has been confirmed by typical mercury poisoning experiment and leaching test.

3.3.5.1 Mercury Poisoning Experiment

To establish the heterogeneity of the **Pd@TpBpy** catalyst, we have conducted mercury poisoning test for tandem catalysis for showing the significant inhibition in the catalytic process, due to the poisoning of the catalytically active metal centers. In a typical mercury poisoning test, two set of reactions for tandem catalysis process were carried out

using phenylacetylene (66 μL , 0.6 mmol), 2-bromophenol (58 μL , 0.5 mmol), potassium carbonate (34.5 mg, 0.25 mmol) and **Pd@TpBpy** (2 mg, 0.6 mol%) in 1 mL dry DMF, under nitrogen atmosphere and allowed to stir at 150 $^{\circ}\text{C}$. In one case, we have added 250 mg of mercury to the reaction mixture during the addition of the substrates and another reaction mixture was heated without adding any trace of mercury. After the 20h reaction, the yields of the products were measured by GC. The reaction mixture without mercury gave 70% yield of the product, whereas the reaction mixture having mercury gave 8% yield of the product, which strongly suggests the heterogeneity of the catalyst. The yield of the product decreased due to the formation of Pd-Hg amalgam on the palladium nanoparticles surface.

3.3.5.2 Pd Leaching Test:

In a typical catalyst leaching test experiment, a mixture of phenyl acetylene (66 μL , 0.6 mmol), 2-bromophenol (58 μL , 0.5 mmol), potassium carbonate (34.5 mg, 0.25 mmol) and **Pd@TpBpy** (2 mg, 0.6 mol%) are added to 1 mL dry DMF under nitrogen atmosphere in a screw cap reaction tube. Then the reaction mixture is allowed to stir at 150 $^{\circ}\text{C}$ for 5 h. After 5h, 55% product conversion is achieved as determined by GC. The solid palladium catalyst is removed quickly from the reaction mixture by centrifugation and the reaction mixture is transferred to another reaction tube under identical condition. There is no additional product conversion observed even after 15 h of heating to the reaction mixture, which suggests the almost negligible leaching of metal from palladium catalyst.

3.3.5.3 Catalyst Recyclability Experiment:

Further, the recyclability test of the **Pd@TpBpy** catalyst has been performed (using 3-bromo-4-hydroxybenzonitrile and phenylacetylene as a coupling partner) for a model reaction (Figure 3.7). The outcomes of the experiments suggest superior recyclability of **Pd@TpBpy** up to five cycles without considerable deactivation of catalytic

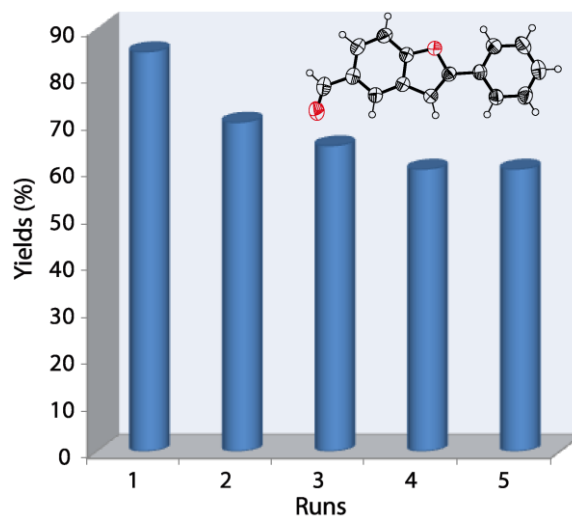


Figure 3.7: Recyclability test of **Pd@TpBpy** catalyst used for tandem catalysis. Yields are calculated by GC peak integration using *m*-Xylene as an internal standard.

activity. This is due to stable and less sintering nature of **Pd@TpBpy** through the catalytic cycles. All these experiments unambiguously confirm the heterogeneity of the **Pd@TpBpy** catalyst.

3.4 Conclusion

In this chapter, we have discussed a unique strategy for *in situ* loading of metal (**Pd**) nanoparticles in the chemically stable, porous, crystalline COF (**Pd@TpBpy**), without using a conventional reducing agent. The **Pd@TpBpy** has been synthesized by simply reacting with 1,3,5-triformylphloroglucinol (**Tp**) and 2,2'-bipyridine-5,5'-diamine palladium chloride (**Bpy-PdCl₂**) in the solvothermal condition in DMAc and Dioxane solvents. Best of our knowledge this is the first report of *in situ* loading of Pd nanoparticles in the covalent organic framework by using Pd anchored building unit for COF synthesis. The TEM images of **Pd@TpBpy** unambiguously confirm the uniform distribution of the Pd nanoparticle in the COF skeleton. The ¹⁵N NMR experiments also confirm the breakage of Pd-N bond takes place in the course of COF formation. The stability and crystalline nature of the **Pd@TpBpy** make it ideal candidates as a heterogeneous catalyst. Therefore, we have successfully used this hybrid material **Pd@TpBpy** as a heterogeneous catalyst for the synthesis of 2-substituted benzofuran derivatives in one-pot way *via* tandem process with the turnover number up to 1101 (Table 3.10). The negligible metal leaching, non-sintering behavior, and good recyclability during the catalytic process confirm the robustness and the green character of the catalyst. Finally, we believe our developed method for *in situ* loading of metal nanoparticles in the Covalent Organic Framework will definitely open up a new domain of exciting research area in the field of heterogeneous catalysis.

3.5 Experimental Procedures

3.5.1 Synthesis of 2,2'-bipyridine-5,5'-diamine palladium chloride (**Bpy-PdCl₂**):

1,3,5-triformylphloroglucinol (**Tp**) is synthesized using a previously reported method and confirmed by IR, ¹HNMR, and ¹³CNMR [3.19].

As shown in Figure 3.8, the compounds, 1-(2-Chloropyridine)-5-yl-2,5-dimethyl-1H-pyrrole (**4**), 5,5'-Bis(2,5-dimethyl-1H-pyrrole)-2,2'-bipyridine (**5**), and 2,2'-bipyridine-5,5'-diamine (**Bpy**) are synthesized using previously reported methods and confirmed by IR, ¹HNMR, and ¹³CNMR [3.20]. In a round bottom flask, palladium chloride (177.3 mg,

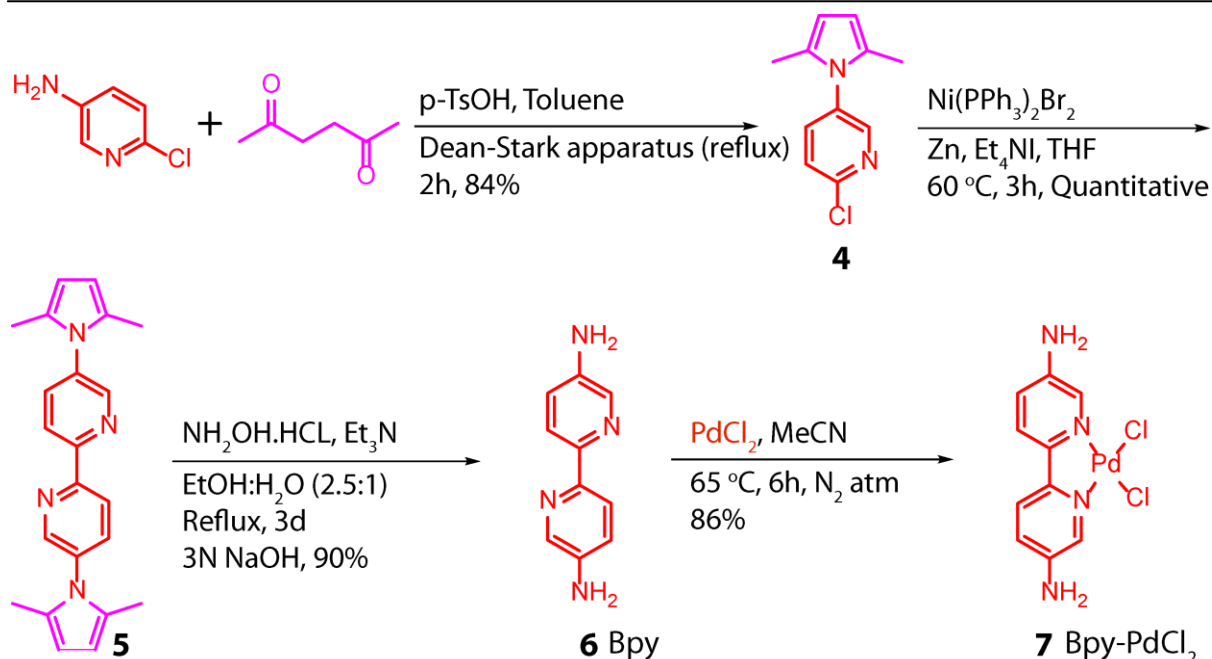


Figure 3.8: General synthetic scheme for the preparation of 2,2'-bipyridine-5,5'-diamine palladium chloride (**Bpy-PdCl₂**).

1 mmol) is added in 30 mL acetonitrile under N₂ atmosphere and allowed to stir the reaction mixture at 65 °C for 1h to get a clear solution. Then the palladium chloride solution is added dropwise to the solution of 2,2'-bipyridine-5,5'-diamine (**Bpy**) (186.2 mg, 1 mmol) in 20 mL acetonitrile solution under N₂ atmosphere. During the addition, the reddish colored precipitate of 2,2'-bipyridine-5,5'-diamine-palladium chloride (**Bpy-PdCl₂**) complex is found, and for complete conversion, the reaction mixture was stirred 5h at 65 °C. The solid precipitate is isolated from the reaction mixture and washed with excess acetonitrile solution to get pure 2,2'-bipyridine-5,5'-diamine palladium chloride (**Bpy-PdCl₂**) product, with 86% yield (Figure 3.8). ¹H NMR (400 MHz, DMSO-*d*₆): δ = 8.33 (s, 2H), 7.74 (d, *J* = 8.7 Hz, 2H), 7.2 (d, *J* = 8.2 Hz, 2H), 6.25 (s, 4H); ¹³C NMR (101 MHz, DMSO-*d*₆) δ = 145.93, 145.14, 135.21, 123.33, 122.23; **Elemental Analysis**; Anal. Calcd. For C₁₀H₁₀N₄Cl₂Pd₁·2HCl: C, 27.52; H, 2.77; N, 12.84; found: C, 27.5; H, 2.21; N, 11.61. **HRMS-ESI (m/z) [M+H]⁺** calcd for C₁₀H₁₁N₄Cl₂Pd₁, 362.9413, found 362.9390. The pure material (**Bpy-PdCl₂**) is crystallized in DMSO solvent and the crystals are solvent exchanged with acetonitrile for 2 days. The PXRD pattern of 2,2'-bipyridine-5,5'-diamine-palladium chloride (**Bpy-PdCl₂**) solvent exchanged crystals are perfectly matching with simulated one. CCDC 1519399 contains the crystallographic data for **Bpy-PdCl₂**.

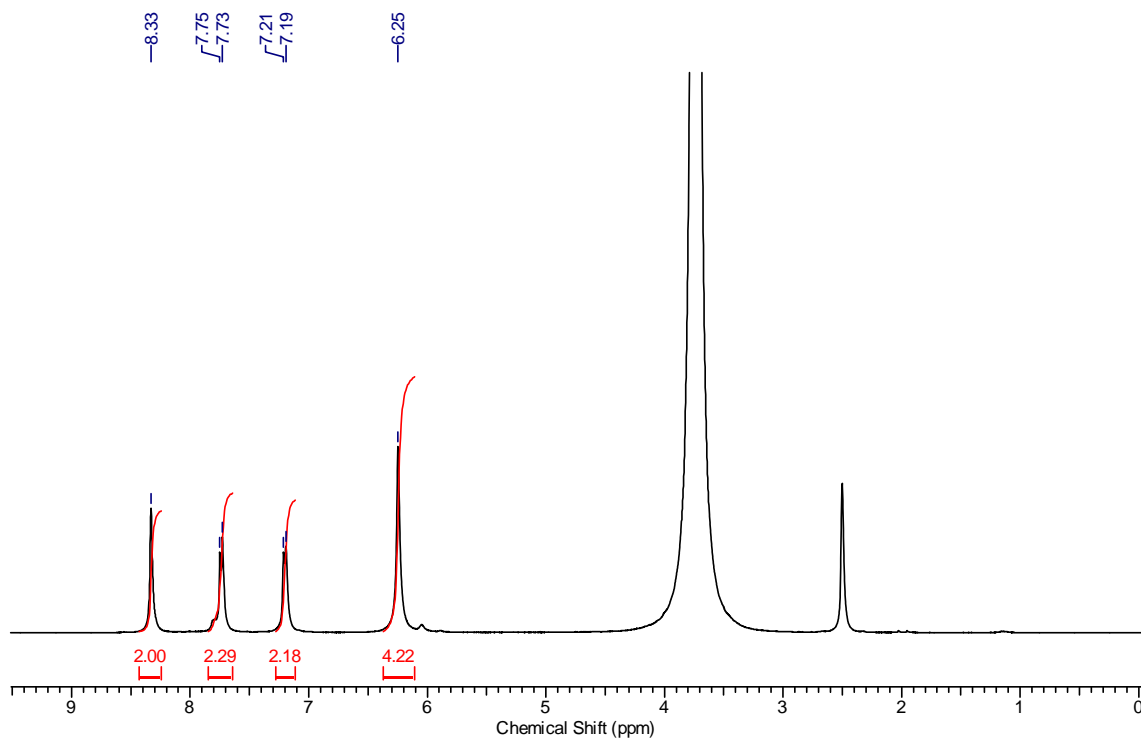


Figure 3.9: ^1H NMR spectrum (in $\text{DMSO-}d_6$) of 2,2'-bipyridine-5,5'-diamine palladium chloride (Bpy-PdCl_2).

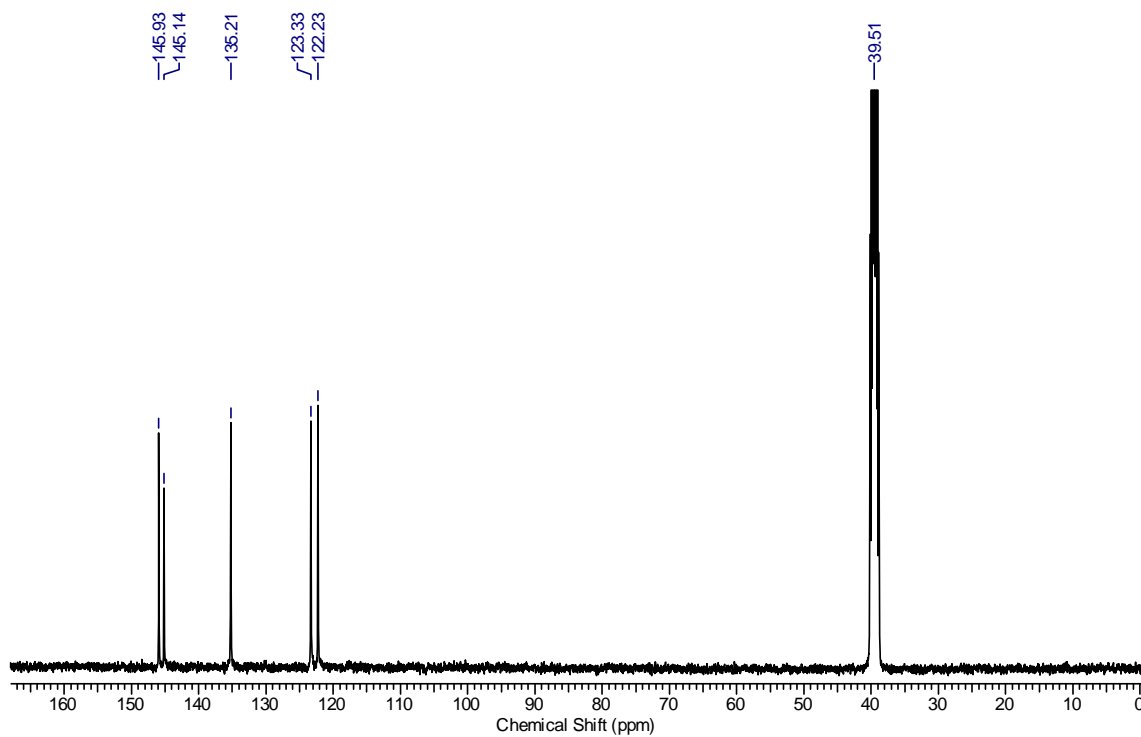


Figure 3.10: ^{13}C NMR spectrum (in $\text{DMSO-}d_6$) of 2,2'-bipyridine-5,5'-diamine palladium chloride (Bpy-PdCl_2).

3.5.2 X-Ray Investigation of Single Crystals of Bpy-PdCl₂Table 3.3 Structural information of Bpy-PdCl₂ single crystal

Structural information	
Empirical formula	C ₁₀ H ₁₀ Cl ₂ N ₄ Pd
Formula weight	363.52
Temperature/K	293
Crystal system	monoclinic
Space group	<i>P</i> 2 ₁ / <i>n</i>
<i>a</i> /Å	10.0173(2)
<i>b</i> /Å	8.6586(2)
<i>c</i> /Å	13.7906(3)
α /°	90.00
β /°	99.382(2)
γ /°	90.00
Volume/Å ³	1180.14(5)
<i>Z</i>	4
ρ_{calc} /mg/mm ³	2.046
μ /mm ⁻¹	2.005
<i>F</i> (000)	712.0
Crystal size/mm ³	0.32 × 0.29 × 0.15
2 θ range for data collection	5.98 to 58°
Index ranges	-11 ≤ <i>h</i> ≤ 12, -10 ≤ <i>k</i> ≤ 6, -16 ≤ <i>l</i> ≤ 17
Reflections collected	4732
Independent reflections	2410[R(int) = 0.0231]
Data/restraints/parameters	2410/0/165
Goodness-of-fit on <i>F</i> ²	1.056
Final <i>R</i> indexes [<i>I</i> ≥ 2 σ (<i>I</i>)]	<i>R</i> ₁ = 0.0266, <i>wR</i> ₂ = 0.0536
Final <i>R</i> indexes [all data]	<i>R</i> ₁ = 0.0337, <i>wR</i> ₂ = 0.0589
Largest diff. peak/hole / e Å ⁻³	0.44/-0.476

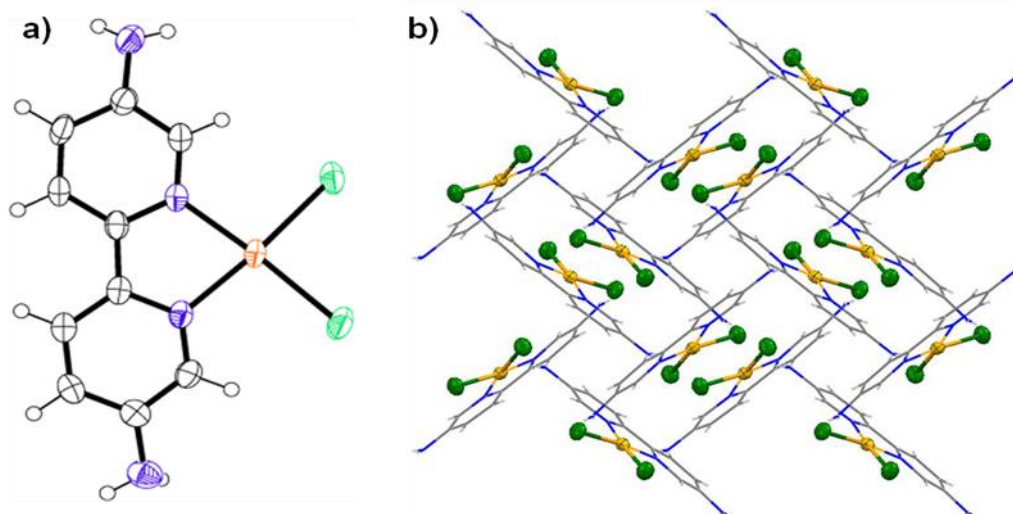


Figure 3.11: (a) Single Crystal X-ray diffraction structure of the reference compound **Bpy-PdCl₂**. In the ORTEP (with 50% probability level); Carbon (light gray), Nitrogen (blue), Palladium (orange), Chloride (green) and Hydrogen (white) have been shown. (b) Crystal packing along *c* axis.

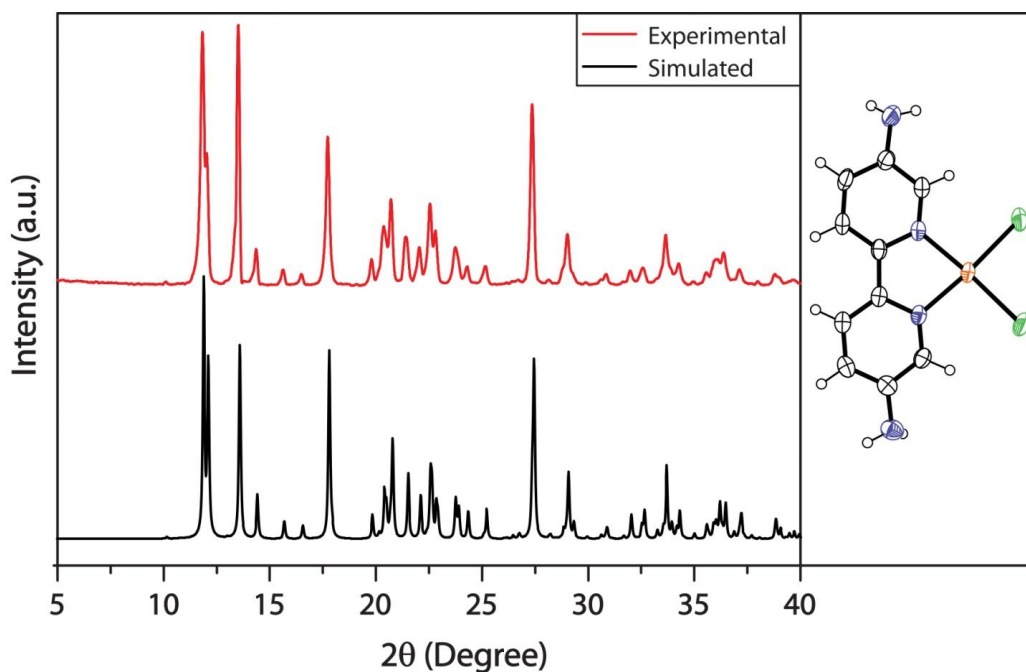


Figure 3.12: PXRD comparison between as-synthesized (**red**) and simulated (**black**) pattern of 2,2'-bipyridine-5,5'-diamine-palladium chloride (**Bpy-PdCl₂**).

3.5.3 Synthesis of Pd@TpBpy:

The **Pd@TpBpy** is synthesized by reacting 1,3,5-triformylphloroglucinol (**Tp**) (21 mg, 0.1 mmol) with 2,2'-bipyridine-5,5'-diamine palladium chloride (**Bpy-PdCl₂**) (54.5 mg,

0.15 mmol) in presence of *N,N*-dimethylacetamide (DMAc) and 1,4-dioxane solvent combination (2.3 : 0.7 mL) with 0.3 mL of 6M aqueous acetic acid using solvothermal process. The reactants are ultrasonicated for 15 min to disperse homogeneously as well as degassed through three successive freeze-pump-thaw cycles. Then the tube is sealed in a vacuum condition and heated at 90 °C in the isothermal oven for 3 days. Finally, the phase pure material is filtered out and washed with DMAc and DMSO solvents to remove the residues of the starting materials. The collected reddish black material is solvent exchanged with DMSO and is washed with excess acetone. Then the powder material is dried at 110 °C for 12 h under vacuum in order to get as synthesized **Pd@TpBpy** COF (88% yield). **IR (powder, cm⁻¹):** 1606, 1566, 1448, 1243, 1147, 1095, 1065, 1030, 994, 923, 906, 844, 813. **Elemental Analysis;** Anal. Calcd. For C₄₈H₃₀N₁₂O₆Cl₆Pd₃: C, 41.1; H, 2.16; N, 11.98; found: C, 40.58; H, 3.16; N, 11.33.

3.5.4 Structure Modelling and Powder X-Ray Diffraction Analysis

Atomic positions and cell sizes of modeled CPP layers were optimized using Self-Consistent-Charge Density-Functional Tight-Binding (SCC-DFTB) method. Stacking of layers is affected by the Coulomb repulsion between the partial atomic charges in adjacent layers. Hence, we performed a Mulliken population analysis for the charges. The adjacent

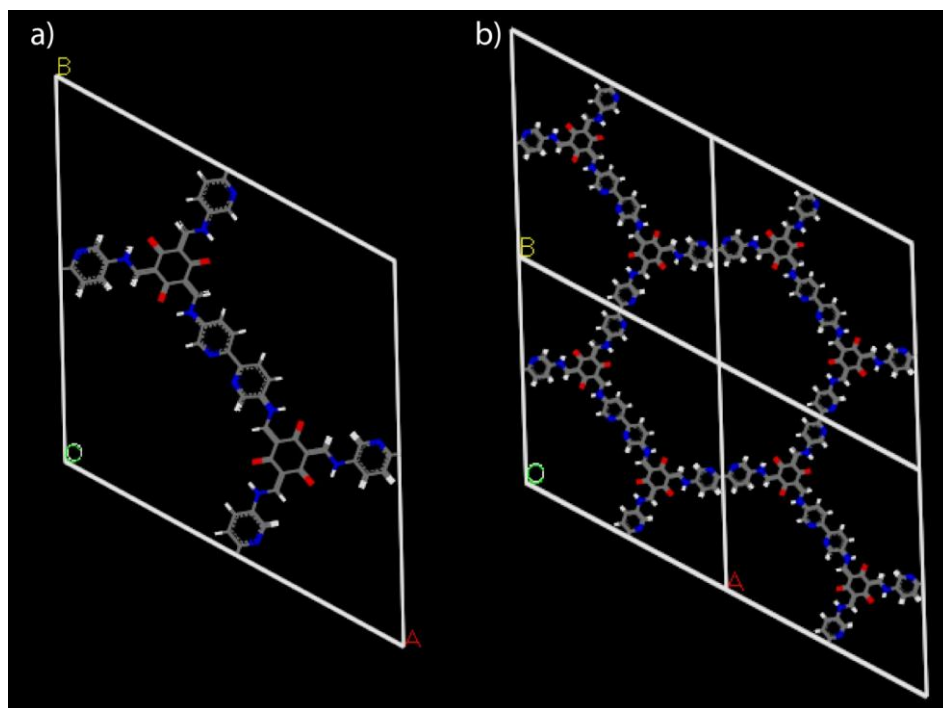


Figure 3.13: (a) Unit cell and (b) Eclipsed crystal lattice packing of *cis* TpBpy.

layers were shifted with respect to each other in different directions in order to avoid Coulomb repulsion from charges alike. Several possibilities were considered, however, the best was taken from a comparison of simulated PXRD pattern with the experimental. Interlayer separation was also determined from the comparison of PXRD patterns. The fractional coordinates of *cis* **TpBpy** are given in Table 3.2 respectively.

In order to elucidate the structure of *cis* **TpBpy** and to calculate the unit cell parameters, possible 2-D models were optimized using Density Functional Tight-Binding method. Several stacking possibilities were considered for reasons reported in the literature. The experimental PXRD patterns are agreeable with the simulated patterns of AA stacking models. Therefore, *cis* **TpBpy** has been modeled in the hexagonal space group ($P6_3$) by comparing the experimental and simulated PXRD patterns.

N.B.: Here we have simulated the unit cell of **Pd@TpBpy** by considering 2,2'-bipyridine-5,5'-diamine (**Bpy**) having both the pyridinic nitrogen in the *cis* position as one of the coupling partners rather than 2,2'-bipyridine-5,5'-diamine palladium chloride (**Bpy-PdCl₂**). Because Pd-N bonds are broken during the reaction. Therefore, it forms Pd nanoparticles over the support which is similar to the *cis* **TpBpy** COF.

3.5.5 FT-IR Spectra and Energy Dispersive X-ray Analysis (EDX)

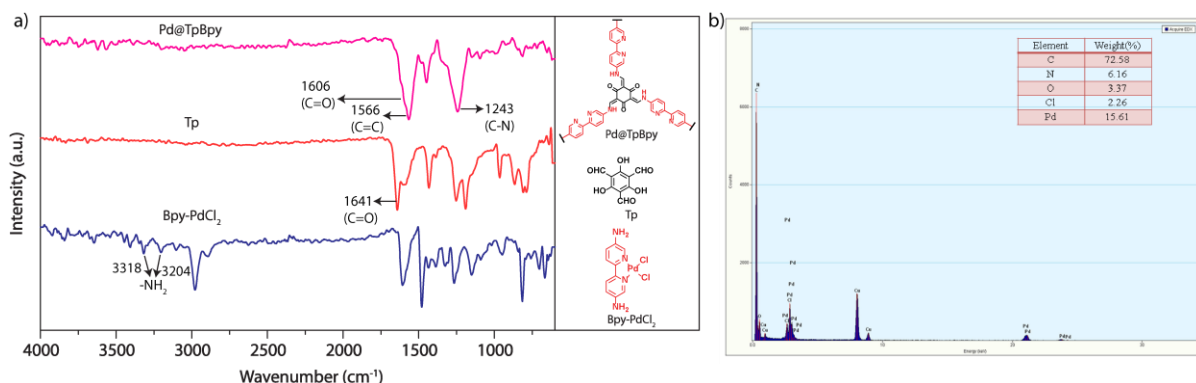


Figure 3.14: (a) FT-IR spectra of 2,2'-bipyridine-5,5'-diamine palladium chloride (**Bpy-PdCl₂**) (blue), 1,3,5-triformylphloroglucinol (**Tp**) (red) and **Pd@TpBpy** (pink). (b) Energy dispersive x-ray analysis of **Pd@TpBpy** showing the presence of C, N, O, Cl and Pd elements.

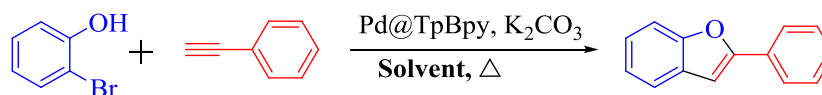
3.5.6 General Procedure for the Tandem Catalysis:

Phenylacetylene (0.6 mmol, 66 μ L), 2-bromophenol (0.5 mmol, 58 μ L), potassium carbonate (34.5 mg, 0.25 mmol) and **Pd@TpBpy** (2 mg, 0.6 mol%) are added to 1 mL dry

DMF under nitrogen atmosphere in a screw cap reaction tube. Then the reaction mixture is allowed to stir at 150 °C for 20h. After the completion of the reaction (monitored by TLC), the reaction mixture is centrifuged to separate the solid and the solid was washed with DCM. The combined organic layer is washed with water to remove potassium carbonate and the organic layer is evaporated under reduced pressure. The crude product is purified by column chromatography to obtain the desired product.

3.5.7 Optimization Details for Tandem Catalysis:

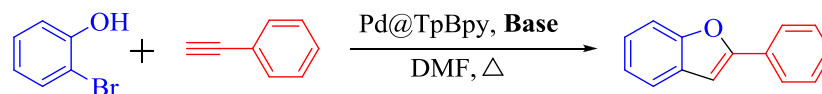
Table 3.4 Optimization of Solvents



Entry	Solvent	GC Yield (%)
1	MeCN	30
2	Toluene	36
3	1,4-Dioxane	47
4	<i>m</i> -Xylene	23
5	THF	27
6	DMSO	11
7	DCE	17
8	NMP	26
9	Mesitylene	20
10	DMA	47
11	DME	25

Reactions are conducted with 0.5 mmol of 2-bromophenol (1 equiv), 0.6 mmol of phenyl acetylene (1.2 equiv), 1.7 mol% of Pd@TpBpy and K₂CO₃ (0.5 equiv) are heated in 1 mL representative solvents for 20 h.

Table 3.5 Optimization of Bases

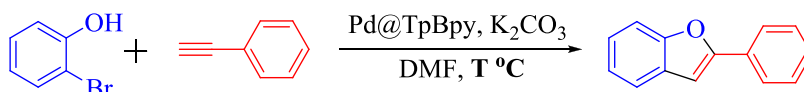


Entry	Base	GC Yield (%)
1	Cs ₂ CO ₃	15
2	Na ₂ CO ₃	22
3	Li ₂ CO ₃	7
4	Ag ₂ CO ₃	-
5	-	-

6	KOAc	13
7	KO ^t Bu	8

Reactions are conducted with 0.5 mmol of 2-bromophenol (1 equiv), 0.6 mmol of phenyl acetylene (1.2 equiv), 1.7 mol% of Pd@TpBpy and base (0.5 equiv) are heated using 1 mL of DMF as a solvent for 20 h.

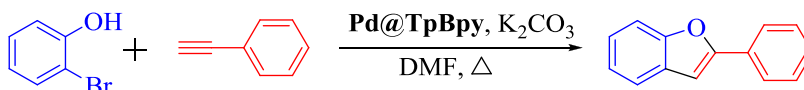
Table 3.6 Temperature Optimization



Entry	Temperature (°C)	GC Yield (%)
1	90	25
2	110	37
3	130	50

Reactions are conducted with 0.5 mmol of 2-bromophenol (1 equiv), 0.6 mmol of phenyl acetylene (1.2 equiv), 1.7 mol% of Pd@TpBpy and K₂CO₃ (0.5 equiv) at Temp. °C in 1 mL DMF for 20 h.

Table 3.7 Optimization of Amount of Catalyst



Entry	Pd@TpBpy (mol%)	GC Yield (%)
1	1.7	58
2	1.1	65
3	-	-
4	2.3	49
5	3.4	40

Reactions are conducted with 0.5 mmol of 2-bromophenol (1 equiv), 0.6 mmol of phenyl acetylene (1.2 equiv), x mol% of Pd@TpBpy and K₂CO₃ (0.5 equiv) heated at 150 °C in 1 mL DMF for 20 h.

Table 3.8 Time Optimization

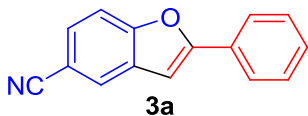


Entry	Time (h)	GC Yield (%)
1	3	42
2	7	45
3	11	49
4	14	55
5	17	59

Reactions are conducted with 0.5 mmol of 2-bromophenol (1 equiv), 0.6 mmol of phenyl acetylene (1.2 equiv), 0.6 mol% of Pd@TpBpy and K₂CO₃ (0.5 equiv) heated at 150 °C in 1 mL DMF for t (h).

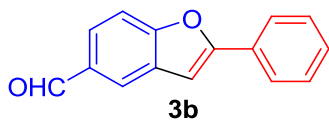
3.5.8 Characteristic Data of Synthesized Compounds

2-phenylbenzofuran-5-carbonitrile (3a) is synthesized by general procedure with 3-bromo-4-hydroxybenzonitrile (0.5 mmol, 99 mg) and phenylacetylene (0.6 mmol, 66 μL) as the substrate. Isolated yield of the product is 77%.



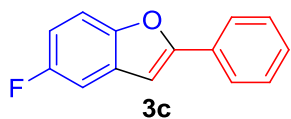
¹H NMR (400 MHz, CDCl₃): δ = 7.93 (s, 1H), 7.88 (d, *J* = 7.3 Hz, 2H), 7.62-7.56 (m, 2H), 7.50 (t, *J* = 7.3 Hz, 2H), 7.43 (t, *J* = 7.3 Hz, 1H), 7.07 (s, 1H); ¹³C NMR (101 MHz, CDCl₃) δ = 158.34, 156.44, 129.87, 129.54, 129.26, 128.98, 127.86, 125.75, 125.24, 119.48, 112.27, 106.86, 100.73; HRMS-ESI (m/z) [M+H]⁺ calcd for C₁₅H₁₀ON, 220.0757, found 220.0757.

2-phenylbenzofuran-5-carbaldehyde (3b) is synthesized by general procedure with 3-bromo-4-hydroxybenzaldehyde (0.5 mmol, 100.5 mg) and phenylacetylene (0.6 mmol, 66 μL) as the substrate. Isolated yield of the product is 64%.



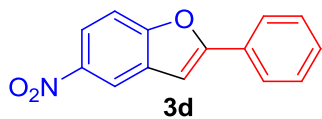
¹H NMR (400 MHz, CDCl₃): δ = 10.07 (s, 1H), 8.11 (s, 1H), 7.89-7.85 (m, 3H), 7.63 (d, *J* = 8.2 Hz, 1H), 7.48 (t, *J* = 7.4 Hz, 2H), 7.41 (t, *J* = 7.3 Hz, 1H), 7.10 (s, 1H); ¹³C NMR (101 MHz, CDCl₃) δ = 191.74, 158.19, 157.90, 132.37, 129.76, 129.56, 129.23, 128.89, 125.88, 125.09, 123.94, 111.82, 101.47; HRMS-ESI (m/z) [M+H]⁺ calcd for C₁₅H₁₁O₂, 223.0754, found 223.0754.

5-fluoro-2-phenylbenzofuran (3c) is synthesized by general procedure with 2-bromo-4-fluorophenol (0.5 mmol, 95.5 mg) and phenylacetylene (0.6 mmol, 66 μL) as the substrate. Isolated yield of the product is 60%.



¹H NMR (500 MHz, CDCl₃): δ = 7.87 (d, *J* = 8.3 Hz, 2H), 7.49-7.44 (m, 3H), 7.39 (t, *J* = 7.3 Hz, 1H), 7.24 (dd, *J* = 8.7, 2.7 Hz, 1H), 7.01 (dt, *J* = 9.15, 2.6 Hz, 1H), 7.00 (s, 1H); ¹³C NMR (126 MHz, CDCl₃) δ = 159.31 (d, *J*_{C-F} = 237.5 Hz), 157.67, 151.1, 130.1, 129.97 (d, *J*_{C-F} = 10.5 Hz), 128.88, 128.83, 124.98, 111.84 (d, *J*_{C-F} = 23.8 Hz), 111.67, 106.30 (d, *J*_{C-F} = 25.7 Hz), 101.42; HRMS-ESI (m/z) [M+H]⁺ calcd for C₁₄H₁₀OF, 213.0734, found 213.0730.

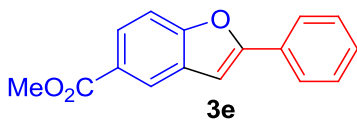
5-nitro-2-phenylbenzofuran (3d) is synthesized by general procedure with 2-bromo-4-



nitrophenol (0.5 mmol, 109 mg) and phenylacetylene (0.6 mmol, 66 μ L) as the substrate. Isolated yield of the product is 43%.

^1H NMR (500 MHz, CDCl_3): δ = 8.49 (s, 1H), 8.21 (dd, J = 8.7, 2.3 Hz, 1H), 7.87 (d, J = 7.2 Hz, 2H), 7.58 (d, J = 8.7 Hz, 1H), 7.50 (t, J = 7.4 Hz, 2H), 7.43 (t, J = 7.3 Hz, 1H), 7.11 (s, 1H); ^{13}C NMR (126 MHz, CDCl_3) δ = 159.18, 157.54, 144.26, 129.64, 129.56, 129.11, 128.96, 125.21, 120.04, 117.21, 111.36, 101.54; HRMS-ESI (m/z) $[\text{M}+\text{Na}]^+$ calcd for $\text{C}_{14}\text{H}_9\text{O}_3\text{NNa}$, 262.0475, found 262.0475.

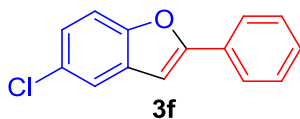
Methyl 2-phenylbenzofuran-5-carboxylate (3e) is synthesized by general procedure with



methyl 3-bromo-4-hydroxybenzoate (0.5 mmol, 115.5 mg) and phenylacetylene (0.6 mmol, 66 μ L) as the substrate. Isolated yield of the product is 37%.

^1H NMR (400 MHz, CDCl_3): δ = 8.33 (s, 1H), 8.03 (d, J = 8.2 Hz, 1H), 7.88 (d, J = 7.8 Hz, 2H), 7.55 (d, J = 8.7 Hz, 1H), 7.48 (t, J = 7.3 Hz, 2H), 7.39 (t, J = 7.3 Hz, 1H), 7.08 (s, 1H), 3.96 (s, 3H); ^{13}C NMR (101 MHz, CDCl_3) δ = 167.27, 157.41, 129.87, 129.23, 129.01, 128.86, 126.04, 125.31, 125.05, 123.29, 110.98, 101.49, 52.09; HRMS-ESI (m/z) $[\text{M}+\text{H}]^+$ calcd for $\text{C}_{16}\text{H}_{13}\text{O}_3$, 253.0858, found 253.0858.

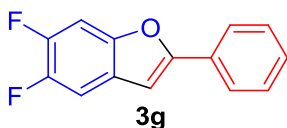
5-chloro-2-phenylbenzofuran (3f) is synthesized by general procedure with 2-bromo-4-



chlorophenol (0.5 mmol, 103.7 mg) and phenylacetylene (0.6 mmol, 66 μ L) as the substrate. Isolated yield of the product is 60%.

^1H NMR (400 MHz, CDCl_3): δ = 7.76 (d, J = 7.8 Hz, 2H), 7.45 (s, 1H), 7.38-7.33 (m, 3H), 7.29 (t, J = 6.9 Hz, 1H), 7.14 (d, J = 8.7 Hz, 1H), 6.86 (s, 1H); ^{13}C NMR (101 MHz, CDCl_3) δ = 157.37, 153.22, 130.55, 129.94, 128.96, 128.83, 128.46, 125.03, 124.36, 120.39, 112.08, 100.76; HRMS-ESI (m/z) $[\text{M}+\text{H}]^+$ calcd for $\text{C}_{14}\text{H}_{10}\text{OCl}$, 229.0417, found 229.0415.

5,6-difluoro-2-phenylbenzofuran (3g) is synthesized by general procedure with 2-bromo-

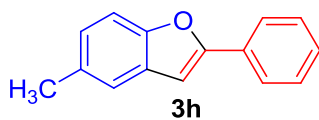


4,5-difluorophenol (0.5 mmol, 57.1 μ L) and phenylacetylene (0.6 mmol, 66 μ L) as the substrate. Isolated yield of the product is 32%.

^1H NMR (400 MHz, CDCl_3): δ = 7.82 (d, J = 7.3 Hz, 2H), 7.47 (t, J = 7.7 Hz, 2H), 7.40-7.30 (m, 3H), 6.95 (s, 1H); ^{13}C NMR (101 MHz, CDCl_3) δ = 157.82,

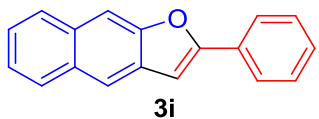
149.76, 149.64, 148.62 (dd, $J_{C-F} = 245.4, 15.3$ Hz), 148.07 (dd, $J_{C-F} = 241.5, 14.4$ Hz), 129.82, 128.9, 128.85, 124.8, 107.49 (d, $J_{C-F} = 21.1$ Hz), 100.99, 100.39 (d, $J_{C-F} = 23$ Hz); HRMS-ESI (m/z) $[M+H]^+$ calcd for $C_{14}H_9OF_2$, 231.0627, found 231.0616.

5-methyl-2-phenylbenzofuran (3h) is synthesized by general procedure with 2-bromo-4-methylphenol (0.5 mmol, 60.4 μ L) and phenylacetylene (0.6 mmol, 66 μ L) as the substrate. Isolated yield of the product is 26%.



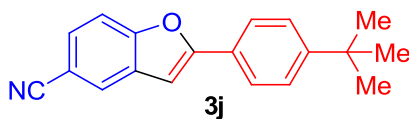
1H NMR (400 MHz, $CDCl_3$): $\delta = 7.87$ (d, $J = 7.8$ Hz, 2H), 7.46 (t, $J = 7.3$ Hz, 2H), 7.42 (d, $J = 8.2$ Hz, 1H), 7.38 (s, 1H), 7.36 (t, $J = 7.3$ Hz, 1H), 7.11 (d, $J = 8.3$ Hz, 1H), 6.97 (s, 1H), 2.47 (s, 3H); ^{13}C NMR (101 MHz, $CDCl_3$) $\delta = 155.97, 153.32, 132.32, 130.61, 129.30, 128.73, 128.39, 125.51, 124.83, 120.71, 110.64, 101.07, 21.33$; HRMS-ESI (m/z) $[M+H]^+$ calcd for $C_{15}H_{13}O$, 209.0961, found 209.0961.

2-phenylnaphtho[2,3-b]furan (3i) is synthesized by general procedure with 3-bromo-2-naphthol (0.5 mmol, 111.5 mg) and phenylacetylene (0.6 mmol, 66 μ L) as the substrate. Isolated yield of the product is 42%.



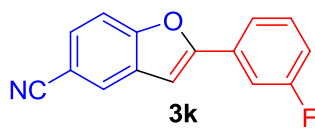
1H NMR (400 MHz, $CDCl_3$): $\delta = 8.06$ (s, 1H), 7.98-7.95 (m, 4H), 7.94 (s, 1H), 7.51 (t, $J = 7.4$ Hz, 2H), 7.47-7.39 (m, 3H), 7.17 (s, 1H); ^{13}C NMR (101 MHz, $CDCl_3$) $\delta = 158.14, 153.90, 131.52, 130.68, 130.24, 130.16, 129.10, 128.84, 127.94, 127.85, 125.32, 124.77, 124.04, 118.54, 106.57, 100.77$; HRMS-ESI (m/z) $[M+H]^+$ calcd for $C_{18}H_{13}O$, 245.0949, found 245.0951.

2-(4-tert-butylphenyl)benzofuran-5-carbonitrile (3j) is synthesized by general procedure with 3-bromo-4-hydroxybenzonitrile (0.5 mmol, 99 mg) and 4-tert-butylphenylacetylene (0.6 mmol, 108.3 μ L) as the substrate. Isolated yield of the product is 79%.



1H NMR (400 MHz, $CDCl_3$): $\delta = 7.89$ (s, 1H), 7.80 (d, $J = 8.6$ Hz, 2H), 7.58-7.54 (m, 2H), 7.51 (d, $J = 8.6$ Hz, 2H), 6.99 (s, 1H), 1.38 (s, 9H); ^{13}C NMR (101 MHz, $CDCl_3$) $\delta = 158.48, 156.29, 152.89, 129.94, 127.53, 126.40, 125.86, 125.46, 124.99, 119.50, 112.10, 106.65, 100.01, 34.80, 31.12$; HRMS-ESI (m/z) $[M+H]^+$ calcd for $C_{19}H_{18}ON$, 276.1379, found 276.1383.

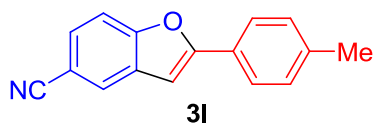
2-(3-fluorophenyl)benzofuran-5-carbonitrile (3k) is synthesized by general procedure with



3-bromo-4-hydroxybenzocyanide (0.5 mmol, 99 mg) and 1-ethynyl-3-fluorobenzene (0.6 mmol, 69.4 μ L) as the substrate. Isolated yield of the product is 62%.

^1H NMR (400 MHz, CDCl_3): δ = 7.92 (s, 1H), 7.64 (d, J = 7.9 Hz, 1H), 7.59 (s, 1H), 7.58-7.54 (m, 2H), 7.44 (q, J = 7.1 Hz, 1H), 7.11 (t, J = 8 Hz, 1H), 7.07 (s, 1H); ^{13}C NMR (101 MHz, CDCl_3) δ = 163.03 (d, $J_{\text{C-F}}$ = 246.6 Hz), 156.85, 156.36, 131.23 (d, $J_{\text{C-F}}$ = 8.5 Hz), 130.63 (d, $J_{\text{C-F}}$ = 7.7 Hz), 129.53, 128.21, 125.94, 120.88, 119.27, 116.37 (d, $J_{\text{C-F}}$ = 21.6 Hz), 112.35, 112.12 (d, $J_{\text{C-F}}$ = 23.9 Hz), 107.07, 101.72; HRMS-ESI (m/z) [$\text{M}+\text{H}$] $^+$ calcd for $\text{C}_{15}\text{H}_9\text{ONF}$, 238.0667, found 238.0663.

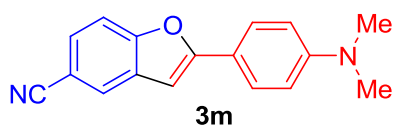
2-*p*-tolylbenzofuran-5-carbonitrile (3l) is synthesized by general procedure with 3-bromo-



4-hydroxybenzocyanide (0.5 mmol, 99 mg) and 4-ethynyltoluene (0.6 mmol, 76.1 μ L) as the substrate. Isolated yield of the product is 70%.

^1H NMR (400 MHz, CDCl_3): δ = 7.87 (s, 1H), 7.74 (d, J = 7.9 Hz, 2H), 7.57-7.51 (m, 2H), 7.28 (d, J = 7.9 Hz, 2H), 6.97 (s, 1H), 2.42 (s, 3H); ^{13}C NMR (101 MHz, CDCl_3) δ = 158.54, 156.26, 139.74, 129.95, 129.61, 127.54, 126.44, 125.45, 125.12, 119.50, 112.08, 106.67, 99.90, 21.39; HRMS-ESI (m/z) [$\text{M}+\text{H}$] $^+$ calcd for $\text{C}_{16}\text{H}_{12}\text{ON}$, 234.0915, found 234.0913.

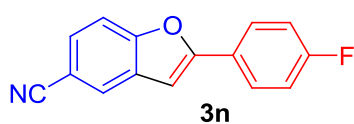
2-(4-(dimethylamino)phenyl)benzofuran-5-carbonitrile (3m) is synthesized by general



procedure with 3-bromo-4-hydroxybenzocyanide (0.5 mmol, 99 mg) and 4-ethynyl-*N,N*-dimethylaniline (0.6 mmol, 87.1 mg) as the substrate. Isolated yield of the product is 62%.

^1H NMR (200 MHz, CDCl_3): δ = 7.83 (s, 1H), 7.74 (d, J = 8.9 Hz, 2H), 7.57-7.44 (m, 2H), 6.81 (s, 1H), 6.77 (d, J = 8.9 Hz, 2H), 3.05 (s, 6H); ^{13}C NMR (101 MHz, CDCl_3) δ = 159.97, 159.56, 156.22, 130.63, 126.78, 126.53, 124.73, 119.80, 119.28, 112.02, 111.73, 106.33, 97.25, 40.22; HRMS-ESI (m/z) [$\text{M}+\text{H}$] $^+$ calcd for $\text{C}_{17}\text{H}_{15}\text{ON}_2$, 263.1174, found 263.1179.

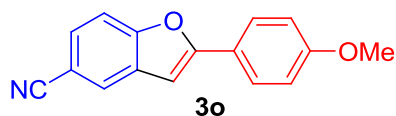
2-(4-fluorophenyl)benzofuran-5-carbonitrile (3n) is synthesized by general procedure with



3-bromo-4-hydroxybenzocyanide (0.5 mmol, 99 mg) and 1-ethynyl-4-fluorobenzene (0.6 mmol, 68.8 μ L) as the substrate. Isolated yield of the product is 65%.

^1H NMR (400 MHz, CDCl_3): $\delta = 7.90$ (s, 1H), 7.86-7.82 (m, 2H), 7.59-7.54 (m, 2H), 7.19-7.15 (m, 2H), 6.98 (s, 1H); ^{13}C NMR (101 MHz, CDCl_3) $\delta = 163.35$ (d, $J_{\text{C-F}} = 250.2$ Hz), 157.34, 156.33, 129.79, 127.84, 127.14 (d, $J_{\text{C-F}} = 8.6$ Hz), 125.66, 125.56, 119.36, 116.12 (d, $J_{\text{C-F}} = 22$ Hz), 112.19, 106.92, 100.42; HRMS-ESI (m/z) $[\text{M}+\text{H}]^+$ calcd for $\text{C}_{15}\text{H}_9\text{ONF}$, 238.0667, found 238.0663.

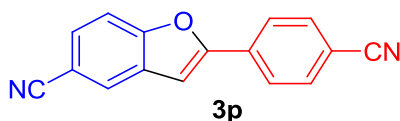
2-(4-methoxyphenyl)benzofuran-5-carbonitrile (3o) is synthesized by general procedure



with 3-bromo-4-hydroxybenzonitrile (0.5 mmol, 99 mg) and 4-ethynylanisole (0.6 mmol, 77.8 μL) as the substrate. Isolated yield of the product is 76%.

^1H NMR (400 MHz, CDCl_3): $\delta = 7.86$ (s, 1H), 7.79 (d, $J = 8.3$ Hz, 2H), 7.56-7.50 (m, 2H), 7.00 (d, $J = 8.3$ Hz, 2H), 6.89 (s, 1H), 3.88 (s, 3H); ^{13}C NMR (101 MHz, CDCl_3) $\delta = 160.65$, 158.43, 156.23, 130.13, 127.33, 126.75, 125.24, 121.94, 119.56, 114.38, 111.97, 106.63, 98.98, 55.36; HRMS-ESI (m/z) $[\text{M}+\text{H}]^+$ calcd for $\text{C}_{16}\text{H}_{12}\text{O}_2\text{N}$, 250.0941, found 250.0943.

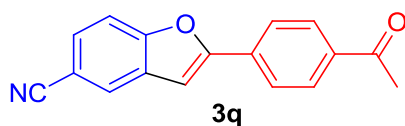
2-(4-cyanophenyl)benzofuran-5-carbonitrile (3p) is synthesized by general procedure with



3-bromo-4-hydroxybenzonitrile (0.5 mmol, 99 mg) and 4-Ethynylbenzonitrile (0.6 mmol, 76.3 mg) as the substrate. Isolated yield of the product is 42%.

^1H NMR (400 MHz, CDCl_3): $\delta = 7.99$ (s, 1H), 7.98 (d, $J = 7.3$ Hz, 2H), 7.78 (d, $J = 8$ Hz, 2H), 7.65 (m, 2H), 7.24 (s, 1H); ^{13}C NMR (101 MHz, CDCl_3) $\delta = 156.69$, 155.94, 133.24, 132.80, 129.30, 128.94, 126.43, 125.55, 119.07, 118.36, 112.71, 112.65, 107.55, 103.66; HRMS-ESI (m/z) $[\text{M}+\text{Na}]^+$ calcd for $\text{C}_{16}\text{H}_8\text{ON}_2\text{Na}$, 267.0528, found 267.0529.

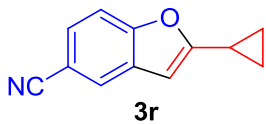
2-(4-acetylphenyl)benzofuran-5-carbonitrile (3q) is synthesized by general procedure with



3-bromo-4-hydroxybenzonitrile (0.5 mmol, 99 mg) and 4'-ethynylacetophenone (0.6 mmol, 86.5 mg) as the substrate. Isolated yield of the product is 32%.

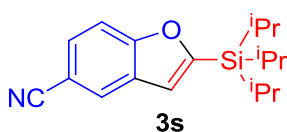
^1H NMR (400 MHz, CDCl_3): $\delta = 8.07$ (d, $J = 8.6$ Hz, 2H), 7.97-7.95 (m, 3H), 7.65-7.59 (m, 2H), 7.20 (s, 1H), 2.66 (s, 3H); ^{13}C NMR (101 MHz, CDCl_3) $\delta = 197.17$, 156.93, 156.65, 137.33, 133.27, 129.51, 129.01, 128.55, 126.20, 125.21, 119.21, 112.52, 107.28, 102.92, 26.65; HRMS-ESI (m/z) $[\text{M}+\text{H}]^+$ calcd for $\text{C}_{17}\text{H}_{12}\text{O}_2\text{N}$, 262.0862, found 262.0863.

2-cyclopropylbenzofuran-5-carbonitrile (3r) is synthesized by general procedure with 3-bromo-4-hydroxybenzonitrile (0.5 mmol, 99 mg) and cyclopropylacetylene (0.6 mmol, 50.8 μ L) as the substrate. Isolated yield of the product is 80%.



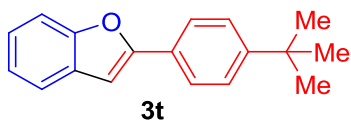
^1H NMR (400 MHz, CDCl_3): δ = 7.75 (s, 1H), 7.45 (d, J = 8.5 Hz, 1H), 7.41 (d, J = 8.5 Hz, 1H), 6.40 (s, 1H), 2.1-1.99 (m, 1H), 1.08-1.04 (m, 2H), 1.03-0.98 (m, 2H); ^{13}C NMR (101 MHz, CDCl_3) δ = 163.15, 155.88, 129.83, 126.71, 124.58, 119.66, 111.56, 106.24, 100.06, 9.29, 7.70; HRMS-ESI (m/z) $[\text{M}+\text{H}]^+$ calcd for $\text{C}_{12}\text{H}_{10}\text{ON}$, 184.0760, found 184.0757.

2-(triisopropylsilyl)benzofuran-5-carbonitrile (3s) is synthesized by general procedure with 3-bromo-4-hydroxybenzonitrile (0.5 mmol, 99 mg) and (triisopropylsilyl)acetylene (0.6 mmol, 134.6 μ L) as the substrate. Isolated yield of the product is 43%.



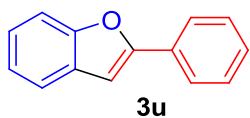
^1H NMR (200 MHz, CDCl_3): δ = 7.94 (s, 1H), 7.57-7.55 (m, 2H), 7.06 (s, 1H), 1.53-1.31 (m, 3H), 1.14 (d, J = 7.1 Hz, 18H); ^{13}C NMR (101 MHz, CDCl_3) δ = 164.11, 159.52, 128.58, 127.66, 125.98, 119.69, 117.59, 112.33, 106.01, 18.47, 10.91; HRMS-ESI (m/z) $[\text{M}+\text{H}]^+$ calcd for $\text{C}_{18}\text{H}_{26}\text{ONSi}$, 300.1776, found 300.1778.

2-(4-*tert*-butylphenyl)benzofuran (3t) is synthesized by general procedure with 2-bromophenol (0.5 mmol, 58 μ L) and 4-*tert*-butylphenylacetylene (0.6 mmol, 108.3 μ L) as the substrate. Isolated yield of the product is 53%.



^1H NMR (400 MHz, CDCl_3): δ = 7.87 (d, J = 8.5 Hz, 2H), 7.63 (d, J = 7.8 Hz, 1H), 7.59 (d, J = 7.8 Hz, 1H), 7.54 (d, J = 8.2 Hz, 2H), 7.34 (t, J = 7.4 Hz, 1H), 7.29 (t, J = 7.3 Hz, 1H), 7.03 (s, 1H), 1.43 (s, 9H); ^{13}C NMR (101 MHz, CDCl_3) δ = 156.14, 154.81, 151.76, 129.34, 127.71, 125.71, 124.72, 123.97, 122.82, 120.74, 111.10, 100.66, 34.73, 31.23; HRMS-ESI (m/z) $[\text{M}+\text{H}]^+$ calcd for $\text{C}_{18}\text{H}_{19}\text{O}$, 251.1439, found 251.1430.

2-phenylbenzofuran (3u) is synthesized by general procedure with 2-bromophenol (0.5 mmol, 58 μ L) and phenylacetylene (0.6 mmol, 66 μ L) as the substrate. The yield of the product is 70%, measured by GC.



^1H NMR (400 MHz, CDCl_3): δ = 7.87 (d, J = 7.8 Hz, 2H), 7.59 (d, J = 7.2 Hz, 1H), 7.53 (d, J = 8.1 Hz, 1H), 7.45 (t, J = 7.6 Hz, 2H), 7.35 (t, J = 7.5 Hz, 1H), 7.29

(t, $J = 7.5$ Hz, 1H), 7.23 (t, $J = 7.5$ Hz, 1H), 7.02 (s, 1H); ^{13}C NMR (101 MHz, CDCl_3) $\delta = 155.89, 154.86, 130.45, 129.19, 128.76, 128.52, 124.90, 124.23, 122.90, 120.87, 111.15, 101.27$; HRMS-ESI (m/z) $[\text{M}+\text{H}]^+$ calcd for $\text{C}_{14}\text{H}_{11}\text{O}$, 195.0805, found 195.0804.

3.5.9 X-Ray Investigation of 2-Phenylbenzofuran-5-Carbaldehyde (3b)

Table 3.9 Structural information of 2-phenylbenzofuran-5-carbaldehyde (3b) single crystal

Structural information	
Empirical formula	$\text{C}_{15}\text{H}_{10}\text{O}_2$
Formula weight	222.23
Temperature/K	293
Crystal system	monoclinic
Space group	$P2_1/n$
$a/\text{\AA}$	8.3515(7)
$b/\text{\AA}$	5.6087(4)
$c/\text{\AA}$	23.3147(19)
$\alpha/^\circ$	90.00
$\beta/^\circ$	98.894(8)
$\gamma/^\circ$	90.00
Volume/ \AA^3	1078.95(15)
Z	4
$\rho_{\text{calc}}/\text{mg}/\text{mm}^3$	1.368
μ/mm^{-1}	0.728
F(000)	464.0
Crystal size/ mm^3	$0.4 \times 0.2 \times 0.2$
2 θ range for data collection	11.8 to 141.1 $^\circ$
Index ranges	$-10 \leq h \leq 9, -6 \leq k \leq 3, -28 \leq l \leq 25$
Reflections collected	3439
Independent reflections	2009[R(int) = 0.0193]
Data/restraints/parameters	2009/0/154
Goodness-of-fit on F^2	1.048
Final R indexes [$I \geq 2\sigma(I)$]	$R_1 = 0.0453, wR_2 = 0.1216$
Final R indexes [all data]	$R_1 = 0.0529, wR_2 = 0.1314$
Largest diff. peak/hole / $e \text{\AA}^{-3}$	0.19/-0.16

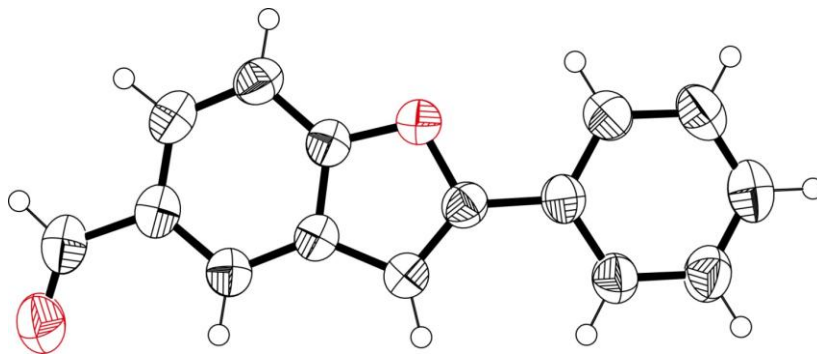


Figure 3.15: Single Crystal X-ray diffraction structure of 2-phenylbenzofuran-5-carbaldehyde (3b). In the ORTEP (with 50% probability level); Carbon (light gray), Oxygen (red), and Hydrogen (white) have been shown.

CCDC 1519400 contains the crystallographic data for 2-phenylbenzofuran-5-carbaldehyde (3b).

3.5.10 Catalyst Recyclability Experiment

In the recycle test, phenylacetylene (66 μL , 0.6 mmol), 3-bromo-4-hydroxybenzofuran-5-carbaldehyde (99 mg, 0.5 mmol), potassium carbonate (34.5 mg, 0.25 mmol), **Pd@TpBpy** (2 mg, 0.6 mol%) and 1 mL dry DMF are mixed under nitrogen atmosphere in a reaction tube and their corresponding yields are analysed for each cycle. After each cycle, the reaction mixture is centrifuged to separate the catalyst, followed by washing with dry acetone. After that catalyst is dried and then used directly without further treatment. For characterization, the recycled catalyst is washed with water, acetone and dried at 110 $^{\circ}\text{C}$ under vacuum.

3.5.11 Large-scale Synthesis (TON and TOF)

In this experiment, a mixture of phenylacetylene (6 mmol, 660 μL), 3-bromo-4-hydroxybenzofuran-5-carbaldehyde (5 mmol, 990 mg), potassium carbonate (345 mg, 2.5 mmol) and **Pd@TpBpy** (2 mg, 0.06 mol%) are added to 10 mL dry DMF under nitrogen atmosphere in a screw cap reaction tube. Then the reaction mixture is allowed to stir at 150 $^{\circ}\text{C}$ for 17h. After the completion of the reaction (monitored by TLC), the crude product is purified by column chromatography to obtain

Table 3.10 TOF in different time intervals

Time (h)	TON	TOF (h^{-1})
1	490	490
2	630	315
17	1101	65

the desired product **3a** in 63% yield (TON = 1101). We have carried out experiments and calculated the TOF in different time intervals. It is observed that Pd@TpBpy shows higher TOF in a shorter time compared to a longer time. The experimental observation is given below in Table 3.10.

3.5.12 Characterization of Pd@TpBpy after Catalysis

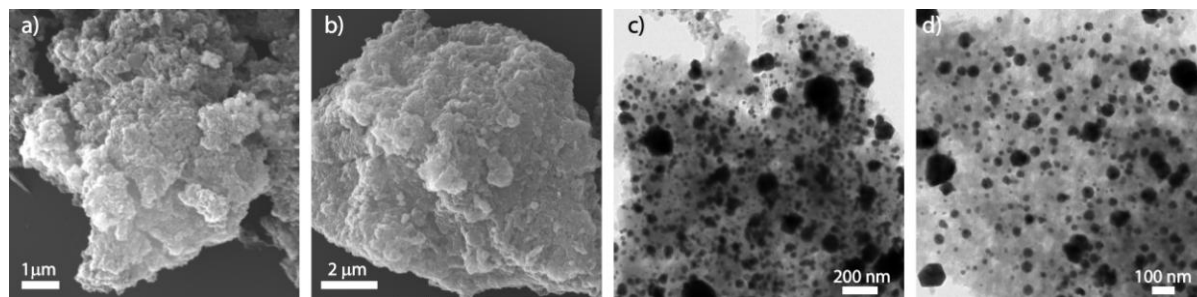


Figure 3.16: (a), (b) are the SEM images; (c), (d) are the TEM images of Pd@TpBpy after catalysis.

3.5.13 General methods for characterization

All reagents were commercially available and used as received.

a) Wide-angle X-Ray Diffraction (WAXD): The Powder X-ray diffraction (PXRD) patterns were recorded on a Phillips PAN analytical diffractometer for Cu K α radiation ($\alpha = 1.5406 \text{ \AA}$), with a scan speed of 1° min^{-1} and a step size of 0.02° in 2θ . The instrument was previously calibrated using a silicon standard.

b) FT-IR spectroscopy: The Fourier Transform Infrared (FTIR) spectra were taken on a Bruker Optics ALPHA-E spectrometer with a universal Zn-Se ATR (attenuated total reflection) accessory in the $600\text{--}4000 \text{ cm}^{-1}$ region.

c) Thermogravimetric analysis: TGA was carried out on a TG50 analyzer (Mettler-Toledo) or an SDT Q600 TG-DTA analyzer under N $_2$ atmosphere at a heating rate of $10 \text{ }^\circ\text{C min}^{-1}$ within a temperature range of $30\text{--}900 \text{ }^\circ\text{C}$.

d) Scanning Electron Microscopy: SEM images were obtained with a Zeiss DSM 950 scanning electron microscope and FEI-QUANTA 200 3D Scanning Electron Microscope with tungsten filament as electron source operated at 10 kV. The samples were sputtered with Au (nano-sized film) prior to imaging by an SCD 040 Balzers Union.

e) Transmission Electron Microscopy: TEM TEM images were recorded using FEI Tecnai G2 F20 X-TWIN TEM at an accelerating voltage of 200 kV. The TEM Samples were

prepared by dropcasting the sample from isopropanol on copper grids (TED PELLA, INC. 200 mesh). The metal nanoparticles size distribution was determined by measuring the size of 700 particles from TEM images.

f) *BET surface area:* BET surface area of the synthesized COFs was measured through N₂ adsorption studies. N₂ adsorption isotherms were collected with a Quantachrome make Autosorb IQ₂ automated surface area analyzer.

g) *Solid-state NMR (SSNMR):* Solid-state NMR (SSNMR) was taken in a Bruker 300 MHz NMR spectrometer and ligand NMR data were taken in Bruker 200/400/500 MHz NMR spectrometer.

h) *Gas Chromatography:* GC analyses were performed on an Agilent 7890B GC system with an FID detector using an HP-5 column (30 m, 0.25 mm, 0.25 μ). As the internal standard *m*-xylene was used.

i) *Inductively Coupled Plasma Optical Emission Spectrometry:* The wt% loading of Pd on TpBpy was analyzed using Inductively Coupled Plasma Optical Emission Spectrometry (ICP-OES) instrument from Spectro analytical instruments GmbH, model ARCOS simultaneous ICP spectrometer, Germany.

j) *X-ray photoelectron spectroscopy:* X-ray photoelectron spectroscopy (XPS) measurement of Pd nanoparticles was carried out by a VG Microtech, model ESCA 3000 instrument equipped with ion gun (EX-05) for cleaning the surface. The binding energy resolution was 0.1eV for the XPS measurement.

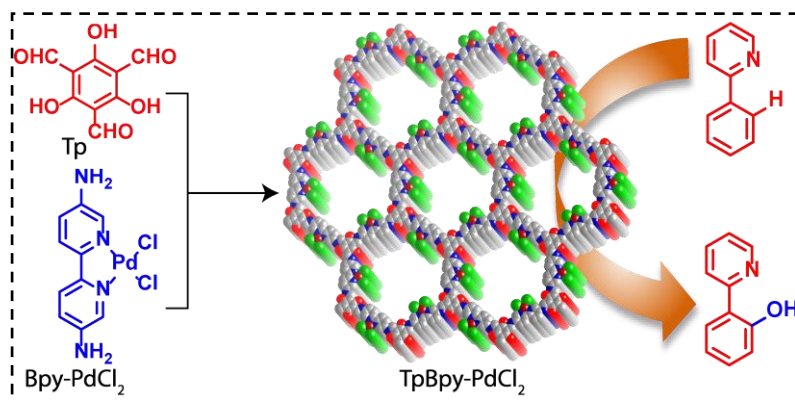
j) *X-ray Diffractometer:* The crystals were mounted on a Super Nova Dual source X-ray Diffractometer system (Agilent Technologies) equipped with a CCD area detector and operated at 250 W power (50 kV, 0.8 mA) to generate Mo K α radiation (λ = 0.71073 Å) and Cu K α radiation (λ = 1.54178 Å) at 298(2) K.

NOTE: The results of this chapter have already been published in *ACS Appl. Mater. Interfaces*, **2017**, 9, 13785–13792 with the title: “*Predesigned Metal-Anchored Building Block for In Situ Generation of Pd Nanoparticles in Porous Covalent Organic Framework: Application in Heterogeneous Tandem Catalysis.*”

CHAPTER 4

Presynthesized Metal Coordinated Stable Covalent Organic Framework as Heterogeneous Catalyst for Chelation Assisted Direct C(sp²)-H Bond Hydroxylation Reaction

Abstract: Metal coordinated heterogeneous catalyst development is highly desired for their applications in the chemical and pharmaceutical industries. Herein, we have developed heterogeneous palladium metal coordinated stable, porous and crystalline covalent organic framework via pre-synthetic method. During the reaction, no palladium nanoparticles formation is observed and is confirmed by PXRD, TEM images. The unchanged metal oxidation state is confirmed by XPS analysis. The material shows good CO₂ and H₂ uptake properties in normal atmospheric pressure. This material is used as an excellent reusable heterogeneous catalyst for the synthesis of biologically and pharmaceutically important alcohol and phenol products. Although selective hydroxylation or C-O bond formation via inert C-H bond activation is a more difficult process compare to the C-C bond formation. Therefore we have synthesized 2-(2-pyridyl)phenol from 2-phenylpyridine in presence of TpBpy-PdCl₂ catalyst using pyridine as a metal chelating agent. The heterogeneity nature of the catalyst is confirmed by mercury poisoning experiment.



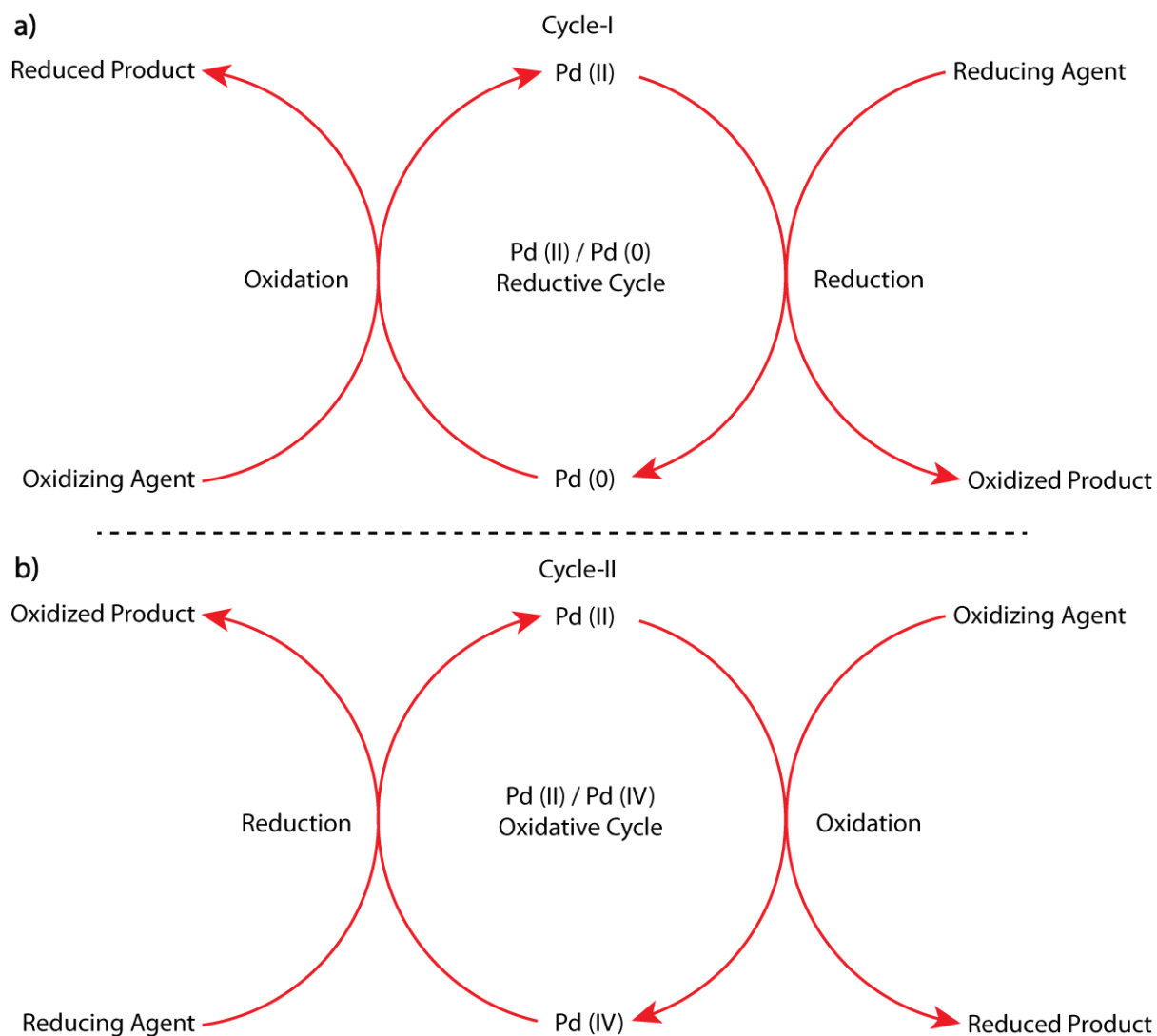
4.1 Introduction:

Importance of 2,2'-bipyridine palladium complex is significant in homogeneous catalysis and has been widely used for direct remote C-H bond activation and functionalization process [4.1]. Palladium (II) complex can possess two distinct mechanisms during the catalytic process: a) Pd (II) / Pd (0) reductive cycle, b) Pd (II) / Pd (IV) oxidative cycle [4.2]. Although, various methods have been reported for Carbon-Carbon (C-C) bond formation reaction using transition metal in last two decades but formation of Carbon-Oxygen (C-O) [4.3] bond through activation of Carbon-Hydrogen (C-H) bond is more difficult and challenging process [4.4]. Traditional approach for synthesizing C-O bond is expensive, multistep and atom deficient process [4.5]. Therefore, developing a mild suitable method for direct conversion of C-H bond into C-O is becoming more prominent not only due to the cost-effective and atom economic process but also the wide application across the chemical field including the synthesis of natural products, pharmaceuticals, polymers, and agrochemicals. Direct functionalization of C-H bond is more challenging due to a) inert nature of C-H bond and b) difficult to control in site-selective functionalization in the molecule having diverse C-H groups. The first problem is overcome by introducing transition metal into the reaction medium where transition metal activates the inert C-H bond *via* C-H activation process¹ and forms reactive Carbon-Metal (C-M) bond which can be further converted to new functional group under mild condition. In case of the second problem, selective functionalization of single C-H bond within a molecule is a major challenging process. The problem is addressed using several different strategies. Among them, the most common strategy is using of substrates having coordinating ligands are often called 'directing groups'. These ligands bind with metal center during the catalytic process and deliver the metal center selectively to the proximal C-H bond. The bond is further activated by forming reactive cyclometalation process as a key intermediate step. Like other transition metals (e.g. Rh, Ru, Pt) Pd also shows ligand directed C-H activation reaction [4.6]. Conversion of homogeneous catalyst into heterogeneous is very important and challenging research area due to recyclability and easy recovery nature from the reaction mixture and vast application in chemical and pharmaceutical industries. Homogeneous catalyst can be converted to heterogeneous by attachment of catalytically active site on stable chelating support [4.7]. Covalent organic frameworks are one kind of emerging crystalline, porous stable

heterogeneous support can be constructed from good metal chelating ligands through reticular chemistry [4.8]. Therefore designing and synthesizing of palladium coordinated covalent organic framework as heterogeneous catalyst (keeping the metal oxidation state intact during the synthesis process) will be the most suitable approach for Carbon-Oxygen (C-O) bond formation reaction.

4.1.1 Mechanism of Pd(II) complex During Catalytic Process :

Palladium (II) catalyst can exhibit two type of mechanism during catalytic process. a) Cycle-I: Reductive Cycle and b) Cycle-II: Oxidative Cycle (Scheme 4.1). In the reductive

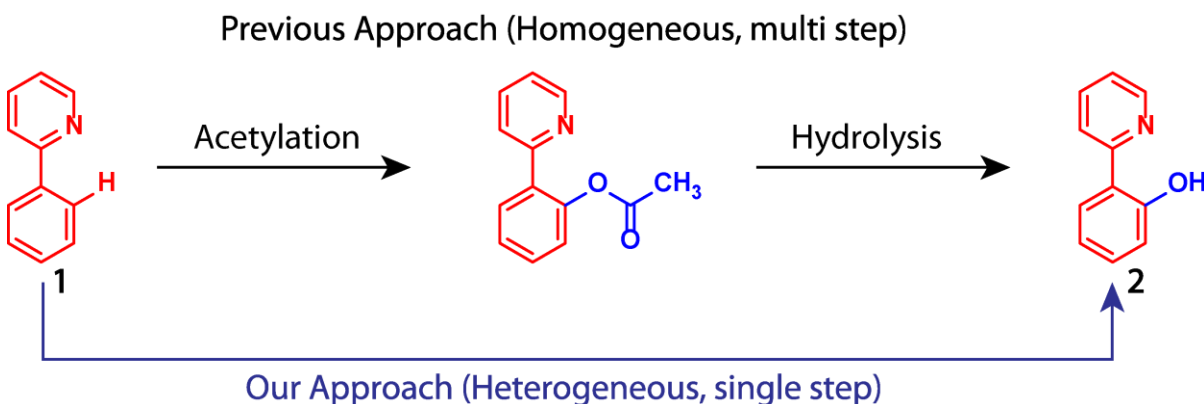


Scheme 4.1: Schematic representation of the catalytic mechanism of Pd (II) complex. a) Cycle-I: Pd (II) / Pd (0) reductive cycle, b) Cycle-II: Pd (II) / Pd (IV) oxidative cycle.

cycle Pd (II) is reduced to Pd (0) through the reductive pathway and the Pd (0) is further oxidized to Pd (II) *via* oxidative pathway. But in case of Cycle-II, first Pd (II) oxidizes to its higher oxidation state Pd (IV) through an oxidizing agent. Then Pd (IV) is further reduced to its original oxidation state Pd (II) *via* a reductive pathway.

4.1.2 Importance of Chelation Assisted Direct C(sp²)-H Bond Hydroxylation Reaction:

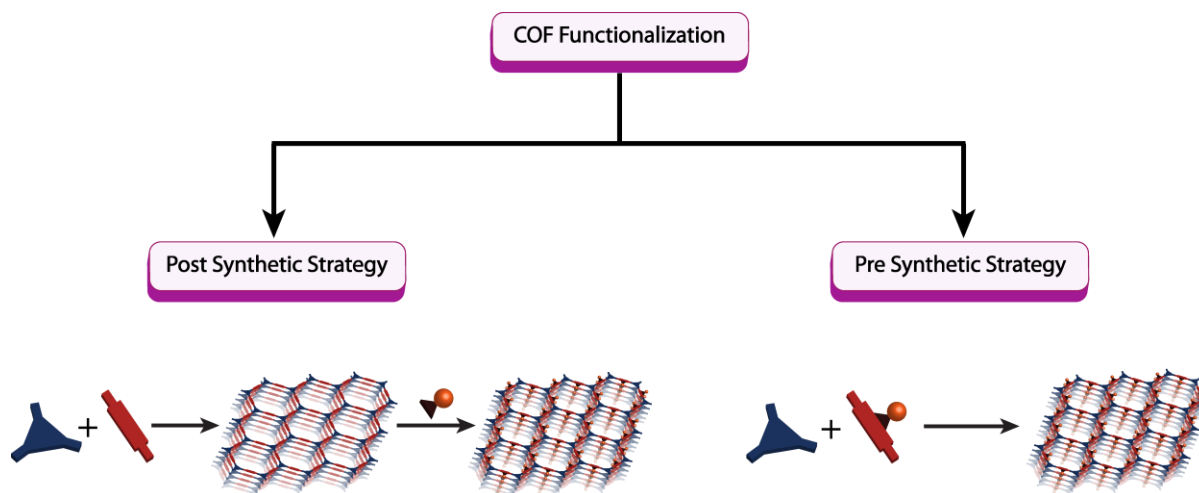
We have discussed previously that transition metal catalyzed Carbon-Oxygen (C-O) bond forming reaction is more challenging compared to Carbon-Carbon (C-C) bond formation reaction. The simple alternative process for selective C-O bond formation is the use of chelating ligand into the substrate which will deliver the metal catalyst for direct and selective activation of C-H bond within a close proximal distance. Transition metal catalyzes the hydroxylation of C-H bond is becoming more important because of the synthesis of industrially important alcohol and phenol products. 2-(2-pyridyl)phenol derivatives are most useful building block for the synthesis of biologically active molecule and light emitting materials [4.9]. The most common method used to synthesize these materials is the formation of acyloxy (-OAc) intermediate which will be converted to hydroxylated (-OH) products *via* further hydrolytic transformation process (Scheme 4.2) [4.10]. Therefore, ligand assisted synthesis of 2-(2-pyridyl)phenol *via* direct C-H activation will be the most convenient single step and atom economical method.



Scheme 4.2: Schematic representation of the synthesis of 2-(2-pyridyl)phenol from 2-phenylpyridine.

4.1.3 Different Methods and their Problems for Covalent Organic Frameworks Functionalization:

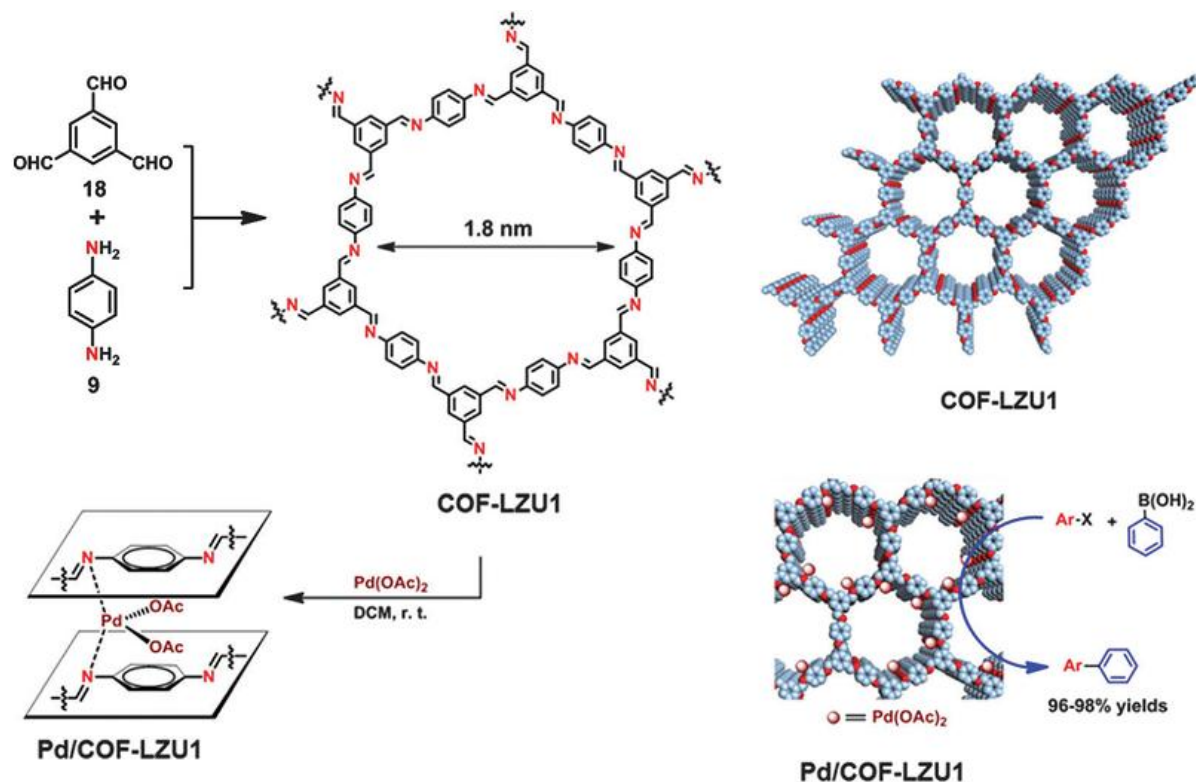
Covalent organic frameworks have been utilized for different applications. It has been observed that different functional groups in the covalent organic framework (COF) are responsible for different applications. Therefore the development of methods for introducing different functional group in the covalent organic framework is a very important and challenging research topic. So far there are two methods for COF functionalization: a) Post Synthetic Method [4.11] and b) Pre Synthetic Method (Scheme 4.3).



Scheme 4.3: Schematic diagram of COF functionalization.

4.1.3.1 Post Synthetic Strategy:

This is the most used method for introducing new functional moiety into the covalent organic framework backbone through chemical transformation or coordinative incorporation. In this strategy, the catalytically active species or functional group is attached after formation of the covalent organic framework. Therefore, there are several disadvantages of using this method. Uneven distribution of catalytically active species: catalytically active species are not homogeneously distributed in the framework [4.12]. Hence lower loading of catalytically active species into the framework may give lower yield during catalytic process. During this process, the crystallinity of the original material will hamper and the framework may lose long-range structural periodicity. Prof. Wang and coworkers have synthesized Pd/COF-LZU1, Pd(OAc)₂ coordinated imine based COF using this strategy and the metal loaded COF has been utilized for Suzuki–Miyaura coupling reaction (Scheme 4.4) [4.13].



Scheme 4.4: Chemical and extended structures of COF-LZU1, Pd/COF-LZU1 and Suzuki-Miyaura coupling reaction. Figures are reproduced with permission from ACS publications.

4.1.3.2 Pre Synthetic Strategy:

This strategy is more straightforward but difficult for covalent organic framework functionalization. Here the functional group should directly attach to the predesigned building block before covalent organic framework synthesis. The advantage of this method is the homogeneous distribution of the functional group in the covalent organic framework will occur and which may improve the thermal and chemical stability compared to the previous framework. During this process, crystallinity and porosity should also get equal priority. Therefore it is always becoming more challenging for synthesizing highly crystalline and porous functionalized covalent organic framework. COFs synthesized *via* pre-synthetic method have shown good performance in ammonia gas uptake, catalysis, and photoelectric application [4.14].

4.2 Statement of the Problem

As we have discussed introduction section that uneven distribution of catalytically active species and low order functionalized covalent organic framework occurs during

functionalization of covalent organic framework *via* post-synthetic approach. Therefore the alternative approach for synthesizing catalytically active covalent organic framework will be pre-synthetic method; although challenging process. Moreover, C-O bond formation is more difficult to compared to C-C bond formation through remote C-H activation. Therefore synthesis of phenol using conventional approach is a multistep and costly process. But palladium (II) complex is used for chelation assisted direct hydroxylation of C-H bond for the synthesis of industrially important, bioactive phenol derivatives.

Keeping this idea in our mind, we have synthesized palladium coordinated crystalline stable covalent organic framework (**TpBpy-PdCl₂**) from palladium chloride coordinated organic precursor through the pre-synthetic approach. Although the previous chapter we have discussed that most of the cases palladium forms palladium nanoparticles during covalent organic framework synthesis *via* pre-synthetic approach where the metal oxidation state is also changed from Pd (II) to Pd (0) [4.15]. But finally, we have overcome the problem and found a suitable condition where palladium oxidation state is unchanged after covalent organic framework formation. The oxidation state of the palladium is confirmed by XPS and PXRD analysis. The synthesized **TpBpy-PdCl₂** is successfully utilized selective hydroxylation of 2-phenylpyridine *via* direct C-H bond activation process.

4.3 Synthesis and Characterization

4.3.1 *TpBpy-PdCl₂* COF Synthesis

To a pyrex tube 1,3,5-triformylphloroglucinol (**Tp**) (21 mg, 0.1 mmol) and 2,2'-bipyridine-5,5'-diamine palladium chloride (**Bpy-PdCl₂**) (54.5 mg, 0.15 mmol) are added in presence of dimethyl sulfoxide (DMSO) 3 mL with 0.3 mL of 6M aqueous acetic acid. In order to disperse homogeneously, the reactants are ultrasonicated for 15 min and degassed through three successive freeze-pump-thaw cycles. After that, the tube is sealed in a vacuum condition and kept for heating at 90 °C in the isothermal oven for 3 days. Finally, the phase pure material is filtered out and washed with DMSO solvents to remove the residues of the starting materials. The collected reddish material is solvent exchanged with DMSO and washed with excess acetone. Then the powder material is dried at 110 °C for 12 h under vacuum in order to get as synthesized **TpBpy-PdCl₂** COF (Figure 4.1a).

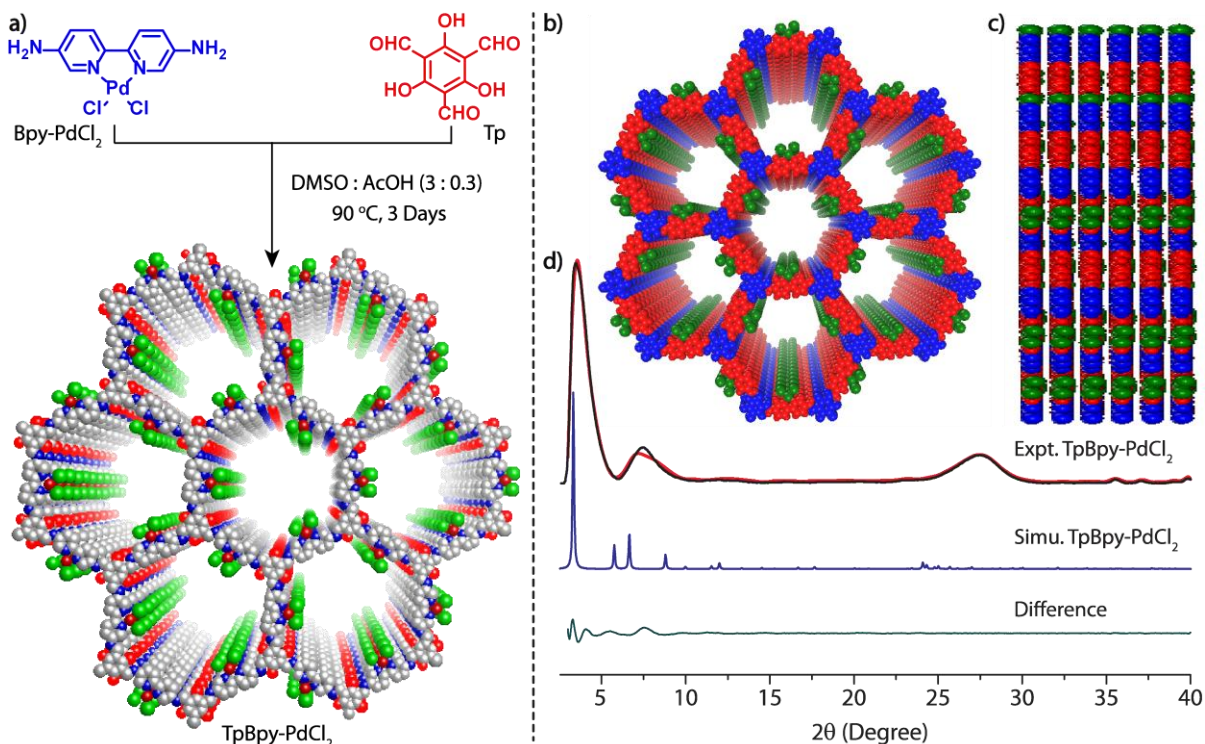


Figure 4.1: (a) Synthesis of the **TpBpy-PdCl₂** using the pre-synthetic method. (b, c) Space-filling models of the AA eclipsed stacking model along c and a axis direction. (d) Comparison of the experimental PXR patterns of **TpBpy-PdCl₂** (black) with the simulated (blue) simulated after Pawley refinement (red), and difference plot (cyan).

4.3.2 Structural simulation and characterization

The crystallinity of the synthesized **TpBpy-PdCl₂** is investigated by PXR analysis. The high crystallinity of **TpBpy-PdCl₂** is observed from intense peak arise at 3.4° (2θ). This intense peak corresponding to the reflection from 100 planes. The other minor peaks appear at 7.5°, and 27.5° (2θ) which are corresponding to the reflection of 200 and 001 plane respectively. The peak at 2θ = 27.5° corresponding to the reflection of 001 planes indicates the presence of π-π stacking between the 2D COF layers. The *d*-spacing between the COF layers is 3.6 Å. In PXR no additional peaks are observed related to palladium nanoparticles which means the Pd-N bond is not breaking under the following synthetic process. In order to elucidate the structure, we have modeled **TpBpy-PdCl₂** in two possible stacking modes (eclipse and staggered) in material studio 6.1. The simulated structure of the eclipse model is well matching with the experimental PXR pattern of **TpBpy-PdCl₂** (Figure 4.1d). The eclipse model is simulated in *P3* space group. To determine the exact unit cell parameter we

have performed Pawley refinement. After refinement the final unit cell values are $a = b = 30.6 \text{ \AA}$, $c = 3.6 \text{ \AA}$, $\alpha = \beta = 90^\circ$, $\gamma = 120^\circ$ with $R_p = 5.3\%$ and $R_{wp} = 7.6\%$ (Figure 4.2 and Table 4.1).

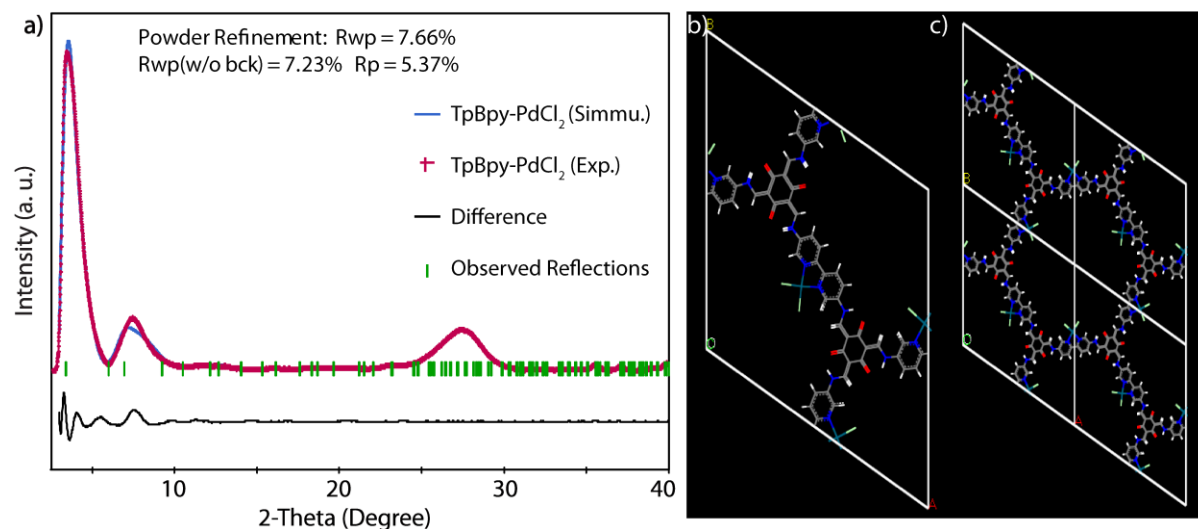


Figure 4.2: (a) Comparison of the PXRD pattern of experimental (crossed) and simulated (blue) *TpBpy-PdCl₂* in eclipsed stacking mode. Difference plot is depicted in black line. Pawley refinement demonstrates good agreement between experimental and simulated eclipsed PXRD pattern (R_{wp} : 7.66%, R_p : 5.37%). (b) Unit cell and (c) eclipsed crystal lattice packing of *TpBpy-PdCl₂*.

Table 4.1 Fractional atomic coordinates for the unit cell of *TpBpy-PdCl₂* (Eclipsed)

TpBpy-PdCl₂							
Hexagonal; P3							
$a = b = 30.6 \text{ \AA}$, $c = 3.6 \text{ \AA}$							
$\alpha = \beta = 90$, $\gamma = 120$							
C2	-0.36415	-0.64415	-0.47512	C73	0.59312	0.45351	1.52992
C3	-0.3844	-0.6983	-0.47308	N74	0.4436	0.48701	1.5457
O9	-0.43855	-0.73218	-0.47	C75	0.53787	0.42485	1.52391
C10	-0.39804	-0.62389	-0.47407	C76	0.42183	0.55632	1.52932
N19	-0.37778	-0.56975	-0.47611	C77	0.51218	0.57682	1.52875
N28	-0.61501	-0.42795	-0.46881	C78	0.58676	0.53225	1.53939
C31	-0.62864	-0.35355	-0.46981	C79	0.47561	0.59321	1.51954
C32	-0.59475	-0.37381	-0.47085	C80	0.61719	0.5086	1.53433

C33	-0.60839	-0.29941	-0.47184	C81	0.5318	0.50168	1.5359
O48	-0.55424	-0.26552	-0.47492	C82	0.49599	0.52314	1.53935
H54	0.66124	0.45468	0.52167	C83	0.40733	0.50256	1.54224
H57	0.34596	0.54762	0.5334	H84	0.60303	0.56918	1.545
H58	0.44533	0.65128	0.52687	H85	0.65412	0.5294	1.53389
H65	0.56188	0.35102	0.5282	H86	0.3714	0.4769	1.54865
Pd69	0.42779	0.41081	1.51627	H87	0.48689	0.62934	1.50684
Cl70	0.41707	0.32756	1.43457	H88	0.54831	0.60189	1.52795
Cl71	0.33735	0.37427	1.53648	H104	0.5179	0.37957	0.51759
N72	0.50836	0.44813	1.52528				

4.3.3 Chemical characterization

The formation of enol to keto tautomerized **TpBpy-PdCl₂** covalent organic framework is investigated by FT-IR and ¹³C CP-MAS solid-state NMR spectra. The FT-IR spectra of **TpBpy-PdCl₂** show the consumption of starting materials. The characteristics

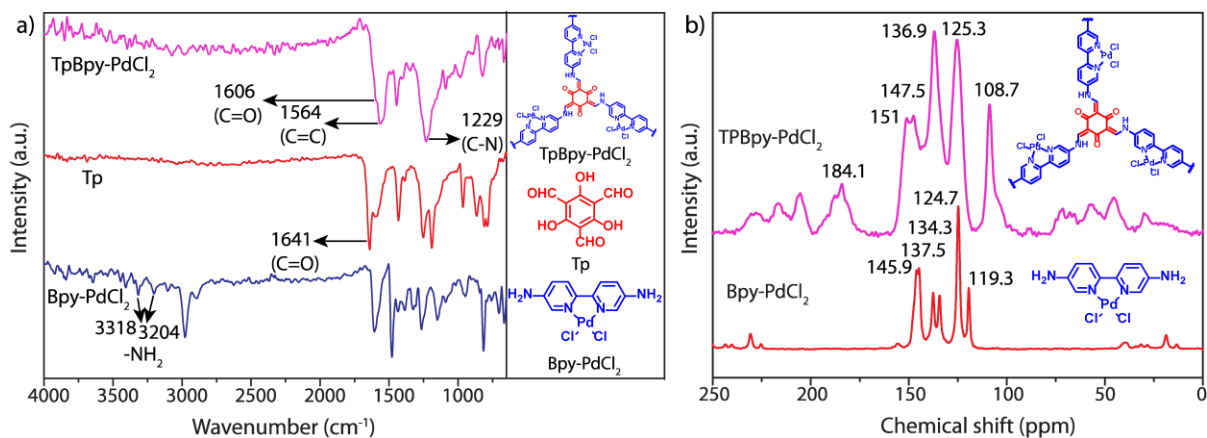


Figure 4.3: (a) FTIR spectra of **Bpy-PdCl₂** (blue), **Tp** (red) and **TpBpy-PdCl₂** (pink). (b) Comparison of solid state ¹³C NMR spectra of **Bpy-PdCl₂** (red) and **TpBpy-PdCl₂** (pink).

stretching band $\text{C}=\text{O}$ (1641 cm^{-1}) of 1,3,5-triformylphloroglucinol (**Tp**) and $\text{N}-\text{H}$ (3318 , 3204 cm^{-1}) stretching band of 2,2'-bipyridine-5,5'-diamine palladium chloride (**Bpy-PdCl₂**) are totally disappeared. In addition, the new intense peaks arise at 1606 cm^{-1} ($\text{C}=\text{O}$), 1564 cm^{-1} ($\text{C}=\text{C}$) and 1229 cm^{-1} ($\text{C}-\text{N}$) indicate the formation of the most stable keto structure (Figure 4.3a). Here the $\text{C}=\text{O}$ peak at 1606 cm^{-1} of **TpBpy-PdCl₂** is merged with $\text{C}=\text{C}$ peak

at 1566 cm^{-1} . The ^{13}C CP-MAS solid-state NMR of **TpBpy-PdCl₂** and **Bpy-PdCl₂** is performed. The signal appears at 184.1 ppm in case of **TpBpy-PdCl₂** corresponding to carbonyl ($-\text{C}=\text{O}$) carbon. The remaining sp^2 carbons appear in the range of 151 to 108 ppm whereas the aromatic carbon in case of **Bpy-PdCl₂** arise 146 ppm to 119 ppm region (Figure 4.3b). To evaluate the permanent porosity and surface area of the synthesized COF, we have performed reversible nitrogen adsorption isotherm of activated **TpBpy-PdCl₂** at 77K which shows type IV adsorption isotherm with mesoporous in nature (Figure 4.4(a,b)). The Brunauer–Emmett–Teller (BET) surface area of **TpBpy-PdCl₂** is $308\text{ m}^2/\text{g}$. Pore size distribution of **TpBpy-PdCl₂** is calculated using the N_2 at 77 K on carbon (cylindr./sphere pores, QSDFT adsorption branch) model which shows three different pores (2.2 nm, 3.2 nm, 6.4 nm) present inside the material. The material shows good CO_2 uptake 44 cc/g at 0°C 1

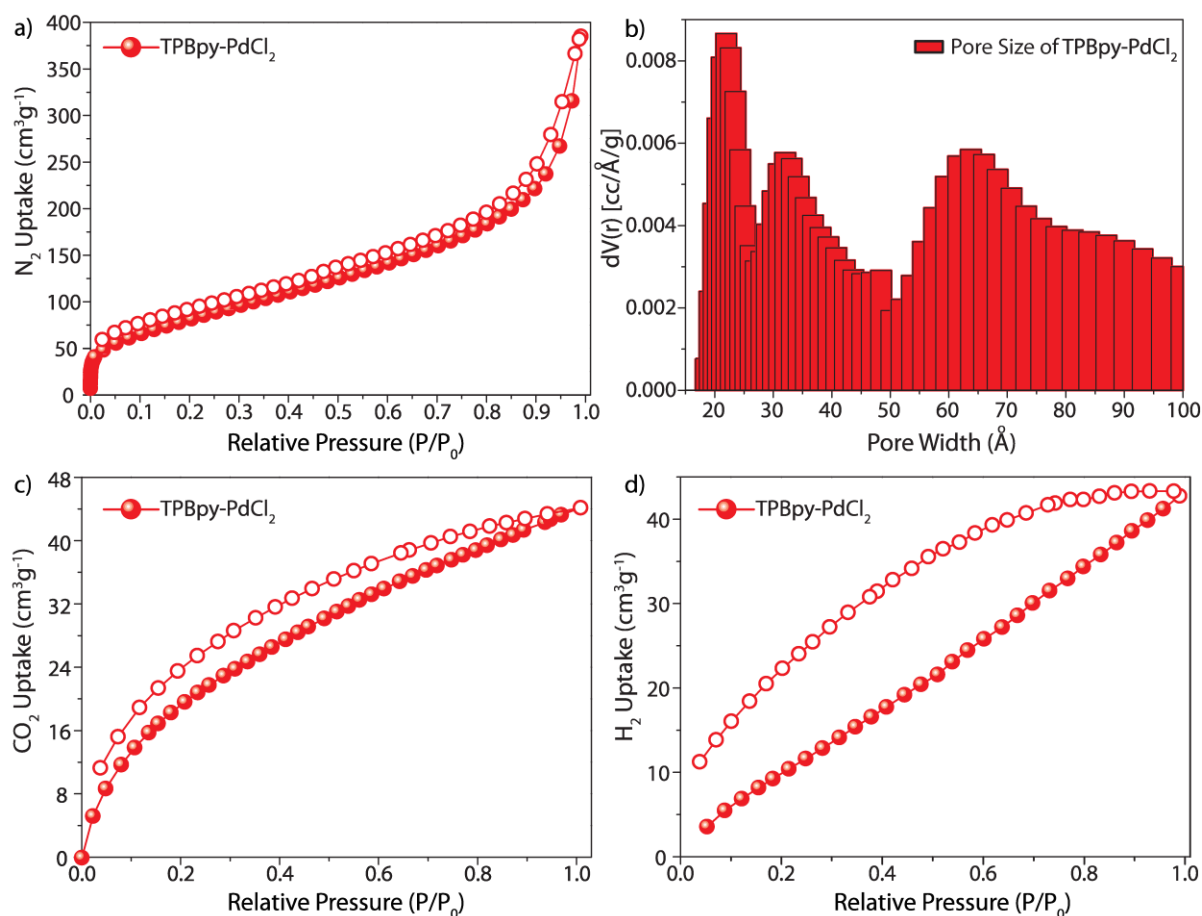


Figure 4.4: (a) N_2 adsorption isotherm of **TpBpy-PdCl₂**. (b) Experimental pore size distributions of **TpBpy-PdCl₂** calculated using the N_2 at 77 K on carbon (cylindr./sphere pores, QSDFT adsorption branch) model. (c) CO_2 adsorption isotherm, (d) Hydrogen adsorption isotherm of **TpBpy-PdCl₂**.

atm pressure and high hydrogen uptake 43 cc/g at 77 K 1 atm pressure (Figure 4.4 (c,d)). As we have discussed previously that after the synthetic process Pd (II) coordinated framework is generated and the oxidation state of the palladium remains unchanged during the whole process. In order to prove the unchanged metal oxidation state, we have carried out the detail XPS analysis of both **Bpy-PdCl₂** complex and **TpBpy-PdCl₂** COF. The 3d XPS spectra of palladium show doublet peaks which represent the corresponding binding energy of Pd 3d_{5/2} and Pd 3d_{3/2} respectively. In **TpBpy-PdCl₂** the characteristic binding energy peaks arise at 337.7 and 342.9 eV of Pd 3d_{5/2} and Pd 3d_{3/2} are corresponding to Pd(II) species which is exactly matching with the binding energy of Pd 3d_{5/2} and Pd 3d_{3/2} in the palladium coordinated synthetic precursor (**Bpy-PdCl₂** complex) appear at 337.7 and 343.1 eV (Figure 4.5a). Also, this signifies the palladium is in the +2 oxidation state after framework formation. The thermal stability of the framework is analyzed by thermogravimetric analysis (TGA) and it shows that the material is stable up to 200 °C (Figure 4.5b).

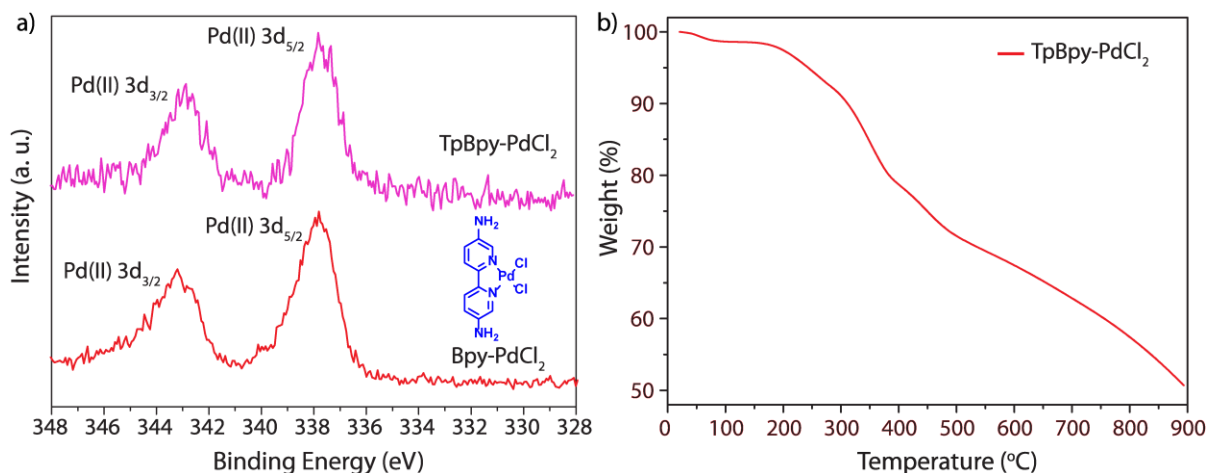


Figure 4.5: (a) XPS spectra of Pd (II) in **Bpy-PdCl₂** (red) and **TpBpy-PdCl₂** (pink). (b) TGA spectra of **TpBpy-PdCl₂**.

To reveal the internal morphology of the synthesized material **TpBpy-PdCl₂** we have performed SEM and TEM analysis. Both the analysis shows the fibrillar nature of the internal structure of the material (Figure 4.6). The Energy Dispersive X-ray (EDX) analysis shows the percentage of elements present in the material **TpBpy-PdCl₂**. But the quantity of palladium metal present in the framework is accurately measured by Inductively Coupled Plasma Atomic Emission Spectroscopy (ICP-OES) analysis and found 13 wt% Pd metal present in the matrix.

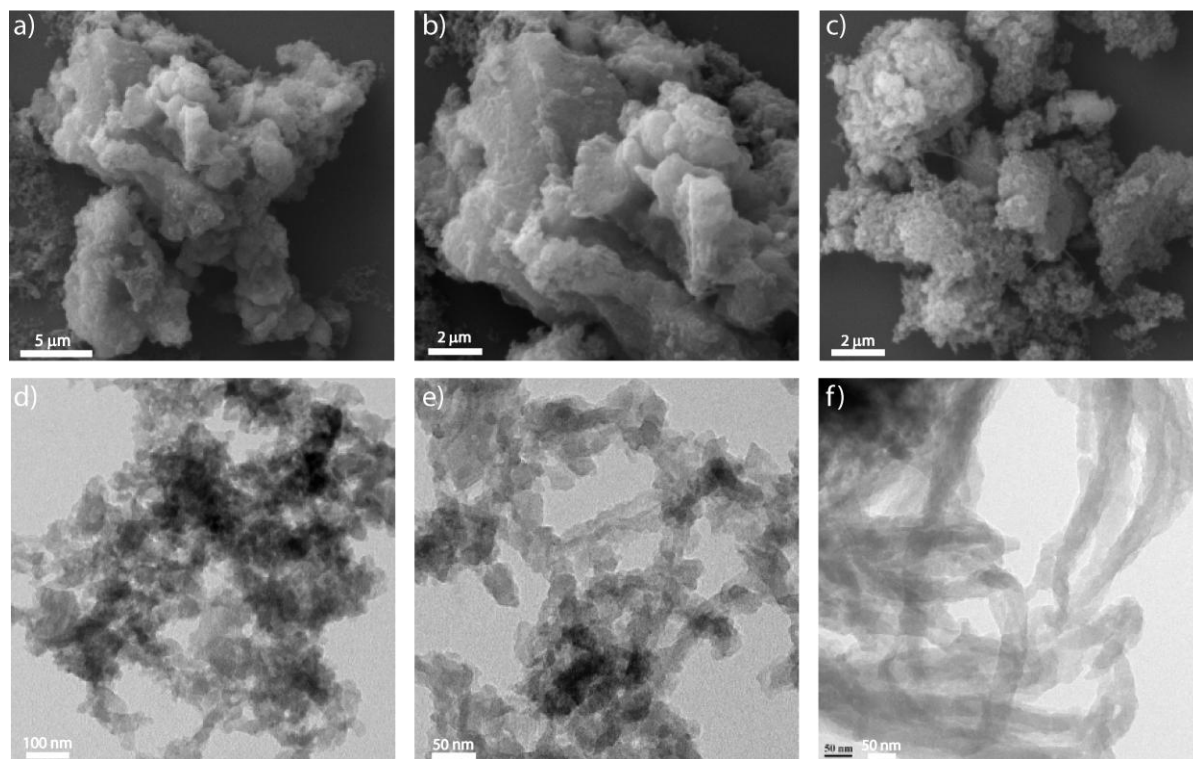


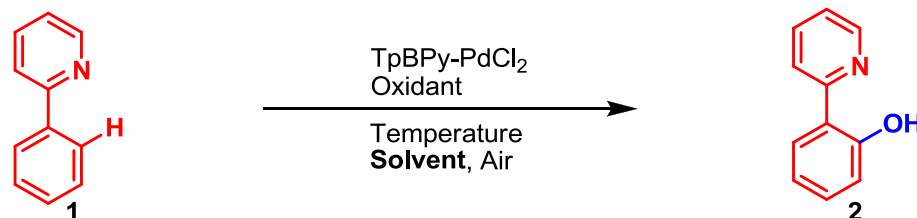
Figure 4.6: Characterization details of *TpBpy-PdCl₂*. (a, b, c) SEM images and (d, e, f) TEM images of *TpBpy-PdCl₂* showing fibrillar morphology.

4.3.4 Optimization Details for Chelation Assisted Direct C(sp²)-H Bond Hydroxylation Reaction

The formation of the C-O bond is more challenging compared to C-C bond formation through inert C-H bond action. Although the problem is solved by introducing transition metal into the reaction medium but selective hydroxylation of a single C-H bond in a molecule is becoming a more difficult process. The simple alternative to overcome this problem is using of directing group into the substrate which will bind with the metal and will allow the metal to activate a particular C-H bond within a proximal distance. Transition metal catalyzes the hydroxylation of C-H bond is becoming more important because of the synthesis of industrially important alcohol and phenol products. 2-(2-pyridyl)phenol derivatives are a most useful building block for the synthesis of the biologically active molecule and light-emitting materials. Therefore we have started optimization of 2-(2-pyridyl)phenol formation from 2-phenylpyridine as precursor where pyridine group acts as a metal chelating agent. First, we have varied different solvents. Among those Mesitylene shows better yield compared to other solvents (Table 4.2). Then the reaction is performed

under acidic condition using glacial AcOH and Ac₂O mixture (Table 4.3). The yield of the hydroxyl product decreases significantly and there is no –OAc product found as a major product under this condition. In presence of very less amount of water, the reaction is quenched. The starting material remains as such after the reaction which means the reaction has to be performed under a moisture free condition (Table 4.3). During the temperature optimization process, as temperature increases, the yield of product increases and 130 °C shows the optimized temperature for this transformation (Table 4.4). Next, we have varied different organic and inorganic oxidizing agent and their amount. Among the oxidant PhI(OAc)₂ shows better yield compared to others (Table 4.5). In presence of only oxygen, there is no reaction occurring which means only oxygen is not sufficient for product formation. Notably, we have found that 2 equiv. of PhI(OAc)₂ is optimum for this reaction and in absence of PhI(OAc)₂, there is no progress in reaction found (Table 4.6). 1 mg catalyst **TpBpy-PdCl₂** is sufficient for this transformation. As the catalyst amount increases, the formation of product decreases and in absence of a catalyst the reaction does not proceed further (Table 4.7). During

Table 4.2 Optimization of Solvents

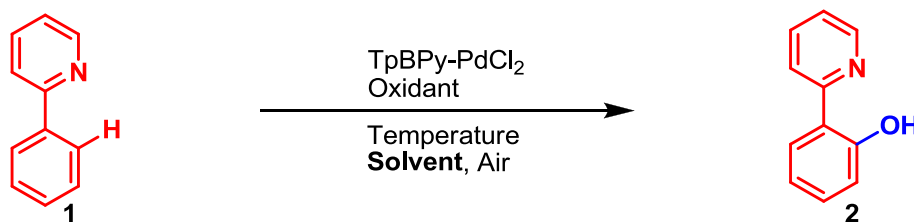


Entry	Solvent	GC Yield (%)
1	MeCN	21
2	Toluene	54
3	1,4-Dioxane	64
4	DMF	18
5	DMA	5
6	Mesitylene	70
7	<i>o</i> -DCB	47
8	THF	8
9	<i>m</i> -Xylene	62
10	DCE	51
11	NMP	-
12	NMF	-

13	DME	54
14	Nitrobenzene	49

Reactions were conducted with 0.4 mmol of 2-phenylpyridine (1 equiv), 4 mg of TpBpy-PdCl₂ and PhI(OAc)₂ (1.8 equiv) were heated at 130 °C in 2 mL representative solvents for 16 h in presence of air.

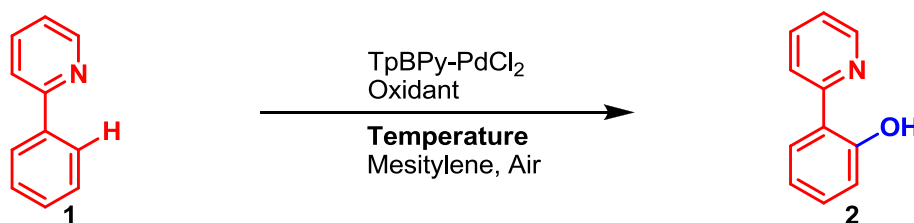
Table 4.3 Optimization in presence of Acid and Water



Entry	Solvent	Additive	GC Yield (%)
1	Mesitylene	H ₂ O (10 eq) = 72 μL	-
2	Glacial AcOH	Ac ₂ O = 400 μL	17
3	Glacial AcOH	Ac ₂ O = 400 μL and H ₂ O (10 eq) = 72 μL	-
4	Mesitylene	Glacial AcOH (1 mL)	20
5	Mesitylene	Glacial AcOH (1 mL) and Ac ₂ O = 200 μL	40
6	Mesitylene	Glacial AcOH (1 mL) and Ac ₂ O = 200 μL and H ₂ O (10 eq) = 72 μL	-

Reactions were conducted with 0.4 mmol of 2-phenylpyridine (1 equiv), 4 mg of TpBpy-PdCl₂ and PhI(OAc)₂ (1.8 equiv) were heated at 130 °C in 2 mL representative solvents for 16 h in presence of air.

Table 4.4 Temperature Optimization

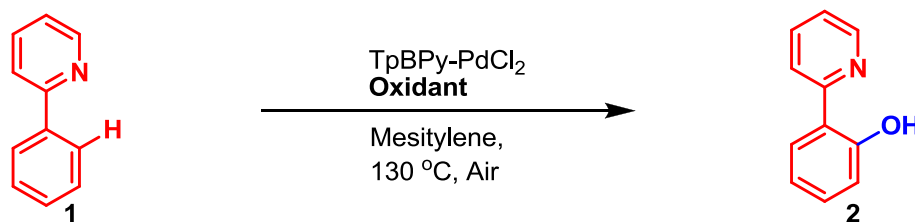


Entry	Temperature (°C)	GC Yield (%)
1	70	12
2	90	43
3	110	64

4	130	70
5	150	70

Reactions were conducted with 0.4 mmol of 2-phenylpyridine (1 equiv), 4 mg of TpBpy-PdCl₂ and PhI(OAc)₂ (1.8 equiv) were heated at different temperature in 2 mL mesitylene for 16 h in presence of air.

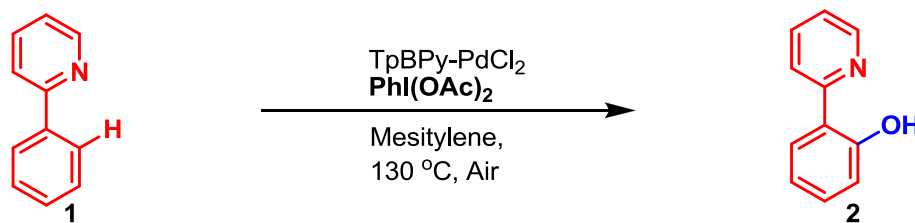
Table 4.5 Optimization of Oxidant



Entry	Oxidant	GC Yield (%)
1	CuCl ₂ .2H ₂ O	-
2	Anhyd. Cu(OAc) ₂	-
3	K ₂ S ₂ O ₈	-
4	PhI(OTf) ₂	-
5	<i>p</i> -Benzoquinone	-
6	Oxone	-
7	NaOCl	-
8	O ₂	-
9	70 wt% TBHP in H ₂ O	-
10	5(M) TBHP in Decane	-
11	30% H ₂ O ₂ in H ₂ O (W/V)	-
12	NMO	-
13	<i>m</i> -CPBA	-
14	DDQ	-
15	9,10-Phenanthrenequinone	-
16	PhI(OAc)₂	76

Reactions were conducted with 0.4 mmol of 2-phenylpyridine (1 equiv), 4 mg of TpBpy-PdCl₂ and different oxidant (2 equiv) were heated at 130 °C in 2 mL mesitylene for 16 h in presence of air.

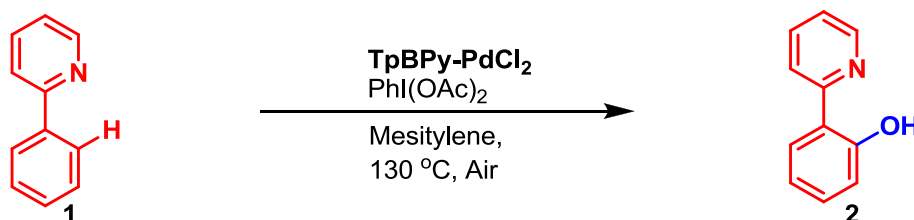
Table 4.6 Optimization of Amount of Oxidant



Entry	PhI(OAc) ₂ (eq)	GC Yield (%)
1	-	-
2	0.5	5
3	1	47
4	1.5	69
5	2	76
6	2.5	73
7	3	63
8	3.5	54
9	4	33

Reactions were conducted with 0.4 mmol of 2-phenylpyridine (1 equiv), 4 mg of TpBpy-PdCl₂ and PhI(OAc)₂ in different equiv were heated at 130 °C in 2 mL mesitylene for 16 h in presence of air.

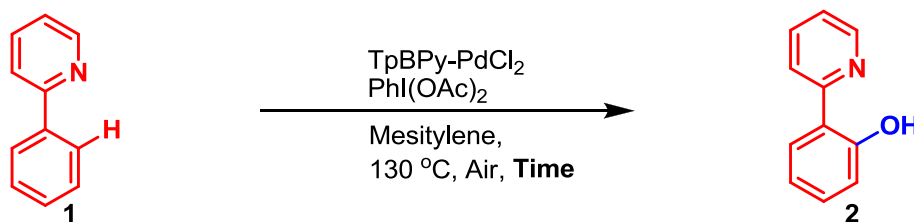
Table 4.7 Optimization of Amount of Catalyst



Entry	TpBpy-PdCl ₂ (mg)	GC Yield (%)
1	-	-
2	1	91
3	2	82
4	3	73
5	6	70
6	8	65

Reactions were conducted with 0.4 mmol of 2-phenylpyridine (1 equiv), different amount of TpBpy-PdCl₂ and PhI(OAc)₂ (2 equiv) were heated at 130 °C in 2 mL mesitylene for 16 h in presence of air.

Table 4.8 Time Optimization



Entry	Time (h)	GC Yield (%)
1	1	66
2	2	67

3	4	68
4	6	78
5	8	84
6	12	90
7	16	91
8	20	80

Reactions were conducted with 0.4 mmol of 2-phenylpyridine (1 equiv), 1 mg of **TpBpy-PdCl₂** and **PhI(OAc)₂** (2 equiv) were heated at 130 °C in 2 mL mesitylene for different time in presence of air. Yields are calculated based on GC analysis using *n*-Decane as an internal standard.

time optimization process, it is observed that 12 h is sufficient to get 90% yield of the product (Table 4.8). The yields in the optimization process are calculated based on GC analysis using *n*-Decane as an internal standard.

4.3.5 Heterogeneity Test:

The heterogeneity of the **TpBpy-PdCl₂** catalyst has been confirmed by typical mercury poisoning experiment.

4.3.5.1 Mercury Poisoning Experiment

The heterogeneity of the **TpBpy-PdCl₂** catalyst is verified by mercury poisoning test for chelation assisted direct C(sp²)-H bond hydroxylation reaction. During the reaction there is a significant inhibition in the catalytic performance is observed due to the poisoning of the catalytically active metal centers. In a typical mercury poisoning test, two sets of reactions are carried out for C(sp²)-H bond hydroxylation reaction using 2-phenylpyridine (57.1 μL, 0.4 mmol), **PhI(OAc)₂** (258 mg, 0.8 mmol) and **TpBpy-PdCl₂** (1 mg, 0.0012 mmol) in 1 mL Mesitylene under air and allowed to stir at 130 °C for 12 h. In one case, we have added 275 mg of mercury to the reaction mixture during the addition of the substrates and another reaction mixture was heated without adding any trace of mercury. After 12 h reaction, the yields of the products were measured by GC. The reaction mixture without mercury gave 90% yield of the product, whereas the reaction mixture having mercury gave 24% yield of the product, which strongly suggests the heterogeneity of the catalyst. The yield of the product decreased due to the formation of Pd-Hg amalgam.

4.4 Conclusion

In this chapter, we have discussed the development of a unique strategy for the synthesis of palladium metal coordinated stable covalent organic framework (**TpBpy-PdCl₂**)

by reacting with 1,3,5-triformylphloroglucinol (**Tp**) and 2,2'-bipyridine-5,5'-diamine palladium chloride (**Bpy-PdCl₂**) in the solvothermal condition in DMSO solvent using pre-synthetic method. This is the only combination we have found where Pd nanoparticles are not forming during the course of the reaction. The palladium coordination into the framework is confirmed from PXRD, TEM, EDX and ICP-OES analysis. Further, the oxidation of palladium (II) is verified by XPS analysis where the 3d spectra of palladium coordinated framework have shown comparable binding energy similar to the palladium metal coordinated organic starting precursor (**Bpy-PdCl₂**). The thermal stability of the framework is analyzed by TGA analysis. The stable and crystalline nature of the **TpBpy-PdCl₂** makes it ideal candidates as a heterogeneous catalyst. Therefore, we have utilized the material **TpBpy-PdCl₂** successfully for the selective hydroxylation of 2-phenylpyridine *via* chelation assisted direct C(sp²)-H bond activation where pyridine unit acts as a metal directing ligand with 90% yield of the formation of the product. Mercury poisoning experiment shows that the material is heterogeneous in nature. Finally, we believe that our developed method for homogeneous metal coordination into the framework *via* pre-synthesized method will definitely open up a new domain of exciting research area in the field of heterogeneous catalysis.

4.5 Experimental Procedures

4.5.1 Synthesis of **TpBpy-PdCl₂**:

To a pyrex tube 1,3,5-triformylphloroglucinol (**Tp**) (21 mg, 0.1 mmol) and 2,2'-bipyridine-5,5'-diamine palladium chloride (**Bpy-PdCl₂**) (54.5 mg, 0.15 mmol) are added in presence of dimethyl sulfoxide (DMSO) 3 mL with 0.3 mL of 6M aqueous acetic acid. In order to disperse homogeneously, the reactants are ultrasonicated for 15 min and degassed through three successive freeze-pump-thaw cycles. After that, the tube is sealed in a vacuum condition and kept for heating at 90 °C in the isothermal oven for 3 days. Finally, the phase pure material is filtered out and washed with DMSO solvents to remove the residues of the starting materials. The collected reddish material is solvent exchanged with DMSO and washed with excess acetone. Then the powder material is dried at 110 °C for 12 h under vacuum in order to get as synthesized **TpBpy-PdCl₂** COF (80% yield). **IR (powder, cm⁻¹):** 1606, 1564, 1445, 1231, 1229, 1088, 984, 821, 732.

4.5.2 Synthesis of 2,2'-bipyridine-5,5'-diamine palladium chloride (**Bpy-PdCl₂**):

1,3,5-triformylphloroglucinol (**Tp**) was synthesized using a previously reported method and confirmed by IR, ¹HNMR, and ¹³CNMR [4.16].

The 2,2'-bipyridine-5,5'-diamine-palladium chloride (**Bpy-PdCl₂**) (Figure 4.7) is synthesized as per reported procedure [4.17] and elaborately discussed in chapter 3.

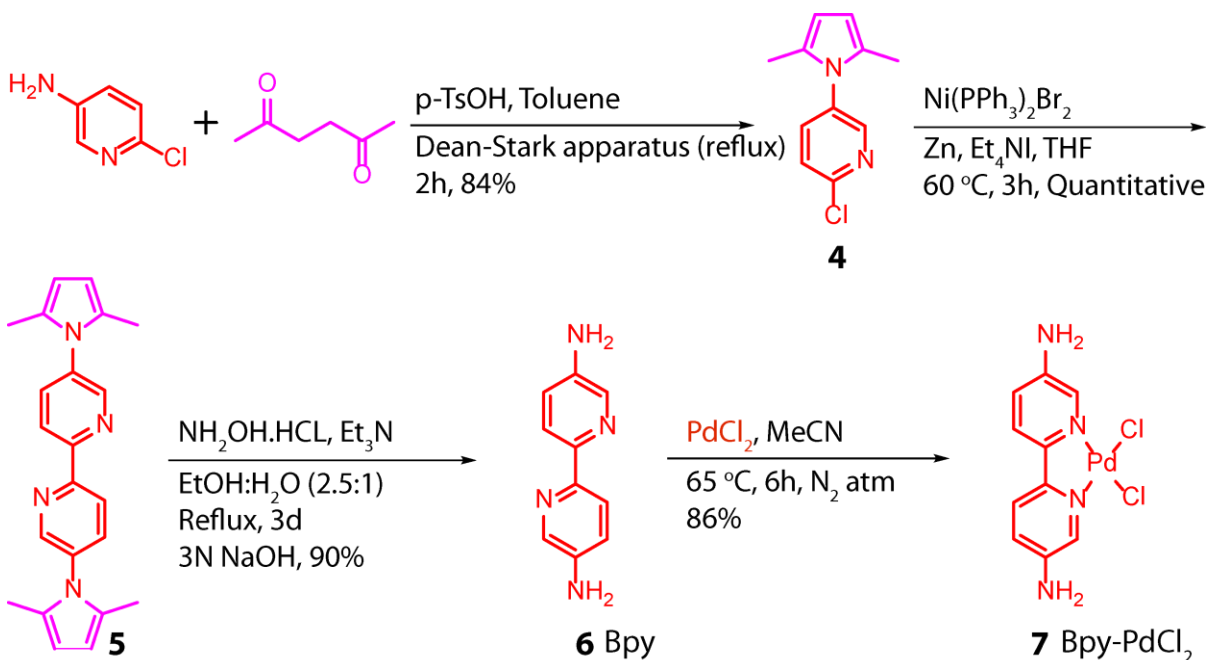


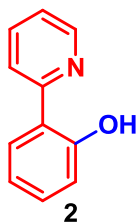
Figure 4.7: General synthetic scheme for the preparation of 2,2'-bipyridine-5,5'-diamine palladium chloride (**Bpy-PdCl₂**).

4.5.3 General Procedure for selective hydroxylation of 2-phenylpyridine via direct C(sp²)-H bond activation:

2-phenylpyridine (57.1 μL, 0.4 mmol), PhI(OAc)₂ (258 mg, 0.8 mmol) and **TpBpy-PdCl₂** (1 mg, 0.0012 mmol) are added in 1 mL Mesitylene under air atmosphere in a screw cap reaction tube. Then the reaction mixture is allowed to stir at 130 °C for 12 h. After the completion of the reaction (monitored by TLC), the reaction mixture is centrifuged to separate the solid and the solid is washed with DCM. The combined organic layer is evaporated under reduced pressure. The crude product is purified by column chromatography to obtain the desired product.

4.5.4 Characteristic Data of Synthesized Compounds

2-(2-pyridyl)phenol (2) is synthesized by general procedure with 2-phenylpyridine (57.1 μL , 0.4 mmol), $\text{PhI}(\text{OAc})_2$ (258 mg, 0.8 mmol) and **TpBpy-PdCl₂** (1 mg, 0.0012 mmol). The yield of the product is 90% measured in GC using n-Decane as an internal standard.



¹H NMR (400 MHz, CDCl_3): δ = 14.38 (s, 1H), 8.54 (d, J = 4.8 Hz, 1H), 7.94 (d, J = 9.2 Hz, 1H), 7.91-7.83 (m, 2H), 7.42 (t, J = 8 Hz, 1H), 7.27 (t, J = 8 Hz, 1H), 7.17 (d, J = 8.9 Hz, 1H), 7.01 (t, J = 8 Hz, 1H); ¹³C NMR (101 MHz, CDCl_3) δ = 159.81, 157.53, 145.52, 137.56, 131.27, 125.96, 121.31, 118.81, 118.58, 118.36; HRMS-ESI (m/z) $[\text{M}+\text{H}]^+$ calcd for $\text{C}_{11}\text{H}_{10}\text{ON}$, 172.0757, found 172.0755.

4.5.5 Characterization of TpBpy-PdCl₂ after Catalysis

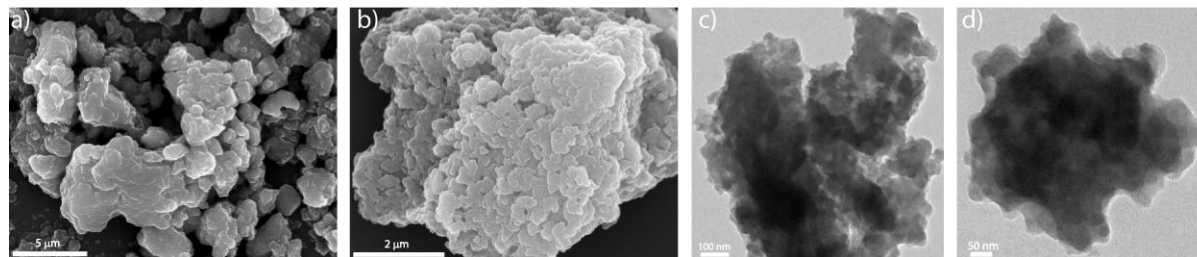


Figure 4.8: (a), (b) are the SEM images; (c), (d) are the TEM images of **TpBpy-PdCl₂** after catalysis.

4.5.6 General methods for characterization

All reagents were commercially available and used as received.

a) Wide-angle X-Ray Diffraction (WAXD): The Powder X-ray diffraction (PXRD) patterns were recorded on a Phillips PAN analytical diffractometer for $\text{Cu K}\alpha$ radiation (α = 1.5406 Å), with a scan speed of 1° min^{-1} and a step size of 0.02° in 2θ . The instrument was previously calibrated using a silicon standard.

b) FT-IR spectroscopy: The Fourier Transform Infrared (FTIR) spectra were taken on a Bruker Optics ALPHA-E spectrometer with a universal Zn-Se ATR (attenuated total reflection) accessory in the $600\text{--}4000 \text{ cm}^{-1}$ region.

c) Thermogravimetric analysis: TGA was carried out on a TG50 analyzer (Mettler-Toledo) or an SDT Q600 TG-DTA analyzer under N_2 atmosphere at a heating rate of $10^\circ \text{ C min}^{-1}$ within a temperature range of $30\text{--}900^\circ \text{ C}$.

d) Scanning Electron Microscopy: SEM images were obtained with a Zeiss DSM 950 scanning electron microscope and FEI-QUANTA 200 3D Scanning Electron Microscope with tungsten filament as electron source operated at 10 kV. The samples were sputtered with Au (nano-sized film) prior to imaging by an SCD 040 Balzers Union.

e) Transmission Electron Microscopy: TEM images were recorded using FEI Tecnai G2 F20 X-TWIN TEM at an accelerating voltage of 200 kV. The TEM Samples were prepared by drop-casting the sample from isopropanol on copper grids (TED PELLA, INC. 200 mesh). The metal nanoparticles size distribution was determined by measuring the size of 700 particles from TEM images.

f) BET surface area: BET surface area of the synthesized COFs was measured through N₂ adsorption studies. N₂ adsorption isotherms were collected with a Quantachrome make Autosorb IQ₂ automated surface area analyzer.

g) Solid-state NMR (SSNMR): Solid-state NMR (SSNMR) was taken in a Bruker 300 MHz NMR spectrometer and ligand NMR data were taken in Bruker 200/400/500 MHz NMR spectrometer.

h) Gas Chromatography: GC analyses were performed on an Agilent 7890B GC system with an FID detector using an HP-5 column (30 m, 0.25 mm, 0.25 μ). As the internal standard *m*-xylene was used.

i) Inductively Coupled Plasma Optical Emission Spectrometry: The wt% loading of Pd on TpBpy was analyzed using Inductively Coupled Plasma Optical Emission Spectrometry (ICP-OES) instrument from Spectro analytical instruments GmbH, model ARCOS simultaneous ICP spectrometer, Germany.

j) X-ray photoelectron spectroscopy: X-ray photoelectron spectroscopy (XPS) measurement of Pd nanoparticles was carried out by a VG Microtech, model ESCA 3000 instrument equipped with ion gun (EX-05) for cleaning the surface. The binding energy resolution was 0.1eV for the XPS measurement.

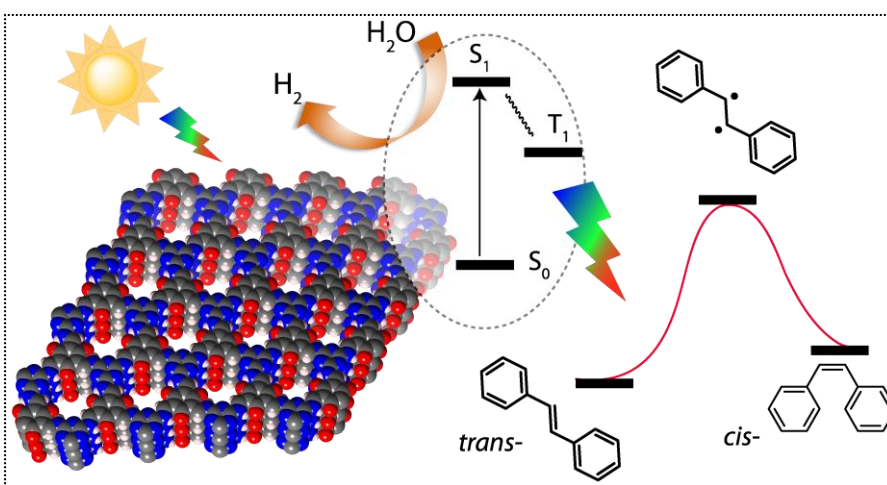
j) X-ray Diffractometer: The crystals were mounted on a Super Nova Dual source X-ray Diffractometer system (Agilent Technologies) equipped with a CCD area detector and operated at 250 W power (50 kV, 0.8 mA) to generate Mo K α radiation (λ = 0.71073 Å) and Cu K α radiation (λ = 1.54178 Å) at 298(2) K.

CHAPTER 5

Photocatalytic Covalent Organic Frameworks: Metal Free Photocatalyst for Trans to Cis Isomerization of Stilbenes and Hydrogen Evolution

Abstract: Conversion of most abundant solar energy into renewable energy in terms of hydrogen can be achieved by performing water-splitting reaction in presence of sunlight. Therefore developing methods for suitable photocatalyst/semiconductor synthesis is essential. Photocatalysts are used not

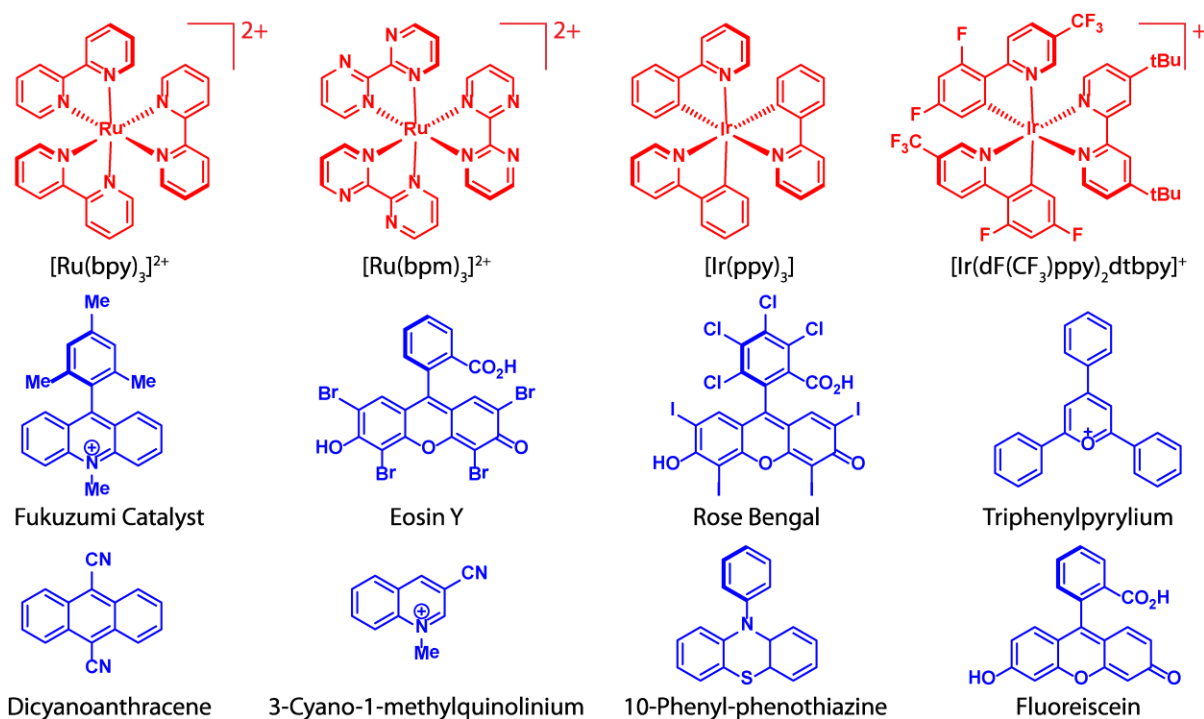
only for water splitting reaction but also for other organic chemical transformation for synthesizing different molecules in presence of visible light. Photochemical reactions are greener, safer and easy to



handle compared to thermal reaction. Hence for good photocatalytic performance, the catalyst should not only have sufficient light absorption ability in visible region but also have suitable band gap and high porosity as well. Although precious metal based homogeneous photocatalyst are developed which are toxic in nature. So, we have synthesized nonmetal based heterogeneous two photocatalysts Tp-OMeTt and TpTt using mild condition. Both the catalysts have shown the excellent photocatalytic conversion of trans stilbene to cis stilbene in presence of blue LED. But during photocatalytic hydrogen evolution reaction, TpTt has shown better activity compared to Tp-OMeTt. The decrease in catalytic activity in case of Tp-OMeTt is due to the lower band gap and low dispersion nature of the catalyst.

5.1 Introduction:

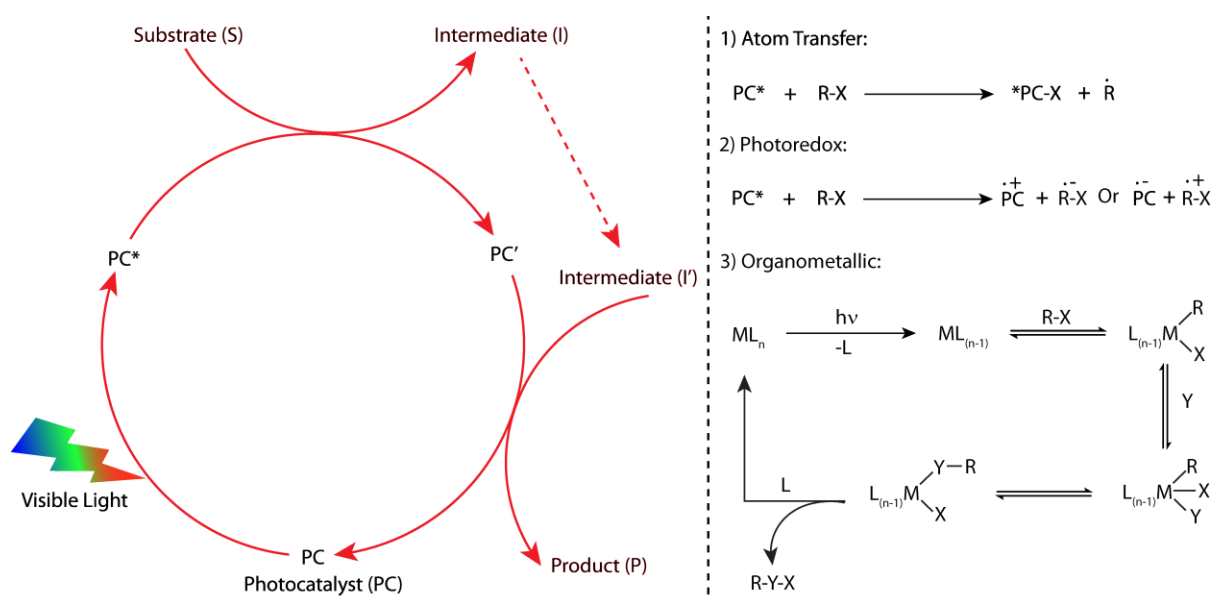
The day by day increasing energy demand and the climate change due to the consumption of fossil fuels (limited) producing greenhouse gases are becoming a serious concern to the scientific community [5.1]. Hence conversion of most abundant solar energy to renewable energy will be the most alternative approach. Therefore designing and synthesis of different photocatalysts and their utilization for different organic transformations have drawn significant attention. The term photocatalysis means the synergetic effect of light and catalyst which helps to promote the reactions [5.2]. Compare to thermal reactions, photochemical organic transformations are very safe, clean, abundant and easy handling process [5.3]. Although significant research on photocatalysis has been done using UV-



Scheme 5.1: Chemical structure of some common photoredox catalysts.

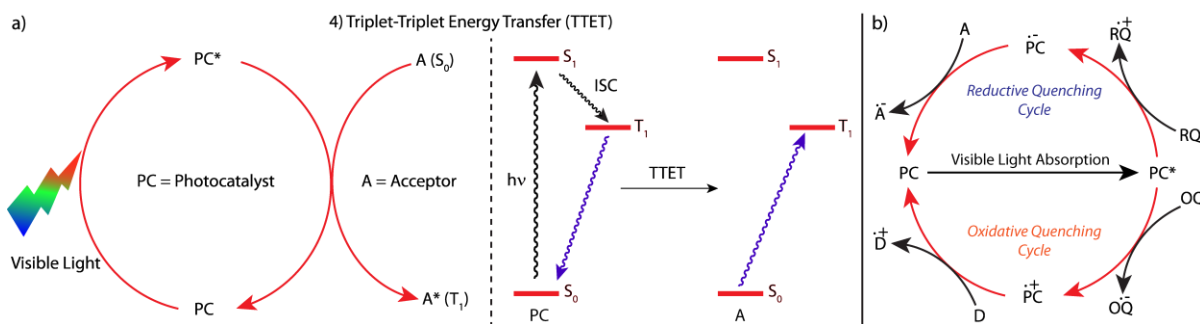
Visible light but performing reaction under visible light is more preferable compared to UV light. The major drawback of utilizing high energy UV light is that it generates various side reactions in the reaction medium [5.4]. The lack of visible light absorption capability of the most common organic molecule becomes a major obstacle for utilization of visible light in the photocatalytic process. Although after significant research, several metal-based and non-metal based organic photosensitizers [5.5] (photocatalysts) are developed which can absorb

visible light and convert solar energy to chemical energy by mimicking natural photosynthetic process (Scheme 5.1) [5.6]. The most common mechanisms involved during this process for selective molecule activation are 1) Light-induced atom transfer: where substrate transfers atom or group to the excited photocatalyst to generate radical; 2) Photoredox catalysis: where radical cation and anion are generated by transferring an electron from the substrate to the photocatalyst or vice versa; 3) Organometallic excitation: where the reaction happens in the metal center (Scheme 5.2);



Scheme 5.2: Schematic representation of photocatalysis and the description of possible mechanisms.

4) Energy transfer: here photocatalyst is excited from its ground singlet state (S_0) to its lowest singlet excited state (S_1) by irradiation and then through intersystem crossing (ISC) it generates the long-lived lowest energy triplet state (T_1). This triplet excited state of the photocatalyst may participate in electron transfer or in a process called triplet-triplet energy transfer (TTET). During the process the decay of energy from triplet state to ground singlet state of the photocatalyst assists to excite an acceptor molecule (A) from its ground singlet state (S_0) to its lowest energy triplet state (T_1). Moreover, there are three processes occurred during photoredox catalysis; a) Light absorption: the catalyst should absorb more light and excite an electron from its ground singlet state (S_0) to singlet excited state. b) Generation of long-lived excited state: then the electron should transfer to the lowest energy triplet state (T_1) through intersystem crossing (ISC). Hence the suitable condition for good photocatalytic performance is the efficient formation of the triplet state with good stability and long half-life



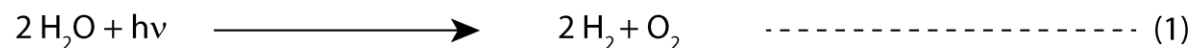
Scheme 5.3: (a) Mechanism of triplet-triplet energy transfer (TTET) from photocatalyst to the acceptor. (b) Photoredox catalysis with visible light: reductive and oxidative quenching cycle. PC = photocatalyst, RQ = reductive quencher, OQ = oxidative quencher, A = electron acceptor, D = electron donor.

after light absorption. c) Quenching process: this process can induce for chemical changing of a substrate which is not able to absorb light. This process occurs in two ways: 1) Reductive quenching and 2) Oxidative quenching. Reductive quencher reduces the excited state catalyst to the corresponding low oxidation state species whereas oxidative quencher oxidizes the excited state catalyst to the corresponding high oxidation state species. Last few decades the photoredox catalysts are extensively utilized for carbon dioxide reduction [5.7], degradations of chemical pollutant [5.8] and water splitting [5.9]. But recently these are used for synthesizing an organic molecule [5.10]. But the high cost and toxicity of the metal catalyst and high soluble nature of photocatalysts limit their applications for the production of large-scale synthesis. Therefore development of metal-free heterogeneous photocatalyst is essential.

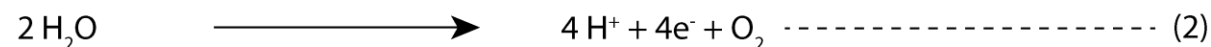
5.1.1 Water Splitting:

Photocatalytic water splitting is an eco-friendly, inexhaustible approach has gained significant attention for production of a renewable energy source as hydrogen using sunlight to fulfill the day by day increasing energy demand. Hydrogen contains high free energy ($\Delta G = +237$ KJ/mol) and in presence of oxygen, it produces nontoxic water as a side product [5.11]. The overall water splitting can be represented in two half reaction: 1) Oxygen evolution reaction (OER), 2) Hydrogen evolution reaction (HER). The oxidation potential for $\text{H}_2\text{O}/\text{O}_2$ is +1.23 V vs NHE at pH 0 (or at pH 7 is +0.82 V vs NHE) and the reduction potential for H^+/H_2 is 0.00 V vs NHE but in pH 7, -0.41 V overpotential is required for the production of H_2 in aqueous solution vs NHE. Therefore for overall water splitting reaction

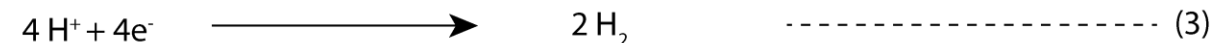
Overall Water Splitting



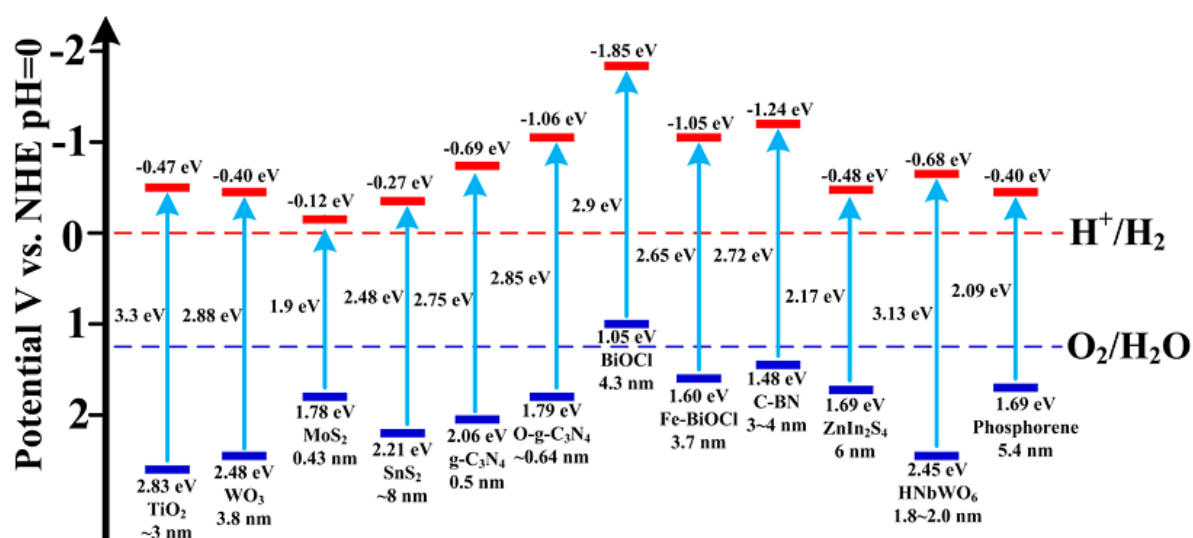
Oxygen evolution reaction (OER)



Hydrogen evolution reaction (HER)



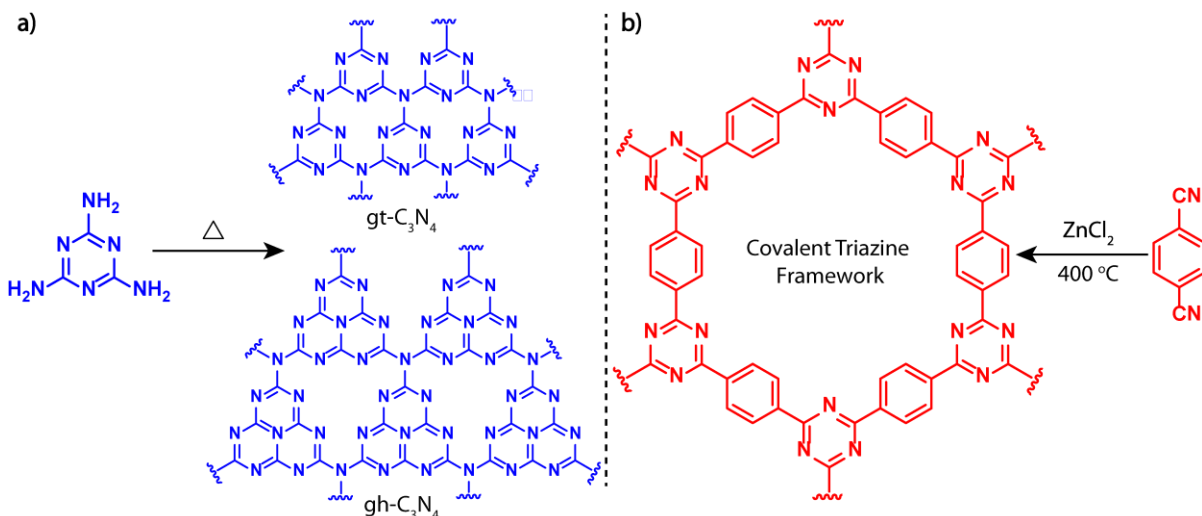
the band gap energy of the semiconductors should be more than 1.23 eV. Although many inorganic metal oxide, sulfide semiconductors [5.12] are developed for photocatalytic water splitting reaction but due to their low band gap, lower light absorption property in the visible region, high charge recombination and toxic nature make them nonideal for bulk scale reaction (Scheme 5.4).



Scheme 5.4: Band gap energies and band position of different semiconductors in relation with the redox potential of water splitting. Figures are reproduced with permission from ACS publications.

Therefore designing and synthesizing of nonmetal based heterogeneous semiconductors having suitable band gap and efficient light absorbing property in the visible region are essential for water splitting reaction. After several research, it has been found that carbon-based heterogeneous materials are suitable for this purpose. Among them, graphitic carbon nitride (g-C₃N₄) and covalent triazine frameworks are suitable candidates [5.13]. But these

materials are synthesized in higher temperature (400 to 600 °C) and in presence of Lewis metal catalyst (ZnCl_2) (Scheme 5.5). Hence, developing a mild method for the preparation of metal-free heterogeneous photocatalytic semiconductor is required.



Scheme 5.5: Synthetic scheme for (a) graphitic carbon nitride ($\text{g-C}_3\text{N}_4$) and (b) covalent triazine framework (CTF).

5.1.2 Importance of Trans (E) to Cis (Z) Isomerization Reaction and the Problems:

Alkene/olefin functional groups are essential building units in many synthetic, polymeric building blocks and drugs [5.14]. Stereo-chemistry of olefin functionalities plays pivotal role in the biological chemistry of molecule such as retinol. Most of the synthetic methods to synthesize alkenes lead to the formation of thermodynamically more stable *trans* (E) form. While, the direct synthesis of energetically less stable *cis* (Z) form, is remarkably challenging and has been restricted to a limited number of available synthetic methods [5.15]. Most of these synthetic methods lack high stereoselectivity and often require expensive high energy metal catalysts [5.16]. The probable solution for the more economic and stereoselective synthesis of *cis* (Z) isomer, is to follow the conventional photo-assisted E to Z isomerization strategy. However most of the low conjugated olefin compounds lacks absorption in the visible range, thus the E to Z transformation can happens only at high energy UV radiation. But UV based photo-conversions are not economic and often require special care due to its high toxicity. UV based reactions can also produces unwanted side products because of the high energy operating conditions. The alternative solution for this problem is to use economic, safe and more abundant sunlight/ visible light to perform the E

to Z isomerization. The implementation of photo-catalyst, which can absorb the visible light and transfer the energy to the E-olefin reactants, is highly essential for the success of full light induced E-Z isomerization. High photochemical stability, optimum band gap, absorption maxima in the visible range, and long-lived excited state are the key features to be considered while selecting an ideal photocatalyst. In literature photocatalysts such as iridium polypyridine complex, riboflavin, and aromatic keto compounds have been employed for the E to Z isomerization of alkenes [5.17]. However, due to the homogenous nature and low photochemical stability, recycling of the costly photocatalyst is tedious in most of the cases. In this perspective, there is a high demand for developing novel heterogenous, chemically stable photo-catalyst for the economic and energy efficient E to Z conversion of alkenes. The triazine core reported catalyzing E to Z photo-isomerization of an alkene, by promoting the close contact π - π interaction with the E alkene reactant. Additionally, Keto functionalities present in the β -ketoenamine core helps to enhance the lifetime of an excited triplet state by promoting the efficient intersystem crossing between singlet and triplet excited states.

By taking virtue of these qualities, we have successfully constructed novel heterogenous COF based photocatalysts for the E to Z isomerization of alkenes and hydrogen evolution from water. The COFs are constructed from two types of distinct photo-active building blocks (triazine and β -ketoenamine) having unique photo-sensitizing properties. We believe the newly generated heterogeneous hybrid COF photocatalysts will display high efficiency towards E to Z photo-isomerization alkenes and in hydrogen evolution process.

5.2 Synthesis and Characterization

5.2.1 *TpTt* COF Synthesis

The **TpTt** is synthesized by reacting 1,3,5-triformylphloroglucinol (**Tp**) (63 mg, 0.3 mmol) with Melamine (**Tt**) (38 mg, 0.3 mmol) in presence of *N,N*-dimethylacetamide (DMAc) and dimethyl sulfoxide solvent combination (2 : 1 mL) with 0.3 mL of 6M aqueous acetic acid using solvothermal process. The reactants are ultrasonicated for 15 min to disperse homogeneously as well as degassed through three successive freeze-pump-thaw cycles. Then the tube is sealed in a vacuum condition and heated at 120 °C in the isothermal oven for 3 days. Finally, the phase pure material is filtered out and is washed with DMAc solvents to remove the residues of the starting materials. The collected yellowish material is solvent exchanged with DMAc, H₂O and washed with excess acetone. Then the powder

material is dried at 120 °C for 8 h under vacuum in order to get as synthesized **TpTt** COF (80% yield) (Figure 5.1a). **IR (powder, cm⁻¹):** 1620, 1523, 1383, 1236, 1123, 1001, 806, 675, 643.

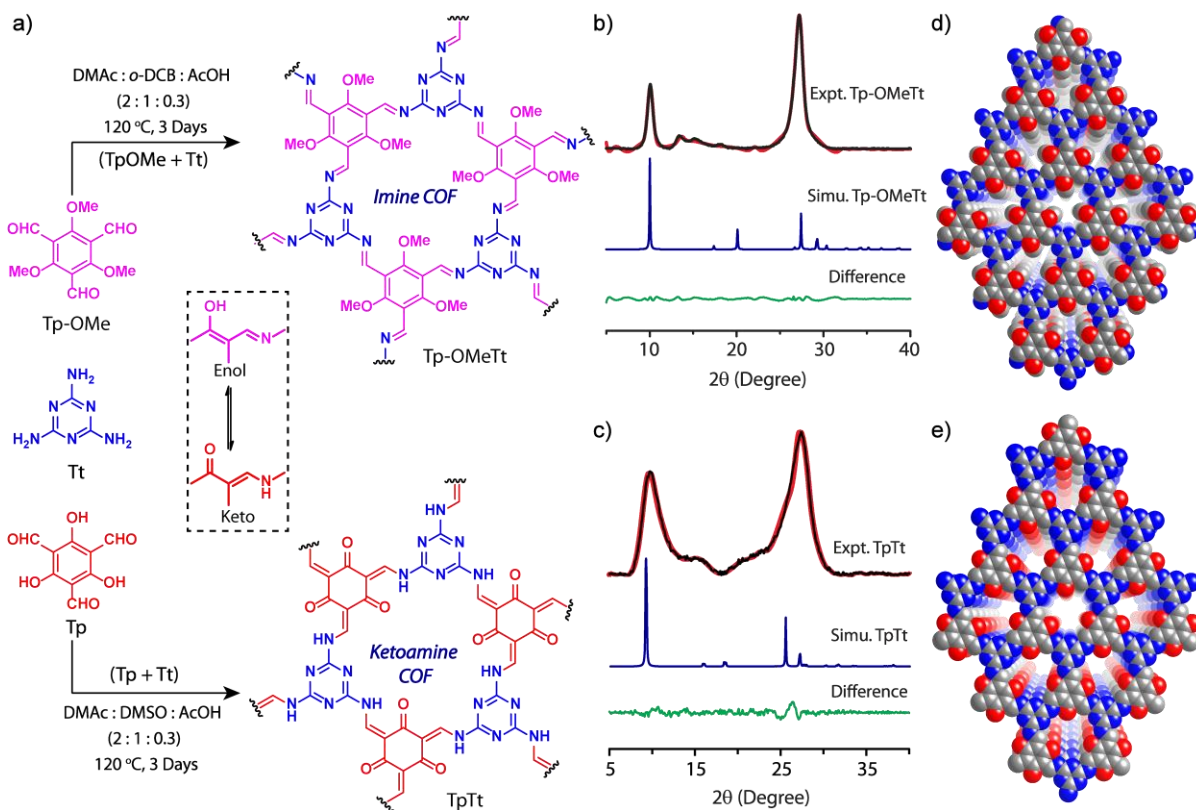


Figure 5.1: (a) Synthesis details of **Tp-OMeTt** (imine based COF) and **TpTt** (Ketoamine based COF). (b) Comparison of the experimental PXRD patterns of **Tp-OMeTt** (black) with the simulated (blue) simulated after Pawley refinement (red), and difference plot (green). (c) Comparison of the experimental PXRD patterns of **TpTt** (black) with the simulated (blue) simulated after Pawley refinement (red), and difference plot (green). (d), (e) Space-filling AA eclipsed stacking models of **Tp-OMeTt** and **TpTt** respectively along c direction.

5.2.2 **Tp-OMeTt** COF Synthesis

The **Tp-OMeTt** is synthesized by reacting 2,4,6-trimethoxybenzene-1,3,5-tricarbaldehyde (**Tp-OMe**) (75.6 mg, 0.3 mmol) with Melamine (**Tt**) (38 mg, 0.3 mmol) in presence of *N,N*-dimethylacetamide (DMAC) and *o*-dichlorobenzene solvent combination (2 : 1 mL) with 0.3 mL of 6M aqueous acetic acid using solvothermal process. The reactants are ultrasonicated for 15 min to disperse homogeneously as well as degassed through three successive freeze-pump-thaw cycles. Then the tube is sealed in a vacuum condition and is

heated at 120 °C in the isothermal oven for 3 days. Finally, the phase pure material is filtered out and is washed with DMAc solvents to remove the residues of the starting materials. The collected blackish material is solvent exchanged with DMAc, H₂O and is washed with excess acetone. Then the powder material is dried at 120 °C for 8 h under vacuum in order to get as synthesized **Tp-OMeTt** COF (82% yield) (Figure 5.1a). **IR (powder, cm⁻¹):** 1605, 1516, 1374, 1225, 996, 797, 733.

5.2.3 Structural Simulation and Characterization

The crystallinity of the synthesized **Tp-OMeTt** and **TpTt** are investigated by PXRD analysis. The PXRD patterns of **Tp-OMeTt** display two main characteristic peaks at $2\theta = 10^\circ$ and 27.2° , which corresponds to the reflections from the 100 and 002 plane respectively. The shift of 100 peak to the higher 2θ region as compared to other reported imine COFs, can be correlated to the small pore channels (1.7 nm) of **Tp-OMeTt** COF. From the d spacing of the 002 peaks, we are able to calculate the interlayer π - π stacking distance between the individual COF layers as 3.2 Å. The similar pattern is also observed in the case of ketoamine based **TpTt** COF. The PXRD patterns of **TpTt** display two main characteristic peaks at $2\theta = 9.7^\circ$ and 27.4° , which corresponds to the reflections from the 100 and 002 plane respectively. The shift of 100 peak to the higher 2θ region as compared to other reported ketoenamine COFs, can be correlated to the small pore channels (1.3 nm) of **TpTt** COF. From the d spacing of the 002 peaks, we are able to calculate the interlayer π - π stacking distance between the individual COF layers as 3.5 Å. In order to find out a reasonably fitting modeled structure of **Tp-OMeTt** and **TpTt** several stacking possibilities such as AA eclipsed, AB staggered, AA inclined are constructed using Material Studio-6.1 software. The simulated structure of the eclipse model is well matching with the experimental PXRD pattern of both the COFs. The eclipse models of **Tp-OMeTt** and **TpTt** are simulated in *P1* space group. To determine the exact unit cell parameter we have performed Pawley refinement. After refinement the final unit cell values are for **Tp-OMeTt** $a = b = 10.2$ Å, $c = 6.5$ Å, $\alpha = 90.4^\circ$, $\beta = 90.2^\circ$, $\gamma = 59.8^\circ$ with $R_p = 12.7\%$ and $R_{wp} = 6.4\%$ (Figure 5.2 and Table 5.1) and for **TpTt** $a = 11.2$ Å, $b = 11$ Å, $c = 6.9$ Å, $\alpha = 89.9^\circ$, $\beta = 90.3^\circ$, $\gamma = 59.9^\circ$ with $R_p = 4.7\%$ and $R_{wp} = 8.1\%$ (Figure 5.3 and Table 5.2).

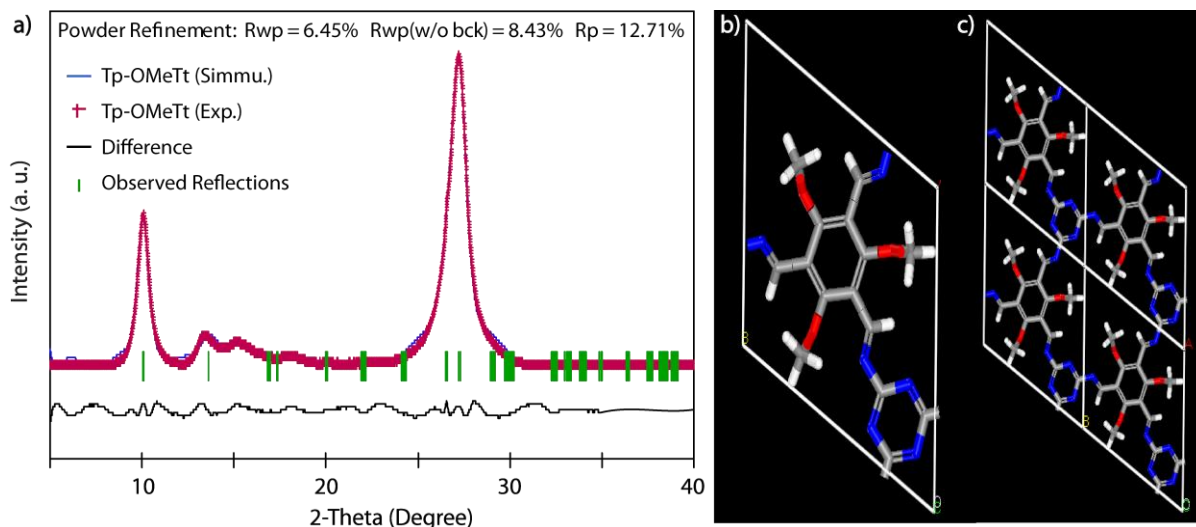


Figure 5.2: (a) Comparison of PXR D pattern of experimental (crossed) and simulated (blue) **Tp-OMeTt** in eclipsed stacking mode. Difference plot is depicted in black line. Pawley refinement demonstrates good agreement between experimental and simulated eclipsed PXR D pattern (Rwp: 8.43%, Rp: 12.71%). (b) Unit cell and (c) eclipsed crystal lattice packing of **Tp-OMeTt**.

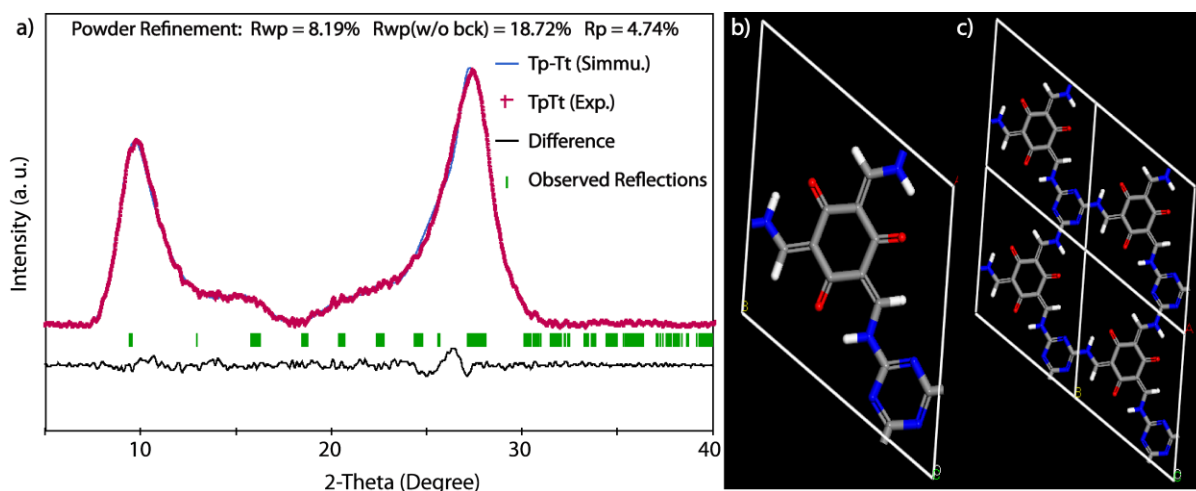


Figure 5.3: (a) Comparison of the PXR D pattern of experimental (crossed) and simulated (blue) **TpTt** in eclipsed stacking mode. Difference plot is depicted in black line. Pawley refinement demonstrates good agreement between experimental and simulated eclipsed PXR D pattern (Rwp: 8.19%, Rp: 4.74%). (b) Unit cell and (c) eclipsed crystal lattice packing of **TpTt**.

Table 5.1 Fractional atomic coordinates for the unit cell of **Tp-OMeTt** (Eclipsed)

<p>Tp-OMeTt P1 a = 10.2 Å, b = 10.2 Å, c = 6.5 Å $\alpha = 90.4, \beta = 90.2, \gamma = 59.8$</p>

C1	0.45442	0.43212	0.00508	C16	0.45442	0.43212	0.50508
C2	0.6017	0.37491	0.0037	C17	0.6017	0.37491	0.5037
C3	0.66253	0.46148	0.00256	C18	0.66253	0.46148	0.50256
C4	0.57222	0.60886	0.00484	C19	0.57222	0.60886	0.50484
C5	0.42447	0.6699	0.00624	C20	0.42447	0.6699	0.50624
C6	0.36748	0.5799	0.00735	C21	0.36748	0.5799	0.50735
C7	0.39537	0.33857	0.99549	C22	0.39537	0.33857	0.49549
H1	0.45877	0.23628	0.92552	H13	0.45877	0.23628	0.42552
N1	0.27717	0.37234	0.06525	N7	0.27717	0.37234	0.56525
C8	0.2284	0.27709	0.06083	C23	0.2284	0.27709	0.56083
C9	0.04497	0.23628	0.06125	C24	0.04497	0.23628	0.56125
C10	0.26974	0.05237	0.06182	C25	0.26974	0.05237	0.56182
N2	0.08864	0.33071	0.06178	N8	0.08864	0.33071	0.56178
N3	0.32294	0.13859	0.06262	N9	0.32294	0.13859	0.56262
N4	0.13126	0.0965	0.06354	N10	0.13126	0.0965	0.56354
C11	0.33081	0.82288	0.99863	C26	0.33081	0.82288	0.49863
H2	0.22722	0.86166	0.93259	H14	0.22722	0.86166	0.43259
C12	0.81567	0.40093	0.99069	C27	0.81567	0.40093	0.49069
H3	0.8543	0.46013	0.91304	H15	0.8543	0.46013	0.41304
N5	0.3654	0.90801	0.06579	N11	0.3654	0.90801	0.56579
N6	0.90056	0.2861	0.06668	N12	0.90056	0.2861	0.56668
O1	0.22283	0.63771	0.97815	O4	0.22283	0.63771	0.47815
O2	0.62756	0.69706	0.97465	O5	0.62756	0.69706	0.47465
O3	0.68851	0.23059	0.97063	O6	0.68851	0.23059	0.47063
C13	0.69754	0.72508	0.11508	C28	0.69754	0.72508	0.61508
H4	0.77946	0.62713	0.17492	H16	0.77946	0.62713	0.67492
H5	0.74726	0.78094	0.05928	H17	0.74726	0.78094	0.55928
H6	0.62032	0.79263	0.21287	H18	0.62032	0.79263	0.71287
C14	0.73006	0.13406	0.11406	C29	0.73006	0.13406	0.61406
H7	0.80051	0.14943	0.20153	H19	0.80051	0.14943	0.70153
H8	0.63777	0.14666	0.18516	H20	0.63777	0.14666	0.68516
H9	0.7871	0.02752	0.05861	H21	0.7871	0.02752	0.55861
C15	0.12803	0.69347	0.12386	C30	0.12803	0.69347	0.62386

H10	0.14512	0.60803	0.21159	H22	0.14512	0.60803	0.71159
H11	0.14056	0.77426	0.19386	H23	0.14056	0.77426	0.69386
H12	0.02089	0.74223	0.07115	H24	0.02089	0.74223	0.57115

Table 5.2 Fractional atomic coordinates for the unit cell of **TpTt** (Eclipsed)

<p style="text-align: center;">TpTt P1 a = 11.2 Å, b = 11.05 Å, c = 6.98 Å $\alpha = 89.9, \beta = 90.3, \gamma = 59.9$</p>							
C1	0.45823	0.42543	0.00372	C13	0.45823	0.42543	0.50016
C2	0.60951	0.36799	0.99797	C14	0.60951	0.36799	0.50152
C3	0.66156	0.46759	0.99808	C15	0.66156	0.46759	0.50164
C4	0.56694	0.62083	0.99658	C16	0.56694	0.62083	0.50013
C5	0.41656	0.67382	0.99564	C17	0.41656	0.67382	0.49919
C6	0.36004	0.57793	0.00268	C18	0.36004	0.57793	0.49913
C7	0.41247	0.3299	0.00352	C19	0.41247	0.3299	0.49996
H1	0.48725	0.21639	0.0043	H7	0.48725	0.21639	0.50075
N1	0.27665	0.36891	0.00234	N7	0.27665	0.36891	0.49878
C8	0.22873	0.27559	0.002	C20	0.22873	0.27559	0.49845
C9	0.04749	0.23584	0.00038	C21	0.04749	0.23584	0.49682
C10	0.26807	0.05205	0.00262	C22	0.26807	0.05205	0.49906
N2	0.09063	0.33012	0.00066	N8	0.09063	0.33012	0.49711
N3	0.3218	0.13748	0.00298	N9	0.3218	0.13748	0.49942
N4	0.13187	0.09591	0.00139	N10	0.13187	0.09591	0.49783
H2	0.20632	0.47686	0.00161	H8	0.20632	0.47686	0.49806
O1	0.61415	0.70121	0.99614	O4	0.61415	0.70121	0.49969
O2	0.23346	0.62583	0.0018	O5	0.23346	0.62583	0.49824
O3	0.68916	0.23978	0.99898	O6	0.68916	0.23978	0.50253
C11	0.32204	0.81579	0.00194	C23	0.32204	0.81579	0.49839
H3	0.21013	0.85315	0.00126	H9	0.21013	0.85315	0.49771
C12	0.80155	0.42167	0.99964	C24	0.80155	0.42167	0.50319
H4	0.83803	0.49798	0.99973	H10	0.83803	0.49798	0.50328
N5	0.36032	0.91454	0.99492	N11	0.36032	0.91454	0.49847

N6	0.89938	0.28423	0.00823	N12	0.89938	0.28423	0.50468
H5	0.86368	0.21264	0.00804	H11	0.86368	0.21264	0.50449
H6	0.46677	0.87797	0.99565	H12	0.46677	0.87797	0.4992

5.2.4 Chemical Characterization

The formation of imine bonded and enol-keto tautomerized covalent organic frameworks are examined by FT-IR spectra analysis (Figure 5.4). The FT-IR spectra show that the starting materials are totally consumed. The characteristic stretching band of primary amine -N-H ($3464, 3415 \text{ cm}^{-1}$) in case of melamine (**Tt**) and carbonyl (-C=O , 1678 cm^{-1}) in case of **Tp-OMe** are disappeared and new peaks arise in **Tp-OMeTt** at $1605, 1516, 1225 \text{ cm}^{-1}$ are corresponding to the stretching band of -C=N , -C=C and -C-N bond. The appearance of -C=N peak at 1605 cm^{-1} indicate the formation of the imine bonded covalent organic framework. The FTIR of **TpTt** does not show of N-H stretching bands ($3464\text{-}3312 \text{ cm}^{-1}$) of Melamine (**Tt**) and C=O stretching frequency (1643 cm^{-1}) of 2,4,6-Triformylphloroglucinol (**Tp**). The successful incorporation of β -ketoenamine links in **TpTt** is indicated by the appearance of intense peaks at 1620 cm^{-1} (-C=O), 1523 cm^{-1} (-C=C) and 1236 cm^{-1} (-C-N) in the FTIR spectra.

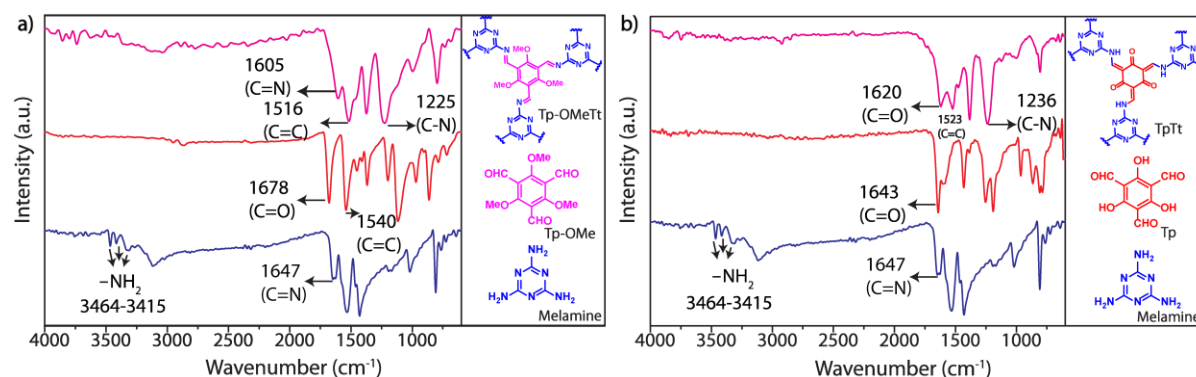


Figure 5.4: (a) FTIR spectra of **Melamine (Tt)** (blue), **Tp-OMe** (red) and **Tp-OMeTt** (pink). (b) FTIR spectra of **Melamine (Tt)** (blue), **Tp** (red) and **TpTt** (pink).

The ¹³C CP-MAS solid-state NMR of **Tp-OMeTt** shows that the formation of imine bonded framework where the signal appears at 167.1 and 162.9 ppm corresponding to imine (-C=N) carbon. The remaining sp^2 carbons appear together at 148.4 and 109.3 ppm (Figure 5.5a). The peak 68.5 ppm corresponding to the methoxy (-OMe) carbon. Whereas ¹³C CP-MAS solid-state NMR of **TpTt** shows the formation enol-keto tautomerized COF. The peak arises

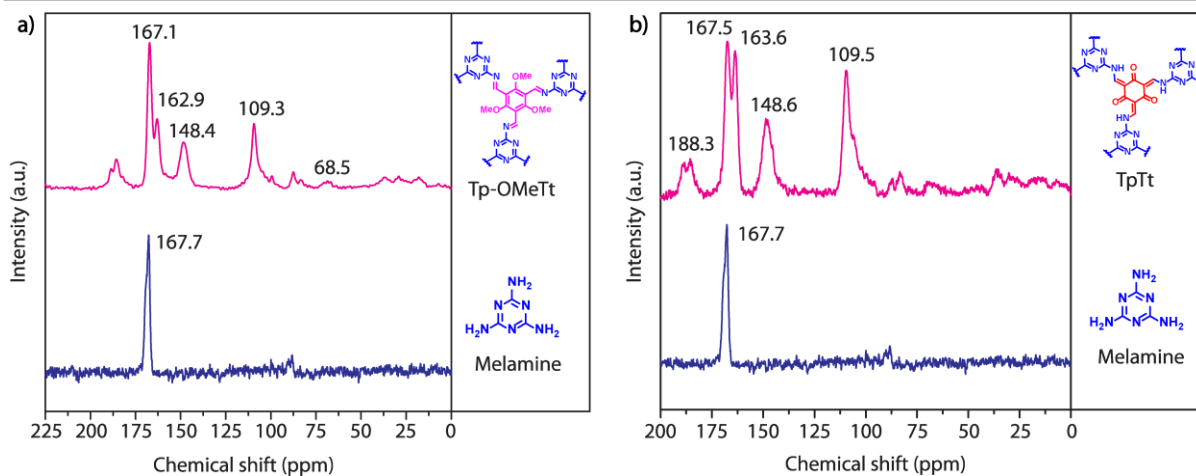


Figure 5.5: (a) Comparison of solid state ^{13}C NMR spectra of **Melamine** (blue) and **Tp-OMeTt** (pink). (b) Comparison of solid state ^{13}C NMR spectra of **Melamine** (blue) and **TpTt** (pink).

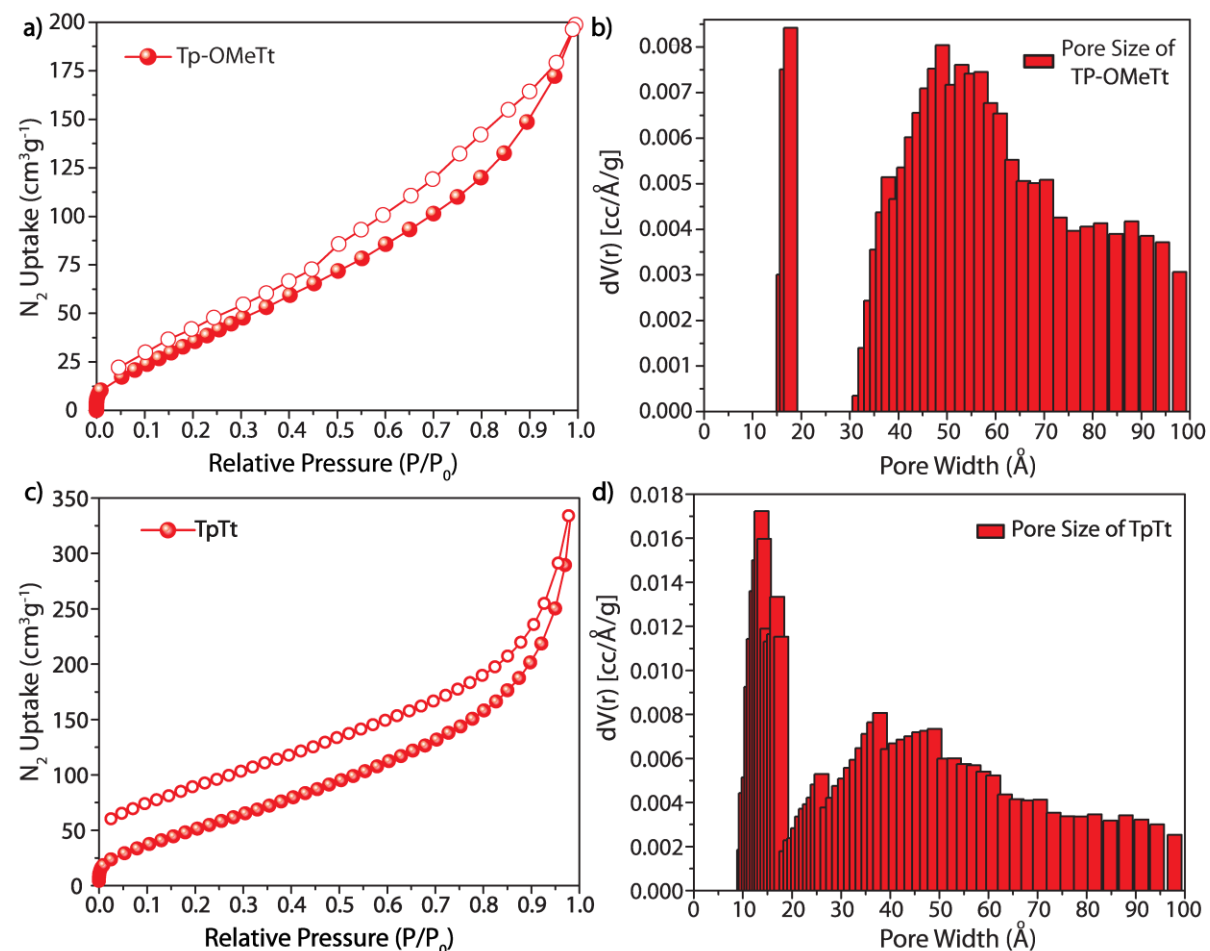


Figure 5.6: (a), (c) N_2 adsorption isotherm of **Tp-OMeTt** and **TpTt**. (b), (d) Experimental pore size distributions of **Tp-OMeTt** and **TpTt** calculated using the N_2 at 77 K on carbon (slit/cylindr. Pores, NLDFT equilibrium) model.

at 188.3 ppm corresponding to carbonyl carbon (-C=O) and the remaining aromatic carbons appear at 167.5 to 109.5 ppm. We have carried out N_2 adsorption isotherm of activated **Tp-OMeTt** and **TpTt** at 77K to evaluate permanent porosity of the respective COFs. Both the COFs show type I reversible N_2 adsorption isotherm with microporous in nature. The Brunauer–Emmett–Teller (BET) surface areas of **Tp-OMeTt** and **TpTt** are found to be 180 and 225 m^2g^{-1} respectively (Figure 5.6 a,c). The pore size distribution is measured on the basis of nonlocal density functional theory (NLDFT) which shows the narrow pore size distribution in the range of 1.7 nm for **Tp-OMeTt** and 1.3 nm for **TpTt** (Figure 6.6 b,d). Also we have performed the H_2 and CO_2 uptake study for both the COFs. The materials show good hydrogen uptake 25 cc/g for **Tp-OMeTt** and 33 cc/g for **TpTt** at 77 K 1atm pressure. The CO_2 uptake properties for **Tp-OMeTt** and **TpTt** are 22 cc/g and 40 cc/g respectively at 0 °C 1 atm pressure (Figure 5.7).

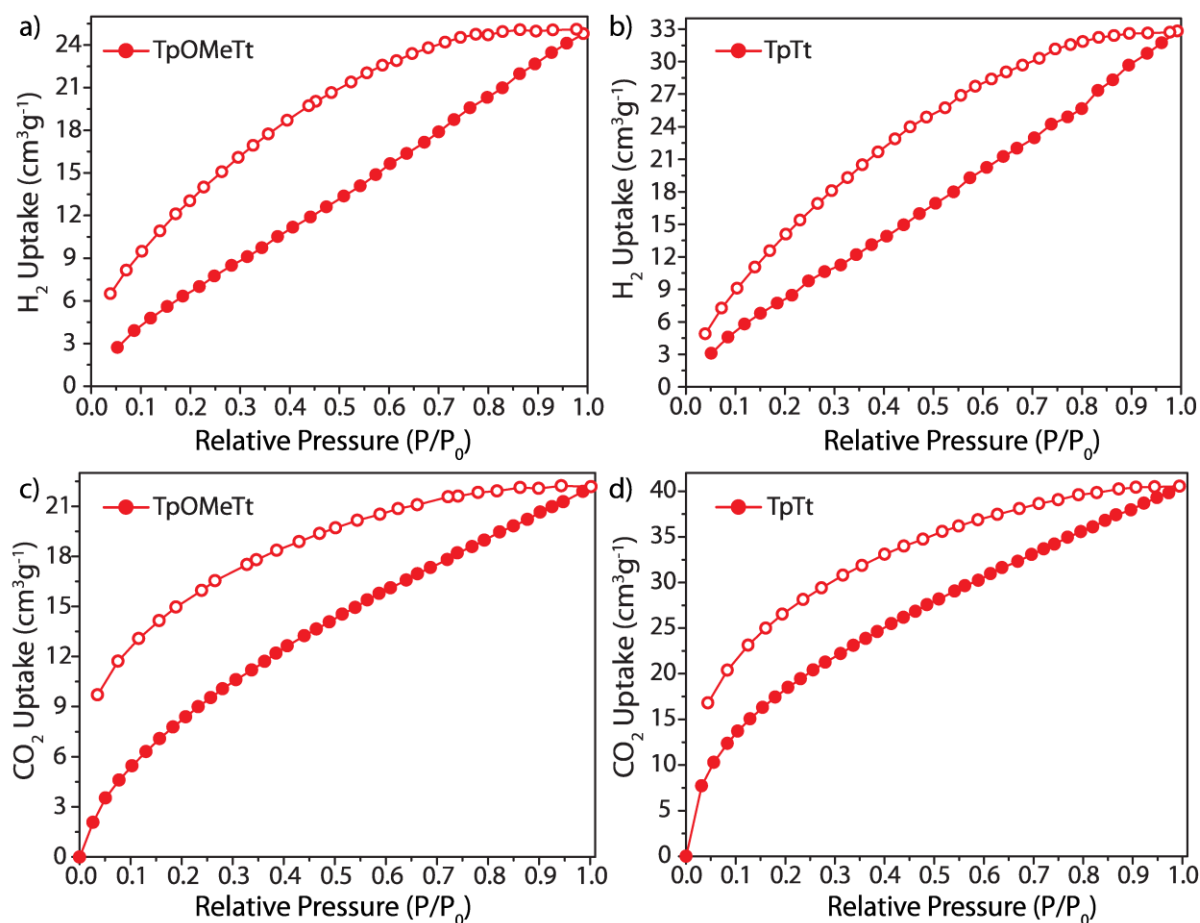


Figure 5.7: (a), (b) H_2 adsorption isotherm of **Tp-OMeTt** and **TpTt**. (c), (d) CO_2 adsorption isotherm of **Tp-OMeTt** and **TpTt**.

The thermal stability of the frameworks is analyzed by thermogravimetric analysis (TGA). It shows that the materials **Tp-OMeTt** and **TpTt** are stable up to 250 °C and 200 °C respectively (Figure 5.8). Whereas the corresponding starting materials Melamine (**Tt**), **Tp-OMe**, **Tp** are started degrading at 224 °C, 141 °C, and 128 °C.

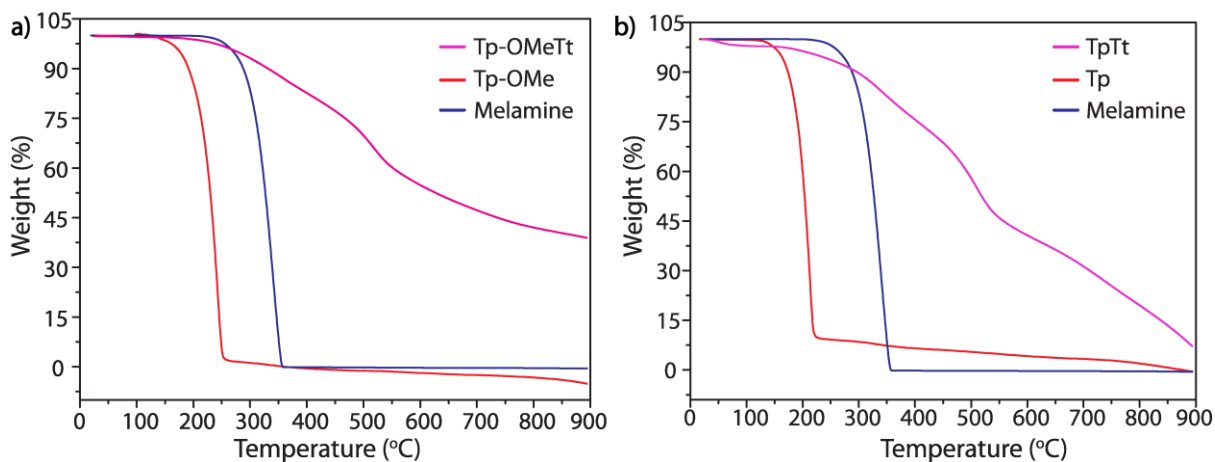


Figure 5.8: (a) TGA spectra of **Melamine (Tt)** (blue), **Tp-OMe** (red) and **Tp-OMeTt** (pink). (b) TGA spectra of **Melamine (Tt)** (blue), **Tp** (red) and **TpTt** (pink).

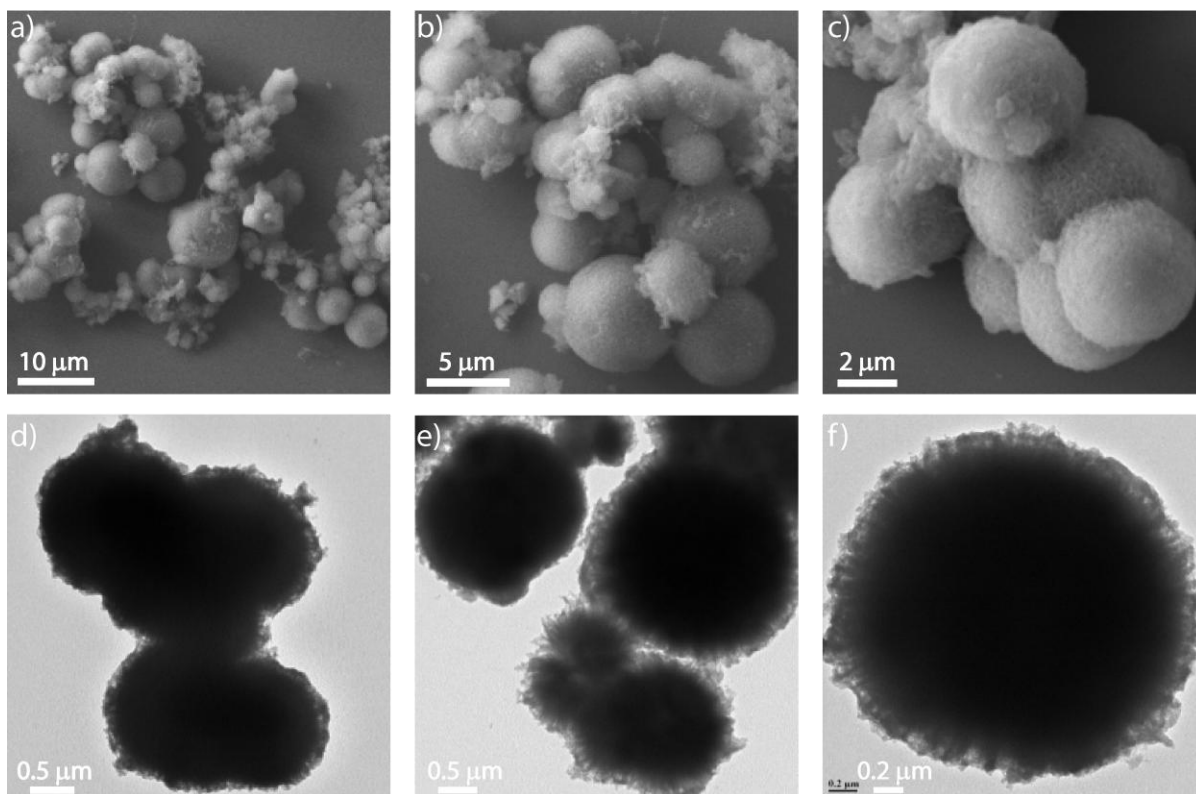


Figure 5.9: (a), (b), (c) SEM images and (d), (e), (f) TEM images of **Tp-OMeTt** showing spherical morphology.

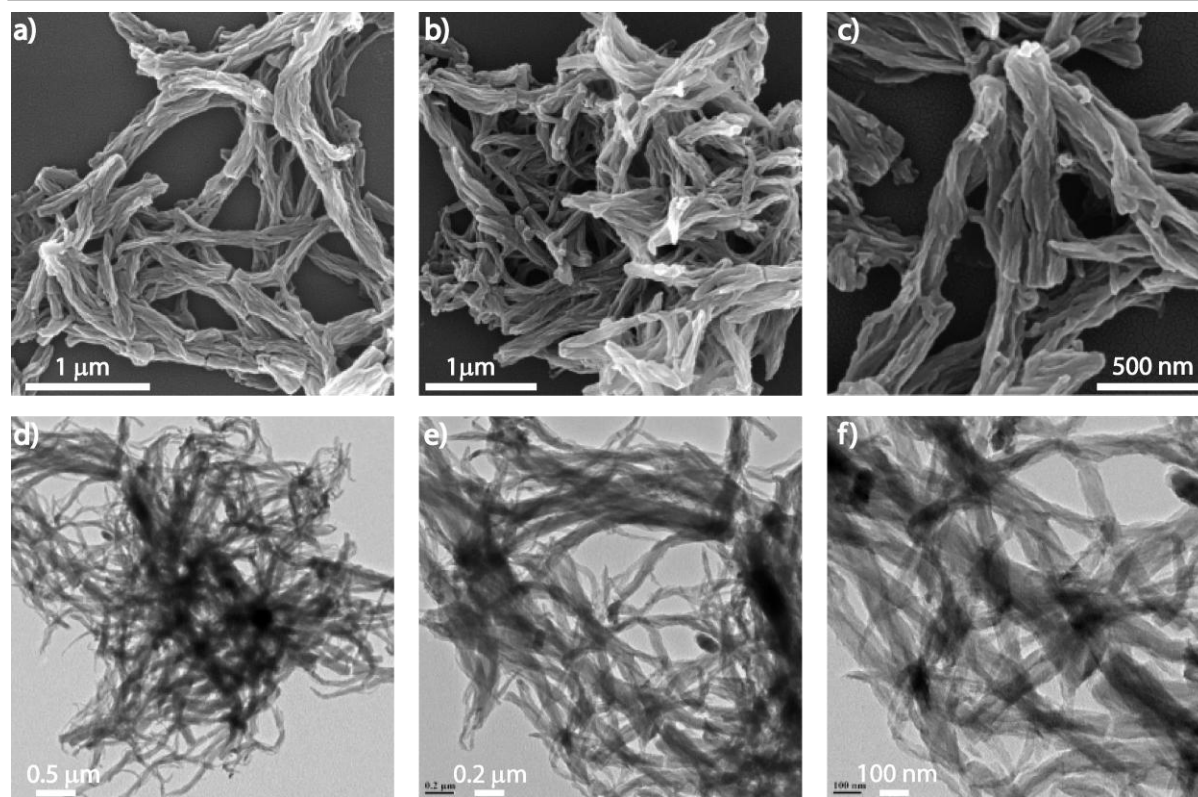


Figure 5.10: (a), (b), (c) SEM images and (d), (e), (f) TEM images of **TpTt** showing fibrillar morphology.

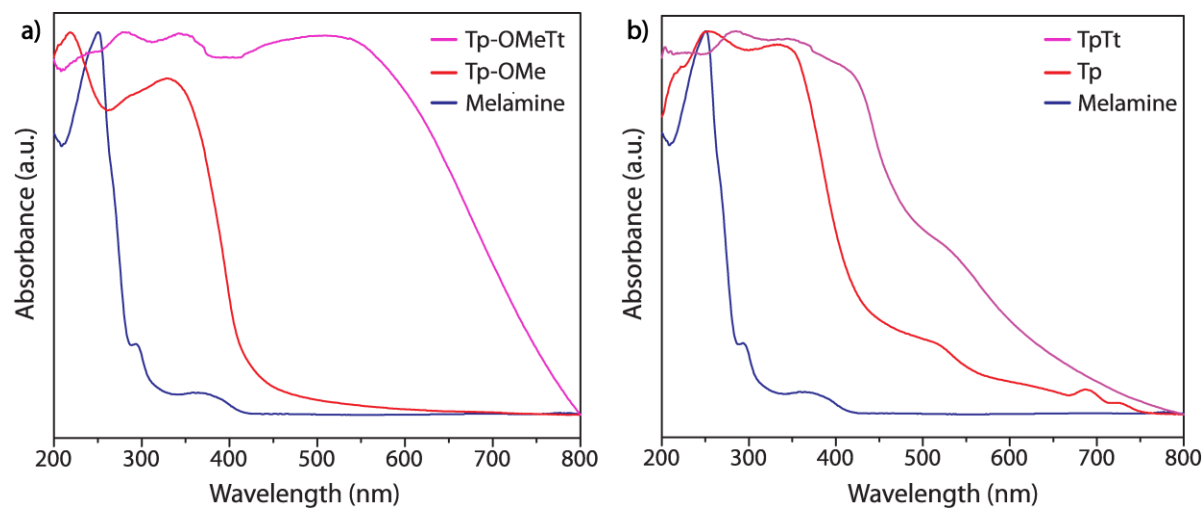


Figure 5.11: (a) Solid state UV-Vis diffuse reflectance spectra of **Melamine (Tt)** (blue), **Tp-OMe** (red) and **TP-OMeTt** (pink). (b) Solid state UV-Vis diffuse reflectance spectra of **Melamine (Tt)** (blue), **Tp** (red) and **TPTt** (pink).

Scanning Electron Microscopy (SEM) and Transmission Electron Microscopy (TEM) images of **Tp-OMeTt** show the spherical morphology (Figure 5.9) whereas in case of **TpTt** the SEM and TEM images show the material is fibrillar in nature (Figure 5.10). The absorption property of the synthesized COFs is investigated by solid-state UV-Vis diffuse reflectance spectra. Both the COFs have shown maximum absorption in the visible region which satisfy one of the essential criteria for visible light mediated photocatalysis. **Tp-OMeTt** shows two absorption maxima at 525 nm and 340 nm which is corresponding to n to π^* and π to π^* transition whereas the absorption maxima of n to π^* and π to π^* for **TpTt** arise at 525 nm and 350 nm. The respective starting materials absorption peaks are observed at 250 nm for Melamine (**Tt**), 330 nm and 218 nm for **TpOMe**, 340 nm and 254 nm for **Tp**. The optical band gaps are calculated from Tauc plots and observed 1.89 eV for **TpOMe** and 2.74 eV for **Tp**. The minimum band gap is required for photocatalytic water splitting is ~ 1.8 eV (Figure 5.12).

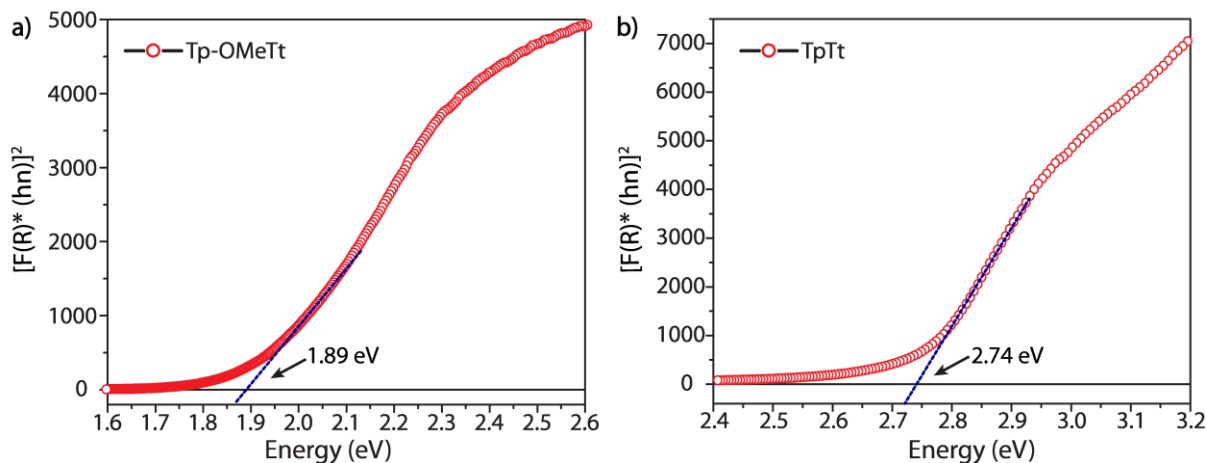


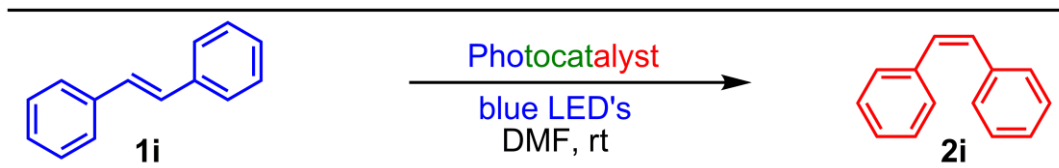
Figure 5.12: Tauc plots. (a) The optical band gap of **Tp-OMeTt**. (b) The optical band gap of **TpTt**.

5.2.5 Photocatalytic *trans* to *cis* Isomerization Reaction:

Although *trans* (E) to *cis* (Z) isomerization is an energetically uphill process and it requires precious metal-based catalyst which is toxic in nature and some homogeneous organic dyes which are not recoverable. Therefore developing heterogeneous metal free materials are suitable for photocatalytic *trans* (E) to the *cis* (Z) isomerization process. We have synthesized two photocatalytic heterogeneous covalent organic frameworks **Tp-OMeTt** and **TpTt** which have shown significant absorption in the visible region and applied as photocatalysts for *trans* (E) to *cis* (Z) isomerization process.

We have started optimizing the process for *trans* to *cis* isomerization by choosing *trans*-stilbene as benchmark substrate (0.5 mmol) and **TpTt** as a photocatalyst. First, we have varied different solvents. Among those DMF shows better yield compared to other solvents (Table 5.3). Next, we have varied catalyst and solvent amount. As the catalyst amount increases, the formation of product increases and 4 mg catalyst **TpTt** and 5 mL solvent is optimum for this transformation. In absence of a catalyst, the reaction does not proceed further and also under similar condition Melamine (**Tt**) produces very less amount of product. During the time optimization process, it is observed that 18 h is sufficient to get 90% yield of the product (Table 4.8). The yields in the optimization process are calculated based on GC analysis using *n*-Decane as an internal standard. Under optimized condition, 90% yield of the desired product *trans*-stilbene is obtained after 18 h stirring using the catalytic amount of **TpTt** (4 mg) in 5 mL DMF solvent at rt in presence of blue LED (36W).

Table 5.3 Optimization table for *trans* to *cis* isomerization process.^a



Entry	Catalyst	Temperature	Solvent	Yield (%) ^b
1	TpTt	rt	DMF	90
2	TpTt	rt	Toluene	34
3	TpTt	rt	MeCN	32
4	TpTt	rt	THF	20
5	TpTt	rt	DMA	65
6	TpTt	rt	MeOH	32
7	TpTt	rt	DCE	44
8	TpTt	rt	NMF	21
9	TpTt	rt	2-Methyl THF	11
10	-	rt	DMF	1
11	Melamine (Tt)	rt	DMF	1
12	TpTt + <i>p</i> -BQ	rt	DMF	4

13	Tp-OMeTt	rt	DMF	81
14	TpTt	80 °C	DMF	-

^aAll the reactions are conducted with 0.5 mmol of *trans*-stilbene (1 equiv), 4 mg TpTt catalyst, in 5 mL solvents at rt under blue LED for 18h. ^bBased on GC analysis using *n*-Decane as an internal standard.

On the other hand in the similar optimized condition, we have tested the photocatalytic activity of the imine bonded covalent organic framework (**Tp-OMeTt**) and shows 81% yield of the expected product formation under similar condition. In order to prove the reaction is not in equilibrium and neither in thermodynamic or kinetic control, we have carried out the experiment at rt and 80 °C. No product (*cis* stilbene) formation is observed under these conditions. The versatility of the reaction condition is proved by synthesizing different *cis*

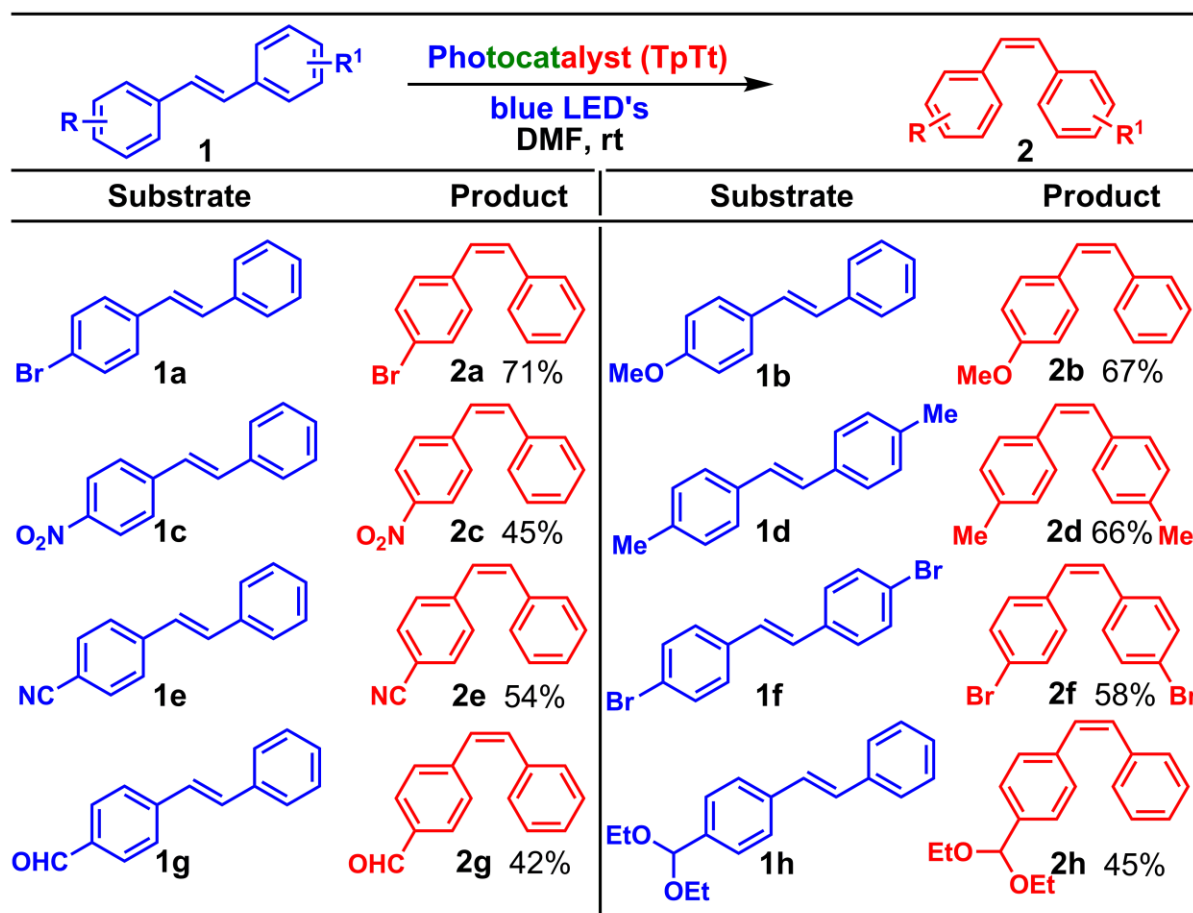


Figure 5.13: Evaluation of the substrate scope.^{a,b} ^aAll the reactions are conducted with 0.5 mmol of *trans*-stilbene (1 equiv), 4 mg TpTt catalyst, in 5 mL *N,N*-dimethylformamide at rt under blue LED for 18h. ^bIsolated yields. ^cBased on GC analysis (**2h**).

stilbene derivatives from different *trans*-stilbene derivatives in presence of blue LED (Figure 5.13). The different substituent electron donating and withdrawing are attached to either one side or both side of the *trans*-stilbene moiety. It has been observed that electron donating groups showed good to excellent yield compared to electron withdrawing groups. Thus, the electron-donating groups such as $-OMe$ (**1b**), $-CH_3$ (**1d**) have given 67 to 66% yield of the desired products whereas electron withdrawing groups $-NO_2$ (**1c**), $-CN$ (**1e**), $-CHO$ (**1g**) have given 42 to 54% yield of the expected products. In case of halogenated compounds like mono-brominated (**1a**) and di-brominated (**1f**) compounds have converted to its individual products with 71% and 58% yield. Moreover, the optimized condition has shown broad substrates scope and large functional group tolerance which implies that it will be most suitable, easiest and economical process for *trans* to *cis* isomerization process. The significance of the light is essential for this transformation and is verified by light on-off experiment which shows that the product formation is happening as long as the light is on. After switching off the light, there no further product is formed. This result suggests that the reaction proceeds *via* photocatalytic pathway (Figure 5.14b). In order to investigate the reaction mechanism and to find out the transition state of the intermediate we have performed controlled photo-reactions using radical scavengers (R.S). In presence of 1.5 eq TEMPO, BHT and p-benzoquinone R.S in the reaction medium, the yield of the *cis* product decreases significantly to 53, 44 and 4% respectively which confirms the reaction proceeds through a biradical intermediate state. To get further insight about the reaction mechanism we have performed theoretical energy states calculations of different reaction intermediate state possible during the photoisomerisation reaction (Figure 5.14a). At first, **TpTt** absorbs visible

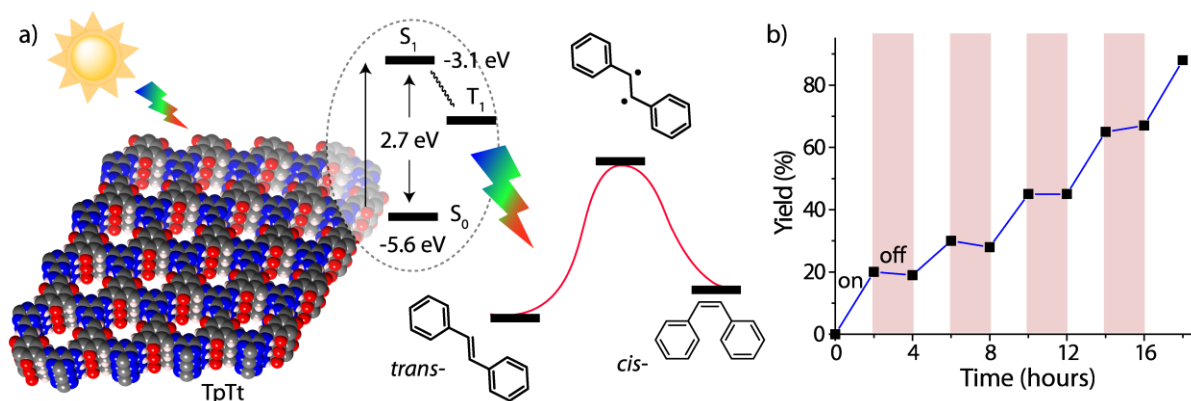


Figure 5.14: (a) Photocatalytic mechanism of **TpTt** COF during *trans* to *cis* isomerization process. (b) Light on off experiment study over time.

light and gets excited from singlet ground to excited state (S_0 to S_1). After intersystem crossing (ISC) COF reaches to the more energetically stable triplet excited state (T_1). Due to the higher lifetime of the T_1 state, COF gets sufficient time to interact with the *trans*-stilbene reactant and transfer its energy to *trans* stilbene reactants. The *trans*-stilbene is then got promoted to the biradical intermediate, through the π to π^* electronic excitation. This triplet intermediate state then gets converted to the product *cis*-stilbene singlet ground state (S_0).

5.2.6 Catalyst Recyclability Experiment:

In the recycle test, first TpTt (4 mg) is kept inside the dialysis tubing cellulose membrane (avg. flat width 33 mm (1.3 in.) having 14 kDa molecular cutoff. Then *trans*-stilbene (0.5 mmol, 90.1 mg) and the dialysis membrane with catalyst are added to 5 mL DMF in a screw cap reaction tube. Then the reaction mixture is sonicated for 5 min and allowed to stir at rt for 27 h in presence of blue LED (total 36W). After each cycle, the dialysis membrane with the catalyst is taken out from the reaction mixture followed by washing with acetone. After that catalyst is dried and then is used for the next cycle (Figure 5.15a). After each cycle, the corresponding yield of the product is analyzed by GC using *n*-decane as an internal standard.

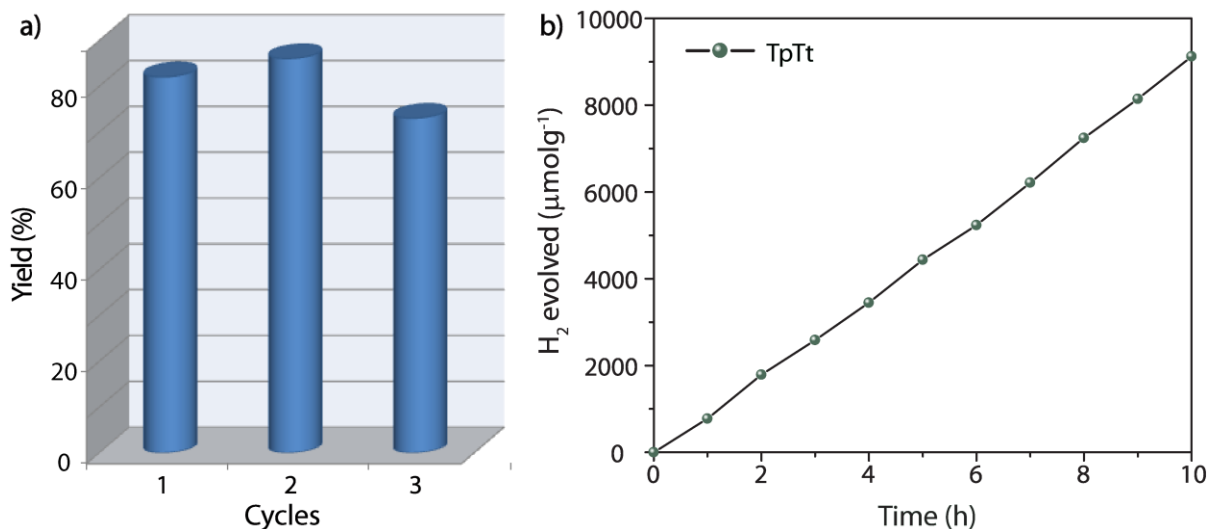


Figure 5.15: (a) Recyclability test of **TpTt** catalyst used in *trans* to *cis* isomerization reaction. Yields are calculated by GC peak integration using *n*-decane as an internal standard. (b) Photocatalytic hydrogen evolution experiments of **TpTt** under visible light irradiation ($\lambda \geq 395$ nm).

5.2.7 Photocatalytic Hydrogen Evolution Reaction:

As the synthesized materials absorb light in the visible region. Therefore we have tried to perform a photocatalytic hydrogen evolution experiment using our materials. Between two COFs, **TpTt** has shown better performance compared to **Tp-OMeTt**. The photocatalytic hydrogen evolution reaction is performed in a 38 mL Teflon reactor fitted with quartz glass window at 25 °C temperature in presence of 10 mg catalyst, 0.1 M ascorbic acid water solution (34 mL) and H₂PtCl₆ (3Wt% Pt). Then the solution is irradiated with a 300 W Xe lamp (L.O.T.-Quantum design) with a cut off filter of 395 nm. After 10h reaction, **TpTt** produces 913 μmolg⁻¹h⁻¹ hydrogen from water (Figure 5.15b) but in the similar condition, **Tp-OMeTt** generates the very negligible amount of hydrogen 10 μmolg⁻¹h⁻¹. Although **Tp-OMeTt** absorbs light in the visible range but the non-dispersive nature and lower band gap may makes as a less effective catalyst for hydrogen evolution from the water.

5.3 Conclusion

In this chapter, we have discussed the synthesis of imine bonded (**Tp-OMeTt**) and enol-keto tautomerized (**TpTt**) covalent organic frameworks by choosing the smallest C₃-C₃ building unit. Both the COFs are fully characterized by different instrumental analysis. The different morphology of two COFs is observed from SEM and TEM analysis. But both the COFs have shown significant absorption in the visible region. By considering this criterion we have utilized both the materials for a photocatalytic application like photocatalytic *trans* to *cis* isomerization as well as photocatalytic hydrogen evolution from the water. For *trans* to *cis* isomerization process, both the COFs have shown similar performance. But we have proceeded further by considering **TpTt** COF for this reaction as it has given higher yield compared to other. The catalyst has shown broad substrates scope with good yield and different functional groups tolerance under optimized condition. The light is essential for this transformation is proved by the light on-off experiment. The reaction is happening through photocatalytic energy transfer process which helps *trans* stilbene to form biradical intermediate for converting to *cis* stilbene as the final product. We have performed the recyclability test up to three cycles of the catalyst for this transformation and observed that the material is showing similar activity even after three cycles without significant decrease in the catalytic activity which suggests heterogeneous nature of the material. Further, we have applied our material for photocatalytic hydrogen evolution reaction. Here enol-keto

tautomerized **TpTt** has shown better performance compared to imine bonded **Tp-OMeTt**. Finally, we believe our developed method for synthesizing metal free photocatalytic Covalent Organic Frameworks will definitely open up a new domain of exciting research area in the field of heterogeneous photocatalysis.

5.4 Experimental Procedures

5.4.1 Synthesis of 2,4,6-trimethoxybenzene-1,3,5-tricarbaldehyde (*Tp-OMe*):

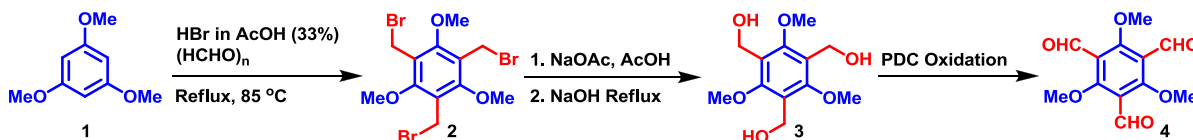


Figure 5.16: General synthetic scheme for the preparation of 2,4,6-trimethoxybenzene-1,3,5-tricarbaldehyde (*Tp-OMe*).

2,4,6-Trimethoxy-benzene-1,3,5-tricarbaldehyde (*TpOMe*) is prepared from 1,3,5-trimethoxybenzene using the reported literature procedure [5.18].

Compound 2 (1,3,5-tris-bromomethyl-2,4,6-trimethoxybenzene): Compound 2 is synthesized according to the reported literature procedure [5.19].

Compound 3 (1,3,5-tris-hydroxymethyl-2,4,6-trimethoxybenzene; triol): Compound 2 (1.00 g, 2.24 mmol) and NaOAc (2.27 g, 27.7 mmol) are added in glacial AcOH (20 mL) in a round bottom flask and the reaction mixture is heated to reflux for 4-6 hours. After cooling to room temperature, the resulting suspension is diluted with dichloromethane (40 mL) and the solid precipitate is removed by filtration. The filtrate is evaporated till a crude white solid form. The crude solid is dissolved in ethyl acetate (50 mL) and extracted with saturated aqueous NaHCO₃ (2 x 50 mL), water (30 mL), brine (30 mL). The collected organic solvent is evaporated in vacuum and the crude triacetate (0.860 g, quant.) is obtained as a white solid. Then the material is dissolved in EtOH (8 mL) and aq. NaOH (1.50 g, 37.5 mmol; 10 mL water) solution and allowed to reflux for 12-18 hours. Next EtOH is removed under vacuum and the remaining aqueous mixture is neutralized with 1.0 M HCl followed by saturated with NaCl. The reaction mixture is extracted with ethyl acetate (3 x 40 mL) and the organic layers are combined, dried over Na₂SO₄, and concentrated to dryness to give the triol (0.48 g, 83%) as a white solid.

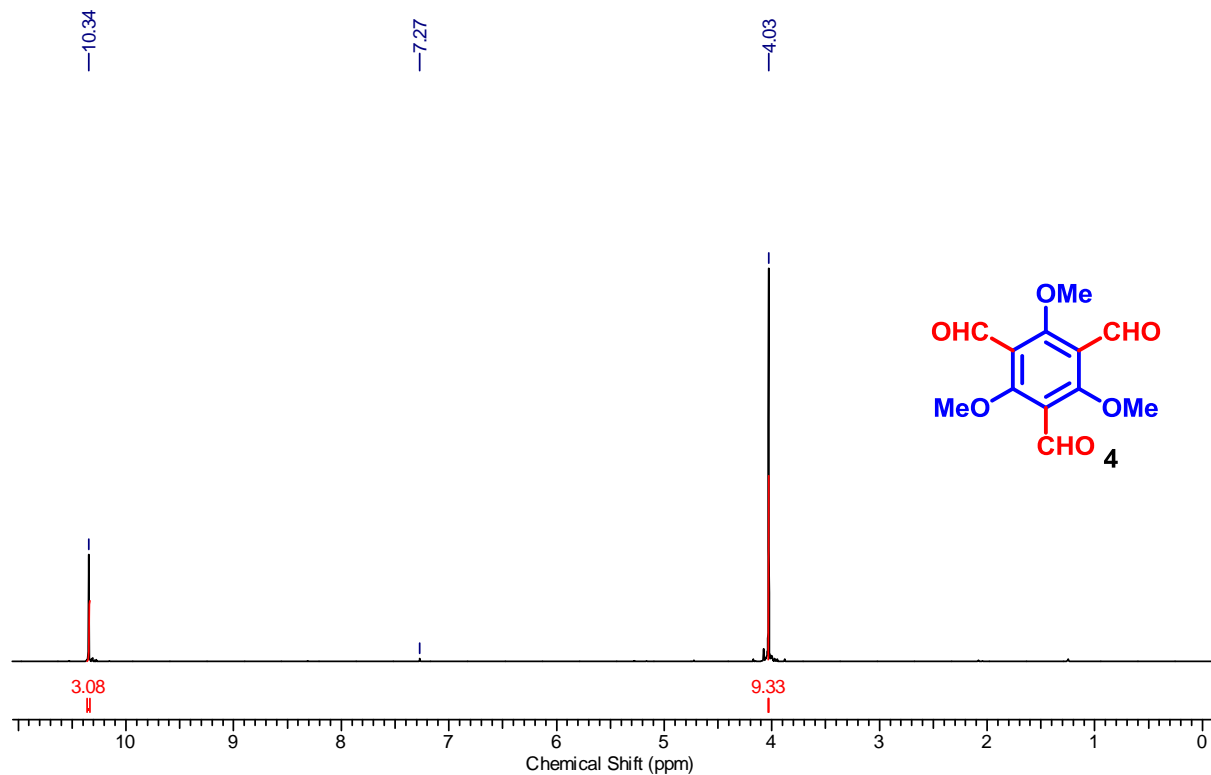


Figure 5.17: ^1H NMR spectrum of **TpOMe**.

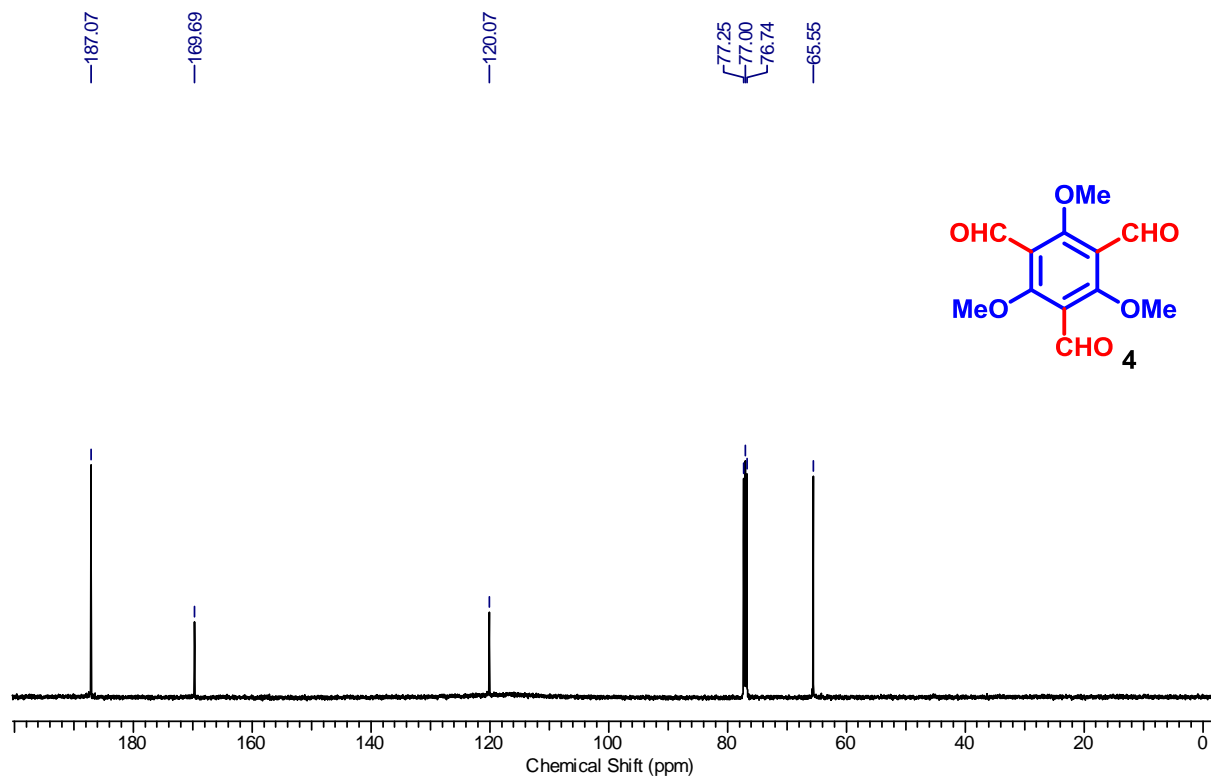
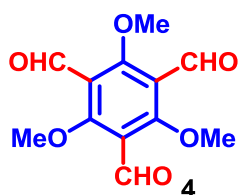


Figure 5.18: ^{13}C NMR spectrum of **TpOMe**.

Compound 4 (2,4,6-Trimethoxy-benzene-1,3,5-tricarbaldehyde). PDC (10.94 g, 29.08 mmol) is added to the stirring mixture of the triol (1.50 g, 5.81 mmol) in dry dichloromethane (35 mL) and 3 Å molecular sieves. The resulting mixture is allowed to stir under argon for overnight and then diluted with DCM (100 mL). The solid suspension is removed *via* suction filtration. The filtrate is concentrated to a crude residue and is purified *via* column chromatography (3:2 hexanes/EtOAc) to afford the trialdehyde (0.98 g, 67%) as a colorless solid (Figure 5.16).



^1H NMR (500 MHz, CDCl_3): δ = 10.34 (s, 3H), 4.03 (s, 9H); ^{13}C NMR (126 MHz, CDCl_3) δ = 187.07, 169.69, 120.07, 65.55; HRMS-ESI (m/z) $[\text{M}+\text{H}]^+$ calcd for $\text{C}_{12}\text{H}_{13}\text{O}_6$, 253.0707, found 253.0702.

5.4.2 General Procedure for Photocatalytic *trans* to *cis* Isomerization:

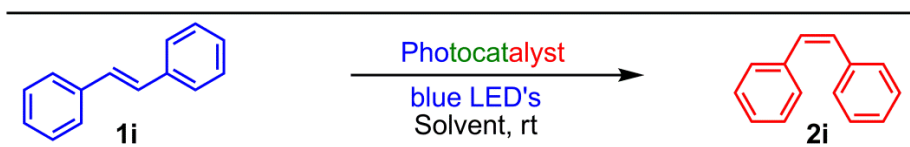
Trans-stilbene (0.5 mmol, 90.1 mg), TpTt (4 mg) are added to 5 mL DMF in a screw cap reaction tube. Then the reaction mixture is sonicated for 5 min and allowed to stir at rt for 18 h in presence of blue LED (total 36W). After 18h the reaction mixture is centrifuged to separate the solid and the solid is washed with EtOAc. The combined organic layer is mixed with water and EtOAc mixture to remove DMF from the reaction mixture and the separated organic layer is evaporated under reduced pressure. The crude product is purified by column chromatography to obtain the pure desired product.

5.4.3 General Procedure for Photocatalytic Hydrogen Evolution Reaction:

Photocatalytic hydrogen evolution experiments are performed in a 38 mL Teflon reactor fitted with quartz glass window and temperature controller maintaining the temperature at $25\pm 1^\circ\text{C}$. The reactor is filled with 10 mg of catalyst, 0.1 M ascorbic acid water solution (34 mL) and H_2PtCl_6 (3Wt% Pt), degassed and then is irradiated with a 300 W Xe lamp (L.O.T.-Quantum design) with a cut off filter of 395 nm. Pressure *vs* time profile is recorded and at the end of the reaction, which is then converted to volume *vs* time, the obtained gas from the headspace is injected into GC to determine the volume % of hydrogen produced. The irradiation area of the light is 12.5 cm^2 . The amount of evolved H_2 in μmol is calculated from the volume.

5.4.4 Optimization Details for *trans* to *cis* Isomerization Reaction:

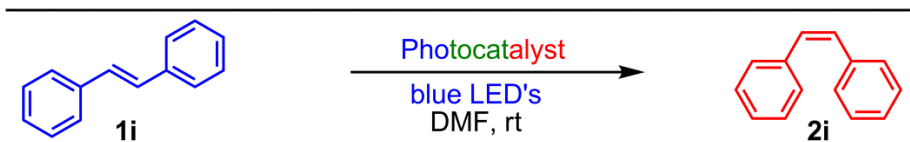
Table 5.4 Optimization of Solvents



Entry	Solvent (mL)	GC Yield (%)
1	Toluene	34
2	MeCN	32
3	DMF	88
4	DMA	65
5	THF	20
6	MeOH	32
7	1,4-Dioxane	54
8	NMF	21
9	DCE	44
10	Acetone	21
11	2-Methyl THF	11

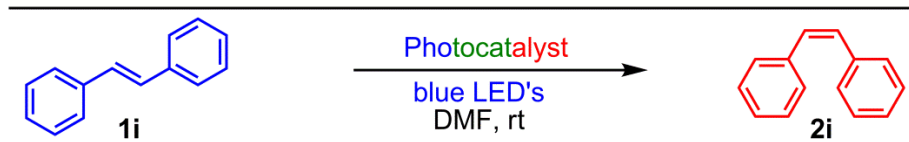
Reactions are conducted with 0.5 mmol of *trans*-stilbene (1 equiv), 4 mg TpTt catalyst, in 5 mL solvents at rt under blue LED for 18h. Yields are calculated based on GC analysis using *n*-Decane as an internal standard.

Table 5.5 Optimization of Catalyst Amount



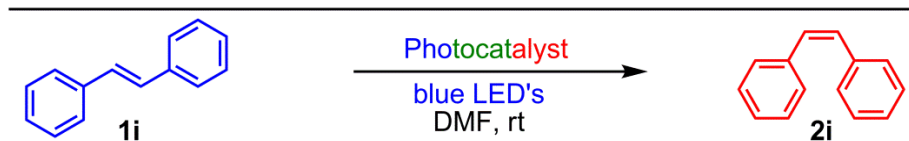
Entry	Catalyst (TpTt) amount (mg)	GC Yield (%)
1	1	64
2	2	75
3	4	89
4	6	84
5	8	84
6	-	1
7	Melamine (SM)	1

Reactions are conducted with 0.5 mmol of *trans*-stilbene (1 equiv), different amount TpTt catalyst (mg), in 5 mL DMF at rt under blue LED for 18h. Yields are calculated based on GC analysis using *n*-Decane as an internal standard.

Table 5.6 Optimization of Solvent Amount

Entry	Solvent Amount (mL)	GC Yield (%)
1	1	58
2	2	79
3	3	82
4	4	83
5	5	88

Reactions are conducted with 0.5 mmol of *trans*-stilbene (1 equiv), 4 mg TpTt catalyst, in a different amount of DMF solvent at rt under blue LED for 18h. Yields are calculated based on GC analysis using *n*-Decane as an internal standard.

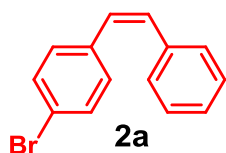
Table 5.7 Time Optimization

Entry	Time (h)	GC Yield (%)
1	2	21
2	4	45
3	6	69
4	12	88
5	18	90
6	24	91

Reactions are conducted with 0.5 mmol of *trans*-stilbene (1 equiv), 4 mg TpTt catalyst, in 5 mL DMF at rt under blue LED for different time. Yields are calculated based on GC analysis using *n*-Decane as an internal standard.

5.4.5 Characteristic Data of Synthesized Compounds

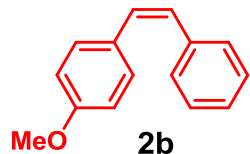
4-bromo-cis-stilbene (2a) is synthesized by following the general procedure with 4-bromo-*trans*-stilbene (0.5 mmol, 129.6 mg) as the substrate. The yield of the isolated product is 71%.



$^1\text{H NMR}$ (400 MHz, CDCl_3): δ = 7.38 (d, J = 8.4 Hz, 2H), 7.32-7.24 (m, 5H), 7.15 (d, J = 7.9 Hz, 2H), 6.67 (d, J = 11.8 Hz, 1H), 6.54 (d, J = 11.8 Hz, 1H); $^{13}\text{C NMR}$

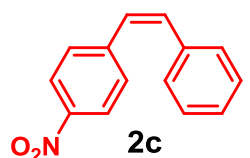
(101 MHz, CDCl₃) δ = 136.78, 136.05, 131.32, 130.99, 130.50, 128.90, 128.76, 128.31, 127.31, 120.90; HRMS-ESI (m/z) [M]⁺ calcd for C₁₄H₁₁Br, 260.0018, found 260.0029.

4-methoxy-cis-stilbene (2b) is synthesized by following the general procedure with 4-methoxy-trans-stilbene (0.5 mmol, 105.1 mg) as the substrate. The yield of the isolated product is 67%.



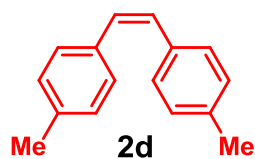
¹H NMR (400 MHz, CDCl₃): δ = 7.38-7.28 (m, 7H), 6.85 (d, *J* = 8.9 Hz, 2H), 6.61 (d, *J* = 1.8 Hz, 2H), 3.87 (s, 3H); ¹³C NMR (101 MHz, CDCl₃) δ = 158.62, 137.56, 130.11, 129.72, 129.60, 128.77, 128.71, 128.19, 126.86, 113.53, 55.14; HRMS-ESI (m/z) [M+H]⁺ calcd for C₁₅H₁₅O, 211.1117, found 211.1169.

4-nitro-cis-stilbene (2c) is synthesized by following the general procedure with 4-nitro-trans-stilbene (0.5 mmol, 112.6 mg) as the substrate. The yield of the isolated product is 45%.



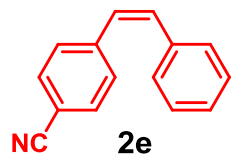
¹H NMR (500 MHz, CDCl₃): δ = 8.17 (d, *J* = 8.7 Hz, 2H), 7.74 (d, *J* = 8.7 Hz, 1H), 7.66 (d, *J* = 8.1 Hz, 1H), 7.48 (d, *J* = 8.7 Hz, 2H), 7.37-7.35 (m, 2H), 7.32-7.30 (m, 1H), 6.92 (d, *J* = 11.2 Hz, 1H), 6.72 (d, *J* = 12.4 Hz, 1H); ¹³C NMR (126 MHz, CDCl₃) δ = 146.51, 144.14, 136.08, 133.91, 129.61, 128.76, 128.52, 127.96, 126.99, 126.82, 123.52; HRMS-ESI (m/z) [M+H]⁺ calcd for C₁₄H₁₂NO₂, 226.0863, found 226.0865.

4,4'-dimethyl-cis-stilbene (2d) is synthesized by following the general procedure with 4,4'-dimethyl-trans-stilbene (0.5 mmol, 104.1 mg) as the substrate. The yield of the isolated product is 66%.



¹H NMR (500 MHz, CDCl₃): δ = 7.23 (d, *J* = 7.91 Hz, 4H), 7.09 (d, *J* = 7.7 Hz, 4H), 6.58 (s, 2H), 2.37 (s, 6H); ¹³C NMR (126 MHz, CDCl₃) δ = 136.67, 134.47, 129.48, 128.85, 128.72, 21.19; HRMS-ESI (m/z) [M+H]⁺ calcd for C₁₆H₁₇, 209.1325, found 209.1335.

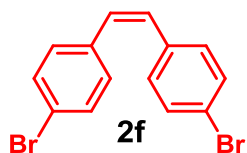
4-cyano-cis-stilbene (2e) is synthesized by following the general procedure with 4-cyano-trans-stilbene (0.5 mmol, 102.6 mg) as the substrate. The yield of the isolated product is 54%.



¹H NMR (500 MHz, CDCl₃): δ = 7.56 (d, *J* = 8.2 Hz, 2H), 7.38 (d, *J* = 8 Hz, 2H), 7.35-7.3 (m, 3H), 7.26 (d, *J* = 7.4 Hz, 2H), 6.83 (d, *J* = 12.1 Hz, 1H), 6.84 (d, *J* =

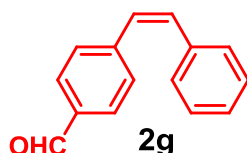
12.2 Hz, 1H); ^{13}C NMR (126 MHz, CDCl_3) δ = 142.01, 136.17, 133.25, 131.93, 129.46, 128.70, 128.43, 128.29, 127.75, 118.86, 110.39; HRMS-ESI (m/z) $[\text{M}+\text{H}]^+$ calcd for $\text{C}_{15}\text{H}_{12}\text{N}$, 206.0964, found 206.0968.

4,4'-dibromo-cis-stilbene (2f) is synthesized by following the general procedure with 4,4'-dibromo-trans-stilbene (0.5 mmol, 169.02 mg) as the substrate. The yield of the isolated product is 58%.



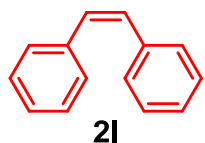
^1H NMR (400 MHz, CDCl_3): δ = 7.37 (d, J = 8 Hz, 4H), 7.10 (d, J = 7.9 Hz, 4H), 6.55 (s, 2H); ^{13}C NMR (101 MHz, CDCl_3) δ = 135.63, 131.48, 130.41, 129.67, 121.20; HRMS-ESI (m/z) $[\text{M}+\text{H}]^+$ calcd for $\text{C}_{14}\text{H}_{11}\text{Br}_2$, 338.9202, found 338.9215.

4-formyl-cis-stilbene (2g) is synthesized by following the general procedure with 4-formyl-trans-stilbene (0.5 mmol, 104.1 mg) as the substrate. The yield of the isolated product is 42%.



^1H NMR (400 MHz, CDCl_3): δ = 9.98 (s, 1H), 7.77 (d, J = 8.6 Hz, 2H), 7.43 (d, J = 8.2 Hz, 2H), 7.35-7.23 (m, 5H), 6.79 (d, J = 12.5 Hz, 1H), 6.65 (d, J = 12 Hz, 1H); ^{13}C NMR (101 MHz, CDCl_3) δ = 191.72, 143.71, 136.45, 134.90, 132.94, 129.65, 129.44, 128.93, 128.79, 128.37, 127.64; ; HRMS-ESI (m/z) $[\text{M}+\text{H}]^+$ calcd for $\text{C}_{15}\text{H}_{13}\text{O}$, 209.0961, found 209.0990.

cis-stilbene (2i) is synthesized by following the general procedure with trans-stilbene (0.5 mmol, 90.1 mg) as the substrate. The yield of the isolated product is 70%.



^1H NMR (400 MHz, CDCl_3): δ = 7.35-7.27 (m, 10H), 6.69 (s, 2H); ^{13}C NMR (101 MHz, CDCl_3) δ = 137.20, 130.22, 128.84, 128.18, 127.05; HRMS-ESI (m/z) $[\text{M}+\text{H}]^+$ calcd for $\text{C}_{14}\text{H}_{12}$, 181.1012, found 181.1038.

5.4.6 General Methods for Characterization

All reagents were commercially available and used as received.

a) Wide-angle X-Ray Diffraction (WAXD): The Powder X-ray diffraction (PXRD) patterns were recorded on a Phillips PAN analytical diffractometer for $\text{Cu K}\alpha$ radiation (α = 1.5406 Å), with a scan speed of 1° min^{-1} and a step size of 0.02° in 2θ . The instrument was previously calibrated using a silicon standard.

- b) FT-IR spectroscopy:** The Fourier Transform Infrared (FTIR) spectra were taken on a Bruker Optics ALPHA-E spectrometer with a universal Zn-Se ATR (attenuated total reflection) accessory in the 600–4000 cm^{-1} region.
- c) Thermogravimetric analysis:** TGA was carried out on a TG50 analyzer (Mettler-Toledo) or a SDT Q600 TG-DTA analyzer under N_2 atmosphere at a heating rate of 10 $^\circ\text{C min}^{-1}$ within a temperature range of 30–900 $^\circ\text{C}$.
- d) Scanning Electron Microscopy:** SEM images were obtained with a Zeiss DSM 950 scanning electron microscope and FEI-QUANTA 200 3D Scanning Electron Microscope with tungsten filament as electron source operated at 10 kV. The samples were sputtered with Au (nano-sized film) prior to imaging by a SCD 040 Balzers Union.
- e) Transmission Electron Microscopy:** TEM TEM images were recorded using FEI Tecnai G2 F20 X-TWIN TEM at an accelerating voltage of 200 kV. The TEM Samples were prepared by dropcasting the sample from isopropanol on copper grids (TED PELLA, INC. 200 mesh). The metal nanoparticles size distribution was determined by measuring the size of 700 particles from TEM images.
- f) BET surface area:** BET surface area of the synthesized COFs was measured through N_2 adsorption studies. N_2 adsorption isotherms were collected with a Quantachrome make Autosorb IQ₂ automated surface area analyzer.
- g) Solid state NMR (SSNMR):** Solid state NMR (SSNMR) was taken in a Bruker 300 MHz NMR spectrometer and ligand NMR data were taken in Bruker 200/400/500 MHz NMR spectrometer.
- h) Gas Chromatography:** GC analyses were performed on a Agilent 7890B GC system with an FID detector using a HP-5 column (30 m, 0.25 mm, 0.25 μ). As the internal standard *m*-xylene was used.
- i) UV-Visible Spectrometer:** UV–visible spectroscopy was carried with a Shimadzu UV-3600 spectrophotometer from 200 nm to 800 nm region.

CHAPTER 6

Conclusions of all Chapters and Future Directive

6.1 Conclusions

The first chapter of the thesis includes the introduction of different heterogeneous catalysts. Heterogeneous catalysts provide many advantages over homogeneous one. Among different heterogeneous catalyst, porous crystalline materials with the high surface area will show high catalytic activity compared to an amorphous one. Porous carbon, Zeolite, Mesoporous silica, and MOFs are porous materials having high surface areas are used as a heterogeneous catalyst. Here we have discussed the disadvantages of using those catalysts. Recently a new class of crystalline porous material has been discovered called as Covalent Organic Frameworks (COFs) are made by strong covalent bonds make them thermally stable. The uniform pore size and pore tenability make them useful for different applications are already discussed here. Also, we have discussed the different methods and the different reversible reaction has been used for COF synthesis. The proper symmetry combination is also important for synthesizing different pores inside the COFs are discussed. Although there are many advantages of using COFs but the major drawback for its practical application is its lower chemical stability in acid, base and water medium. The improvement of COFs stability is discussed stepwise and finally, stable COFs are made by reversible followed by irreversible enol-keto tautomerization process. Then the stable COFs have been utilized for different heterogeneous catalytic reaction. Nitrogen-rich frameworks are useful for many applications including stabilizing metal nanoparticles for making a heterogeneous catalyst. Finally, we have discussed the importance of synthesizing nitrogenous COFs and COFs functionalization processes.

In chapter 2, we have discussed the importance of synthesizing nitrogen-rich frameworks. The presence of more basic nitrogen atoms in the frameworks increases the acidic gas uptake and selective gas separation (CO_2/N_2). Moreover, methods for synthesizing such materials are limited for bulk scale production. 2,2'-Bipyridine is a very good chelating

ligand for anchoring different metal ions and is applied for different catalytic organic transformation in homogeneous catalysis. Therefore we have developed methods for synthesizing bipyridine based crystalline porous heterogeneous materials in solvothermal (TpBpy-ST) and green environment-friendly, cost-efficient mechanochemical process (TpBpy-MC). Although solvothermally synthesized TpBpy-ST shows high crystallinity and high surface area ($S_{\text{BET}} = 1746 \text{ m}^2\text{g}^{-1}$) compared to mechanochemical one ($S_{\text{BET}} = 293 \text{ m}^2\text{g}^{-1}$). The decrease in surface area in TpBpy-MC is due to random displacement of COF sheet layers for continuous applying mechanical force during the synthesis. Moreover first time we have developed bulk scale synthesis of COF in the mechanochemical process. Both the COFs shows high uptake of greenhouse gas (CO_2), renewable energy source H_2 and H_2O at 1 atm pressure. Finally, we believe our developed method for synthesizing bipyridine based Covalent Organic Frameworks will be applicable as heterogeneous support for stabilizing metal nanoparticles in making heterogeneous catalyst, proton conduction, energy storage, gas storage and separation purpose.

In chapter three, we have discussed the advantages of synthesizing metal nanoparticles in stable nitrogenous covalent organic frameworks by *in situ* process over *ex-situ*. Nanoparticles are used for catalyzing different organic transformations. The uniformly distributed non agglomerated nanoparticles show better catalytic activity compared to bulk particles. Metal nanoparticles are already loaded on COFs *via ex situ* method in presence of a strong reducing agent which hampers the porosity and rigidity of the frameworks. Therefore leaching and sintering of the nanoparticles have observed in the recyclability test which decreases the subsequent catalytic activity in the repeated cycles. We have synthesized palladium metal nanoparticles loaded by pyridine COF (Pd@TpBpy) *via in situ* process without using a strong reducing agent, a capping agent at moderate temperature. The formation of nanoparticles is confirmed by PXRD, ^{15}N , TEM images and XPS spectral analysis. The average size of the Pd nanoparticles is found 12 ± 4 nm from the nanoparticles size distribution plot and 15.2 wt% loading of metal into the frameworks is measured by ICP analysis. Finally, the synthesized hybrid materials are used for synthesizing biologically important 2-substituted benzofuran derivatives *via* the tandem process. The catalyst shows broad substrates scope and different functional group tolerance with excellent yield under the optimized condition and performed better catalytic activity compared to the commercially

available homogeneous and heterogeneous catalysts. Mercury poisoning experiment and leaching test prove the catalyst is heterogeneous in nature.

In the fourth chapter, we have discussed the development of a unique strategy for the synthesis of palladium metal coordinated stable covalent organic framework (TpBpy-PdCl₂) by reacting with 1,3,5-triformylphloroglucinol (Tp) and 2,2'-bipyridine-5,5'-diamine palladium chloride (Bpy-PdCl₂) using pre-synthetic method. This is the only combination we have found where Pd nanoparticles are not generating during the course of the reaction. The palladium coordination into the framework is confirmed from PXRD, TEM, EDX and ICP-OES analysis. Further, the oxidation of palladium (II) is verified by XPS analysis. The synthesized material is successfully used for the selective hydroxylation of 2-phenylpyridine *via* chelation assisted direct C(sp²)-H bond activation where pyridine unit acts as a metal directing ligand with 90% yield of the formation of the product. The catalyst and oxidant are required for this transformation are observed from control experiments. Mercury poisoning experiment shows that the material is heterogeneous in nature.

In the fifth chapter, we have discussed the synthesis of photocatalytically active imine bonded (Tp-OMeTt) and enol-keto tautomerized (TpTt) covalent organic frameworks by choosing the smallest C₃-C₃ building unit. Although they have different morphology observed from SEM and TEM images but both the COFs have shown significant absorption in the visible region. Therefore we have used both COFs for photocatalytic *trans* to *cis* isomerization as well as photocatalytic hydrogen evolution reaction from the water. Both the catalysts have shown broad substrates scope with good yield and different functional groups tolerance under optimized condition. The light is essential for this transformation is proved by the light on-off experiment. In presence of radical quencher the reaction yield decreases which indicate the reaction proceeds *via* a radical mechanism. Further, we have applied our material for photocatalytic hydrogen evolution reaction. Here enol-keto tautomerized TpTt has shown better performance compared to imine bonded Tp-OMeTt. Finally, we believe our developed method for synthesizing metal free photocatalytic Covalent Organic Frameworks will definitely open up a new domain of exciting research area in the field of heterogeneous photocatalysis.

6.2 Future directive

Synthesis of Photocatalytic Redox-Active Covalent Organic Frameworks for C(sp³)-H bond Functionalization, Alcohol Oxidation, and Phenazine Formation.

COFs are new class organic porous framework materials, which possesses ordered pore channels. Although COFs are widely applied in gas storage, drug delivery and metal-loaded organic thermal catalysis, but COFs are used as photocatalyst for synthesizing organic molecule is limited. Photocatalytic organic transformation is a green clean safe and cost-effective process which is the most alternative approach for replacing the complicated thermal process. COFs have ordered structure with suitable band gap as like semiconductors and absorb light significantly in a visible region similar to other photocatalysts. Therefore COFs can be used as heterogeneous photocatalyst for catalyzing organic reactions in presence of visible light. A keto-functionalized small molecule like anthraquinone is used as a photocatalyst for C(sp³)-H bond Functionalization [6.1]. After exciting by light anthraquinone (AQN) generates a triplet state (³AQN). Then the energy transfer happens from singlet (¹AQN) to the triplet (³AQN) state. During this process, the energy is sufficient to elongate the N-F bond to produce selectfluor radical cation which further abstract hydrogen from alkane give alkyl radical species (\dot{R}). The alkyl radical species will further abstract fluorine from AQN-F complex to afford alkyl fluorinated product. Therefore we have designed diketo based COF for photocatalytic 1) C-F bond formation via remote C(sp³)-H bond activation, 2) alcohol oxidation and biologically active phenazine formation.

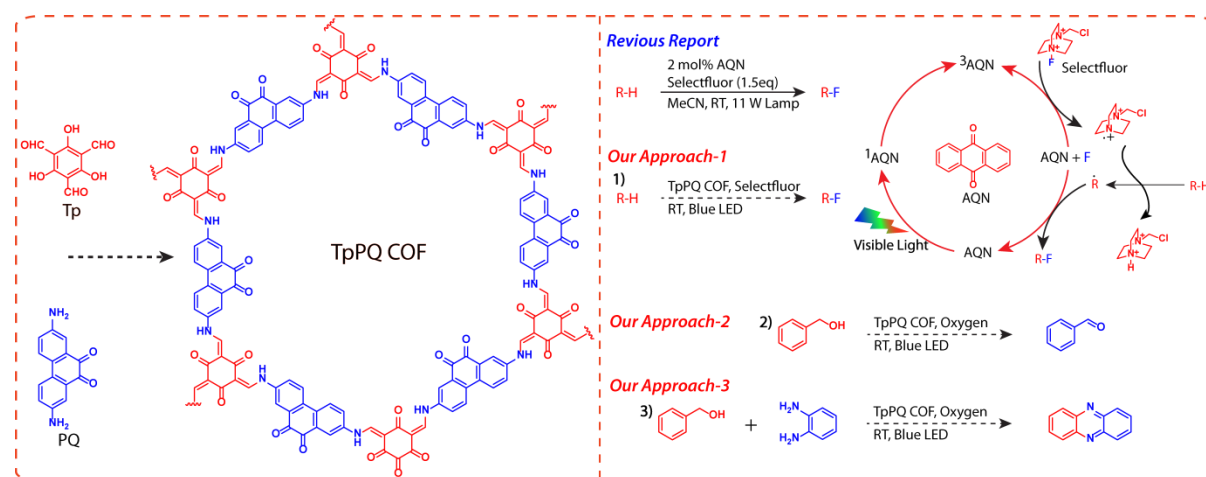


Figure 6.1. A synthetic scheme of TpPQ COF and utilization for photocatalytic C-F bond formation (Approach-1), Alcohol oxidation (Approach-2) and Phenazine formation (Approach-3).

REFERANCES**CHAPTER 1**

- [1.1] (a) Y. Jiang, Q. Gao, *J. Am. Chem. Soc.*, **2006**, *128*, 716. (b) C. A. Witham, W. Huang, C.-K. Tsung, J. N. Kuhn, G. A. Somorjai, F. D. Toste, *Nat. Chem.*, **2010**, *2*, 36. (c) F. A. Westerhaus, R. V. Jagadeesh, G. Wienhöfer, M.-M. Pohl, J. Radnik, A.-E. Surkus, J. Rabeah, K. Junge, H. Junge, M. Nielsen, A. Brückner, M. Beller, *Nat. Chem.*, **2013**, *5*, 537.
- [1.2] (a) M. Benaglia, A. Puglisi, F. Cozzi, *Chem. Rev.*, **2003**, *103*, 3401. (b) S. Ikegami, H. Hamamoto, *Chem. Rev.*, **2009**, *109*, 583. (c) D. J. Cole-Hamilton, *Science*, **2003**, *299*, 1702. (d) K. Mennecke, R. Cecilia, T. N. Glasnov, S. Gruhl, C. Vogt, A. Feldhoff, M. A. L. Vargas, C. O. Kappe, U. Kunz, A. Kirschning, *Adv. Synth. Catal.*, **2008**, *350*, 717. (e) W. Huang, J. H.-C. Liu, P. Alayoglu, Y. Li, C. A. Witham, C.-K. Tsung, F. D. Toste, G. A. Somorjai, *J. Am. Chem. Soc.*, **2010**, *132*, 16771. (f) E. G. Moschetta, S. Negretti, K. M. Chepiga, N. A. Brunelli, Y. Labreche, Y. Feng, F. Rezaei, R. P. Lively, W. J. Koros, H.M. L. Davies, C. W. Jones, *Angew. Chem., Int. Ed.*, **2015**, *54*, 6470.
- [1.3] (a) J. Lee, J. Kim, T. Hyeon. *Adv. Mater.* **2006**, *18*, 2073. (b) M. C. Orilall, U. Wiesner. *Chem. Soc. Rev.* **2011**, *40*, 520. (c) Y. Zhou, Y. Kim, C. Jo, J. Lee, C. W. Lee, S. Yoon. *Chem. Commun.* **2011**, *47*, 4944. (d) Y. Ishii, Y. Kanamori, T. Kawashita, I. Mukhopadhyay, S. Kawasaki. *J. Phys. Chem. Solids*, **2010**, *71*, 511. (e) L. Fu, H. Liu, H. Zhang, C. Li, T. Zhang, Y. Wu, H. Wu. *J. Power Sources*, **2006**, *159*, 219. (f) D.-H. Lee, J.-G. Park, K. Jin Choi, H.-J. Choi, D.-W. Kim. *Eur. J. Inorg. Chem.* **2008**, 878.
- [1.4] (a) Y. Ma, W. Tong, H. Zhou, S. L Suib, *Microporous Mesoporous Mater.*, **2000**, *37*, 243, (b) S. Cavenati, C. A. Grande, A. E. Rodrigues, *J. Chem. Eng. Data*, **2004**, *49*, 1095. (c) J. Rouquerol, D. Avnir, C. W. Fairbridge, D. H. Everett, J. H. Haynes, N. Pernicone, J. D. F. Ramsay, K. S. W. Sing, K. K. Unger, *Pure and Applied Chemistry*, **1994**, *66*, 1739. (d) T. Sawaki, T. Dewa, Y. Aoyama, *J. Am. Chem. Soc.*, **1998**, *120*, 8539. (e) R. E. Morris, P. S. Wheatley. *Angew. Chem., Int. Ed.* **2008**, *47*, 4966.

- [1.5] (a) Breck, D. W., *Zeolite molecular sieves: structure, chemistry, and use*. Wiley: New York, **1974**. (b) Cundy, C. S., Cox, P. A., *Chem. Rev.* **2003**, *103*, 663. (c) Z. Wang, J. Yu, R. Xu, *Chem. Soc. Rev.*, **2012**, *41*, 1729. (d) J. Yu and R. Xu, *Acc. Chem. Res.*, **2010**, *43*, 1195. (e) J. J. Pluth, J. V. Smith, *Am. Mineral.*, **1990**, *75*, 501. (f) R. M. Barrer, P. J. Denny, *J. Chem. Soc.*, **1961**, 971. (g) A. F. Cronsted, *Akad. Handl.*, **1756**, *17*, 20.
- [1.6] (a) F. Schuth, K. S. W. Sing, J. Weitkamp, editors. *Handbook of Porous Solids*. Wiley-VCH Verlag GmbH, **2002**. (b) Wingenfelder, U., Hansen, C., Furrer, G., Schulin, R., *Environ. Sci. Technol.* **2005**, *39*, 4606. (c) Moreno, N., Querol, X., Ayora, C., Pereira, C. F., Janssen-Jurkovicová, M., *Environ. Sci. Technol.* **2001**, *35*, 3526. (d) Clearfield, A., *Chem. Rev.* **1988**, *88*, 125.
- [1.7] (a) M. Eddaoudi, D. B. Moler, H. Li, B. Chen, T. M. Reinecke, M. O’Keeffe, O. M. Yaghi, *Acc. Chem. Res.* **2001**, *34*, 319. (b) C. Janiak, *Angew. Chem., Int. Ed. Engl.*, **1997**, *36*, 1431. (c) A. J. Blake, N. R. Champness, P. Hubberstey, W.-S. Li, M. A. Withersby, M. Schroder, *Coord. Chem. Rev.*, **1999**, *183*, 117. (d) O. M. Yaghi, G. Li, H. Li, *Nature*, **1995**, *378*, 703. (e) S. Kitagawa, R. Kitaura, S. -I. Noro, *Angew. Chem., Int. Ed.*, **2004**, *43*, 2334. (f) G. Ferey, *Chem. Soc. Rev.* **2008**, *37*, 191. (g) B. Chen, S. Xiang, G. Qian, *Acc. Chem. Res.*, **2010**, *43*, 1115. (h) L. Ma, C. Abney, W. Lin, *Chem. Soc. Rev.*, **2009**, *38*, 124. (i) Z. G. Gu, Y. P. Cai, H. C. Fang, Z. Y. Zhou, P. K. Thallapally, J. A. Tian, J. Liu, G. J. Exarhos, *Chem. Commun.*, **2010**, *46*, 5373. (j) B. Chen, M. Eddaoudi, S. T. Hyde, M. O’Keeffe, O. M. Yaghi, *Science*, **2001**, *291*, 1021. (k) P. Pachfule, Y. Chen, J. Jiang, R. Banerjee *J. Mater. Chem.*, **2011**, *21*, 17737. (l) J. W. Yoon, S. H. Jung, Y. K. Hwang, S. M. Humphrey, P. T. Wood, J. -S. Chang, *Adv. Mater.* **2007**, *19*, 1830. (m) K. L. Mulfort, O. K. Farha, C. D. Malliakas, M. G. Kanatzidis, J. T. Hupp, *Chem. Eur. J.*, **2010**, *16*, 276. (n) H. -S. Choi, M. P. Suh, *Angew. Chem.* **2009**, *121*, 6997. (o) X. Gu, Z.-H. Lu, Q. Xu, *Chem. Commun* **2010**, *46*, 7400. (p) S. -T. Zheng, J. T. Bu, Y. Li, T. Wu, F. Zuo, P. Feng, X. Bu. *J. Am. Chem. Soc.* **2010**, *132*, 17062. (q) J. An, N. L. Rosi, *J. Am. Chem. Soc.* **2010**, *132*, 5578. (r) A. G. Wong-Foy, O. Lebel, A. J. Matzger, *J. Am. Chem. Soc.* **2007**, *129*, 15740. (s) H. Chun, D. N. Dybtsev, H. Kim, K. Kim, *Chem. Eur. J.* **2005**, *11*, 3521. (t) J. Rowsell, A. Millward, K. Park, O. Yaghi *J. Am. Chem. Soc.* **2004**, *126*, 5666. (u)

- Y. Cui, H. Xu, Y. Yue, Z. Guo, J. Yu, Z. Chen, J. Gao, Y. Yang, G. Qian, B. Chen, *J. Am. Chem. Soc.* **2012**, *134*, 3979. (v) A. M. Shultz, O. K. Farha, J. T. Hupp, S. T. Nguyen, *J. Am. Chem. Soc.* **2009**, *131*, 4204. (w) V. Stavila, R. K. Bhakta, T. M. Alam, E. H. Majzoub, M. D. Allendorf, *ACS Nano* **2012**, *6*, 9807. (x) Y. Lee, J. Kim, W. Ahn, *Korean J. Chem. Eng.* **2013**, *30*, 1667. (y) A. Schneemann, V. Bon, I. Schwedler, I. Senkowska, S. Kaskel, R. A. Fischer *Chem. Soc. Rev.*, **2014**, *43*, 6062. (z) F. X. Coudert, *Chem. Mater.*, **2015**, *27*, 1905.
- [1.8] (a) H. Furukawa, K. E. Cordova, M. O’Keeffe, O. M. Yaghi, *Science*, **2013**, *341*, 6149. (b) R. J. Kupplera, D. J. Timmons, Q. –R. Fanga, J. –R. Lia, T. A. Makala, M. D. Younga, D. Yuana, D. Zhaoa, W. Zhuanga, H. –C. Zhou. *Coord. Chem. Rev.*, **2009**, *253*, 3042. (c) A. Morozan, F. Jaouen, *Energy Environ. Sci.*, **2012**, *5*, 9269. (d) A. U. Czaja, N. Trukhan, U. Müller, *Chem. Soc. Rev.*, **2009**, *38*, 1284. (e) U. Mueller, M. Schubert, F. Teich, H. Puetter, K. Schierle-Arndt, J. Pastré *J. Mater. Chem.*, **2006**, *16*, 626.
- [1.9] (a) Y. Li, R. T. Yang, *AIChE J.* **2008**, *54*, 269. (b) Z. Liang, M. Marshall, A. L. Chaffee, *Energy Fuels* **2009**, *23*, 2785. (c) F. Gul-E-Noor, B. Jee, A. Poppl, M. Hartmann, D. Himsl, M. Bertmer, *Phys. Chem. Chem. Phys.* **2011**, *13*, 7783. (d) N. C. Burtch, H. Jasuja, K. S. Walton, *Chem. Rev.*, **2014**, *114*, 10575.
- [1.10] (a) Y. Luo, B. Li, W. Wang, K. Wu and B. Tan, *Advanced Materials*, **2012**, *24*, 5703. (b) D. C. Wu, F. Xu, B. Sun, R. W. Fu, H. K. He, K. Matyjaszewski, *Chem. Rev.*, **2012**, *112*, 3959. (c) P. kaur, J. T. Hupp and S. T. Nguyen, *ACS Catal.*, **2011**, *1*, 819. (d) Z. H. Xiang and D. P. Cao, *J. Mater. Chem. A*, **2013**, *1*, 2691.
- [1.11] (a) Y. Luo, B. Li, W. Wang, K. Wu, B. Tan, *Advanced Materials*, **2012**, *24*, 5703. (b) T. Ben, S. L. Qiu, *CrystEngComm*, **2013**, *15*, 17. (c) T. Ben, H. Ren, S. Q. Ma, D. P. Cao, J. H. Lan, X. F. Jing, W. C. Wang, J. Xu, F. Deng, J. M. Simmons, S. L. Qiu, G. S. Zhu, *Angew. Chem., Int. Ed.*, **2009**, *48*, 9457. (d) S. Y. Ding, W. Wang, *Chem. Soc. Rev.*, **2013**, *42*, 548. (e) P. M. Budd, B. S. Ghanem, S. Makhseed, N. B. McKeown, K. J. Msayib, C. E. Tattershall, *Chem. Commun.*, **2004**, 230. (f) X. Feng, X. Ding, D. Jiang, *Chem. Soc. Rev.*, **2012**, *41*, 6010.

- [1.12] (a) G. Cheng, T. Hasell, A. Trewin, D. J. Adams, A. I. Cooper, *Angew. Chem., Int. Ed.*, **2012**, *51*, 12727. (b) L. Chen, Y. Honsho, S. Seki, D. Jiang, *J. Am. Chem. Soc.*, **2010**, *132*, 6742. (c) J. X. Jiang, F. B. Su, A. Trewin, C. D. Wood, N. L. Campbell, H. J. Niu, C. Dickinson, A. Y. Ganin, M. J. Rosseinsky, Y. Z. Khimyak, A. I. Cooper, *Angew. Chem., Int. Ed.*, **2007**, *46*, 8574. (d) J. X. Jiang, A. Trewin, D. J. Adams, A. I. Cooper, *Chem. Sci.*, **2011**, *2*, 1777. (e) Y. H. Xu, L. Chen, Z. Q. Guo, A. Nagai, D. Jiang, *J. Am. Chem. Soc.*, **2011**, *133*, 17622. (f) S. W. Yuan, B. Dorney, D. White, S. Kirklin, P. Zapol, L. P. Yu, D. J. Liu, *Chem. Commun.*, **2010**, *46*, 4547. (g) A. Li, R. F. Lu, Y. Wang, X. Wang, K. L. Han, W. Q. Deng, *Angew. Chem., Int. Ed.*, **2010**, *49*, 3330. (h) A. Li, H. X. Sun, D. Z. Tan, W. J. Fan, S. H. Wen, X. J. Qing, G. X. Li, S. Y. Li, W. Q. Deng, *Energy Environ. Sci.*, **2011**, *4*, 2062. (i) Q. Chen, J. X. Wang, F. Yang, D. Zhou, N. Bian, X. J. Zhang, C. G. Yan, B. H. Han, *J. Mater. Chem.*, **2011**, *21*, 13554. (j) Y. Kou, Y. Xu, Z. Guo, D. Jiang, *Angew. Chem., Int. Ed.*, **2011**, *50*, 8753. (k) A. I. Cooper, *Advanced Materials*, **2009**, *21*, 1291. (l) J.-X. Jiang, F. Su, A. Trewin, C. D. Wood, H. Niu, J. T. Jones, Y. Z. Khimyak, A. I. Cooper, *J. Am. Chem. Soc.*, **2008**, *130*, 7710.
- [1.13] (a) A. P. Cote, A. I. Benin, N. W. Ockwig, M. O’Keeffe, A. J. Matzger, O. M. Yaghi, *Science*, **2005**, *310*, 1166. (b) E. L. Spitler, W. R. Dichtel, *Nat. Chem.*, **2010**, *2*, 672. (c) J. X. Jiang, A. I. Cooper, *Top. Curr. Chem.*, **2010**, *293*, 1. (d) P. J. Waller, F. Gandara and O. M. Yaghi, *Acc. Chem. Res.*, **2015**, *48*, 3053.
- [1.14] H. M. El-Kaderi, J. R. Hunt, J. L. Mendoza-Cortes, A. P. Cote, R. E. Taylor, M. O’Keeffe, O. M. Yaghi, *Science*, **2007**, *316*, 268.
- [1.15] (a) E. L. Spitler, W. R. Dichtel, *Nat. Chem.*, **2010**, *2*, 672. (b) J. X. Jiang, A. I. Cooper, *Top. Curr. Chem.*, **2010**, *293*, 1. (c) P. J. Waller, F. Gandara and O. M. Yaghi, *Acc. Chem. Res.*, **2015**, *48*, 3053. (d) S. Y. Ding, W. Wang, *Chem. Soc. Rev.*, **2013**, *42*, 548. (e) P. M. Budd, B. S. Ghanem, S. Makhseed, N. B. McKeown, K. J. Msayib, C. E. Tattershall, *Chem. Commun.*, **2004**, 230. (f) X. Feng, X. Ding, D. Jiang, *Chem. Soc. Rev.*, **2012**, *41*, 6010.
- [1.16] A. P. Cote, A. I. Benin, N. W. Ockwig, M. O’Keeffe, A. J. Matzger, O. M. Yaghi, *Science*, **2005**, *310*, 1166.

- [1.17] S. Dalapati, M. Addicoat, S. Jin, T. Sakurai, J. Gao, H. Xu, S. Irle, S. Seki, D. Jiang, *Nat. Commun.*, **2015**, *6*, 7786.
- [1.18] F. J. Uribe-Romo, J. R. Hunt, H. Furukawa, C. Klock, M. O’Keeffe, O. M. Yaghi, *J. Am. Chem. Soc.*, **2009**, *131*, 4570.
- [1.19] E. L. Spitler, B. T. Koo, J. L. Novotney, J. W. Colson, F. J. Uribe-Romo, G. D. Gutierrez, P. Clancy, W. R. Dichtel, *J. Am. Chem. Soc.*, **2011**, *133*, 19416.
- [1.20] H. M. El-Kaderi, J. R. Hunt, J. L. Mendoza-Cortes, A. P. Cote, R. E. Taylor, M. O’Keeffe, O. M. Yaghi, *Science*, **2007**, *316*, 268.
- [1.21] (a) Côté, A. P., El- Kaderi, H. M., Furukawa, H., Hunt, J. R. & Yaghi, O. M. *J. Am. Chem. Soc.* **2007**, *129*, 12914. (b) A. Nagai, Z. Guo, X. Feng, S. Jin, X. Chen, X. Ding, D. Jiang, *Nat. Commun.*, **2011**, *2*, 536.
- [1.22] (a) P. Kuhn, M. Antonietti, A. Thomas, *Angew. Chem., Int. Ed.*, **2008**, *47*, 3450. (b) M. J. Bojdys, J. Jeromenok, A. Thomas, M. Antonietti, *Adv. Mater.*, **2010**, *22*, 2202. (c) R. Palkovits, M. Antonietti, P. Kuhn, A. Thomas, F. Schuth, *Angew. Chem., Int. Ed.*, **2009**, *48*, 6909. (d) C. E. Chan-Thaw, A. Villa, L. Prati, A. Thomas, *Chem.–Eur. J.*, **2011**, *17*, 1052.
- [1.23] (a) F. J. Uribe-Romo, C. J. Doonan, H. Furukawa, K. Oisaki, O. M. Yaghi, *J. Am. Chem. Soc.*, **2011**, *133*, 11478. (b) S.-Y. Ding, J. Gao, Q. Wang, Y. Zhang, W.-G. Song, C.-Y. Su, W. Wang, *J. Am. Chem. Soc.*, **2011**, *133*, 19816. (c) S. Wan, F. Gandara, A. Asano, H. Furukawa, A. Saeki, S. K. Dey, L. Liao, M. W. Ambrogio, Y. Y. Botros, X. Duan, S. Seki, J. F. Stoddart, O. M. Yaghi, *Chem. Mater.*, **2011**, *23*, 4094.
- [1.24] (a) L. M. Lanni, R. W. Tilford, M. Bharathy, J. J. Lavigne, *J. Am. Chem. Soc.*, **2011**, *133*, 13975. (b) R. W. Tilford, W. R. Gemmill, H.-C. Z. Loye, J. J. Lavigne, *Chem. Mater.*, **2006**, *18*, 5296. (c) B. M. Rambo, J. J. Lavigne, *Chem. Mater.*, **2007**, *19*, 3732. (d) Y. Du, K. Mao, P. Kamakoti, P. Ravikovitch, C. Paur, S. Cundy, Q. Li, D. Calabro, *Chem. Commun.* **2012**, *48*, 4606. (e) R. W. Tilford, S. J. Mugavero III, P. J. Pellechia, J. J. Lavigne, *Adv. Mater.*, **2008**, *20*, 2741.

- [1.25] (a) N. L. Campbell, R. Clowes, L. K. Ritchie, A. I. Cooper, *Chem. Mater.*, **2009**, *21*, 204. (b) M. Dogru, A. Sonnauer, A. Gavryushin, P. Knochel, T. Bein, *Chem. Commun.*, **2011**, *47*, 1707.
- [1.26] (a) B. P. Biswal, S. Chandra, S. Kandambeth, B. Lukose, T. Heine, R. Banerjee, *J. Am. Chem. Soc.*, **2013**, *135*, 5328. (b) S. Kandambeth, B. P. Biswal, H. D. Chaudhari, K. C. Rout, H. S. Kunjattu, S. Mitra, S. Karak, A. Das, R. Mukherjee, U. K. Kharul, R. Banerjee, *Adv. Mater.* **2017**, *29*, 1603945. (c) S. Karak, S. Kandambeth, B. P. Biswal, H. S. Sasmal, S. Kumar, P. Pachfule, R. Banerjee, *J. Am. Chem. Soc.* **2017**, *139*, 1856. (d) S. Kandambeth, V. Venkatesh, D. B. Shinde, S. Kumari, A. Halder, S. Verma, R. Banerjee, *Nat. Commun.* **2015**, *6*, Article No. 6786. (e) S. Kandambeth, A. Mallick, B. Lukose, M. V. Mane, T. Heine, R. Banerjee, *J. Am. Chem. Soc.* **2012**, *134*, 19524. (f) J. H. Chong, M. Sauer, B. O. Patrick, M. J. MacLachlan, *Org. Lett.* **2003**, *5*, 3823 (g) S. Kandambeth, D. B. Shinde, M. K. Panda, B. Lukose, T. Heine, R. Banerjee, *Angew. Chem. Int. Ed.* **2013**, *52*, 13052. (h) H. Xu, J. Gao, D. Jiang, *Nat. Chem.* **2015**, *7*, 905. (i) P. F. Wei, M. Z. Qi, Z. P. Wang, S. Y. Ding, W. Yu, Q. Liu, L. Wang, H. Z. Wang, W. K. An, W. Wang, *J. Am. Chem. Soc.* **2018**, *140*, 4623.
- [1.27] (a) N. A. A. Zwaneveld, R. Pawlak, M. Abel, D. Catalin, D. Gigmes, D. Bertin, L. Porte, *J. Am. Chem. Soc.*, **2008**, *130*, 6678. (b) J. W. Colson, A. R. Woll, A. Mukherjee, M. P. Levendorf, E. L. Spitler, V. B. Shields, M. G. Spencer, J. Park, W. R. Dichtel, *Science*, **2011**, *332*, 228. (c) X. H. Liu, C. Z. Guan, S. Y. Ding, W. Wang, H. J. Yan, D. Wang, L. J. Wan, *J. Am. Chem. Soc.*, **2013**, *135*, 10470.
- [1.28] (a) M. P. Suh, H. J. Park, T. K. Prasad, D.-W. Lim, *Chem. Rev.*, **2012**, *112*, 782. (b) H. Furukawa, O. M. Yaghi, *J. Am. Chem. Soc.*, **2009**, *131*, 8875. (c) E. Klontzas, E. Tylianakis, G. E. Froudakis, *J. Phys. Chem. C*, **2009**, *113*, 21253. (d) F. Li, J. Zhao, B. Johansson, L. Sun, *Int. J. Hydrogen Energy*, **2010**, *35*, 266. (e) H. Furukawa, N. Ko, Y. B. Go, N. Aratani, S. B. Choi, E. Choi, A. O. Yazaydin, R. Q. Snurr, M. O’Keeffe, J. Kim, O. M. Yaghi, *Science*, **2010**, *329*, 424. (f) C. J. Doonan, D. J. Tranchemontagne, T. G. Glover, J. R. Hunt, O. M. Yaghi, *Nat. Chem.*, **2010**, *2*, 235.
- [1.29] (a) S. Wan, J. Guo, J. Kim, H. Ihee, D. Jiang, *Angew. Chem., Int. Ed.*, **2009**, *48*, 5439. (b) S. Wan, J. Guo, J. Kim, H. Ihee, D. Jiang, *Angew. Chem., Int. Ed.*, **2008**, *47*, 8826. (c) X. Feng, L. Liu, Y. Honsho, A. Saeki, S. Seki, S. Irle, Y. Dong, A. Nagai, D.

- Jiang, *Angew. Chem., Int. Ed.*, **2012**, *51*, 2618. (d) X. S. Ding, J. Guo, X. Feng, Y. Honsho, J. D. Guo, S. Seki, P. Maitarad, A. Saeki, S. Nagase, D. Jiang, *Angew. Chem., Int. Ed.*, **2011**, *50*, 1289. (e) X. Feng, L. Chen, Y. Honsho, O. Saengsawang, L. Liu, L. Wang, A. Saeki, S. Irle, S. Seki, Y. Dong, D. Jiang, *Adv. Mater.*, **2012**, *24*, 3026.
- [1.30] (a) C. R. DeBlase, K. E. Silberstein, T. T. Truong, H. D. Abruna, W. R. Dichtel, *J. Am. Chem. Soc.*, **2013**, *135*, 16821. (b) C. R. DeBlase, K. Hernandez-Burgos, K. E. Silberstein, G. G. Rodriguez-Calero, R. P. Bisbey, H. D. Abruna, W. R. Dichtel, *ACS Nano*, **2015**, *9*, 3178. (c) F. Xu, H. Xu, D. Wu, Y. Wu, H. Liu, C. Gu, R. Fu, D. Jiang Chen, *Angew. Chem Int. Ed.* **2015**, *54*, 6814.
- [1.31] (a) H. Lu, C. Wang, J. Chen, R. Ge, W. Leng, B. Dong, J. Huang, Y. Gao, *Chem. Commun.* **2015**, *51*, 15562. (b) B. P. Biswal, H. D. Chaudhari, R. Banerjee, U. K. Kharul, *Chem. Eur. J.*, **2016**, *22*, 4695. (c) L. C. Lin, J. Choi, J. C. Grossman, *Chem. Commun.*, **2015**, *51*, 14921.
- [1.32] (a) S. Chandra, T. Kundu, S. Kandambeth, R. BabaRao, Y. Marathe, S. M. Kunjir, R. Banerjee, *J. Am. Chem. Soc.*, **2014**, *136*, 6570–6573. (b) S. Chandra, T. Kundu, K. Dey, M. Addicoat, T. Heine, R. Banerjee, *Chem. Mater.*, **2016**, *28*, 1489–1494. (c) D. B. Shinde, H. B. Aiyapp, M. Bhadra, B. P. Biswal, P. Wadge, S. Kandambeth, B. Garai, T. Kundu, S. Kurungot, R. Banerjee, *J. Mater. Chem. A*, **2016**, *4*, 2682–2690. (d) H. Xu, S. Tao, D. Jiang, *Nat. Mater.*, **2016**, *15*, 722–726.
- [1.33] Q. Fang, J. Wang, S. Gu, R. B. Kaspar, Z. Zhuang, J. Zheng, H. Guo, S. Qiu, Y. Yan, *J. Am. Chem. Soc.*, **2015**, *137*, 8352.
- [1.34] (a) L. M. Lanni, R. W. Tilford, M. Bharathy, J. J. Lavigne, *J. Am. Chem. Soc.*, **2011**, *133*, 13975. (b) Y. Du, K. Mao, P. Kamakoti, P. Ravikovitch, C. Paur, S. Cundy, Q. Li, D. Calabro, *Chem. Commun.* **2012**, *48*, 4606. (c) S. Kandambeth, D. B. Shinde, M. K. Panda, B. Lukose, T. Heine, R. Banerjee, *Angew. Chem., Int. Ed.*, **2013**, *52*, 13052–13056. (d) P. J. Waller, S. Lyle, T. Osborn Popp, C. S. Diercks, J. A. Reimer, O. M. Yaghi, *J. Am. Chem. Soc.*, **2016**, *138*, 15519. (e) S. Kandambeth, A. Mallick, B. Lukose, M. V. Mane, T. Heine, R. Banerjee, *J. Am. Chem. Soc.*, **2012**, *134*, 19524.
- [1.35] (a) Z. Wang, S. M. Cohen, *Chem. Soc. Rev.*, **2009**, *38*, 1315. (b) S. M. Cohen, *Chem. Rev.*, **2012**, *112*, 970. (c) Trindade, A. F.; Gois, P. M. P.; Afonso, C. A. M. *Chem.*

- Rev.*, **2009**, *109*, 418. (d) Heitbaum, M.; Glorius, F.; Escher, I. *Angew. Chem., Int. Ed.*, **2006**, *45*, 4732. (e) A. Nagai, Z. Guo, X. Feng, S. Jin, X. Chen, X. Ding, D. Jiang, *Nat. Commun.*, **2011**, *2*, 536. (f) M. Gruttadauria, F. Giacalone, R. Noto, *Chem. Soc. Rev.*, **2008**, *37*, 1666. (g) F. Hoffmann, M. Cornelius, J. Morell, M. Fröba, *Angew. Chem., Int. Ed.*, **2006**, *45*, 3216. (h) S.-Y. Ding, J. Gao, Q. Wang, Y. Zhang, W.-G. Song, C.-Y. Su, W. Wang, *J. Am. Chem. Soc.*, **2011**, *133*, 19816.
- [1.36] (a) H.-S. Xu, S.-Y. Ding, W.-K. An, H. Wu, W. Wang, *J. Am. Chem. Soc.*, **2016**, *138*, 11489. (b) C. J. Doonan, D. J. Tranchemontagne, T. G. Glover, J. R. Hunt, O. M. Yaghi, *Nat. Chem.*, **2010**, *2*, 235. (c) S. Wan, J. Guo, J. Kim, H. Ihee, D. Jiang, *Angew. Chem., Int. Ed.*, **2008**, *47*, 8826.
- [1.37] (a) L. Yang, S. Jiang, Y. Zhao, L. Zhu, S. Chen, X. Wang, Q. Wu, J. Ma, Y. Ma, Z. Hu, *Angew. Chem.* **2011**, *123*, 7270. (b) Z. Yang, Z. Yao, G. Li, G. Fang, H. Nie, Z. Liu, X. Zhou, X. Chen, S. Huang, *ACS Nano*, **2012**, *6*, 205. (c) Y. Wang, H. Li, J. Yao, X. Wang, M. Antonietti, *Chem. Sci.* **2011**, *2*, 446. (d) Y. Wang, J. Zhang, X. Wang, M. Antonietti, H. Li, *Angew. Chem., Int. Ed.*, **2010**, *49*, 3356. (e) W. J. Lee, U. N. Maiti, J. M. Lee, J. Lim, T. H. Han, S. O. Kim, *Chem. Commun.* **2014**, *50*, 6818. (f) W. Xia, A. Mahmood, R. Zou, Q. Xu, *Energy Environ. Sci.* **2015**, *8*, 1837. (g) J. Lahaye, G. Nanse, A. Bagreev, V. Strelko, *Carbon*, **1999**, *37*, 585. (h) K. Jurewicz, K. Babel, A. Zi'olkowski, H. Wachowska, M. Kozłowski, *Fuel Process. Technol.*, **2002**, *191*, 77. (i) K. Jurewicz, K. Babel, A. Zi'olkowski, H. Wachowska, *Electrochim. Acta*, **2003**, *48*, 1491. (j) K. Jurewicz, K. Babel, A. Zi'olkowski, H. Wachowska, *J. Phys. Chem. Solids*, **2004**, *65*, 269. (k) S. M. Mahurin, J. S. Lee, X. Wang, S. Dai, *J. Membr. Sci.*, **2011**, *368*, 41. (l) J. R. Pels, F. Kapteijn, J. A. Moulijn, Q. Zhu, K. M. Thomas, *Carbon*, **1995**, *33*, 1641. (m) A. Bagreev, J. A. Menendez, I. Dukhno, Y. Tarasenko, T. J. Bandosz, *Carbon*, **2004**, *42*, 469. (n) K. P. Gong, F. Du, Z. H. Xia, M. Durstock, L. M. Dai, *Science*, **2009**, *323*, 760. (o) Y. Tang, B. L. Allen, D. R. Kauffman, A. Star, *J. Am. Chem. Soc.*, **2009**, *131*, 13200. (p) P. Pachfule, V. M. Dhavale, S. Kandambeth, S. Kurungot, R. Banerjee, *Chem. Eur. J.* **2013**, *19*, 974. (q) M. Tiemann, *Chem. Mater.* **2008**, *20*, 961. (r) K. E. Shopsowitz, W. Y. Hamad, M. J. MacLachlan, *Angew. Chem.* **2011**, *123*, 11183. *Angew. Chem. Int. Ed.*, **2011**, *50*, 10991. (s) X. Q. Wang, J. S. Lee, Q. Zhu, J. Liu, Y. Wang, S. Dai, *Chem. Mater.*,

- 2010, 22, 2178. (t) D. Hulicowa, J. Yamashita, Y. Soneda, H. Hatori, M. Kodama, *Chem. Mater.*, **2005**, 17, 1241. (u) F. B´eguin, K. Szostak, G. Lota, E. Frackowiak, *Adv. Mater.*, **2005**, 17, 2380. (v) D. Hulicowa, M. Kodama, H. Hatori, *Chem. Mater.*, **2006**, 18, 2318. (w) I. Florea, O. Ersen, R. Arenal, D. Ihiawakrim, C. Messaoudi, K.Chizari, I. Janowska, C. Pham-Huu, *J. Am. Chem. Soc.* **2012**, 134, 9672.
- [1.38] S.-Y. Ding, J. Gao, Q. Wang, Y. Zhang, W.-G. Song, C.-Y. Su, W. Wang, *J. Am. Chem. Soc.*, **2011**, 133, 19816.
- [1.39] P. Pachfule, M. K. Panda, S. Kandambeth, S. M. Shivaprasad, D. D. Díaz, R. Banerjee, *J. Mater. Chem. A*, **2014**, 2, 7944.
- [1.40] Q. Fang, S. Gu, J. Zheng, Z. Zhuang, S. Qiu, Y. Yan, *Angew. Chem., Int. Ed.*, **2014**, 53, 2878.
- [1.41] X. Wang, X. Han, J. Zhang, X. Wu, Y. Liu, Y. Cui, *J. Am. Chem. Soc.*, **2016**, 138, 12332.
- [1.42] H.-S. Xu, S.-Y. Ding, W.-K. An, H. Wu, W. Wang, *J. Am. Chem. Soc.*, **2016**, 138, 11489.
- [1.43] V. S. Vyas, F. Haase, L. Stegbauer, G. Savasci, F. Podjaski, C. Ochsenfeld, B. V. Lotsch, *Nat. Commun.*, **2015**, 6, 8508.
- [1.44] J. Thote, H. B. Aiyappa, A. Deshpande, D. D. Díaz, S. Kurungot, R. Banerjee, *Chem.-Eur. J.* **2014**, 20, 15961.
- [1.45] S. Lin, C. S. Diercks, Y.-B. Zhang, N. Kornienko, E. M. Nichols, Y. Zhao, A. R. Paris, D. Kim, P. Yang, O. M. Yaghi, C. J. Chang, *Science*, **2015**, 349, 1208.

CHAPTER 2

- [2.1] M. Beller, A. Renken, an R. A. E. Santen, *Catalysis: From Principles to Applications*, 1st ed., Wiley-VCH: Weinheim, **2012**.
- [2.2] (a) J. Hagen, *Industrial Catalysis: A Practical Approach*, 2nd ed., Wiley-VCH: Weinheim, **2015**. (b) G. Ertl, H. Knözinger, F. Schüth, J. E. Weitkamp, *Handbook Of Heterogeneous Catalysis*, 2nd ed., Wiley-VCH: Weinheim, **2008**.
- [2.3] (a) L. D. Bergelson, M. M. Shemyakin, *Tetrahedron*, **1963**, 19, 149. (b) J. Motoyoshiya, *Trends Org. Chem.*, **1998**, 7, 63. (c) L. F. V. Staden, D. Gravestock, D.

- J. Ager, *Chem. Soc. Rev.*, **2002**, *31*, 195. (d) E.-I. Negishi, Z. Huang, G. Wang, S. Mohan, C. Wang, H. Hattori, *Acc. Chem. Res.*, **2008**, *41*, 1474. (e) Z. Huang, E.-I. Negishi, *J. Am. Chem. Soc.*, **2007**, *129*, 14788. (f) H. Lindlar, *Helv. Chim. Acta*, **1952**, *35*, 446. (g) S. J. Meek, R. V. O'Brien, J. Llaveria, R. R. Schrock, A. H. Hoveyda, *Nature*, **2011**, *471*, 461. (h) M. J. Koh, R. K. M. Khan, S. Torker, A. H. Hoveyda, *Angew. Chem., Int. Ed.*, **2014**, *53*, 1968. (i) K. Endo, R. H. Grubbs, *J. Am. Chem. Soc.*, **2011**, *133*, 8525.
- [2.4] (a) S. H. Joo, S. J. Choi, I. Oh, J. Kwak, Z. Liu, O. Terasaki, R. Ryoo, *Nature*, **2001**, *412*, 169. (b) C. D. Liang, Z. J. Li, S. Dai, *Angew. Chem., Int. Ed.*, **2008**, *47*, 3696. (c) Y. Wan, Y. F. Shi, D. Y. Zhao, *Chem. Mater.*, **2008**, *20*, 932.
- [2.5] (a) G. Rothenberg, *Catalysis: Concepts and Green Applications*, 1st ed., Wiley-VCH: Weinheim, **2008**. (b) G. G. Wildgoose, C. E. Banks, R. G. Compton, *Small* **2006**, *2*, 182. (c) D. Tasis, N. Tagmatarchis, A. Bianco, M. Prato, *Chem. Rev.* **2006**, *106*, 1105. (d) D. R. Dreyer, C. W., Bielawski, *Chem. Sci.* **2011**, *2*, 1233. (e) V. Georgakilas, J. A. Perman, J. Tucek, R. Zboril, *Chem. Rev.* **2015**, *115*, 4744.
- [2.6] (a) P. Albers, K. Deller, B. M. Despeyroux, A. Schäfer, K. Seibold, *J. Catal.* **1992**, *133*, 467. (b) M. Li, Y. Li, L. Jia, Y. Wang, *Catal. Commun.* **2018**, *103*, 88. (c) G. Marck, A. Villiger, R. Buchecker, *Tetrahedron Lett.* **1994**, *35*, 3277.
- [2.7] Y. Cao, S. Mao, M. Li, Y. Chen, Y. Wang, *ACS Catal.*, **2017**, *7*, 8090.
- [2.8] (a) L. Yang, S. Jiang, Y. Zhao, L. Zhu, S. Chen, X. Wang, Q. Wu, J. Ma, Y. Ma, Z. Hu, *Angew. Chem.* **2011**, *123*, 7270. (b) Z. Yang, Z. Yao, G. Li, G. Fang, H. Nie, Z. Liu, X. Zhou, X. Chen, S. Huang, *ACS Nano*, **2012**, *6*, 205. (c) Y. Wang, H. Li, J. Yao, X. Wang, M. Antonietti, *Chem. Sci.* **2011**, *2*, 446. (d) Y. Wang, J. Zhang, X. Wang, M. Antonietti, H. Li, *Angew. Chem., Int. Ed.*, **2010**, *49*, 3356.
- [2.9] K. N. Wood, R. O'Hayre, S. Pylypenko, *Energy Environ. Sci.* **2014**, *7*, 1212.
- [2.10] (a) W. J. Lee, U. N. Maiti, J. M. Lee, J. Lim, T. H. Han, S. O. Kim, *Chem. Commun.* **2014**, *50*, 6818. (b) W. Xia, A. Mahmood, R. Zou, Q. Xu, *Energy Environ. Sci.* **2015**, *8*, 1837.
- [2.11] J. Lahaye, G. Nanse, A. Bagreev, V. Strelko, *Carbon*, **1999**, *37*, 585.

- [2.12] (a) K. Jurewicz, K. Babel, A. Zi'olkowski, H. Wachowska, M. Kozlowski, *Fuel Process. Technol.*, **2002**, *191*, 77. (b) K. Jurewicz, K. Babel, A. Zi'olkowski, H. Wachowska, *Electrochim. Acta*, **2003**, *48*, 1491. (c) K. Jurewicz, K. Babel, A. Zi'olkowski, H. Wachowska, *J. Phys. Chem. Solids*, **2004**, *65*, 269. (d) S. M. Mahurin, J. S. Lee, X. Wang, S. Dai, *J. Membr. Sci.*, **2011**, *368*, 41. (e) J. R. Pels, F. Kapteijn, J. A. Moulijn, Q. Zhu, K. M. Thomas, *Carbon*, **1995**, *33*, 1641. (f) A. Bagreev, J. A. Menendez, I. Dukhno, Y. Tarasenko, T. J. Bandosz, *Carbon*, **2004**, *42*, 469.
- [2.13] (a) K. P. Gong, F. Du, Z. H. Xia, M. Durstock, L. M. Dai, *Science*, **2009**, *323*, 760. (b) Y. Tang, B. L. Allen, D. R. Kauffman, A. Star, *J. Am. Chem. Soc.*, **2009**, *131*, 13200. (c) P. Pachfule, V. M. Dhavale, S. Kandambeth, S. Kurungot, R. Banerjee, *Chem. Eur. J.* **2013**, *19*, 974. (d) M. Tiemann, *Chem. Mater.* **2008**, *20*, 961. (e) K. E. Shopsowitz, W. Y. Hamad, M. J. MacLachlan, *Angew. Chem.* **2011**, *123*, 11183. *Angew. Chem. Int. Ed.*, **2011**, *50*, 10991.
- [2.14] (a) X. Q. Wang, J. S. Lee, Q. Zhu, J. Liu, Y. Wang, S. Dai, *Chem. Mater.*, **2010**, *22*, 2178. (b) D. Hulicowa, J. Yamashita, Y. Soneda, H. Hatori, M. Kodama, *Chem. Mater.*, **2005**, *17*, 1241. (c) F. B'eguine, K. Szostak, G. Lota, E. Frackowiak, *Adv. Mater.*, **2005**, *17*, 2380. (d) D. Hulicowa, M. Kodama, H. Hatori, *Chem. Mater.*, **2006**, *18*, 2318.
- [2.15] I. Florea, O. Ersen, R. Arenal, D. Ihiwakrim, C. Messaoudi, K. Chizari, I. Janowska, C. Pham-Huu, *J. Am. Chem. Soc.* **2012**, *134*, 9672.
- [2.16] (a) A. D. Ryabov, *Chem. Rev.*, **1990**, *90*, 403. (b) A. E. Shilov, G. B. Shul'pin, *Chem. Rev.*, **1997**, *97*, 2879. (c) V. Ritleng, C. Sirlin, M. Pfeffer, *Chem. Rev.*, **2002**, *102*, 1731. (d) A. R. Dick, M. S. Sanford, *Tetrahedron*, **2006**, *62*, 2439. (e) I. A. I. Mkhaliid, J. H. Barnard, T. B. Marder, J. M. Murphy, J. F. Hartwig, *Chem. Rev.*, **2010**, *110*, 890. (f) M. P. Doyle, R. Duffy, M. Ratnikov, L. Zhou, *Chem. Rev.*, **2010**, *110*, 704. (g) H. M. Davies, J. Du Bois, J. Q. Yu, *Chem. Soc. Rev.*, **2011**, *40*, 1855. (h) D. A. Colby, R. G. Bergman, J. A. Ellman, *Chem. Rev.*, **2009**, *110*, 624. (a) X. Chen, K. M. Engle, D. Wang, J. Q. Yu, *Angew. Chem., Int. Ed.*, **2009**, *48*, 5094. (b) T. W. Lyons, M. S. Sanford, *Chem. Rev.*, **2010**, *110*, 1147. (c) L. Ackermann, *Chem. Rev.*, **2011**, *111*, 1315. (d) S. R. Neufeldt, M. S. Sanford, *Acc. Chem. Res.*, **2012**, *45*, 936.

- [2.17] (a) K. M. Choi, D. Kim, B. Rungtaweevoranit, C. A. Trickett, J. T. D. Barmanbek, A. S. Alshammari, P. Yang, O. M. Yaghi, *J. Am. Chem. Soc.* **2017**, *139*, 356.
- [2.18] (a) C. K. Prier, D. A. Rankic, D. W. C. MacMillan, *Chem. Rev.* **2013**, *113*, 5322. (b) N. A. Romero, D. A. Nicewicz, *Chem. Rev.* **2016**, *116*, 10075. (c) D. P. Hari, B. König, *Chem. Commun.* **2014**, *50*, 6688. (d) S. Fukuzumi, H. Kotani, K. Ohkubo, S. Ogo, N. V. Tkachenko, H. Lemmetyinen, *J. Am. Chem. Soc.* **2004**, *126*, 1600. (e) I. Ghosh, T. Ghosh, J. I. Bardagi, B. König, *Science*, **2014**, *346*, 725. (f) I. Ghosh, B. König, *Angew. Chem. Int. Ed.* **2016**, *55*, 7676. (g) I. Ghosh, L. Marzo, A. Das, R. Shaikh, B. König, *Acc. Chem. Res.* **2016**, *49*, 1566. (h) M. M. Li, Y. Wei, J. Liu, H. W. Chen, L. Q. Lu, W. J. Xiao, *J. Am. Chem. Soc.* **2017**, *139*, 14707. (i) Y. Y. Liu, X. Y. Yu, J. R. Chen, M. M. Qiao, X. Qi, D. Q. Shi, W. J. Xiao, *Angew. Chem. Int. Ed.* **2017**, *56*, 9527. *Angew. Chem.*, **2017**, *129*, 9655. (j) D. A. Nicewicz, D. W. C. MacMillan, *Science*, **2008**, *322*, 77. (k) X. H. Zhang, D. W. C. MacMillan, *J. Am. Chem. Soc.* **2017**, *139*, 11353. (l) H. Bartling, A. Eisenhofer, B. König, R. M. Gschwind, *J. Am. Chem. Soc.* **2016**, *138*, 11860. (m) A. U. Meyer, A. Wimmer, B. König, *Angew. Chem. Int. Ed.*, **2017**, *56*, 409, *Angew. Chem.* **2017**, *129*, 420. (n) S. Senaweera, J. D. Weaver, *J. Am. Chem. Soc.* **2016**, *138*, 2520. (o) M. Chhowalla, H. S. Shin, G. Eda, L. J. Li, K. P. Loh, H. Zhang, *Nat. Chem.*, **2013**, *5*, 263. (p) W. J. Ong, L. L. Tan, Y. H. Ng, S. T. Yong, S. P. Chai, *Chem. Rev.*, **2016**, *116*, 7159. (q) C. Tan, X. Cao, X. J. Wu, Q. He, J. Yang, X. Zhang, J. Chen, W. Zhao, S. Han, G. H. Nam, M. Sindoro, H. Zhang, *Chem. Rev.* **2017**, *117*, 6225. (r) Grätzel, M. *Acc. Chem. Res.* **1981**, *14*, 376. (s) Meyer, T. J. *Acc. Chem. Res.* **1989**, *22*, 163.
- [2.19] (a) A. P. Côté, A. I. Benin, N. W. Ockwig, M. O'Keeffe, A. J. Matzger, O. M. Yaghi, *Science*, **2005**, *310*, 1166. (b) X. Feng, X. Ding, D. Jiang, *Chem. Soc. Rev.*, **2012**, *41*, 6010. (c) C. J. Doonan, D. J. Tranchemontagne, T. G. Glover, J. R. Hunt, O. M. Yaghi, *Nat. Chem.*, **2010**, *2*, 235. (d) Y. Zeng, R. Zou, Z. Luo, H. Zhang, X. Yao, X. Ma, R. Zou, Y. Zhao, *J. Am. Chem. Soc.*, **2015**, *137*, 1020. (e) D. D. Medina, J. M. Rotter, Y. Hu, M. Dogru, V. Werner, F. Auras, J. T. Markiewicz, P. Knochel, T. Bein, *J. Am. Chem. Soc.*, **2015**, *137*, 1016.
- [2.20] (a) H. Furukawa, O. M. Yaghi, *J. Am. Chem. Soc.*, **2009**, *131*, 8875. (b) Y. -B. Zhang, J. Su, H. Furakawa, Y. Yun, F. Gándara, A. Duong, X. Zou, O. M. Yaghi, *J. Am.*

- Chem. Soc.* **2013**, *135*, 16336. (c) M. G. Rabbani, A. K. Sekizkardes, Z. Kahveci, T. E. Reich, R. Ding, H. M. El-Kaderi, *Chem. Eur. J.*, **2013**, *19*, 3324. (d) K. T. Jackson, T. E. Reich, H. M. El-Kaderi, *Chem. Commun.*, **2012**, *48*, 8823. (e) S. Kandambeth, D. B. Shinde, M. K. Panda, B. Lukose, T. Heine, R. Banerjee, *Angew. Chem. Int. Ed.* **2013**, *52*, 13052. (f) M. Dogru, A. Sonnauer, A. Gavryushin, P. Knochel, T. Bein, *Chem. Commun.*, **2011**, *47*, 1707. (g) S. -Y. Ding, J. Gao, Q. Wang, Y. Zhang, W. -G. Song, C. -Y. Su, W. Wang, *J. Am. Chem. Soc.*, **2011**, *133*, 19816. (h) Q. Fang, S. Gu, J. Zheng, Z. Zhuang, S. Qiu, Y. Yan, *Angew. Chem. Int. Ed.*, **2014**, *53*, 2878. (i) D. B. Shinde, S. Kandambeth, P. Pachfule, R. R. Kumar, R. Banerjee, *Chem. Commun.*, **2015**, *51*, 310. (j) S. Wan, J. Guo, J. Kim, H. Ihee, D. Jiang, *Angew. Chem. Int. Ed.*, **2008**, *47*, 8826. (k) S. Dalapati, S. Jin, J. Gao, Y. Xu, A. Nagai, D. Jiang, *J. Am. Chem. Soc.*, **2013**, *135*, 17310. (l) C. R. DeBlase, K. E. Silberstein, T. -T. Truong, H. D. Abruña, W. R. Dichtel, *J. Am. Chem. Soc.*, **2013**, *135*, 16821. (m) S. Wan, F. Gándara, A. Asano, H. Furukawa, A. Saeki, S. K. Dey, L. Liao, M. W. Ambrogio, Y. Y. Botros, X. Duan, S. Seki, J. F. Stoddart, O. M. Yaghi, *Chem. Mater.*, **2011**, *23*, 4094.
- [2.21] (a) E. L. Spitler, W. R. Dichtel, *Nat. Chem.*, **2010**, *2*, 672. (b) J. X. Jiang, A. I. Cooper, *Top. Curr. Chem.*, **2010**, *293*, 1. (c) P. J. Waller, F. Gandara and O. M. Yaghi, *Acc. Chem. Res.*, **2015**, *48*, 3053.
- [2.22] (a) P. Kuhn, M. Antonietti, A. Thomas, *Angew. Chem., Int. Ed.*, **2008**, *47*, 3450. (b) M. J. Bojdys, J. Jeromenok, A. Thomas, M. Antonietti, *Adv. Mater.*, **2010**, *22*, 2202. (c) R. Palkovits, M. Antonietti, P. Kuhn, A. Thomas, F. Schuth, *Angew. Chem., Int. Ed.*, **2009**, *48*, 6909. (d) C. E. Chan-Thaw, A. Villa, L. Prati, A. Thomas, *Chem.–Eur. J.*, **2011**, *17*, 1052.
- [2.23] (a) N. L. Campbell, R. Clowes, L. K. Ritchie, A. I. Cooper, *Chem. Mater.*, **2009**, *21*, 204. (b) M. Dogru, A. Sonnauer, A. Gavryushin, P. Knochel, T. Bein, *Chem. Commun.*, **2011**, *47*, 1707.
- [2.24] (a) N. A. A. Zwaneveld, R. Pawlak, M. Abel, D. Catalin, D. Gigmès, D. Bertin, L. Porte, *J. Am. Chem. Soc.*, **2008**, *130*, 6678. (b) J. W. Colson, A. R. Woll, A. Mukherjee, M. P. Levendorf, E. L. Spitler, V. B. Shields, M. G. Spencer, J. Park, W.

- R. Dichtel, *Science*, **2011**, 332, 228.(c) X. H. Liu, C. Z. Guan, S. Y. Ding, W. Wang, H. J. Yan, D. Wang, L. J. Wan, *J. Am. Chem. Soc.*, **2013**, 135, 10470.
- [2.25] (a) R. B. N. Baig, R. S. Varma, *Chem. Soc. Rev.*, **2012**, 41, 1559. (b) C. Jiménez-González, D. J. C. Constable, C. S. Ponder, *Chem. Soc. Rev.* **2012**, 41, 1485.
- [2.26] (a) M. K. Beyer, H. Clausen-Schaumann, *Chem. Rev.*, **2005**, 105, 2921. (b) R. E. Morris, S. L. James, *Angew. Chem. Int. Ed.*, **2013**, 52, 2163. (c) T. Friščić, I. Halasz, P. J. Beldon, A. M. Belenguer, F. Adams, S. A. J. Kimber, V. Honkimäki, R. E. Dinnebier, *Nat. Chem.*, **2013**, 5, 66. (d) T. Friščić, D. G. Reid, I. Halasz, R. S. Stein, R. E. Dinnebier, M. J. Duer, *Angew. Chem. Int. Ed.*, **2010**, 49, 712.
- [2.27] T. Friščić, W. Jones, *Cryst. Growth Des.* **2009**, 9, 1621.
- [2.28] J. H. Chong, M. Sauer, B. O. Patrick, M. J. MacLachlan, *Org. Lett.*, **2003**, 5, 3823.
- [2.29] M. Albrecht, I. Janser, A. Lützen, M. Hapke, R. Fröhlich, P. Weis, *Chem. Eur. J.*, **2005**, 11, 5742.

CHAPTER 3

- [3.1] (a) M. Benaglia, A. Puglisi, F. Cozzi, *Chem. Rev.*, **2003**, 103, 3401. (b) S. Ikegami, H. Hamamoto, *Chem. Rev.*, **2009**, 109, 583. (c) D. J. Cole-Hamilton, *Science*, **2003**, 299, 1702. (d) K. Mennecke, R. Cecilia, T. N. Glasnov, S. Gruhl, C. Vogt, A. Feldhoff, M. A. L. Vargas, C. O. Kappe, U. Kunz, A. Kirschning, *Adv. Synth. Catal.*, **2008**, 350, 717. (e) W. Huang, J. H.-C. Liu, P. Alayoglu, Y. Li, C. A. Witham, C.-K. Tsung, F. D. Toste, G. A. Somorjai, *J. Am. Chem. Soc.*, **2010**, 132, 16771. (f) E. G. Moschetta, S. Negretti, K. M. Chepiga, N. A. Brunelli, Y. Labreche, Y. Feng, F. Rezaei, R. P. Lively, W. J. Koros, H.M. L. Davies, C. W. Jones, *Angew. Chem., Int. Ed.*, **2015**, 54, 6470.
- [3.2] (a) Y. Jiang, Q. Gao, *J. Am. Chem. Soc.*, **2006**, 128, 716. (b) C. A. Witham, W. Huang, C.-K. Tsung, J. N. Kuhn, G. A. Somorjai, F. D. Toste, *Nat. Chem.*, **2010**, 2, 36. (c) F. A. Westerhaus, R. V. Jagadeesh, G. Wienhöfer, M.-M. Pohl, J. Radnik, A.-E. Surkus, J. Rabeah, K. Junge, H. Junge, M. Nielsen, A. Brückner, M. Beller, *Nat. Chem.*, **2013**, 5, 537.

- [3.3] (a) D. Wang, D. Astruc, *Chem. Rev.*, **2014**, *114*, 6949. (b) R. Pool, *Science*, **1990**, *248*, 1186. (c) D. Astruc, F. Lu, J. R. Aranzaes, *Angew. Chem., Int. Ed.*, **2005**, *44*, 7852.
- [3.4] (a) X. Zhang, A. Corma, *Angew. Chem., Int. Ed.*, **2008**, *47*, 4358. (b) J. Han, Y. Liu, R. Guo, *J. Am. Chem. Soc.*, **2009**, *131*, 2060. (c) M. Bernechea, E. de Jesús, C. López-Mardomingo, P. Terreros, *Inorg. Chem.*, **2009**, *48*, 4491. (d) F. Wang, J. Mielby, F. H. Richter, G. Wang, G. Prieto, T. Kasama, C. Weidenthaler, H.-J. Bongard, S. Kegnaes, A. Fürstner, F. Schüth, *Angew. Chem., Int. Ed.*, **2014**, *53*, 8645. (e) G.-H. Wang, X. Deng, D. Gu, K. Chen, H. Tüysüz, B. Spliethoff, H.-J. Bongard, C. Weidenthaler, W. Schmidt, F. Schüth, *Angew. Chem., Int. Ed.*, **2016**, *55*, 11101, (f) L.-C. Lee, J. He, J.-Q. Yu, C. W. Jones, *ACS Catal.*, **2016**, *6*, 5245.
- [3.5] (a) D. E. Fogg, E. N. dos Santos, *Coord. Chem. Rev.*, **2004**, *248*, 2365. (b) J.-C. Wasilke, S. J. Obrey, R. T. Baker, G. C. Bazan, *Chem. Rev.*, **2005**, *105*, 1001. (c) C. Roberta, C. M. Thomas, *Chem. Soc. Rev.*, **2013**, *42*, 9392. (d) A. C. Atesin, N. A. Ray, P. C. Stair, T. J. Marks, *J. Am. Chem. Soc.*, **2012**, *134*, 14682. (e) Z. Li, R. S. Assary, A. C. Atesin, L. A. Curtiss, T. J. Marks, *J. Am. Chem. Soc.*, **2014**, *136*, 104. (f) Y. Yuki, K. Takahashi, Y. Tanaka, K. Nozaki, *J. Am. Chem. Soc.*, **2013**, *135*, 17393. (g) D. C. Leitch, Y. C. Lam, J. A. Labinger, J. E. Bercaw, *J. Am. Chem. Soc.*, **2013**, *135*, 10302. (h) L.-C. Lee, J. Lu, M. Weck, C. W. Jones, *ACS Catal.*, **2016**, *6*, 784.
- [3.6] (a) A. P. Côté, A. I. Benin, N. W. Ockwig, M. O’Keeffe, A. J. Matzger, O. M. Yaghi, *Science*, **2005**, *310*, 1166. (b) X. Feng, X. Dinga, D. Jiang, *Chem. Soc. Rev.*, **2012**, *41*, 6010. (c) J. W. Colson, W. R. Dichtel, *Nat. Chem.*, **2013**, *5*, 453. (d) S.-Y. Dinga, W. Wang, *Chem. Soc. Rev.*, **2013**, *42*, 548. (e) M. Calik, T. Sick, M. Dogru, M. Döblinger, S. Datz, H. Budde, A. Hartschuh, F. Auras, T. Bein, *J. Am. Chem. Soc.*, **2016**, *138*, 1234. (f) D. Wu, F. Xu, B. Sun, R. Fu, H. He, K. Matyjaszewski, *Chem. Rev.*, **2012**, *112*, 3959. (g) T.-Y. Zhou, S.-Q. Xu, Q. Wen, Z.-F. Pang, X. Zhao, *J. Am. Chem. Soc.*, **2014**, *136*, 15885.
- [3.7] (a) Q. Fang, Z. Zhuang, S. Gu, R. B. Kaspar, J. Zheng, J. Wang, S. Qiu, Y. Yan, *Nat. Commun.*, **2014**, *5*, 4503. (b) G. Das, B. P. Biswal, S. Kandambeth, V. Venkatesh, G. Kaur, M. Addicoat, T. Heine, S. Verma, R. Banerjee, *Chem. Sci.*, **2015**, *6*, 3931.

- [3.8] (a) C. J. Doonan, D. J. Tranchemontagne, T. G. Glover, J. R. Hunt, O. M. Yaghi, *Nat. Chem.*, **2010**, 2, 235. (b) Y. Zhu, H. Long, W. Zhang, *Chem. Mater.*, **2013**, 25, 1630. (c) Y. Pramudya, J. L. Mendoza-Cortes, *J. Am. Chem. Soc.*, **2016**, 138, 15204.
- [3.9] (a) E. L. Spitler and W. R. Dichtel, *Nat. Chem.*, **2010**, 2, 672. (b) M. Dogru, M. Handloser, F. Auras, T. Kunz, D. Medina, A. Hartschuh, P. Knochel, T. Bein, *Angew. Chem., Int. Ed.*, **2013**, 52, 2920.
- [3.10] (a) Y. Zhang, S. N. Riduana, *Chem. Soc. Rev.*, **2012**, 41, 2083. (b) Q. Fang, S. Gu, J. Zheng, Z. Zhuang, S. Qiu, Y. Yan, *Angew. Chem., Int. Ed.*, **2014**, 53, 2878. (c) V. S. Vyas, F. Haase, L. Stegbauer, G. Savasci, F. Podjaski, C. Ochsenfeld, B. V. Lotsch, *Nat. Commun.*, **2015**, 6, 8508. (d) D. B. Shinde, S. Kandambeth, P. Pachfule, R. R. Kumar, R. Banerjee, *Chem. Commun.*, **2015**, 51, 310.
- [3.11] (a) H. L. Nguyen, F. Gándara, H. Furukawa, T. L. H. Doan, K. E. Cordova, O. M. Yaghi, *J. Am. Chem. Soc.*, **2016**, 138, 4330. (b) P. Pachfule, M. K. Panda, S. Kandambeth, S. M. Shivaprasad, D. D. Díaz, R. Banerjee, *J. Mater. Chem. A*, **2014**, 2, 7944.
- [3.12] (a) S. Kandambeth, A. Mallick, B. Lukose, M. V. Mane, T. Heine, R. Banerjee, *J. Am. Chem. Soc.*, **2012**, 134, 19524. (b) B. P. Biswal, S. Chandra, S. Kandambeth, B. Lukose, T. Heine, R. Banerjee, *J. Am. Chem. Soc.*, **2013**, 135, 5328.
- [3.13] (a) S.-Y. Ding, J. Gao, Q. Wang, Y. Zhang, W.-G. Song, C.-Y. Su, W. Wang, *J. Am. Chem. Soc.*, **2011**, 133, 19816. (b) L. A. Baldwin, J. W. Crowe, D. A. Pyles and P. L. McGrier, *J. Am. Chem. Soc.*, **2016**, 138, 15134. (c) P. Pachfule, M. K. Panda, S. Kandambeth, S. M. Shivaprasad, D. D. Díaz, R. Banerjee, *J. Mater. Chem. A*, **2014**, 2, 7944.
- [3.14] (a) R. Zhou, W. Wang, Z.-j. Jiang, K. Wang, X.-l. Zheng, H.-y. Fu, H. Chen, R.-x. Li, *Chem. Commun.*, **2014**, 50, 6023. (b) M. J. Bosiak, *ACS Catal.*, **2016**, 6, 2429.
- [3.15] (a) C. A. Witham, W. Huang, C.-K. Tsung, J. N. Kuhn, G. A. Somorjai, F. D. Toste, *Nat. Chem.*, **2010**, 2, 36. (b) W. Huang, J. H.-C. Liu, P. Alayoglu, Y. Li, C. A. Witham, C.-K. Tsung, F. D. Toste, G. A. Somorjai, *J. Am. Chem. Soc.*, **2010**, 132, 16771. (c) Y. Li, J. H.-C. Liu, C. A. Witham, W. Huang, M. A. Marcus, S. C. Fakra,

- P. Alayoglu, Z. Zhu, C. M. Thompson, A. Arjun, K. Lee, E. Gross, F. D. Toste, G. A. Somorjai, *J. Am. Chem. Soc.*, **2011**, *133*, 13527.
- [3.16] D. B. Shinde, H. B. Aiyappa, M. Bhadra, B. P. Biswal, P. Wadge, S. Kandambeth, B. Garai, T. Kundu, S. Kurungot, R. Banerjee, *J. Mater. Chem. A*, **2016**, *4*, 2682.
- [3.17] (a) L. Pazderski, *Magn. Reson. Chem.* **2008**, *46*, S3. (b) T. Pawlak, L. Pazderski, J. Sitkowski, L. Kozerski, E. Szłyk, *Magn. Reson. Chem.* **2011**, *49*, 59.
- [3.18] (a) H. N. C. Wong, K.-S. Yeung, Z. Yang, in *Comprehensive Heterocyclic Chemistry III*, ed. A. R. Katritzky, C. A. Ramsden, E. F. V. Scriven, R. J. K. Taylor, Elsevier, Oxford, **2008**, *3*, pp. 407. (b) P. Stehrer-Schmid, H.-U. Wolf, *Mutat. Res., Rev. Genet. Toxicol.*, **1995**, *339*, 61. (c) J. Knoll, *CNS Drug Rev.*, **2001**, *7*, 317. (d) H. Khanam, Shamsuzzaman, *Eur. J. Med. Chem.*, **2015**, *97*, 483. (e) R. Naik, D. S. Harmalkar, X. Xu, K. Jang, K. Lee, *Eur. J. Med. Chem.*, **2015**, *90*, 379. (f) A. Blanc, V. Bénéteau, J.-M. Weibel, P. Pale, *Org. Biomol. Chem.*, **2016**, *14*, 9184.
- [3.19] J. H. Chong, M. Sauer, B. O. Patrick, M. J. MacLachlan, *Org. Lett.*, **2003**, *5*, 3823.
- [3.20] M. Albrecht, I. Janser, A. Lützen, M. Hapke, R. Fröhlich, P. Weis, *Chem. Eur. J.* **2005**, *11*, 5742.

CHAPTER 4

- [4.1] (a) A. D. Ryabov, *Chem. Rev.*, **1990**, *90*, 403. (b) A. E. Shilov, G. B. Shul'pin, *Chem. Rev.*, **1997**, *97*, 2879. (c) V. Ritleng, C. Sirlin, M. Pfeffer, *Chem. Rev.*, **2002**, *102*, 1731. (d) A. R. Dick, M. S. Sanford, *Tetrahedron*, **2006**, *62*, 2439. (e) I. A. I. Mkhaliid, J. H. Barnard, T. B. Marder, J. M. Murphy, J. F. Hartwig, *Chem. Rev.*, **2010**, *110*, 890. (f) M. P. Doyle, R. Duffy, M. Ratnikov, L. Zhou, *Chem. Rev.*, **2010**, *110*, 704. (g) H. M. Davies, J. Du Bois, J. Q. Yu, *Chem. Soc. Rev.*, **2011**, *40*, 1855. (h) D. A. Colby, R. G. Bergman, J. A. Ellman, *Chem. Rev.*, **2009**, *110*, 624. (a) X. Chen, K. M. Engle, D. Wang, J. Q. Yu, *Angew. Chem., Int. Ed.*, **2009**, *48*, 5094. (b) T. W. Lyons, M. S. Sanford, *Chem. Rev.*, **2010**, *110*, 1147. (c) L. Ackermann, *Chem. Rev.*, **2011**, *111*, 1315. (d) S. R. Neufeldt, M. S. Sanford, *Acc. Chem. Res.*, **2012**, *45*, 936.
- [4.2] (a) D. C. Powers, E. Lee, A. Ariaforde, M. S. Sanford, B. F. Yates, A. J. Canty, T. Ritter, *J. Am. Chem. Soc.*, **2012**, *134*, 12002. (b) D. C. Powers, T. Ritter, *Acc. Chem.*

- Res.*, **2012**, 45, 840. (c) L. T. Pilarski, N. Selander, D. Bose, K. J. Szabo, *Org. Lett.*, **2009**, 11, 5518. (d) N. Selander, B. Willy, K. J. Szabo, *Angew. Chem., Int. Ed.*, **2010**, 49, 4051. (e) R. Alam, L. T. Pilarski, E. Pershagen, K. J. Szabo, *J. Am. Chem. Soc.*, **2012**, 134, 8778.
- [4.3] (a) J. K. Stille, *Angew. Chem., Int. Ed.*, **1986**, 25, 508. (b) N. Miyaura, A. Suzuki, *Chem. Rev.*, **1995**, 95, 2457. (c) B. M. Trost, M. L. Crawley, *Chem. Rev.*, **2003**, 103, 2921. (d) K. C. Nicolaou, P. G. Bulger, D. Sarlah, *Angew. Chem. Int. Ed.*, **2005**, 44, 4442. (e) D. S. Surry, S. L. Buchwald, *Angew. Chem., Int. Ed.*, **2008**, 47, 6338. (f) J. F. Hartwig, *Nature*, **2008**, 455, 314. (g) S. E. Denmark, C. S. Regens, *Acc. Chem. Res.* **2008**, 41, 1486. (h) A. F. Littke, G. C. Fu, *Angew. Chem., Int. Ed.*, **1998**, 37, 3387. (i) B. C. Hamann, J. F. Hartwig, *J. Am. Chem. Soc.*, **1998**, 120, 7369.
- [4.4] (a) T. Furuya, A. S. Kamlet, T. Ritter, *Nature*, **2011**, 473, 470. (b) K. E. Torraca, X. Huang, C. A. Parrich, S. L. Buchwald, *J. Am. Chem. Soc.*, **2001**, 123, 10770. (c) S. Gowrisankar, A. G. Sergeev, P. Anbarasan, A. Spannenberg, H. Neumann, M. Beller, *J. Am. Chem. Soc.*, **2010**, 132, 11592.
- [4.5] *The Chemistry of Phenols*; Z. Rappoport, Ed.; John Wiley & Sons Ltd.: Chichester, U.K., **2003**.
- [4.6] (a) V. V. Dunina, O. A. Zalevskaya, V. M. Potapov, *Russ. Chem. Rev.*, **1988**, 57, 250. (b) A. D. Ryabov, *Chem. Rev.*, **1990**, 90, 403. (c) G. Dyker, *Angew. Chem., Int. Ed.*, **1999**, 38, 1698. (d) J. Dupont, C. S. S. Consorti, *J. Chem. Rev.*, **2005**, 105, 2527.
- [4.7] (a) Y. Jiang, Q. Gao, *J. Am. Chem. Soc.*, **2006**, 128, 716. (b) C. A. Witham, W. Huang, C.-K. Tsung, J. N. Kuhn, G. A. Somorjai, F. D. Toste, *Nat. Chem.*, **2010**, 2, 36. (c) F. A. Westerhaus, R. V. Jagadeesh, G. Wienhöfer, M.-M. Pohl, J. Radnik, A.-E. Surkus, J. Rabeah, K. Junge, H. Junge, M. Nielsen, A. Brückner, M. Beller, *Nat. Chem.*, **2013**, 5, 537. (d) M. Benaglia, A. Puglisi, F. Cozzi, *Chem. Rev.*, **2003**, 103, 3401. (e) S. Ikegami, H. Hamamoto, *Chem. Rev.*, **2009**, 109, 583. (f) D. J. Cole-Hamilton, *Science*, **2003**, 299, 1702. (h) W. Huang, J. H. -C. Liu, P. Alayoglu, Y. Li, C. A. Witham, C. -K. Tsung, F. D. Toste, G. A. Somorjai, *J. Am. Chem. Soc.* **2010**, 132, 16771.

- [4.8] (a) A. P. Côté, A. I. Benin, N. W. Ockwig, M. O’Keeffe, A. J. Matzger, O. M. Yaghi, *Science*, **2005**, *310*, 1166. (b) X. Feng, X. Dinga, D. Jiang, *Chem. Soc. Rev.*, **2012**, *41*, 6010. (c) J. W. Colson, W. R. Dichtel, *Nat. Chem.*, **2013**, *5*, 453. (d) S.-Y. Dinga, W. Wang, *Chem. Soc. Rev.*, **2013**, *42*, 548. (e) M. Calik, T. Sick, M. Dogru, M. Döblinger, S. Datz, H. Budde, A. Hartschuh, F. Auras, T. Bein, *J. Am. Chem. Soc.*, **2016**, *138*, 1234. (f) D. Wu, F. Xu, B. Sun, R. Fu, H. He, K. Matyjaszewski, *Chem. Rev.*, **2012**, *112*, 3959. (g) T.-Y. Zhou, S.-Q. Xu, Q. Wen, Z.-F. Pang, X. Zhao, *J. Am. Chem. Soc.*, **2014**, *136*, 15885. (h) S. Kandambeth, A. Mallick, B. Lukose, M. V. Mane, T. Heine, R. Banerjee, *J. Am. Chem. Soc.*, **2012**, *134*, 19524. (i) B. P. Biswal, S. Chandra, S. Kandambeth, B. Lukose, T. Heine, R. Banerjee, *J. Am. Chem. Soc.*, **2013**, *135*, 5328. (j) D. B. Shinde, H. B. Aiyappa, M. Bhadra, B. P. Biswal, P. Wadge, S. Kandambeth, B. Garai, T. Kundu, S. Kurungot, R. Banerjee, *J. Mater. Chem. A*, **2016**, *4*, 2682.
- [4.9] (a) S. D. Roughley, A. M. Jordan, *J. Med. Chem.* **2011**, *54*, 3451. (b) D. Frath, J. Massue, G. Ulrich, R. Ziessel, *Angew. Chem., Int. Ed.*, **2014**, *53*, 2290. (c) D. Li, H. Zhang, Y. Wang, *Chem. Soc. Rev.*, **2013**, *42*, 8416. (d) L. V. Desai, K. L. Hull, M. S. Sanford, *J. Am. Chem. Soc.*, **2004**, *126*, 9542. (e) G. J. Chuang, W. Wang, E. Lee, T. Ritter, *J. Am. Chem. Soc.* **2011**, *133*, 1760. (f) M. A. Bigi, S. A. Reed, M. C. White, *J. Am. Chem. Soc.* **2012**, *134*, 9721. (g) M. A. Bigi, S. A. Reed, M. C. White, *Nat. Chem.*, **2011**, *3*, 216. (h) M. S. Chen, M. C. White, *Science*, **2007**, *318*, 783. (i) M. G. Charest, C. D. Lerner, J. D. Brubaker, D. R. Siegel, A. G. Myers, *Science*, **2005**, *308*, 395.
- [4.10] (a) X. Chen, X.-S. Hao, G. E. Goodhue, J.-Q. Yu, *J. Am. Chem. Soc.*, **2006**, *128*, 6790. (b) J. Gallardo-Donaire, R. Martin, *J. Am. Chem. Soc.*, **2013**, *135*, 9350. (c) W. Liu, L. Ackermann, *Org. Lett.*, **2013**, *15*, 3484. (d) F. Mo, L. J. Trzpekowski, G. Dong, *Angew. Chem., Int. Ed.*, **2012**, *51*, 13075. (e) G. Shan, X. Yang, L. Ma, Y. Rao, *Angew. Chem., Int. Ed.*, **2012**, *51*, 13070. (f) V. S. Thirunavukkarasu, J. Hubrich, L. Ackermann, *Org. Lett.*, **2012**, *14*, 4210.
- [4.11] (a) Z. Wang, S. M. Cohen, *Chem. Soc. Rev.*, **2009**, *38*, 1315. (b) S. M. Cohen, *Chem. Rev.*, **2012**, *112*, 970. (c) Trindade, A. F.; Gois, P. M. P.; Afonso, C. A. M. *Chem. Rev.*, **2009**, *109*, 418. (d) Heitbaum, M.; Glorius, F.; Escher, I. *Angew. Chem., Int.*

-
- Ed.*, **2006**, *45*, 4732. (e) A. Nagai, Z. Guo, X. Feng, S. Jin, X. Chen, X. Ding, D. Jiang, *Nat. Commun.*, **2011**, *2*, 536.
- [4.12] (a) M. Gruttadauria, F. Giacalone, R. Noto, *Chem. Soc. Rev.*, **2008**, *37*, 1666. (b) F. Hoffmann, M. Cornelius, J. Morell, M. Fröba, *Angew. Chem., Int. Ed.*, **2006**, *45*, 3216.
- [4.13] S.-Y. Ding, J. Gao, Q. Wang, Y. Zhang, W.-G. Song, C.-Y. Su, W. Wang, *J. Am. Chem. Soc.*, **2011**, *133*, 19816.
- [4.14] (a) H.-S. Xu, S.-Y. Ding, W.-K. An, H. Wu, W. Wang, *J. Am. Chem. Soc.*, **2016**, *138*, 11489. (b) C. J. Doonan, D. J. Tranchemontagne, T. G. Glover, J. R. Hunt, O. M. Yaghi, *Nat. Chem.*, **2010**, *2*, 235. (c) S. Wan, J. Guo, J. Kim, H. Ihee, D. Jiang, *Angew. Chem., Int. Ed.*, **2008**, *47*, 8826.
- [4.15] M. Bhadra, H. S. Sasmal, A. Basu, S. P. Midya, S. Kandambeth, P. Pachfule, E. Balaraman, R. Banerjee, *ACS Appl. Mater. Interfaces*, **2017**, *9*, 13785.
- [4.16] J. H. Chong, M. Sauer, B. O. Patrick, M. J. MacLachlan, *Org. Lett.*, **2003**, *5*, 3823.
- [4.17] M. Albrecht, I. Janser, A. Lützen, M. Hapke, R. Fröhlich, P. Weis, *Chem. Eur. J.*, **2005**, *11*, 5742.

CHAPTER 5

- [5.1] (a) I. Dincer, *Renewable Sustainable Energy Rev.*, **2000**, *4*, 157. (b) J. Wang, L. Feng, X. Tang, Y. Bentley, M. Höök, *Futures*, **2017**, *86*, 58. (c) T.-m. Su, Z.-z. Qin, H.-b. Ji, Y.-x. Jiang, G. Huang, *Environ. Chem. Lett.*, **2016**, *14*, 99.
- [5.2] (a) D. Ravelli, D. Dondi, M. Fagnoni, A. Albini, *Chem. Soc. Rev.*, **2009**, *38*, 1999. (b) M. Fagnoni, D. Dondi, D. Ravelli, A. Albini, *Chem. Rev.*, **2007**, *107*, 2725. (c) N. Serpone, E. Pelizzetti, *Photocatalysis: fundamentals and applications*, Wiley, New York, **1989**.
- [5.3] (a) A. C. Arias, J. D. MacKenzie, I. McCulloch, J. Rivnay, A. Salleo, *Chem. Rev.*, **2010**, *110*, 3. (b) A. Facchetti, *Angew. Chem. Int. Ed.*, **2011**, *50*, 6001, *Angew. Chem.*, **2011**, *123*, 6125.

- [5.4] (a) D. H. Waldeck, *Chem. Rev.*, **1991**, *91*, 415. (b) T. Arai, K. Tokumaru, *Chem. Rev.*, **1993**, *93*, 23. (c) F. D. Lewis, B. A. Yoon, T. Arai, T. Iwasaki, K. Tokumaru, *J. Am. Chem. Soc.*, **1995**, *117*, 3029. (d) T. Arai, M. Moriyama and K. Tokumaru, *J. Am. Chem. Soc.*, **1994**, *116*, 3171.
- [5.5] (a) C. K. Prier, D. A. Rankic, D. W. C. MacMillan, *Chem. Rev.* **2013**, *113*, 5322. (b) N. A. Romero, D. A. Nicewicz, *Chem. Rev.* **2016**, *116*, 10075. (c) D. P. Hari, B. König, *Chem. Commun.* **2014**, *50*, 6688. (d) S. Fukuzumi, H. Kotani, K. Ohkubo, S. Ogo, N. V. Tkachenko, H. Lemmetyinen, *J. Am. Chem. Soc.* **2004**, *126*, 1600. (e) I. Ghosh, T. Ghosh, J. I. Bardagi, B. König, *Science*, **2014**, *346*, 725. (f) I. Ghosh, B. König, *Angew. Chem. Int. Ed.* **2016**, *55*, 7676. (g) I. Ghosh, L. Marzo, A. Das, R. Shaikh, B. König, *Acc. Chem. Res.* **2016**, *49*, 1566. (h) M. M. Li, Y. Wei, J. Liu, H. W. Chen, L. Q. Lu, W. J. Xiao, *J. Am. Chem. Soc.* **2017**, *139*, 14707. (i) Y. Y. Liu, X. Y. Yu, J. R. Chen, M. M. Qiao, X. Qi, D. Q. Shi, W. J. Xiao, *Angew. Chem. Int. Ed.* **2017**, *56*, 9527. *Angew. Chem.*, **2017**, *129*, 9655. (j) D. A. Nicewicz, D. W. C. MacMillan, *Science*, **2008**, *322*, 77. (k) X. H. Zhang, D. W. C. MacMillan, *J. Am. Chem. Soc.* **2017**, *139*, 11353. (l) H. Bartling, A. Eisenhofer, B. König, R. M. Gschwind, *J. Am. Chem. Soc.* **2016**, *138*, 11860. (m) A. U. Meyer, A. Wimmer, B. König, *Angew. Chem. Int. Ed.*, **2017**, *56*, 409, *Angew. Chem.* **2017**, *129*, 420. (n) S. Senaweera, J. D. Weaver, *J. Am. Chem. Soc.* **2016**, *138*, 2520. (o) M. Chhowalla, H. S. Shin, G. Eda, L. J. Li, K. P. Loh, H. Zhang, *Nat. Chem.*, **2013**, *5*, 263. (p) W. J. Ong, L. L. Tan, Y. H. Ng, S. T. Yong, S. P. Chai, *Chem. Rev.*, **2016**, *116*, 7159. (q) C. Tan, X. Cao, X. J. Wu, Q. He, J. Yang, X. Zhang, J. Chen, W. Zhao, S. Han, G. H. Nam, M. Sindoro, H. Zhang, *Chem. Rev.* **2017**, *117*, 6225. (r) Grätzel, M. *Acc. Chem. Res.* **1981**, *14*, 376. (s) Meyer, T. J. *Acc. Chem. Res.* **1989**, *22*, 163.
- [5.6] (a) D. Gust, T. A. Moore, *Science*, **1989**, *244*, 35. (b) T. J. Meyer, *Acc. Chem. Res.*, **1989**, *22*, 163. (c) D. Gust, T. A. Moore, A. L. Moore, *Acc. Chem. Res.*, **1993**, *26*, 198.
- [5.7] H. Takeda, O. Ishitani, *Coord. Chem. Rev.*, **2010**, *254*, 346.
- [5.8] (a) N. Serpone, E. Pelizzetti, *Photocatalysis: fundamentals and applications*, Wiley, New York, **1989**. (b) N. Serpone, A. V. Emeline, *Int. J. Photoenergy*, **2002**, *4*, 91.

- [5.9] (a) M. Grätzel, *Acc. Chem. Res.*, **1981**, *14*, 376. (b) T. J. Meyer, *Acc. Chem. Res.*, **1989**, *22*, 163.
- [5.10] (a) E. C. Gentry, R. R. Knowles, *Acc. Chem. Res.*, **2016**, *49*, 1546. (b) I. Ghosh, L. Marzo, A. Das, R. Shaikh, B. Kçnig, *Acc. Chem. Res.* **2016**, *49*, 1566. (c) M. N. Hopkinson, A. Tlahuext-Aca, F. Glorius, *Acc. Chem. Res.* **2016**, *49*, 2261. (d) K. A. Margrey, D. A. Nicewicz, *Acc. Chem. Res.* **2016**, *49*, 1997. (e) N. A. Romero, D. A. Nicewicz, *Chem. Rev.*, **2016**, *116*, 10075. (f) D. Staveness, I. Bosque, C. R. J. Stephenson, *Acc. Chem. Res.*, **2016**, *49*, 2295. (g) J. Twilton, C. Le, P. Zhang, M. H. Shaw, R. W. Evans, D. W. C. MacMillan, *Nat. Rev. Chem.*, **2017**, *1*, 0052. (h) T. P. Yoon, *Acc. Chem. Res.*, **2016**, *49*, 2307.
- [5.11] (a) A. Züttel, A. Borgschulte, L. Schlapbach, *Hydrogen as a future energy carrier*, John Wiley & Sons, **2011**. (b) J. A. Turner, *Science*, **2004**, *305*, 972.
- [5.12] (a) S. Anantharaj, S. R. Ede, K. Sakthikumar, K. Karthick, S. Mishra, S. Kundu, *ACS Catal.*, **2016**, *6*, 8069. (b) J. Tian, Q. Liu, A. M. Asiri, X. Sun, *J. Am. Chem. Soc.*, **2014**, *136*, 7587. (c) Q. Zhang, Z. Li, S. Wang, R. Li, X. Zhang, Z. Liang, H. Han, S. Liao, C. Li, *ACS Catal.*, **2016**, *6*, 2182.
- [5.13] (a) A. Thomas, A. Fischer, F. Goettmann, M. Antonietti, J. O. Muller, R. Schlogl, J. M. Carlsson, *J. Mater. Chem.* **2008**, *18*, 4893. (b) Y. Wang, J. S. Zhang, X. C. Wang, M. Antonietti, H. R. Li, *Angew. Chem.*, **2010**, *122*, 3428, *Angew. Chem. Int. Ed.*, **2010**, *49*, 3356. (e) S. Cao, J. Low, J. Yu, M. Jaroniec, *Adv. Mater.* **2015**, *27*, 2150.
- [5.14] (a) A. Boëdec, H. Sicard, J. Dessolin, G. Herbette, S. Ingoure, C. Raymond, C. Belman, J. -L. Kraus, *J. Med. Chem.* **2008**, *51*, 1747. (b) N. Chhabra, M. L. Aseri, D. Padmanabhan, *Int. J. Appl. Basic Med. Res.*, **2013**, *3*, 16. (c) M. L. Williams, M. S. Lennard, I. J. Martin, G. T. Tucker, *Carcinogenesis*, **1994**, *15*, 2733.
- [5.15] W. -Y. Siau, Y. Zhang, Y. Zhao, *Top. Curr. Chem.*, **2012**, *327*, 33.
- [5.16] (a) L. F. V. Staden, D. Gravestock D. J. Ager, *Chem. Soc. Rev.*, **2002**, *31*, 195. (b) E.-I. Negishi, Z. Huang, G. Wang, S. Mohan, C. Wang, H. Hattori, *Acc. Chem. Res.*, **2008**, *41*, 1474. (c) Z. Huang, E.-I. Negishi, *J. Am. Chem. Soc.*, **2007**, *129*, 14788. (d) S. J. Meek, R. V. O'Brien, J. Llaveria, R. R. Schrock, A. H. Hoveyda, *Nature*, **2011**, *471*, 461. (e) M. J. Koh, R. K. M. Khan, S. Torker, A. H. Hoveyda, *Angew. Chem.*,

- Int. Ed.*, **2014**, 53, 1968. (f) K. Endo, R. H. Grubbs, *J. Am. Chem. Soc.*, **2011**, 133, 8525.
- [5.17] (a) K. Singh, S. J. Staig, J. D. Weaver, *J. Am. Chem. Soc.*, **2014**, 136, 5275. (b) D. C. Fabry, M. A. Ronge, M. Rueping, *Chem. – Eur. J.*, **2015**, 21, 5350. (c) A. Singh, C. J. Fennell, J. D. Weaver, *Chem. Sci.*, **2016**, 7, 6796. (d) J. B. Metternich, R. Gilmour, *J. Am. Chem. Soc.*, **2016**, 138, 1040. (e) W. G. Herkstroeter, G. S. Hammond, *J. Am. Chem. Soc.*, **1966**, 88, 4769. (f) R. S. H. Liu, N. J. Turro, G. S. Hammond, *J. Am. Chem. Soc.*, **1965**, 87, 3406. (g) J. Saltiel, G. S. Hammond, *J. Am. Chem. Soc.*, **1963**, 85, 2516.
- [5.18] B. W. Domagalska, L. Syper, K. A. Wilk, *Tetrahedron*, **2004**, 60, 1931.
- [5.19] H. F. Li, E. A. Homan, A. J. Lampkins, I. Ghiviriga, R. K. Castellano, *Org. Lett.* **2005**, 7, 443.
- [6.1] C. W. Kee, K. F. Chin, M. W. Wong, C.-H. Tan, *Chem. Commun.*, **2014**, 50, 8211.

ABOUT THE AUTHOR



Mr. Mohitosh Bhadra, son of Mrityunjoy Bhadra and Shantilata Bhadra, was born in Samsara village of Paschim Medinipur district, West Bengal, India, in 1990. He did his schooling from Samsara Patpara High School (2006) and higher secondary education from Panchrol High School (2008). He has completed his B.Sc. (Chemistry) from Ramakrishna Mission Vivekananda Centenary College, Rahara, Kolkata (2011) under West Bengal State University. Then he moved to Department of Chemistry, Indian Institute of Technology, Bombay, Mumbai, Maharashtra to pursue his M.Sc. in Chemistry (2013). He has worked under the supervision of Prof. Debabrata Maiti in homogeneous catalysis project at IIT Bombay. After qualifying all India CSIR-UGC National Eligibility Test (NET-JRF) examination, he joined Physical and Materials Chemistry Division, CSIR-National Chemical Laboratory, Pune, India to pursue his Ph.D. degree in July 2014 under the guidance of Prof. Dr. Rahul Banerjee. He has received the research fellowship (JRF and SRF) from Council of Scientific and Industrial Research (CSIR), New Delhi, India for the period of July 2014 - August 2018 to carry out the Ph.D. thesis work.

LIST OF PUBLICATIONS

1. **Mohitosh Bhadra**, Himadri Sekhar Sasmal, Arghya Basu, Siba P. Midya, Sharath Kandambeth, Pradip Pachfule, Ekambaram Balaraman* and Rahul Banerjee*, “*Pre-designed Metal-Anchored Building Block for In Situ Generation of Pd Nanoparticles in Porous Covalent Organic Framework: Application in Heterogeneous Tandem Catalysis*”. *ACS Appl. Mater. Interfaces*, **2017**, 9, 13785–13792.
2. Digambar Balaji Shinde†, Harshitha Barike Aiyappa†, **Mohitosh Bhadra**†, Bishnu P. Biswal, Pritish Wadge, Sharath Kandambeth, Bikash Garai, Tanay Kundu, Sreekumar Kurungot* and Rahul Banerjee.*, “*A mechanochemically synthesized covalent organic framework as a proton-conducting solid electrolyte*”. *J. Mater Chem. A*, **2016**, 4, 2682-2690. † Authors are contributed equally.
3. Abdul Khayum M., Vidyanand Vijayakumar, Suwendu Karak, Sharath Kandambeth, **Mohitosh Bhadra**, Karthika Suresh, Nikhil Acharambath, Sreekumar Kurungot*, and Rahul Banerjee*, “*Convergent Covalent Organic Framework Thin Sheets as Flexible Supercapacitor Electrodes*”. *ACS Appl. Mater. Interfaces*, **2018**, DOI: 10.1021/acsami.8b10486.
4. Atanu Modak, Uttam Dutta, Rajesh Kancharla, Soham Maity, **Mohitosh Bhadra**, Saikh M. Mobin, and Debabrata Maiti*, “*Predictably Selective (sp^3)C–O Bond Formation through Copper Catalyzed Dehydrogenative Coupling: Facile Synthesis of Dihydro-oxazinone Derivatives*”. *Org. Lett.* **2014**, 16, 2602–2605.

CONFERENCES AND PRESENTATIONS

1. Presented an oral presentation at *24th Congress & General Assembly of the International Union of Crystallography 2017 (IUCr-2017)* held at Hyderabad, India (2017).
2. Presented Poster in *Sustainable Catalytic Technologies* held at CSIR-NCL, Pune, India (2017).
3. Participated in *Modern Trends in Inorganic Chemistry (MTIC XVII)* held at CSIR-NCL, Pune, India (2017).
4. Participated in *RSC India Road show* held at CSIR-NCL, Pune, India (2017).
5. Participated in *17th CRSI-National Symposium in Chemistry, 2015* held at CSIR-NCL, Pune, India (2015).
6. Participated in *International Conference on Structural and Inorganic Chemistry* held at CSIR-NCL, Pune, India (2014).